Multilayer Microwave Structures

Using Thick-Film Technology

A thesis submitted to Middlesex University in partial fulfilment of the requirements for the degree of Doctor of Philosophy

By

Zhengrong Tian

Communication Research Group, School of Computing Science
Middlesex University

November 2002

Abstract

Multilayer techniques, in conjunction with thick-film technology have been applied to the design and fabrication of several multilayer microwave structures to achieve the low cost and high performance goals set by modern microwave circuits and systems.

To provide accurate material parameters for the design of multilayer thick-film components, a novel slit cavity resonator method has been developed that enables the relative permittivity and loss tangent of dielectric samples to be measured easily, and with high accuracy. A particular feature of this method is that it can be used to measure thick-film samples that are normally only available in relatively thin layers in a two-layer format. Rigorous electromagnetic analysis on a slit cavity has been performed that accounts for the effect of the fringing fields and the radiation from the slits. The method has been verified through measurement on several thick-film materials over X-band.

Both the analytical methods and the fabrication techniques for multilayer microwave microstrip structures are presented. Several multilayer thick-film microstrip line test structures have been designed and characterised, and these provide a basic database for the design of multilayer microstrip components.

A new design procedure for the multilayer end-coupled filter has been developed that enables the designer to arrive at the physical dimensions of the multilayer structure based on the filter specification. This design technique is effective as it combines the accuracy of electromagnetic (EM) analysis and the efficiency of circuit simulation. The multilayer gap, which is the most critical element of multilayer end-coupled filters, has been characterised using EM analysis and the data is incorporated into a

circuit simulator. Measured and simulated results are presented that verify the new design technique. A 40% bandwidth has been achieved experimentally, which shows a very significant improvement over conventional single layer structures, where the bandwidth achievable is normally less than 5%.

Novel, octave band DC blocks have been designed, fabricated and tested using a new multilayer format. The tight coupling required between the coupled lines in this component was realized by overlapping these lines in a multilayer structure. Very good agreement was obtained between measured and simulated data. The multilayer approach was also applied to the design of coupled line bandpass filters where a measured 80% bandwidth was achieved.

For the first time, the properties of multilayer coupled lines using a range of different thick-film dielectrics are examined using their coupled-mode parameters. Design curves for multilayer coupled lines are obtained, that provide important information on the design of multilayer directional couplers.

A practical design strategy for multilayer directional couplers is developed, which overcomes the problem of excessive computation that is normally associated with the electromagnetic optimization of multilayer circuit designs. The methodology has been verified through the design and measurement of wide bandwidth 2dB and 3dB directional couplers that were fabricated using multilayer, thick-film technology.

New techniques for the design and fabrication of multilayer microwave thick-film components have thus been established, both theoretically and through practical circuit fabrication and measurement.

Acknowledgements

I would like to thank my supervisor, Dr. Charles Free, for his valuable help and guidance throughout the duration of this project. Without his help the completion of this work would have not been possible.

I would like to thank Prof. Colin Aitchison, Dr. Peter Barnwell and Mr. Keith Pitt for their support and helpful discussion.

Thanks to James Wood of Heraeus Inc. who helped with the preparation of dielectric samples and fabrication of the circuits.

I would like to thank University of Surrey for allowing me the use of their HP8510 Vector Network Analyzer.

Contents

Introduction

Interest in multilayer microwave structures has increased recently due to their potential to meet size, performance and cost requirements of the modern wireless market. With multilayer techniques one can employ several layers of metals sandwiched by insulators, this leads to an efficient solution for system miniaturization. Also, some of the circuit functions that are difficult to realize in conventional single layer structures can be easily obtained by a multilayer arrangement. For example, the strong coupling that is often required in the design of broadband directional couplers and filters can be obtained easily by overlapping multilayer coupled lines, with less stringent geometrical requirements. The multilayer approach will aid circuit integration and compaction, it also provides the microwave designer with an additional degree of design freedom. Whilst showing many advantages, multilayer structures offer a challenge to the microwave circuit designer. As multilayer microwave structures may comprise several layers of dielectrics and metallizations, there is complicated electromagnetic coupling between conductors in the same or different layers. Simple, accurate equivalent circuit models are not available. In general, full wave analysis has to be employed to characterize circuits of this kind. Since electromagnetic (EM) analysis usually requires a considerable amount of computation time, practical and effective design strategies are critical in the development of multilayer microwave structures, and it is the generation of these design strategies that is the primary focus of this project.

A good understanding of the coupling mechanisms involved in multilayer structures is crucial for effective multilayer circuit design. A number of the basic multilayer microstrip building blocks investigated in this study are shown in Table 1. The intention is that a detailed examination of the behaviour of these basic elements will

Table 1: Basic Multilayer Microstrip Building Blocks Studied

	Single layer version	Multilayer version	Applications
Gap (Overlap)	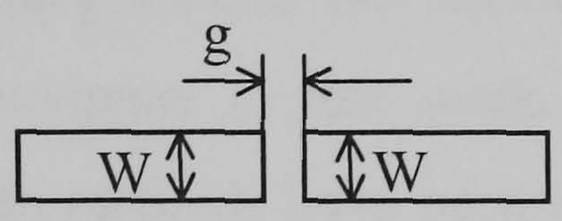	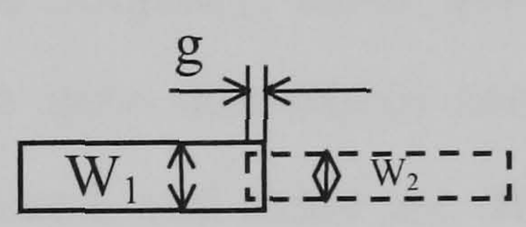	End-coupled bandpass filter
Two-Port coupled-line section	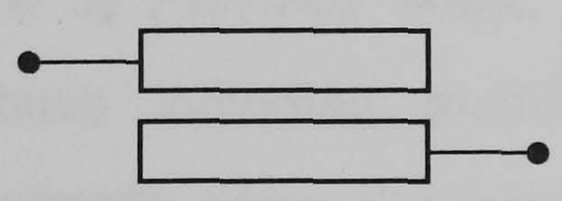	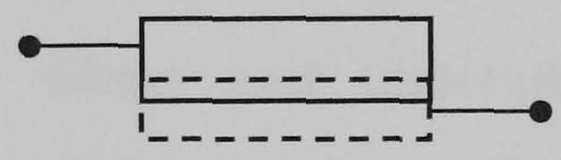	Coupled-line bandpass filter; DC block
Four-Port coupled-line section	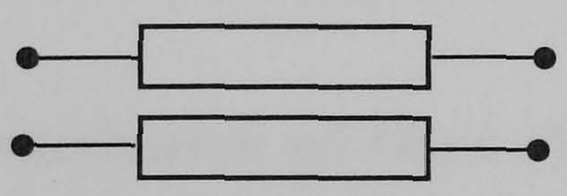	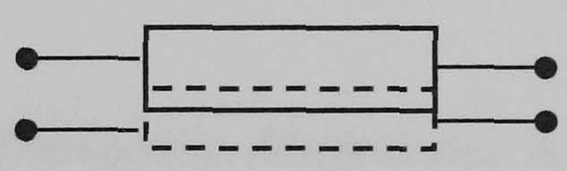	Directional coupler

Top conductor Bottom conductor

lead to an efficient and systematic design methodology for multilayer microwave structures. The multilayer microstrip structures studied cover multilayer end-coupled filters, multilayer coupled-line filters, multilayer DC blocks and multilayer tight directional couplers.

Fabrication technology is another important issue associated with the development of low cost microwave circuits. Whilst most of the multilayer structures previously reported in the literature use MMIC technology, thick-film technology, that is not only low cost but is naturally suited to the fabrication of multilayer structures, has been neglected. In this study, multilayer thick-film technology is employed in order to offer a low cost, high performance solution. As precise knowledge about material parameters is crucial for the design of multilayer microwave structures, techniques

for characterizing thick-film dielectric materials are also addressed in this thesis.

Fabrication and measurement of several multilayer circuits using thick-film technology, including filters, DC blocks, and couplers, have verified the design methodologies developed in this work. Some new theoretical methods of circuit analysis and design methods have been introduced, and these are discussed in some detail in the appropriate chapters.

Chapter 1. Review of Previous Work. The status of current work on multilayer microwave structures including multilayer filters and directional couplers is described and discussed. Since the intention of the present work is to implement circuits using thick-film fabrication techniques, a review of dielectric measurement techniques applicable to thick-film dielectric materials is also presented.

Chapter 2. Characterization of Thick-Film Dielectric Materials. A comprehensive error analysis especially for thin film two-layer dielectric measurement was performed. By recognizing the most significant error contribution for thin sample measurement, a novel slit cavity resonator method has been developed to enable dielectric materials to be more easily measured. Rigorous electromagnetic analysis on the slit cavity has been performed which accounts for the radiation effect from the slits. The filling factor for calculating the dielectric constant and loss tangent is obtained through electromagnetic calculation. The design of a slit cavity resonator and sample preparation is described in detail. The method was verified through measurements on a range of thick-film materials.

Chapter 3. Multilayer Microstrip Structures: Analysis and Fabrication. Microwave structures in multilayer format are introduced and the general analytical methods and fabrication techniques used are described. Several multilayer thick-film microstrip lines were designed and characterized, and these provide a basic database for the design of multilayer microstrip structures. The advantages of using multilayer microstrip lines and their applications are also discussed.

Chapter 4. Multilayer End-Coupled Bandpass Filters. A new design procedure for a multilayer end-coupled filter is developed, that allows the physical dimensions of the filter to be obtained from given filter specifications. The new design technique combines the accuracy of electromagnetic (EM) analysis with the efficiency of circuit simulation. Multilayer overlap is characterized through EM simulation and the results are incorporated into a circuit simulator for the simulation of the multilayer end-coupled filters. Measured results are presented that show a significant improvement in bandwidth performance when compared with the performance of conventional single layer structures.

Chapter 5. Broadband Multilayer DC Blocks and Coupled-line Bandpass Filters. The design and measured performance of ultra-broadband DC blocks and bandpass filters are presented, that make use of multilayer quarter wavelength coupled-line sections, with two ports open-circuited. Analytical results show that this simple, multilayer two-port quarter wavelength coupled-line section exhibits very strong coupling when there is an overlap between the two coupled lines. These results lead to design of several DC blocks with more than one octave bandwidth and very low insertion loss. Furthermore, as these coupled-line sections exhibit strong resonant performance, they were used to construct coupled-line filters that yielded ultra-broadband performance.

Chapter 6. Multilayer Directional Couplers. A new, practical design strategy for multilayer directional couplers is presented. The properties of multilayer coupled lines using a range of different thick-film dielectrics are examined using their coupled-mode parameters. Design curves for multilayer coupled lines are obtained, that provide important information in the design of multilayer directional couplers. A practical design strategy for multilayer directional couplers is developed, which overcomes the problem of excessive computation that is normally associated with the electromagnetic optimization of multilayer circuit designs. The methodology has been verified through the design and subsequent measurement of wide bandwidth 2dB and 3dB directional couplers that were fabricated using multilayer, thick-film

technology.

Chapter 7. Conclusions and Suggestions for Further Work. This provides a summary of the main outcomes of the work, and is supplemented in Appendix A by details of the publications that have resulted from this project. Some suggestions are provided for using circular cavities for measuring lower loss materials. Some proposals are given for extending the design techniques developed in this study to the design of multilayer coplanar circuits.

Chapter 1

Review of Previous Work

1.1 Summary

The principal aim of the present work is to study design techniques for multilayer microwave structures fabricated using thick-film technology. The combination of multilayer technique and thick-film technology has the potential to achieve the low cost and high performance goals required by modern microwave circuits and systems. The work will focus on the exploration of an efficient design methodology for multilayer microwave structures through the design, fabrication and testing of several typical multilayer microwave structures, including multilayer filters, DC blocks and directional couplers. To provide accurate material parameters for the design of these multilayer microwave structures, it is the intention to develop a dielectric measurement technique that is suitable for characterization of thick-film dielectric materials at microwave frequencies. Thus the review of previous work has

been divided into two sections. The first section concentrates on the work that has been reported on dielectric measurement techniques, especially the measurement techniques suitable for thin sample measurement. The second section is concerned with the existing studies on multilayer microwave structures, including multilayer filters and directional couplers. Both the current status of the design techniques and multilayer circuits performances that have been achieved are summarized.

1.2 Dielectric Measurement Techniques

Precise data for the dielectric constant and loss tangent of dielectric materials used in multilayer circuits at microwave frequencies is essential for accurate circuit design. These material parameters are critical for obtaining the correct characteristic impedance of the transmission lines and interconnections as well as for determining propagation delays and predicting line loss. Without this material data, the physical layout and performance parameters of the multilayer microwave circuits cannot be accurately established.

Numerous methods for the characterization of dielectric materials at microwave frequencies have been reported in the literature. However, these methods vary significantly in respect of accuracy, applicable frequency range, requirements for sample preparation, sample thickness and geometry, measurement system equipment, measurement speed, and also in the level of complexity required in processing the measured data.

At low frequencies, the dielectric measurement techniques are quite mature. Complex permittivity of the material is generally determined through a capacitance measurement with the sample held in a simple parallel-plate fixture. Capacitance and dissipation factors of the lumped capacitors are measured using a bridge or a resonant circuit [1]. The complex permittivity of the material is then calculated from this data. However, this technique is only useful up to the lower end of the VHF band.

At microwave frequencies, the sample may be placed inside a microwave transmission line or a resonant cavity. The electrical properties of the line or cavity are then measured to obtain the dielectric parameters. Since the propagation characteristics of an electromagnetic wave are influenced by the property of the medium through which it propagates, the material can be characterized by monitoring either the reflected or transmitted waves. At the present time, there are several techniques for measuring dielectric constant and loss tangent at microwave frequencies. These are:

Transmission line method [2] - The transmission line technique involves positioning a sample of the material under test in a length of coaxial or waveguide transmission line. The dielectric and magnetic properties of the sample modify the propagation constant of the line in the region occupied by the sample and also introduce reflections at both ends of the sample. These changes to the properties of the transmission line are monitored by measuring the scattering parameters of the line. The S-parameters are vector quantities, which can be readily measured using a vector network analyzer. Once the S-parameters are known, they can be used to calculate the complex permittivity of the sample, providing its exact length and position are known.

Using this method, materials can be characterized over a wide frequency range, since no resonant elements are involved. The transmission line technique is most suitable for measuring the loss factors of medium to high loss materials.

Resonant cavity and cavity perturbation method - Resonant cavity and cavity perturbation techniques have been extensively and successfully employed to measure the dielectric constant and loss tangent of low-loss materials at microwave frequencies [3-20]. These measurements are performed by inserting a sample with a specified shape into a microwave resonant cavity. In the case of a small sample, the dielectric parameters can be determined from the shift of the resonant frequency and the change of the cavity Q-factor. Figure 1.1 shows the components of a typical

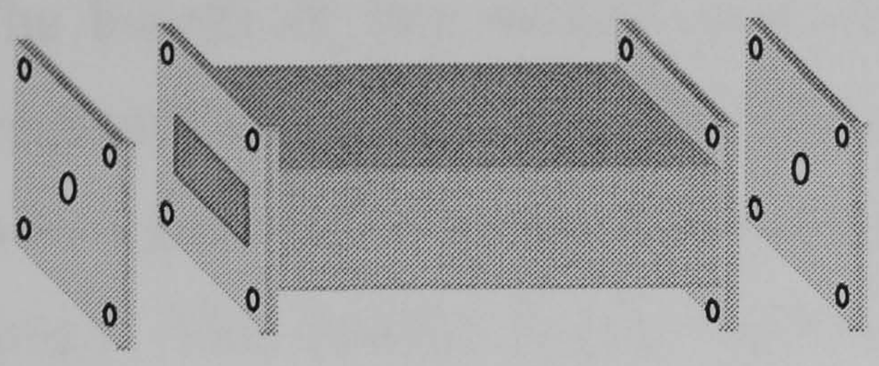

Figure 1.1: Components of a microwave resonant cavity

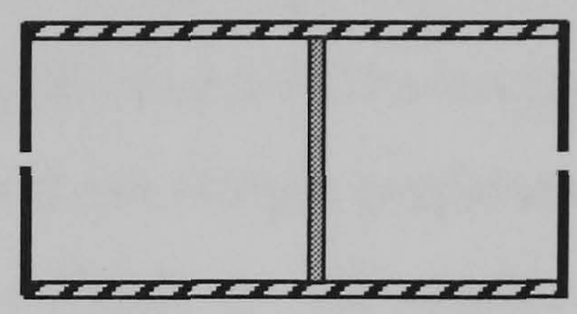

Figure 1.2: The longitudinal view of a cavity loaded with the sample

microwave resonant cavity. This is usually formed from a length of standard rectangular or circular waveguide, with transverse metallic plates bolted to the end flanges. An iris hole in each end plate allows energy to be fed in and out of the cavity. Figure 1.2 shows the longitudinal view of a cavity loaded with a sample. The length of the cavity, together with the reactance of the irises, determines the resonant frequency.

Open-ended transmission line method – In this method the dielectric sample under test is placed in close contact with the end of an open-ended microwave transmission line, which may be coaxial cable [21], as shown in Figure 1.3, or a piece of circular waveguide [22]. The input reflection coefficient is measured using a vector network analyzer and the dielectric properties of the sample can be inferred through numerical electromagnetic analysis.

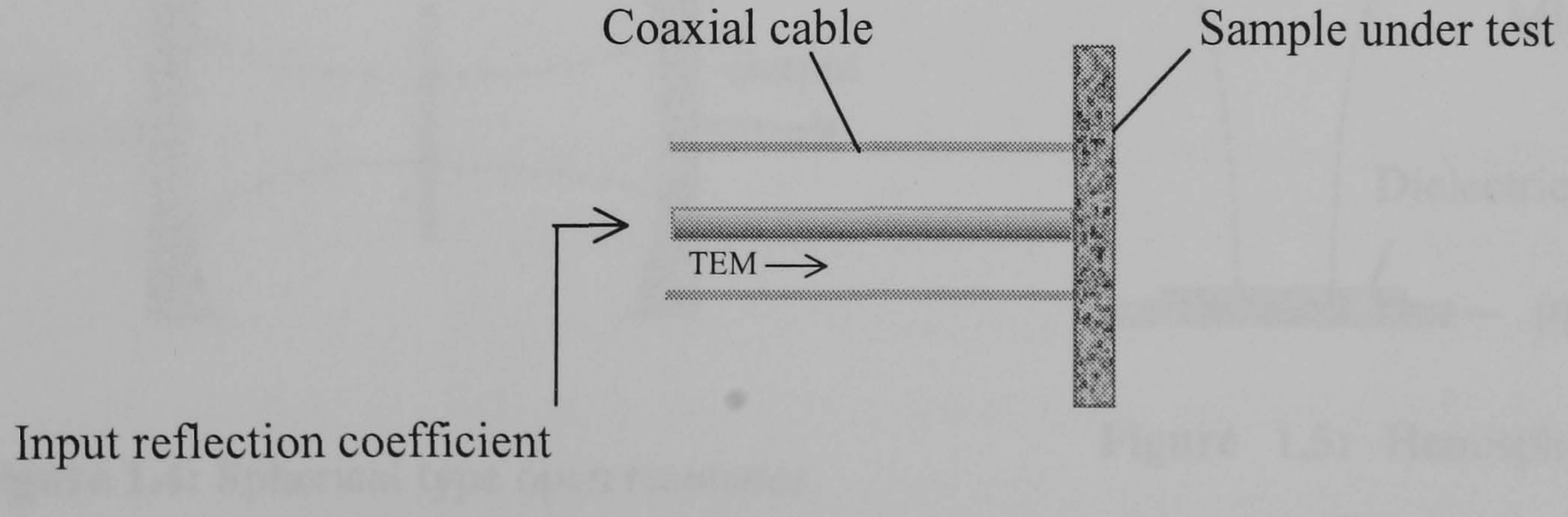

Figure 1.3: Open-ended coaxial line measurement

The benefit of this method is it can be used to measure samples over a wide frequency range rather than limited discrete frequencies as with the cavity method. It is also quick to set up the measurement system and the sample preparation is rather simple. This method is also useful when it is difficult or undesirable to cut the sample, such as when on-line quality control is needed. But the problem is that the data processing is complicated since it involves a large amount of electromagnetic computation.

Open resonator methods — Here, the sample is placed in an open resonator. Open resonator methods are regarded as precise measurement methods for low loss dielectric materials in the millimetre wave range 30-300 GHz[23-27]. Commonly used open resonators are either of the confocal type in which two spherical mirrors form the Fabry-Perot cavity, or the hemispherical type in which one spherical mirror and one flat mirror form the cavity. Figures 1.4 and 1.5 show the configurations of spherical and hemispherical type open resonators respectively. Both types of mirror are machined from brass and gold-plated after polishing. By measuring the resonant frequency and Q-factor of the resonator with and without the sample loaded, the complex permittivity of the materials can be determined.

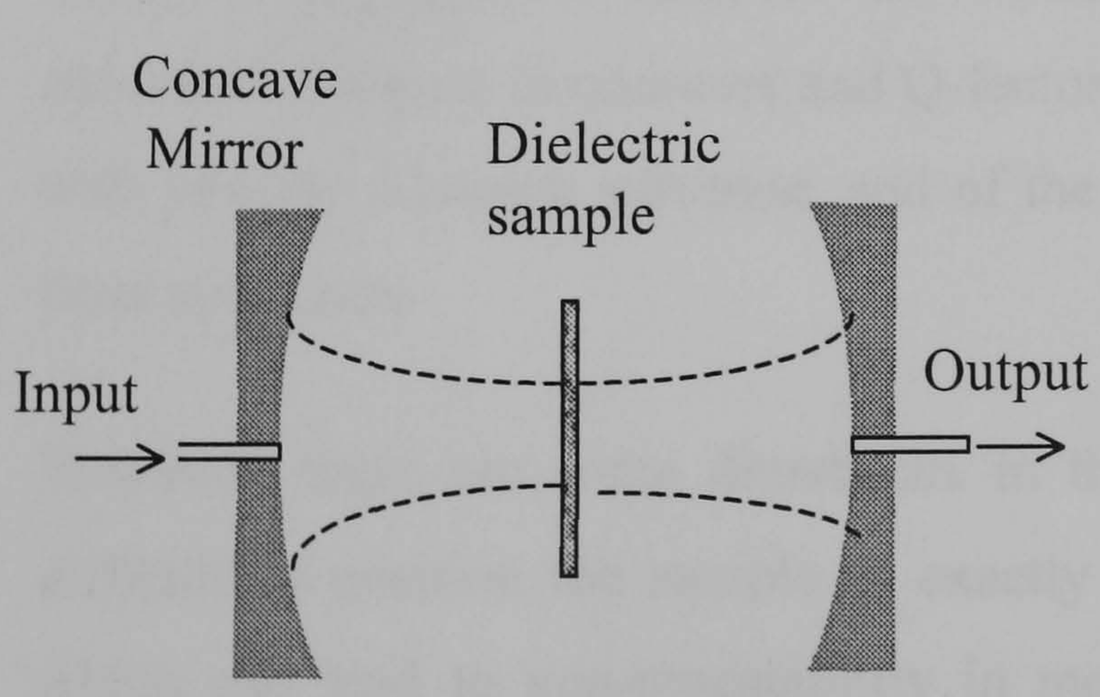

Figure 1.4: Spherical type open resonator

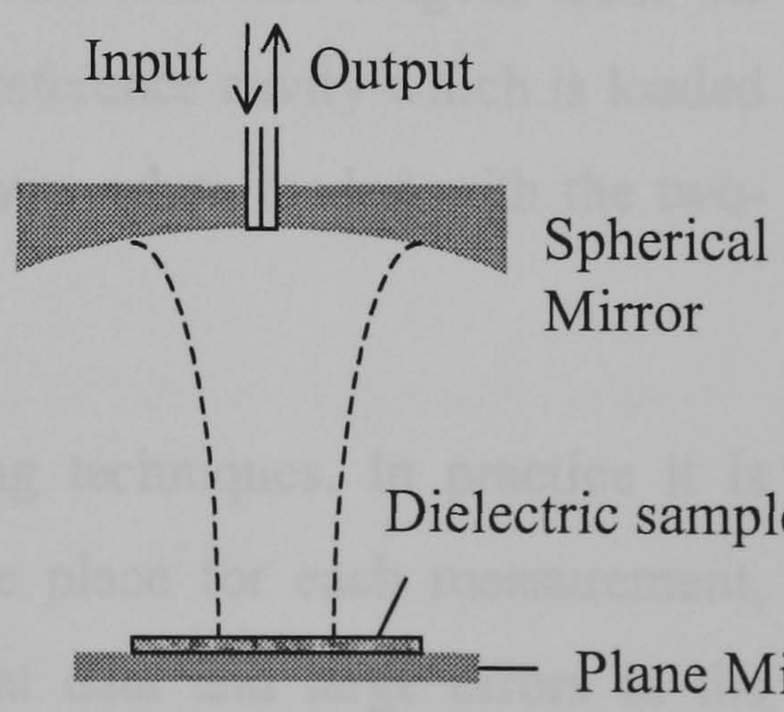

Figure 1.5: Hemispherical type open resonator

The above-mentioned techniques have been mainly used for measuring bulk materials. The measurement on thin samples, as in the case of thick-film dielectrics, is always more challenging, as the sample is so small. Consequently, a very sensitive technique is required.

The cavity perturbation technique has long been regarded as the most sensitive technique and has been used in the thin sample measurement. For thin sample measurement, one important advance was made by Janezic [9] who recognised that to obtain high sensitivity in measuring thin samples, the sample should be positioned in the area having maximum electric field strength so as to have maximum interaction with the electric field. This is achieved by loading a thin sample against a thick one in a circular cavity resonator so the thin sample is positioned in a strong field and has more interaction with the field. From the shift of the resonant frequency introduced by the thin sample, its dielectric constant can be calculated. Li [18] further developed this method to suit the measurement of thick-film dielectric in two-layer format. In Li's method, a movable short-circuit is introduced to position the sample at a location away from the end of the cavity so that the dielectric film can always be loaded in the area of maximum electric field. This new positioning technique maximised the shift of resonant frequency caused by the dielectric film and consequently increased the accuracy of the measurement. Cavity perturbation theory is employed to calculate the dielectric constant and loss tangent from the measured resonant frequencies and Q-factors of the reference cavity which is loaded with just the Alumina substrate, and of the same cavity when loaded with the two-layer specimen.

However, there are some drawbacks in the existing techniques. In practice it is difficult to position the sample at exactly the same place for each measurement, which can lead to non-repeatability in measurement data and large errors in the measured values. In addition, the samples require precise machining, and the cavity needs to be dismantled and reassembled each time a new sample is tested, which makes the measurement time-consuming. A new technique needs to be developed to

solve this problem so as to provide a more efficient measurement technique, whilst retaining high measurement accuracy.

1.3 Multilayer Microwave Structures

Although multilayer circuit structures have been widely used for digital and low frequency systems, RF and microwave circuits are usually fabricated in single-layer configurations. However, there has been considerable research interest in multilayer circuits in recent years, as the use of multilayer circuit configurations make microwave circuits more compact and the design more flexible. An example of a conventional single layer microstrip structure and the corresponding multilayer structure is shown in Figure 1.6. In the conventional single layer structure, the conductor patterns are fabricated on the same layer over a common ground plane. With a multilayer technique one can employ several layers of metals sandwiched by

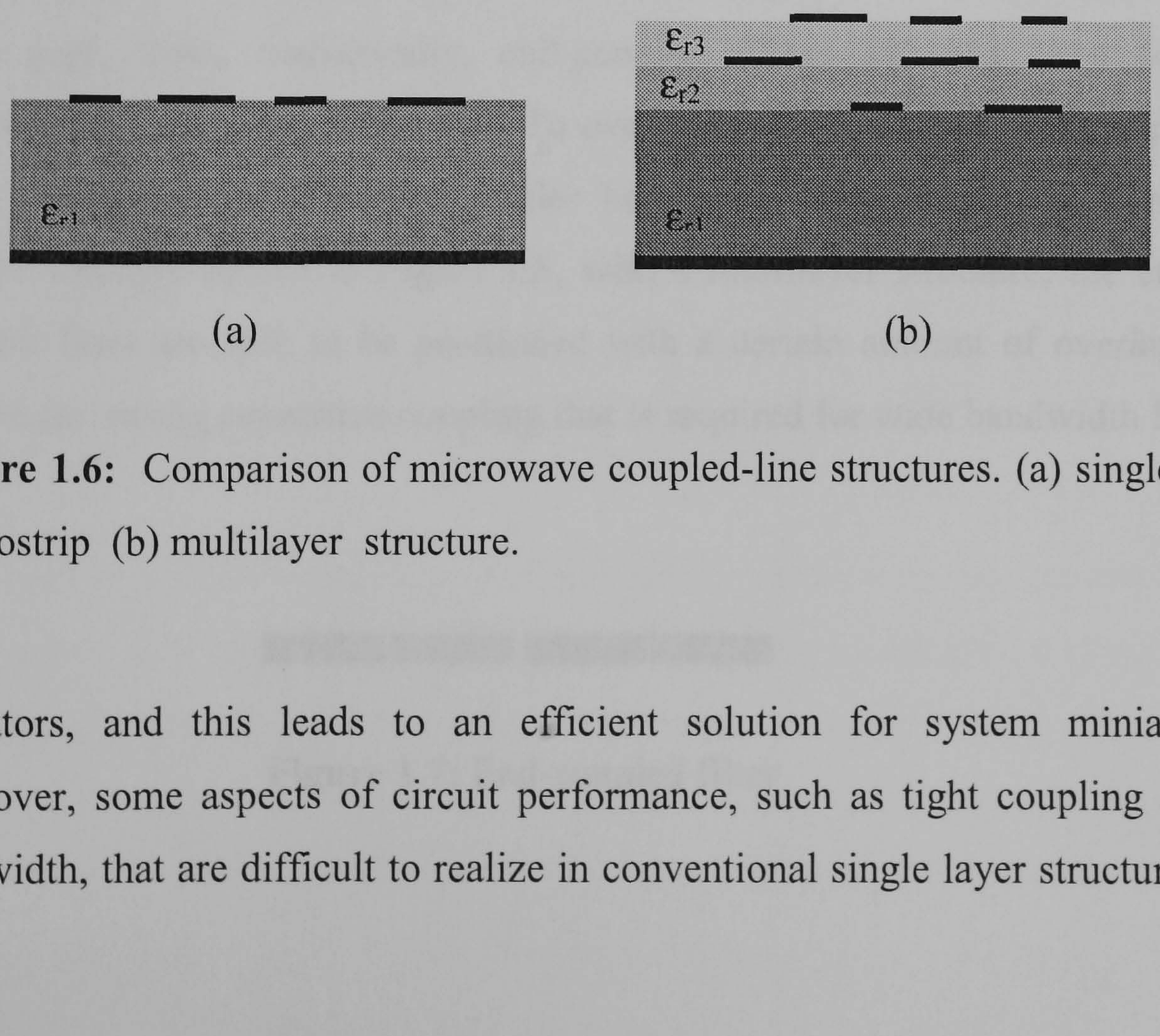

Figure 1.6: Comparison of microwave coupled-line structures. (a) single-layer microstrip (b) multilayer structure.

insulators, and this leads to an efficient solution for system miniaturization. Moreover, some aspects of circuit performance, such as tight coupling and broad bandwidth, that are difficult to realize in conventional single layer structures, can be

easily obtained by a multilayer arrangement. The strong coupling is obtained by overlapping multilayer coupled-lines, with less stringent geometrical requirements.

Multilayer technologies also provide another degree of freedom in the design of compact microwave components. This approach also offers flexibility in the design of circuits and subsystems, with the inherent advantages of high packing density and improved circuit performance.

Multilayer structures have been found useful in the design of filters and couplers, as well as DC blocks, baluns and antennas.

1.3.1 Multilayer End-Coupled Bandpass Filters

End-coupled bandpass filters (Figure 1.7) consist of transmission-line resonators that are approximately a half-wavelength long at the midband frequency. The resonators are coupled by means of the gap capacitance between the ends of adjacent resonator sections. The design of single layer end-coupled bandpass filters is well documented in the literature [28-30]. The structure of this kind of filter is simple and can be easily implemented. However, the bandwidth is restricted due to the requirement for very small gaps. Thus, traditionally, end-coupled filters are only used for narrow bandwidth applications (about 5%). To overcome this limitation, end-coupled filters have been explored to achieve wider bandwidth using multilayer configuration (Figure 1.8). As shown in Figure 1.8, with a multilayer structure, the ends of the adjacent lines are able to be positioned with a certain amount of overlap so as to achieve the strong capacitive coupling that is required for wide bandwidth filter.

Figure 1.7: End-coupled filter

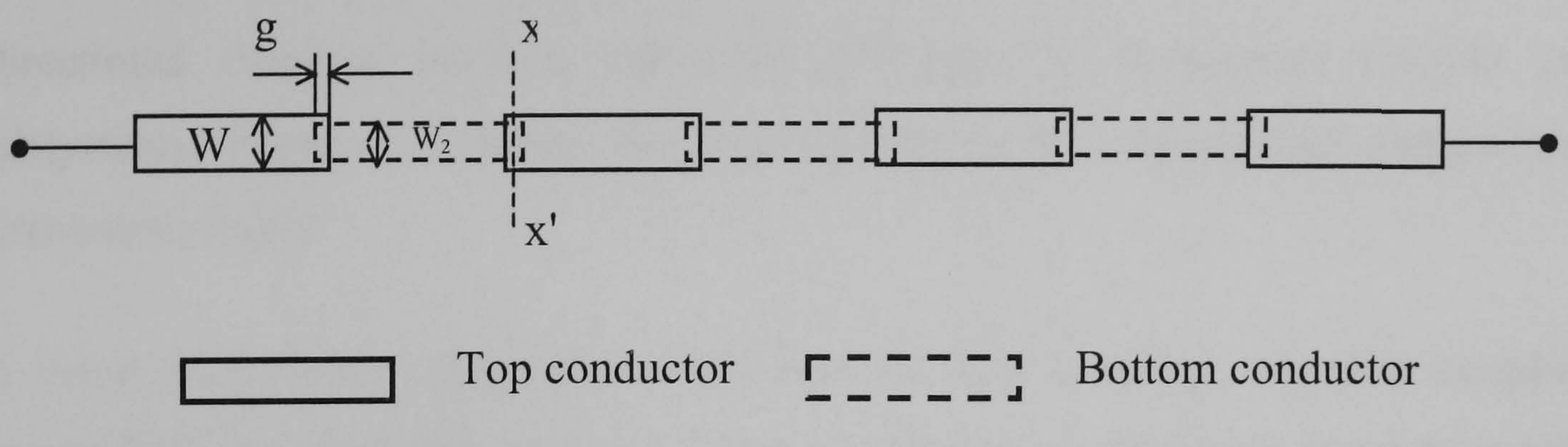

Figure 1.8: The layout of a multilayer end-coupled bandpass filter

Schwab and Menzel[31] proposed a two-layer end-coupled bandpass filter using suspended striplines. They reported a 10GHz filter with 400 MHz bandwidth and a measured passband insertion loss of 0.8dB.

Schwab, Boegelsack, and Menzal [32] also discussed this kind of narrow band filters in CPW configurations.

Cho and Gupta [33] presented a numerical optimisation design procedure for end-coupled bandpass filters in multilayer microstrip configurations. A two-layer end-coupled bandpass filter with 30% bandwidth was achieved at 3GHz, using a full wave electromagnetic simulator for the design. However, both simulated and measured return loss is rather poor (of the order of 10dB, or less). Also, the characteristic impedance of each line resonator is set to a different value and these values can only be obtained through a complicated optimization computation. Although this is a very general design approach, it makes the design unduly complicated and hence impractical for many situations.

The reported results on multilayer end-coupled filters show the potential of these structures to give improved bandwidth. However, the creation of a practical design procedure has not been addressed in the literature.

1.3.2 Multilayer Directional Couplers

Directional couplers perform numerous functions in microwave circuits and subsystems. Figure 1.9 shows the basic geometry of a microstrip coupled-line directional coupler.

In many applications, directional couplers with tight coupling, i.e. with coupling around 3dB, are frequently required. There is considerable difficulty in achieving the tight coupling with single-layer configurations, because of the narrow spacing required between the coupled-lines. For example, the minimum achievable line spacing for a conventional screen-printing thick-film process is about 100 μm, this limits the maximum coupling achievable to about 8dB using a quarter wavelength section. A similar problem occurs in MMICs. Here the conductors must have spacing between each other greater than 8 μm to achieve high yields. Unfortunately, dimensions of half this size are required for the realization of a 3dB coupler on a 75μm thick GaAs substrate.

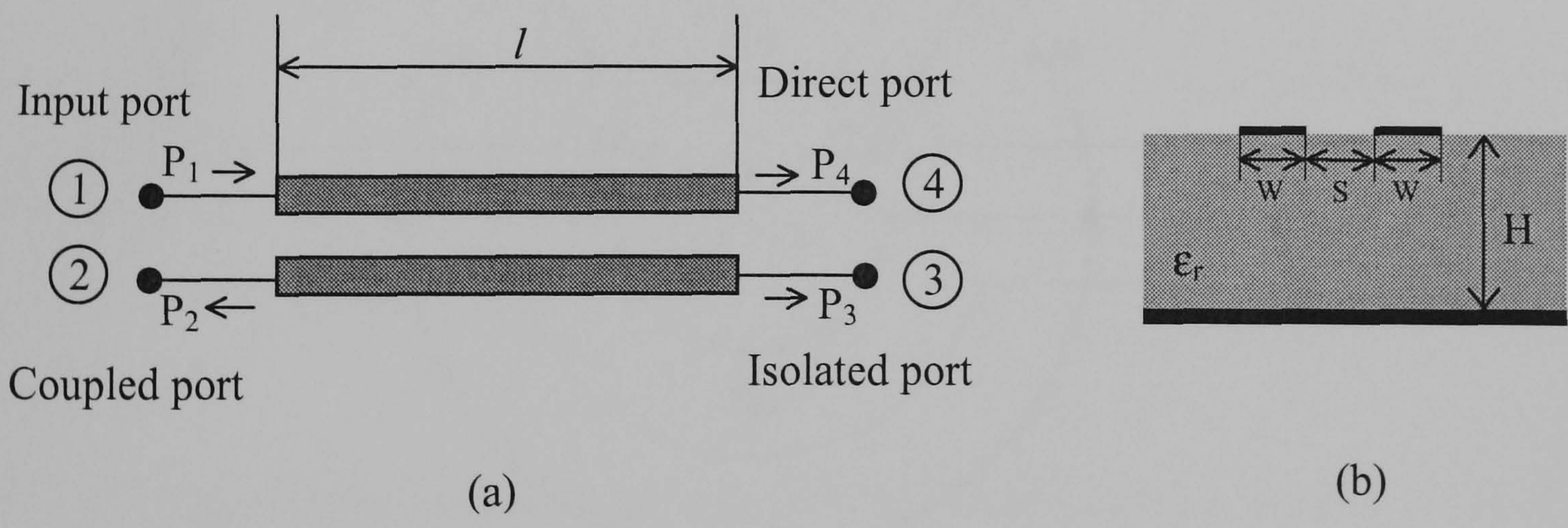

Figure 1.9: Microstrip coupled-line directional coupler.

(a) Schematic, (b) Cross-section view.

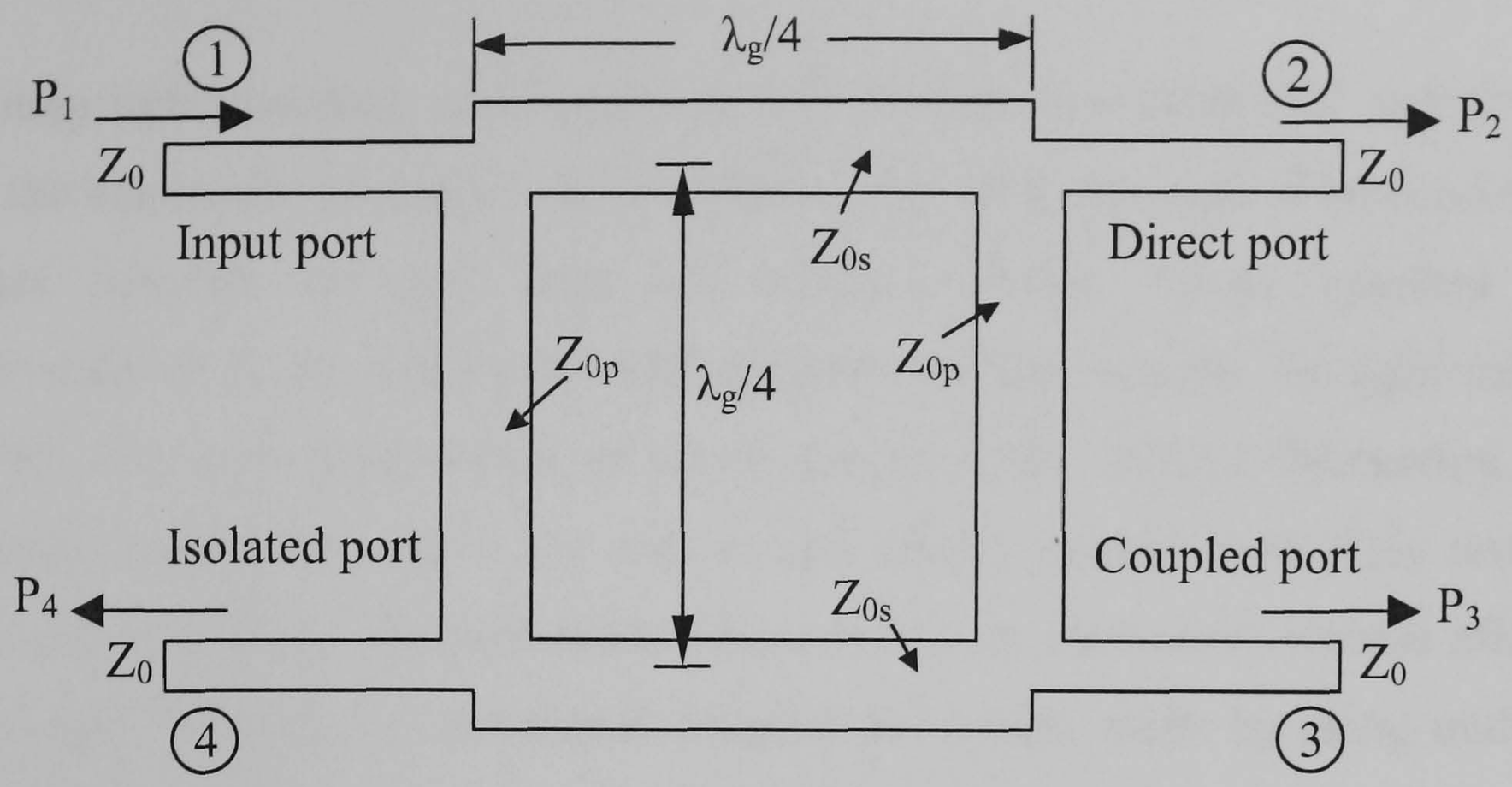

Figure 1.10: Layout of a branch-line coupler in planar circuit configuration

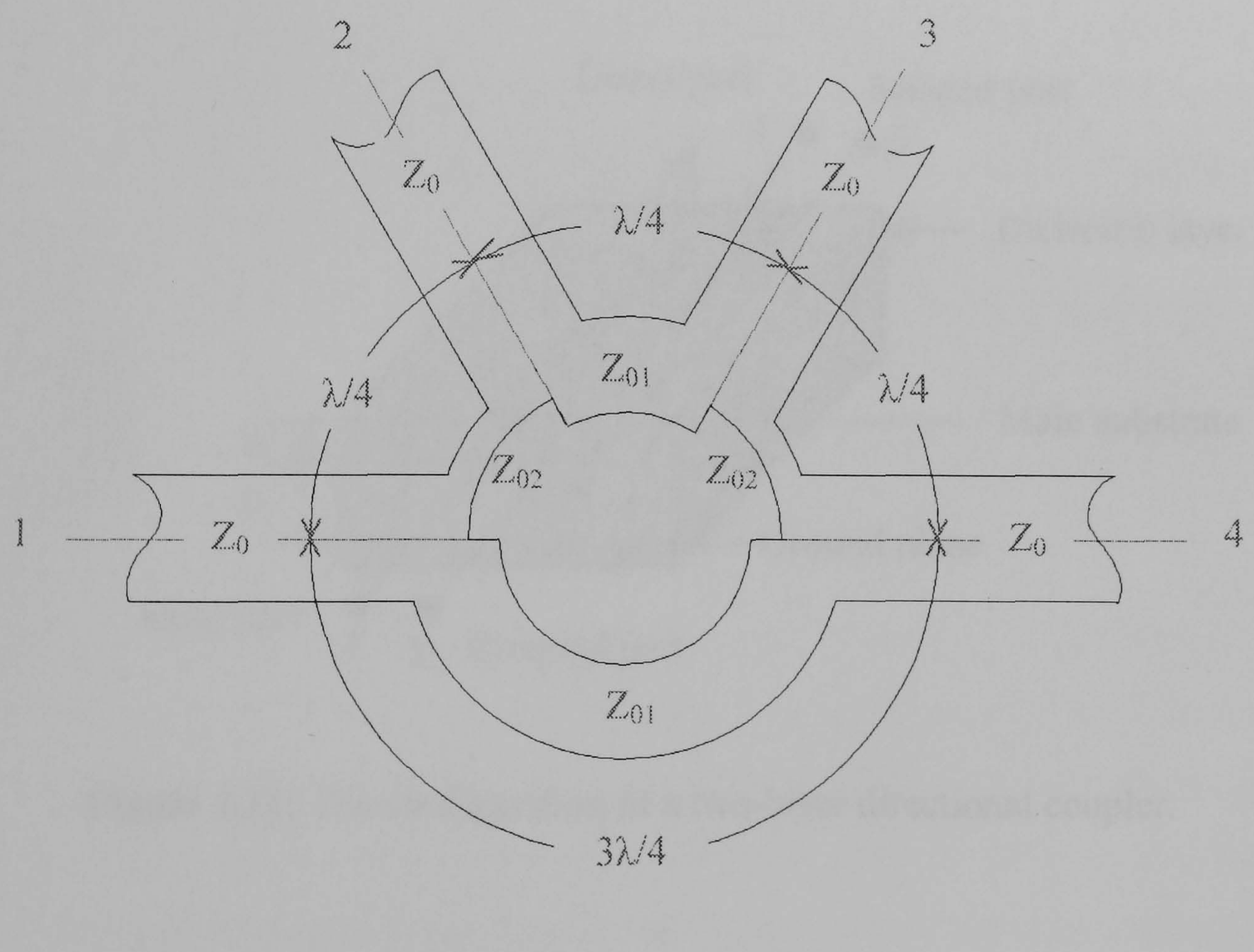

Figure 1.11: Layout of a rat-race coupler in planar circuit configuration

Branch-line (Figure 1.10) and rat-race (Figure 1.11) couplers are suitable for

obtaining tight coupling values such as 3dB but they are inherently narrow band, with the bandwidth normally less than 20% [34]. Also, the size of branch-line and rat-race couplers are too large for compact design. Lange couplers using multiconductor in an interdigital configuration are also suitable for tight coupling [35-38]. The main disadvantage of Lange coupler is the difficult fabrication of the necessary bond wires across the narrow and closely spaced lines. This results in increased sensitivity to dimensional tolerances. As an alternative, various efforts to obtain tight coupling for directional couplers have been made by using multilayer configurations [39-47]. The general configuration of a multilayer directional coupler is shown in Figure 1.12. The two conductors are positioned in different layers with a certain amount of overlap.

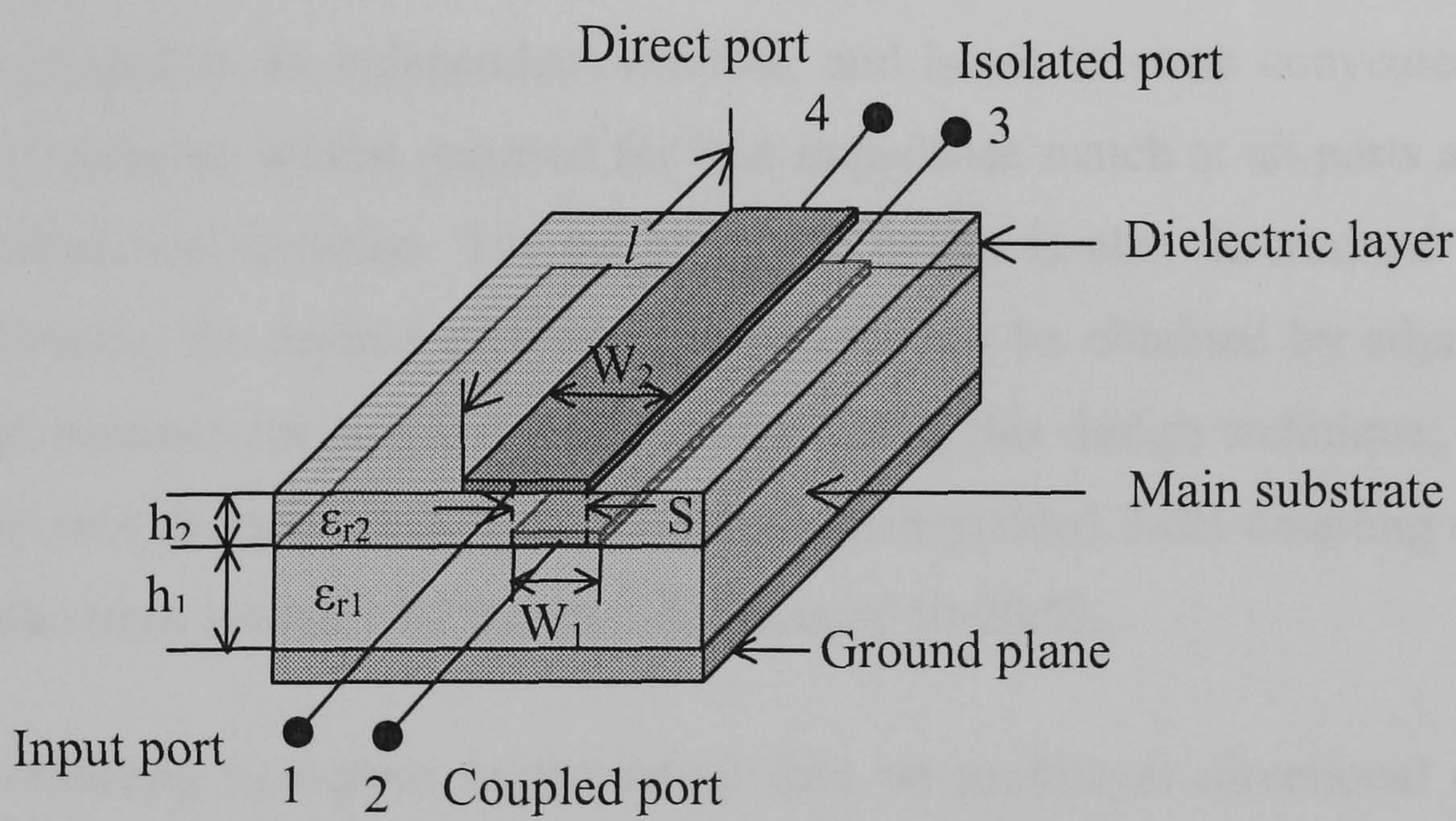

Figure 1.12: The configuration of a two-layer directional coupler.

The potential use of multilayer microstrip structures was first recognised by Marczewski and Niemyjski [39].

Robertson and Aghvami [40] reported the first practical multilayer monolithic 3dB

coupler operating over 2 to 10 GHz. The measured isolation was 12dB.

Willems and Bahl [43] presented a highly manufacturable coupled-line structure for MMIC's that used embedded microstrip to achieve tight coupling. Three-dimensional electromagnetic simulation, using Sonnet in this instance, was used to analyze the multilayer structure. This 3dB coupler had a maximum amplitude variation of ±1.5dB between the coupled and direct ports over a 16 GHz bandwidth. The measured return loss at all ports was greater than 13dB from 0.5 to 24GHz. The phase difference between the coupled ports was 93±9°, and the isolation better than 10dB across the 0.5-20GHz frequency range.

Prouty and Schwarz [44] investigated the performance of a bilevel microstrip structure in which two strips are positioned to give broadside coupling, with one strip directly above the other. In their design, the separation between the two conductor layers is treated as an independent variable, and is set to some convenient value. Then the conductor widths required for best impedance match at all ports are found through numerical iteration. The coupling coefficient is also determined by these widths. Finally, the desired coupling coefficient may be obtained by adjusting the separation between the two conductor layers. Using this design technique, a bilevel microstrip was designed and built on GaAs which yielded 3-dB coupling over 300 MHz, with return loss of 10-25dB and isolation of 10-20dB.

Besides reporting numerous experimental data on multilayer directional couplers, Tsai and Gupta [48] derived a network model for asymmetrical and inhomogeneous coupled-lines based on normal-mode parameters. Given the specifications of the directional coupler including the port impedances and coupling factor, the desired normal-mode parameters are determined through numerical optimization. However the problem of finding actual physical dimensions to yield these normal-mode parameters was not addressed.

Sachse[49] derived the conditions for asymmetric directional couplers with perfect

match and isolation based on coupled-mode parameters. It was shown that the asymmetric coupled two-line structures terminated in a set of impedances which are equal to the characteristic impedances of the individual, uncoupled lines can provide an ideal, backward-coupling directional coupler. In this case the coupler is perfectly matched, with infinite isolation between the uncoupled ports at all frequencies. However, this does require that the inductive and capacitive coupling coefficients of the coupled-lines are equal.

Sachse and Sawicki [50] further investigated the properties of multilayer two- and three-strip asymmetric coupled-lines and pointed out that if the dielectric constant and thickness of each dielectric layer can be chosen properly, it is possible to obtain a set of design parameters such that the inductive and capacitive coupling coefficients are equal, and that the directional coupler can be ideally matched and isolated. Couplers, centred at 3GHz, with 3dB coupling have been designed in microstrip hybrid technology and the measured results show good isolation performance - better than 25dB in a one-octave bandwidth.

Many efforts to improve the performance of directional couplers using multilayer structures have been reported in the literature. It has been shown that multilayer directional couplers have the potential to achieve tight coupling and wide bandwidth. However, multilayer structures are complicated and there are no closed-form design expressions available. Design is usually carried out using EM simulation and involves iterative numerical optimization of the S-parameters for good match and good isolation between the direct and the coupled ports. A good initial design is crucial for efficient design and this has not so far been addressed in the literature.

1.4 Conclusions

The reported work show very promising possibilities to achieve higher performance microwave circuits by using multilayer structures whilst the circuit size remains compact. However, there is a shortage of efficient and feasible systematic design

methods for multilayer microstrip structures. The published literature on multilayer thick-film microwave structures is particularly sparse.

1.5 References

[1] Misra, D. K., 'Permittivity measurement,' *The measurement, Instrumentation, and Sensors handbook*, CRC Press/IEEE Press, 1999.

[2] Dudeck, K. E., 'Dielectric material measurement of thin samples at millimeter wavelengths,' *IEEE T-IM* vol.41, No.5, pp723-725, 1992

[3] Horner, F., Taylor, T. A., Dunsmuir, R., Lamb, J. and Jackson, W., 'Resonance methods of dielectric measurement at centimetre wavelengths,' *J. IEE*, Vol. 93, Pt. III, pp. 53-68, 1946.

[4] Rzepecka, M. A. and Hamid, M. A. K., 'Automatic digital method for measuring the permittivity of thin dielectric films,' *IEEE Trans. Microwave Theory Tech.* Vol. 20 , No.1, pp30-37, Jan. 1972.

[5] Parkash, A., Vaid, J. K. and Mansingh, A., 'Measurement of Dielectric Parameters at Microwave Frequencies by Cavity Perturbation Technique,' *IEEE Trans. microwave Theory Tech.* Vol.27, No.9, pp.791-795, Sept. 1979.

[6] Martinelli, M., Rolla, P. A. and Tombari, E., 'A method for dielectric loss measurements by a microwave cavity in fixed resonance condition,' *IEEE Trans. microwave Theory Tech.* Vol.33, No.9, pp.779-783, Sept. 1985.

[7] Ni, E. and Stunper, U., 'Permittivity measurements using a frequency-tuned microwave TE01 Cavity resonator,' *IEE Proceedings*, Vol. 132, Pt. H, No.1, pp. 27-32, Feb. 1985.

[8] Vanzura, E. J. and Kissick, W. A., 'Advances in NIST permittivty measurement

sapability using a mode-filtered cylindrical cavity,' *IEEE MTT-S International Microwave Symposium Digest,* Vol. III, Part EE, pp. 901-904, 1989.

[9] Janezic, M. D. and Grosvenor, J. H., 'Improved techniques for measuring permittivity of thin dielectrics with a cylindrical resonant cavity,' *1991 IEEE Instrumentation and measurement technology conference,* pp580-584, 1991.

[10] Estin, A. J., and Janezic, M. D., 'Improvement in dielectric measurements with a resonant cavity,' *1991 IEEE Instrumentation and measurement technology conference,* pp573-579, 1991.

[11] Molla, J., Ibarra, A., Margineda, J., Zamarro, J. M. and Hernandez, A., 'Dielectric property measurement system at cryogenic temperature and microwave frequencies,' *IEEE Trans. Instrumentation Meas.* Vol. 42, No. 4, pp.817-821, Aug. 1993.

[12] Kajfez D., and Gundavajhala, A., 'Measurement of material properties with a tunable resonant cavity,' *Electronics letters*, vol.29, No.22 pp.1936-1937, Oct. 1993.

[13] Pohl, V., Fricke, D. and Muhlbauer, A., 'Correction procedures for the measurement of permittivities with cavity perturbation method,' *Journal of Microwave power and electromagnetic energy,* Vol. 30 No1, pp10-26, 1995.

[14] Meng, B., Booske, J. and Cooper, R., 'Extended cavity perturbation technique to determine the complex permittivity of dielectric materials,' *IEEE Trans. Microwave Theory Tech.* Vol. 43 , No.11, pp2633-2636, Nov. 1995.

[15] Gallone, G., Lucardesi, P., Martinelli, M. and Rolla, P. A., 'A fast and precise method for the measurement of dielectric permittivity at microwave frequencies,' *Journal of Microwave Power and Electromagnetic Energy*, Vol.31. No.3, pp.158-164, 1996.

[16] Kraszewski, A. W. and Nelson, S. O., 'Resonant cavity perturbation ---some new applications of an old measuring technique,' *Journal of Microwave Power and Electromagnetic Energy,* Vol.31, No.3 , pp178-187, 1996.

[17] Thomas, R. and Dube, D. C., 'Extended techniques for complex permittivity measurement of dielectric films in the microwave region,' *Electroniics letters*, Vol. 33, No.3, pp218-220, Jan. 1997.

[18] Li, D., Free, C. E., Barnwell, P. G. and Pitt, K. E. G., 'Perturbation method for dielectric constant measurement of thick-film dielectric materials,' *Electronics Letters*, Vol. 34, No.21, pp. 2042-2044, 1998.

[19] Kobayashi, Y. and Shimizu, T., 'Millimeter wave measurements of temperature dependence of complex permittivity of dielectric plates by a cavity resonance method,' *IEEE MTT-S Digest Int. Microwave Symp. Dig.,* pp1885-1888, 1999.

[20] Noskov, Y. N., 'Method for measuring properties of high relative dielectric constant materials in a cutoff waveguide cavity,' *IEEE Trans. Microwave Theory Tech.*, Vol. 48, No. 3, pp. 329-333, March, 2000.

[21] Pournaropoulos, C. L. and Misra, D. K., 'The coaxial aperture electromagnetic sensor and its application in material characterization,' *Measurement Science and Technology* (U.K.), Vol. 8, Issue 11, November 1997.

[22] Tantot, O., Chatard-Moulin, M. and Guillon, P., 'Dielectric measurement of multi-layered medium using an open-ended waveguide,' *Microwave processing of materials V Materials research society symposium proceeding,* Vol. 430, p245-251, 1996.

[23] Jones, R. G., 'Precise dielectric measurements at 35 GHz using an open microwave resonator,' *Proc. IEE,* Vol. 123, No.4, pp. 285-290, April 1976.

[24] Afsar, M. N., Li, X. and Chi, H., 'An automated 60GHz open resonator system for precision dielectric measurement,' *IEEE Trans. Microwave Theory Tech.,* Vol. 38, No. 12, pp. 1845-1853, Dec. 1990.

[25] Komiyama, B., Kiyokawa, M. and Matsui, T., 'Open resonator for precision dielectric measurements in the 100 GHz band,' *IEEE Trans. Microwave Theory Tech.,* Vol. 39, No. 10, pp. 1792-1796, Oct. 1991.

[26] Hirvonen, T. M., Vainikainen, P., Lozowski, A. and Raisanen, A. V., 'Measurement of dielectrics at 100 GHz with an open resonator connected to a network analyzer,' *IEEE Trans. Instrum. Meas.,* Vol. 45, No. 4., pp. 780-786, Aug. 1996.

[27] Afsar, M. N., Ding, H. and Tourshan, K., 'A new open-resonator technique at 60 GHz for premittivity and loss-tangent measurement of low-loss materials,' *IEEE MTT-S Digest Int. Microwave Symp. Dig.,* pp. 1755-1758, 1999.

[28] Matthaei, G., Young, L. and Jones, E. M. T., *Microwave Filters, Impedance – Matching Networks, and Coupling Structures*, Artech House, Dedham, MA, 1990.

[29] Nguyen, C. and Chang, K., 'Design and performance of millimeter-wave end-coupled bandpass filters,' *International Journal of Infrared and Millimeter Waves*, Vol. 6, No. 7, pp. 497-509, 1985.

[30] Cunningham, G. J., Blenkinsop, P. A. And Palmer, J. H., 'Microstrip end-coupled filter design at MM-wave frequencies,' *Proc. 19th European Microwave Conf.*, pp. 1210-1213, Sept. 1989.

[31] Schwab, W. and Menzel, W., 'On the design of planar microwave components using multilayer structures,' *IEEE Trans. Microwave Theory Tech.,* Vol. 40 No. 1, pp. 67-71, Jan. 1992.

[32] Schwab, W., Boegelsack, F., and Menzal, W., 'Multilayer suspended stripline and coplanar line filters,' *IEEE Trans. Microwave Theory Tech.,* Vol. 42 No. 7, pp. 1403-1407, July, 1994.

[33] Cho, C. and Gupta, K. C., 'Design of end-coupled band-pass filters in multilayer microstrip configurations,' *1999 IEEE MTT-S Digest Int. Microwave Symp. Dig.,* pp. 711-714, 1999.

[34] Lippmann, B. A., ' Theory of directional couplers,' *M.I.T.Rad. Lab. Rep.*, No. 860, Dec. 28, 1945.

[35] Reed, J., and G. J. Wheeler, ' A method of analysis of symmetrical four-port networks,' *IRE Tran.*, Vol. MTT-4, pp. 246-253, Oct. 1956.

[36] Lange, J., 'Interdigitated stripline quadrate hybrid,' *IEEE Trans. Microwave Theory Tech.,* vol. MTT-17, pp. 1150-1151, Dec. 1969.

[37] Presser, A., 'Interdigitated microstrip coupler design,' *IEEE Trans. Microwave Theory Tech.,* vol. MTT-26, pp. 801-805, Oct. 1978.

[38] Mongia, R., Bahl, I. and Bhartia, P., *RF and Microwave Coupler-Line Circuits*, Artech House, 1999.

[39] Marczewski, W. and Niemyjski, W., 'The overlapped microstrip for MICs and MMICs', *Proceedings of 14th European Microwave Confere*nce, pp. 166-171, 1984.

[40] Robertson, I. D. and Aghvami, A. H., 'Novel coupler For Gallium Arsenide monolithic microwave integrated circuit applications,' *Electronics Letters*, Vol. 24, No.25, pp1577-1578, Dec. 1988.

[41] Pavio, A. M., Kikel, A. and Sutton, S. K., 'Designing multilayer Ics,' *Applied Microwave Mag.*, Vol. 2, No. 4, pp. 75-81, Winter 1990.

[42] Masot, F., Medina, F., and Horno, M., "Accurate Quasi-TEM Analysis of Modified Coupled Suspended Microstriplines and Its Application to Directional Coupler Design," *Microwave Opt. Technol. Lett.,* Vol. 4, No.2, pp.66-72. Jan. 1991.

[43] Willems, D. and Bahl, I., 'An MMIC-compatible tightly coupled line structure using embedded microstrip,' *IEEE Trans. Microwave Theory Tech.,* vol. MTT-41, No. 12, pp. 2303-2310, Dec. 1993.

[44] Prouty, M. D. and Schwarz, S. E., "Hybrid couplers in bilevel microstrip", *IEEE Trans. Microwave Theory Tech.,* Vol. MTT-41, No.11, pp 1939-1944, Nov. 1993.

[45] Mernyei, F., Aoki, I. and Matsuura, H., "A Novel MMIC Coupler-Measured and Simulated Data," *1994 IEEE MTT-S International Microwave Symposium,* pp.229-232, 1994.

[46] Person, C., Coupez, J. P., Toutain, S. and Morvan, M., "Wideband 3 dB/90 coupler in multilayer thick-film technology," *Electronics Letters*, Vol.31, No.10, pp. 812-813, May 1995.

[47] Al-taei, S., Lane, P. and Passiopoulous, G., ' Design of high directivity couplers in multilayer ceramic technologies,' *2001 IEEE MTT-S Digest Int. Microwave Symp. Dig.,* 2001.

[48] Tsai C. and Gupta, K. C., "A Generalized model for coupled lines and its applications to two-layer planar circuits", *IEEE Trans. Microwave Theory Tech.,* Vol. MTT-40, No.12, pp. 2190-2198, Dec. 1992.

[49] Sachse, K., ' The scattering parameters and directional coupler analysis of characteritically terminated asymmetric coupled translission lines in an inhomogeneous medium', *IEEE Trans. Microwave Theory Tech.,* Vol. MTT-38,

No.4, pp.417-425, Apr. 1990.

[50] Sachse, K. and Sawicki, A., 'Quasi-ideal multilayer two- and three-strip directional couplers for monolithic and hybrid MIC's', *IEEE Trans. Microwave Theory Tech.*, vol. MTT-47, No. 9, pp. 1873-1882, Sept. 1999.

Chapter 2

Characterization of Thick-Film Dielectric Materials

2.1 Summary

A novel slit cavity resonator method is developed that enables the dielectric constant and loss tangent of dielectric samples to be measured easily, and with high accuracy. A particular feature of this method is that it can be used to measure thick-film samples that are normally only available in relatively thin layer in a two-layer format. Rigorous electromagnetic analysis of a slit cavity has been performed that

accounts for the radiation effect from the slits. The filling factor for calculating the dielectric constant and loss tangent is obtained through EM analysis. The new technique is particularly attractive for large-scale quality-control purposes, because it enables the characterization of dielectric samples to be made quickly and without the need for specialized measurement personnel. The method has been verified through measurement on several thick-film materials over X-band.

2.2 Introduction

Dielectric constant (ε_r) and loss tangent ($\tan\delta$) are critical parameters in the design of multilayer structures. The available formats of thick-film dielectric specimens make it difficult to employ the conventional characterization techniques used for bulk materials. Firstly, the thick-film dielectric is not self-supported, and is only available in a two-layer format as shown in Figure 2.1. Here, the thick-film dielectric paste is printed onto a supporting Alumina substrate and fired to form the specimen. Secondly, the thickness of the thick-film sample is relatively thin. Normally it is in the range of 30 to 100μm. Measurements have to be carried out on the two-layer specimen and the dielectric parameters of the thin dielectric is extracted from the measured data on the two-layer sample.

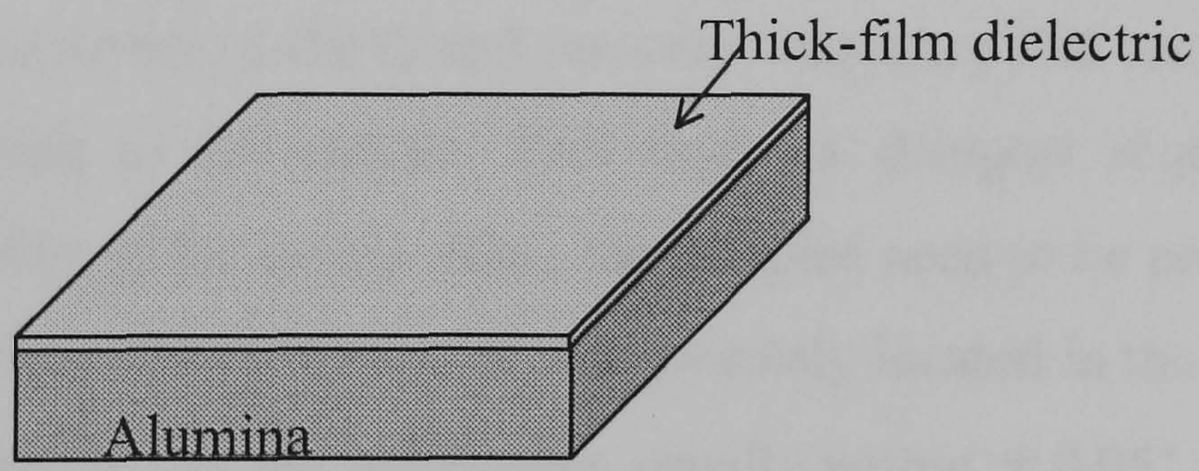

Figure 2.1: Thick-film dielectric sample in a two-layer format

The cavity perturbation technique discussed in chapter 1 is very sensitive and well suited to the measurement of low-loss thin sample [1]. Based on cavity perturbation

theory, Li [2-3] developed a method for measuring the properties of a two-layer thick-film dielectric sample. In Li's method, the cavity loaded with the blank supporting substrate is considered as a reference cavity. After measuring the resonant frequency and Q-factor of the reference cavity, the cavity is dismantled and the supporting substrate coated with the dielectric under test is positioned at the same location as the reference substrate. The shift in the resonant frequency and change of Q-factor are then used to calculate the dielectric constant and loss tangent. A critical requirement of this method is that the blank substrate and the two-layer sample must be located at exactly the same position.

In theory, this method overcomes the difficulty of measuring thin samples. One of the features of Li's method is that the sample being tested is positioned in a high field by means of a movable transverse plate, that has a micrometer drive. However, in reality, there are some drawbacks in using this existing technique.

As the name "perturbation" implies, the insertion of the sample into the reference cavity causes a small change in the properties of the cavity. But the key point here is that the properties of the reference cavity itself must be exactly the same before and after the insertion of the sample. Thus the disassembly and assembly of the cavity, which is needed to insert the sample, must not alter the properties of the cavity. For a high-Q cavity this is very difficult to achieve, as a slight change in the mechanical assembly can cause errors in the Q and resonant frequency that are comparable with the perturbation due to the sample. This imposes stringent requirements on the mechanical assembly of the cavity. Also, the samples need to be precisely formed to the inside dimensions of the waveguide and precisely located in the transverse plane, perpendicular to the axis of the waveguide, usually within $\pm 0.05^\circ$. In the case that the sample is not properly machined or positioned, i.e. it may slant, tilt, or shift from the right position, significant errors will occur in the measured result.

To overcome these problems, a novel slit cavity technique was developed in this study that allows the sample to be loaded through a slit. The slit ensures the sample is in exactly the same position for each measurement, and that it is also in a high field

region. In particular it ensures that, for the measurement of a film on a reference substrate, both the two-layer sample and the reference substrate can be located in exactly the same position and plane. The measurement is thus made accurate and repeatable.

A rigorous electromagnetic analysis on the slit cavity has been carried out which takes into account the radiation effect from the slit. From this analysis a filling factor was obtained for calculating the dielectric constant and loss tangent.

2.3 Two-layer Specimen Measurement Using Cavity Perturbation Theory

The cavity perturbation method is very suitable for the measurement of thin samples. The perturbation approach makes it unnecessary to precisely represent many of the details of the cavity. This leads to high accuracy, particularly when measuring the loss tangent of low-loss specimens and where the volume of the specimen is small.

For the measurement of a two-layer thick-film dielectric specimen, the cavity loaded with the blank alumina substrate is defined as a reference cavity, and this is shown in Figure 2.2(a). The same cavity loaded with the two-layer specimen is defined as the perturbed cavity, and this is shown in Figure 2.2(b). The difference in the resonant frequencies and Q-factors between the two cavities then can be regarded as due only to the dielectric film. This difference is used to calculate the relative permittivity and loss tangent of thick-film dielectric. The equations are:

$$\varepsilon_r = 1 + \frac{2}{\eta}\frac{f_0 - f_1}{f_1}$$

$$\tan\delta = \frac{f_1}{\eta f_1 + 2(f_0 - f_1)}\left(\frac{1}{Q_1} - \frac{1}{Q_0}\right)$$

where f_0 and Q_0 are the resonant frequency and the Q-factor of the reference cavity, respectively. f_1 and Q_1 are the corresponding quantities of perturbed cavity.

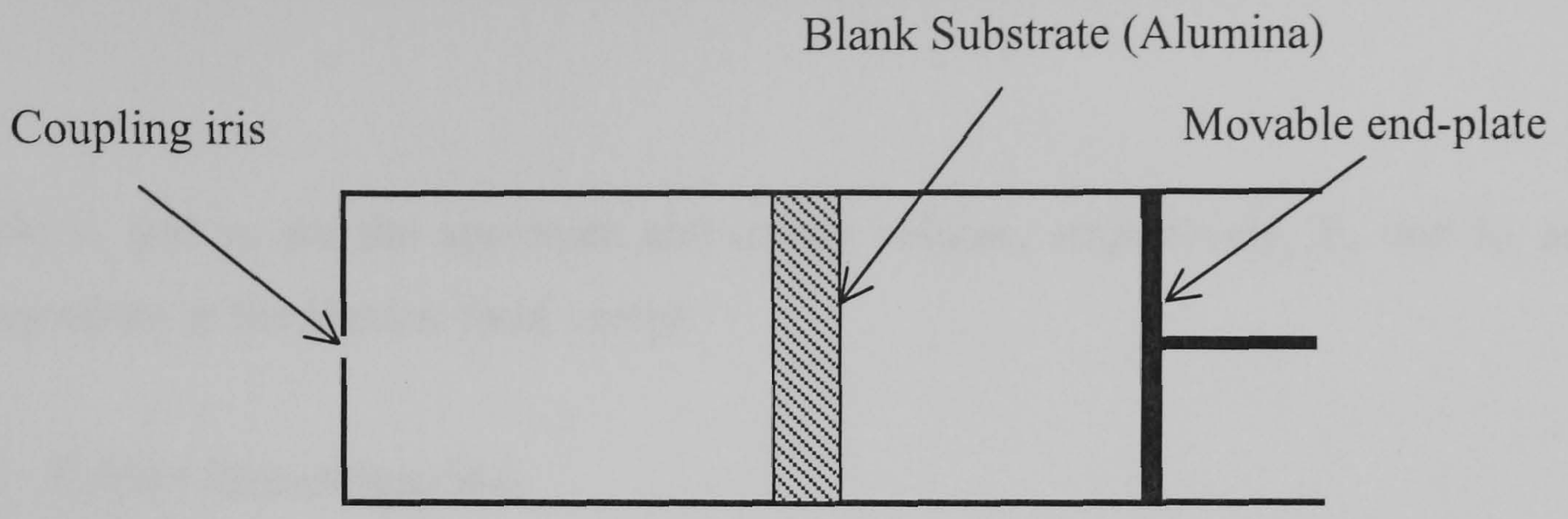

Figure 2.2: Two-layer specimen measurement using cavity perturbation theory. (a) Reference cavity; (b) Perturbed cavity.

η is the filling factor, which is related to the sample geometry and given by:

$$\eta = \frac{\int_{v_s} \vec{E}_1 \cdot \vec{E}_2 \cdot dv}{\int_{v_c} |E_1|^2 \cdot dv}$$

where v_s and v_c are the specimen and cavity volume, respectively. E_1 and E_2 are components of the electric field vector.

where v_s and v_c are the specimen and cavity volume, respectively. E_1 and E_2 are components of the electric field vector.

2.4 Error Investigation

For a perturbation measurement, the need to ensure that properties of the reference cavity remain unchanged after insertion of the specimen has already been discussed. Any differences, either in the properties of the cavity, with and without the specimen, or in the location and properties of the reference substrate, may cause errors in the measured dielectric parameters. Some of the sources of error are as follows:

a) errors in positioning both the two-layer and reference samples

b) error in the length of the cavity

c) error due to differences in the permittivity of the reference substrate and that used in the two-layer test specimen

d) error due to differences in the thickness of the reference substrate and that used in the two-layer test specimen

Table 2.1 shows the error sources along with their contribution to the errors in ε_r and tanδ for a given sample.

It can be seen that the measurement on a two-layer thin sample is very sensitive, and that small errors of the type described above can have a significant effect on the results. This indicates that great care has to be taken to achieve high accuracy.

Table 2.1: Error sources and their contributions towards the errors in dielectric constant and loss tangent for a sample with nominal dielectric constant of 4 and tanδ of 0.007 (Sample thickness: 30 μm)

Variable		Error (±)	Error (±) in ε_r	Error (±) in tanδ
Sample position	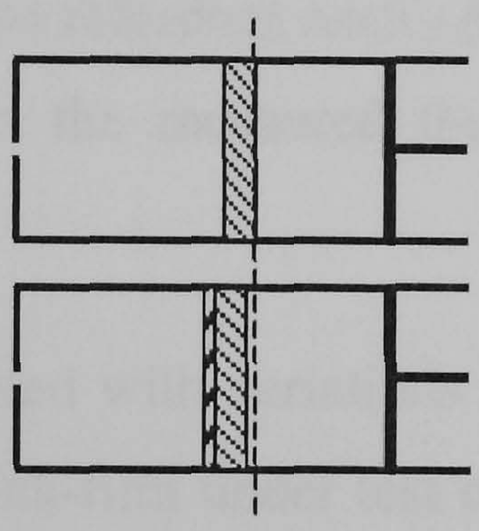	10 μm	0.6	0.0026
ε_r of supporting alumina	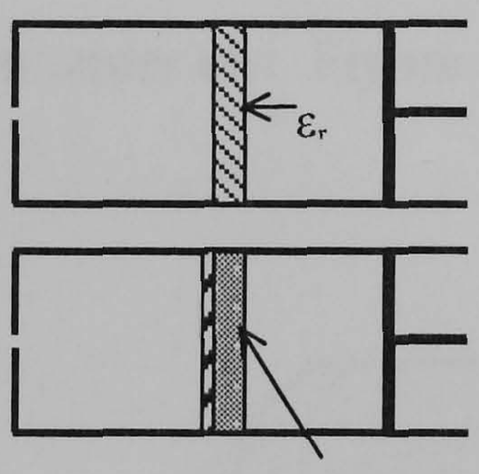	0.05	0.3	0.001
Thickness of supporting alumina	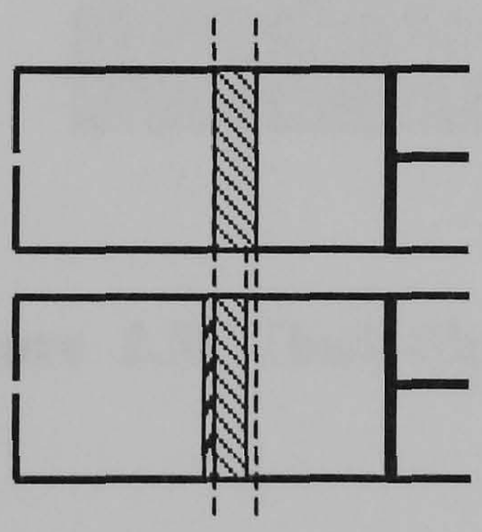	5 μm	0.4	0.001
The length of the cavity	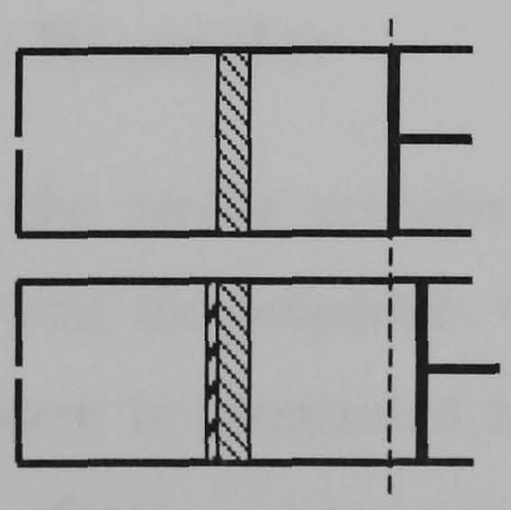	5 μm	0.5	0.0039

2.5 Sample Preparation

From Table 2.1, we can see that, for a certain sample, a difference in thickness of 10μm between the blank substrate used in the reference cavity and that used to support the film will cause an error of 10% in the measured dielectric constant and 15% in the loss tangent. A difference of 0.05 between the dielectric constant of the substrate used in the reference cavity and that used to support the film causes error of 7.5% and 11% in the measured thick-film dielectric constant and loss tangent, respectively.

The errors associated with variations in the properties of the alumina are overcome by printing the thick-film under test on half of an alumina tile, and then cutting the tile to provide a blank reference sample with exactly the same properties as that supporting the film under test. Figure 2.3 shows the prepared sample before it is cut.

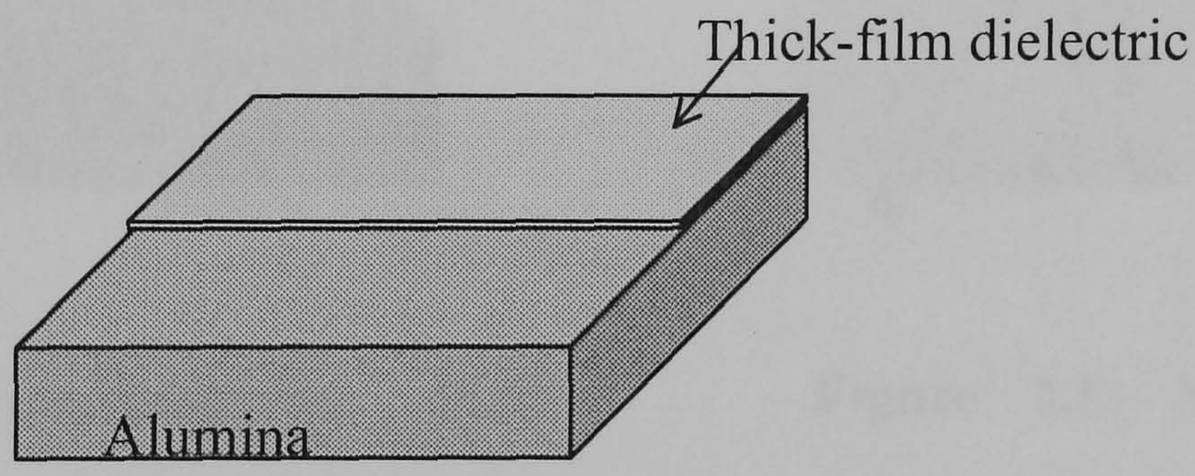

Figure 2.3: Thick-film dielectric sample

2.6 Slit Cavity Resonator

As stated earlier, the cavity perturbation measurement technique can be highly accurate provided that the properties of the cavity can be maintained exactly the same after the system is dismantled and reassembled each time a new sample is tested. Also, the reference sample and two-layer sample need to be positioned exactly at the same location.

All of these problems of the conventional cavity perturbation technique suggest that an opening (slit) in the cavity would be ideal to load and unload the sample from the cavity without disturbing the cavity. Also, this opening may provide good support for the sample and ensure that it is always located at the same position. This will greatly improve the consistency, and accuracy, of the measurement.

Figure 2.4 shows the electromagnetic field distribution of TE_{10n} mode in a rectangular cavity. If we cut a slit in the narrow wall of the cavity, as shown in Figure 2.5, the cavity performance will be essentially unchanged since the slit is parallel to the current flow. Only if a slit is cut in such a way as to interrupt the current flow lines will there be radiation from the slit, and a consequent change in cavity performance.

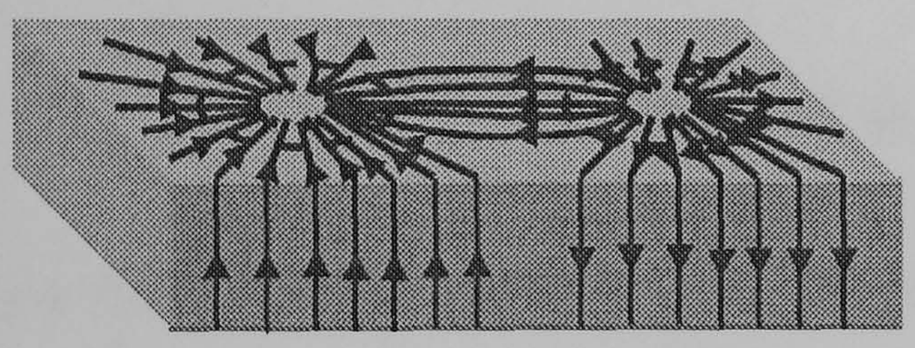

Figure 2.4: Electromagnetic field distribution of TE_{10n} mode in a rectangular cavity

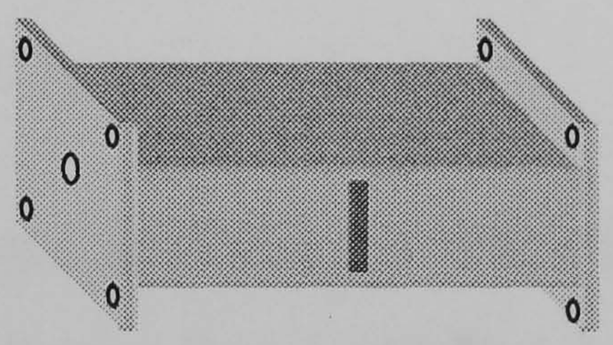

Figure 2.5: Microwave resonant cavity with slit.

With this arrangement shown in Figure 2.5, the measurement on the thick-film dielectric material is simple and quick. The measurement procedure is:

(a) Insert the blank alumina substrate into the slit to form the reference cavity. Note that the substrate must completely fill the waveguide cross-section. Measure the resonant frequency and Q-factor.

(b) Remove the reference sample from the slit and insert the sample deposited with

thick-film into the slit. Again making sure that the sample projects completely through the guide. Measure the resonant frequency and Q–factor.

(c) Proceed to the computation of the complex permittivity.

With this arrangement of slits, there is no need to disassemble the cavity. Any errors associated with cavity loading or poor assembly of the cavity will be exactly the same in both of the measurement states and will therefore cancel out.

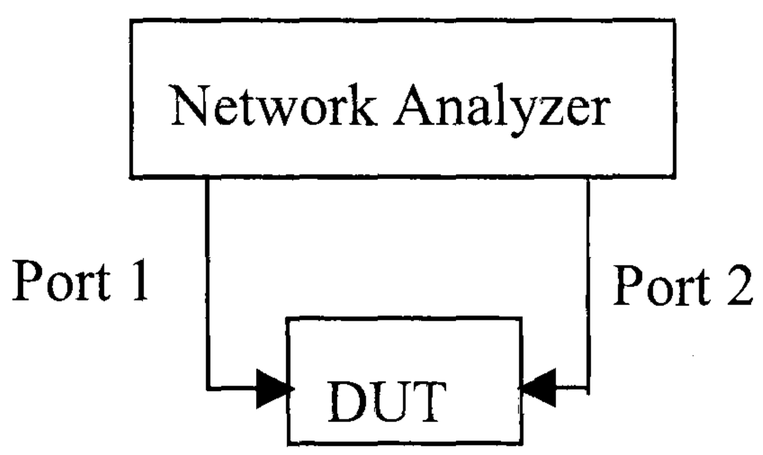

Figure 2.6: Measurement set-up

The measurement set-up is quite simple, and is shown in Figure 2.6. The slit cavity resonator is connected with the network analyzer between Port 1 and Port 2 through waveguide and coaxial transitions. S21 is measured for the cavity with and without the sample to obtain the resonant frequency and Q-factor of the cavity.

2.7 Corrected Filling Factor

To examine the radiation from the slit, electromagnetic analysis was performed on the slit cavity using full wave EM simulation (HFSS^{TM}).

Figure 2.7 shows a slit cavity simulated in HFSS layout window. The outer box is used for simulation of the radiation from the slit. The field pattern at the plane of iris, an arbitrary plane inside the cavity and the plane of the sample are shown in Figures 2.8, 2.9 and 2.10, respectively. Figure 2.11 shows the radiation from the slit. It is

seen there is a certain electromagnetic leakage from the slit but it is a relatively small amount as the slit is cut in such a way not to disturb the current flow in the waveguide wall.

The S parameters for both the reference cavity and sample cavity are obtained from the simulation, and this enables the filling factor for the slit cavity to be calculated. This is listed in Table 2.2, along with the filling factor for the closed cavity. It is seen that the performance of the cavity is only slightly changed due to the presence of the slit. The change in the filling factor caused by the slit is only around 1.7%.

Table 2.2: Filling factor

Sample Thickness	Filling factor for closed cavity	Filling factor for slit cavity
30 μm	0.002787	0.002794

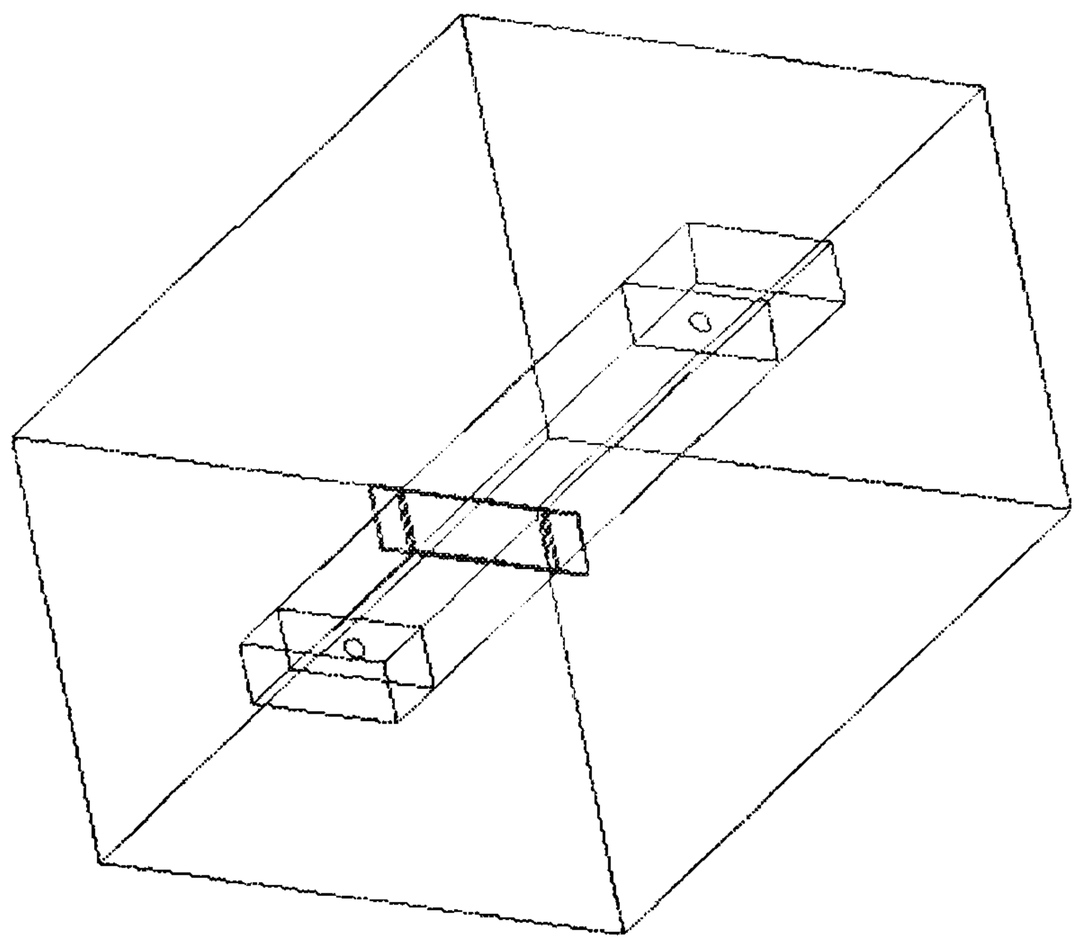

Figure 2.7: Slit cavity with sample loaded. (Outer box is air box for simulation of radiation from the slit)

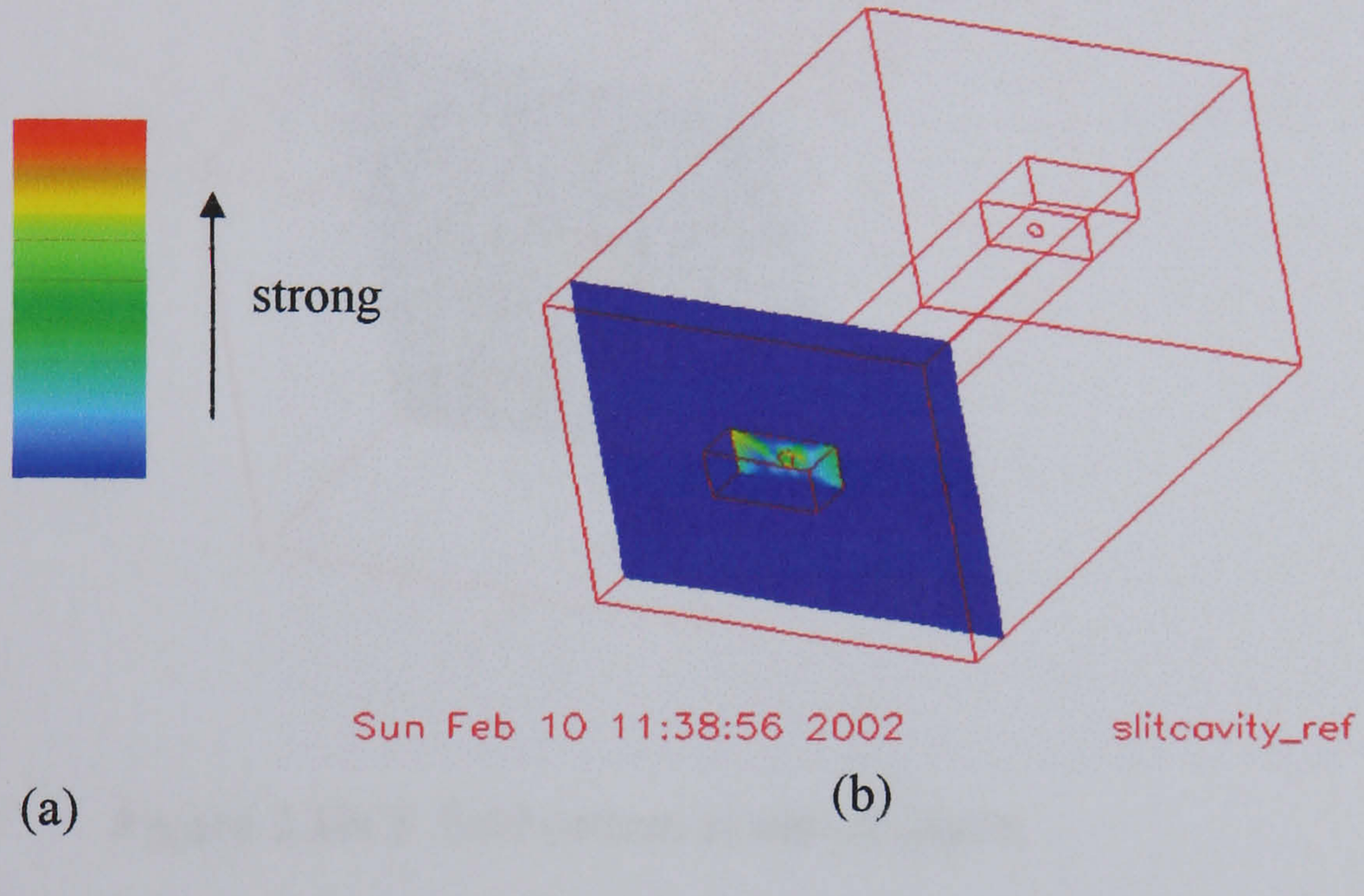

Figure 2.8: (a) Scale; (b) E field at iris plane.

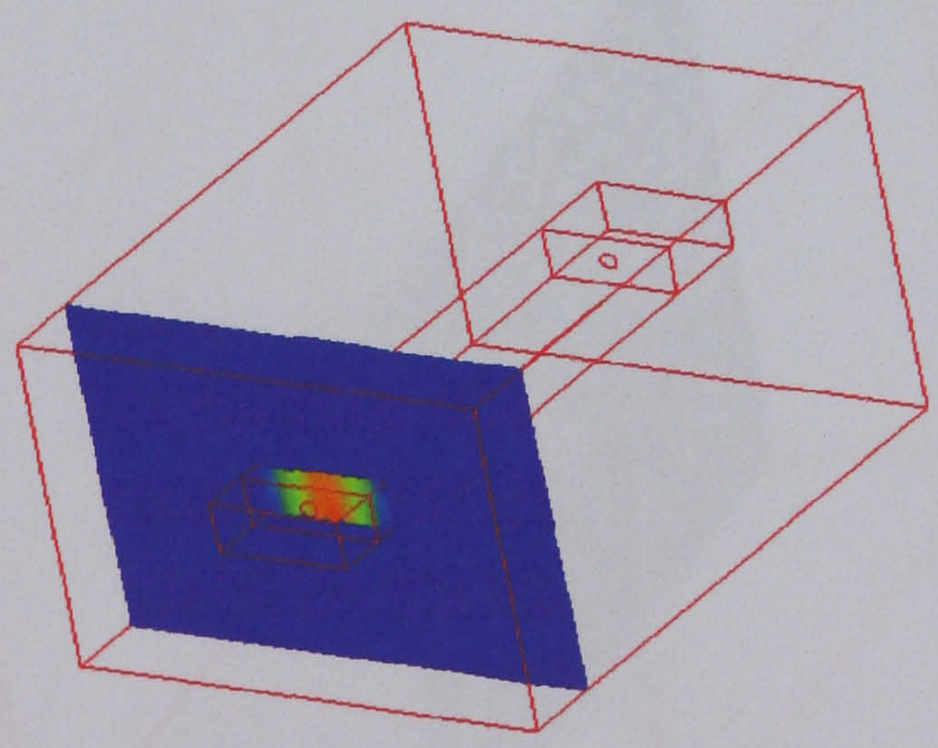

Figure 2.9: E field pattern at an arbitrary plane inside the cavity

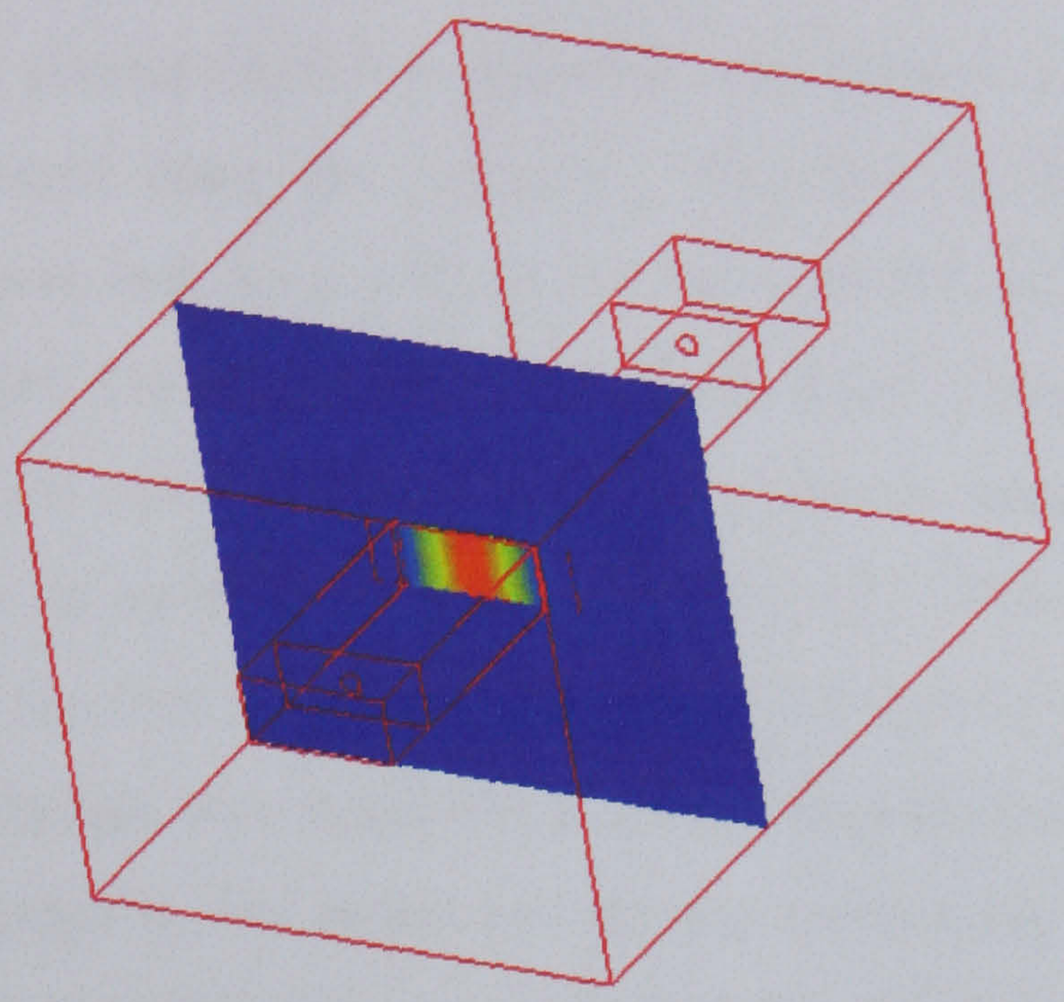

Figure 2.10: E field pattern at sample plane

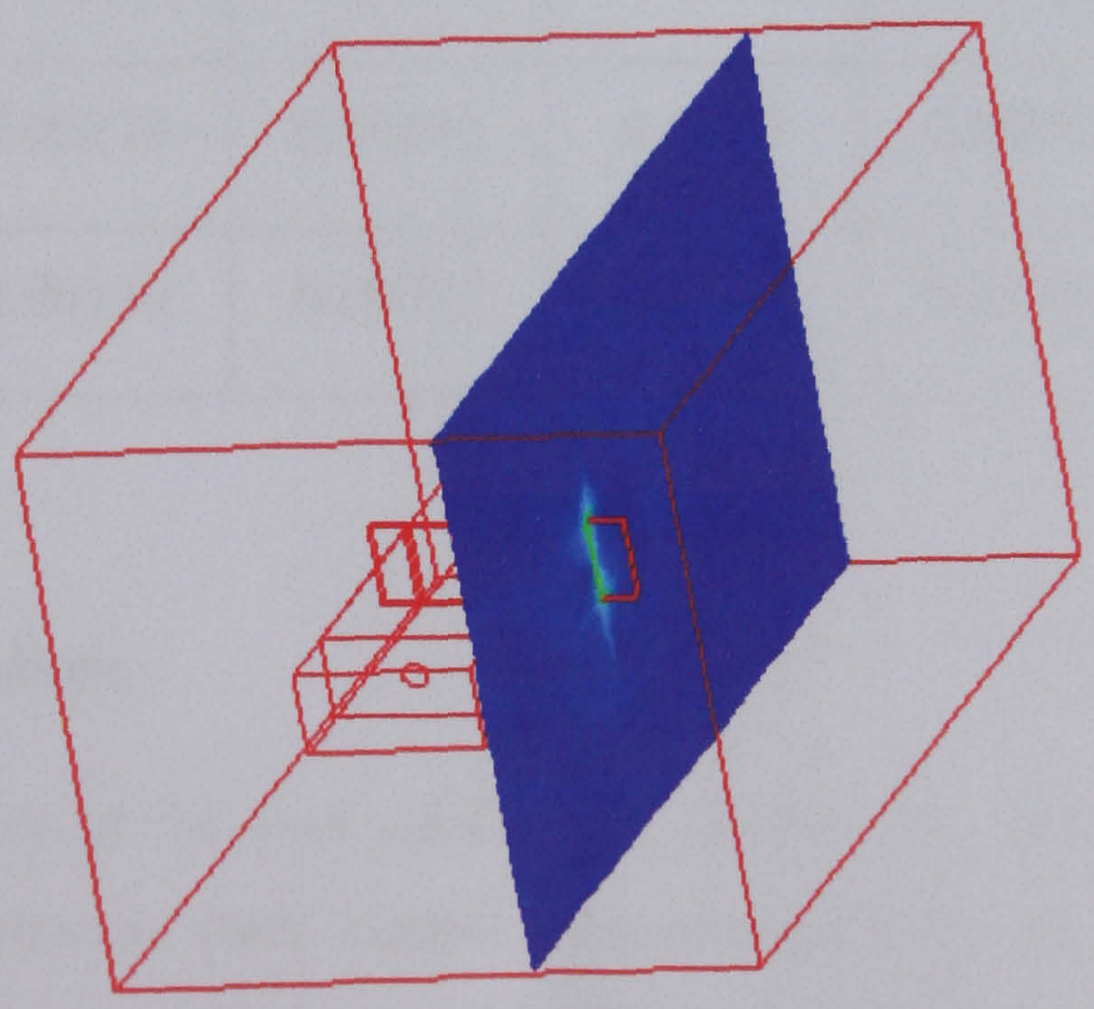

Figure 2.11: E field pattern at the plane of the slit

2.8 Measured Results and Discussion

Measurements on several thick-film materials, identified as A, B and C in Table 2.3, have been performed using the slit cavity technique. In this case the thick-film dielectric under test had been printed onto microwave quality alumina having a thickness of 635μm. The precautions already described in respect of the consistency of the alumina were observed, and the blank reference sample was taken from the same alumina tile on which the dielectric was printed. The thickness of the printed dielectric was of the order of 30μm. The results for the loss tangent are shown in Table 2.3. Each sample was measured four times and the measured results are listed in Columns 1 through 4. The objective here was to examine the repeatability of the measurement. It is seen that very good repeatability has been achieved by using the slit cavity technique.

Table 2.3: Measured loss tangent at 10 GHz

	1	2	3	4	Average
A	0.00725	0.00797	0.00762	0.00814	0.0077±0.0004
B	0.00273	0.00281	0.0027	0.00275	0.0027±0.00006
C	0.00739	0.00777	0.00796	0.00752	0.0076±0.0003

2.9 Conclusions

The key features of the new method are (i) that the cavity does not need to be disassembled between each sample measurement and (ii) that the sample can be located precisely in a high field region. The new slit cavity enables the measurement on thick-film dielectric material in a two-layer format to be characterized accurately and easily. Results that have been obtained show that the simplicity of the new

technique does not compromise the accuracy of the measurement.

2.10 References

[1] Sucher, M. and Fox, J., *Hand book of microwave measurements*, Polytechnic Press of the Polytechnic Institute of Brooklyn, Vol. II, 1963.

[2] Li, D., Free, C. E., Barnwell, P. G. and Pitt, K. E. G., 'Perturbation method for dielectric constant measurement of thick-film dielectric materials,' *Electronics Letters*, Vol. 34, No.21, pp. 2042-2044, 1998.

[3] Li, D., '*Multi-chip module interconnections at microwave frequencies: electromagnetic simulation and material characterisation'*, PhD thesis, Middlesex University, 1999

Chapter 3

Multilayer Microstrip Structures: Analysis and Fabrication

3.1 Summary

Both the methods of analysis and the thick-film fabrication techniques applicable to multilayer microwave structures are discussed in this chapter. Several multilayer thick-film microstrip lines have been designed and characterized, and these provide a

basic database for the design of multilayer microstrip structures. The advantages of using multilayer microstrip lines and their applications are also discussed.

3.2 Introduction

Multilayer configurations have recently received increasing attention because they make design more compact, increase design flexibility, and can reach levels of performance not possible in a planar geometry. In multilayer microstrip structure, there are several layers of metals sandwiched by insulators over a common ground plane. The electromagnetic coupling between conductors in the same or different layer is more complicated than in the conventional single layer structures. The different methods of analysis suitable for multilayer microstrip structures are discussed in this chapter, which also provides a theoretical background for the design and analysis of the various multilayer structures involved in this study.

Thick-film technology is employed in this work for the fabrication of multilayer structure as it is well established for the low-cost manufacture of hybrid microcircuits. Thick-film allows designers to combine microwave and digital functions on common high thermal conductivity Alumina substrates and to incorporate capacitors and resistors into the main microwave structures. It has the potential to combine baseband and RF circuitry that enables the mixed signal systems to be realized more cost effectively. Advanced thick-film technology including advanced thick-film material and patterning techniques employed in the fabrication of multilayer microwave structures is discussed.

The performance of several multilayer thick-film microstrip line structures is studied using full wave analysis. Some experimental results on the multilayer line loss and relative permittivity of multilayer substrate are also presented.

3.3 Configurations of Multilayer Microstrip Lines

Multilayer microstrip lines are the basic building blocks for multilayer microwave structures. These structures can be used as interconnections, or for impedance matching in mixers and amplifiers, and as resonant elements in filters. The configurations of the multilayer microstrip lines studied are shown in Figure 3.1. Figure 3.1(a) shows a conductor track on top of a two-layer dielectric. Figure 3.1(b) and (c) shows conductor track buried between two dielectrics. The dielectric constant and thickness of the Alumina base are ε_{r1} and h_1. This base acts as the main supporting substrate for the multilayer structure. The dielectric constants and thickness of the printed thick-film dielectric layers are ε_{r2}, ε_{r3}, h_2 and h_3.

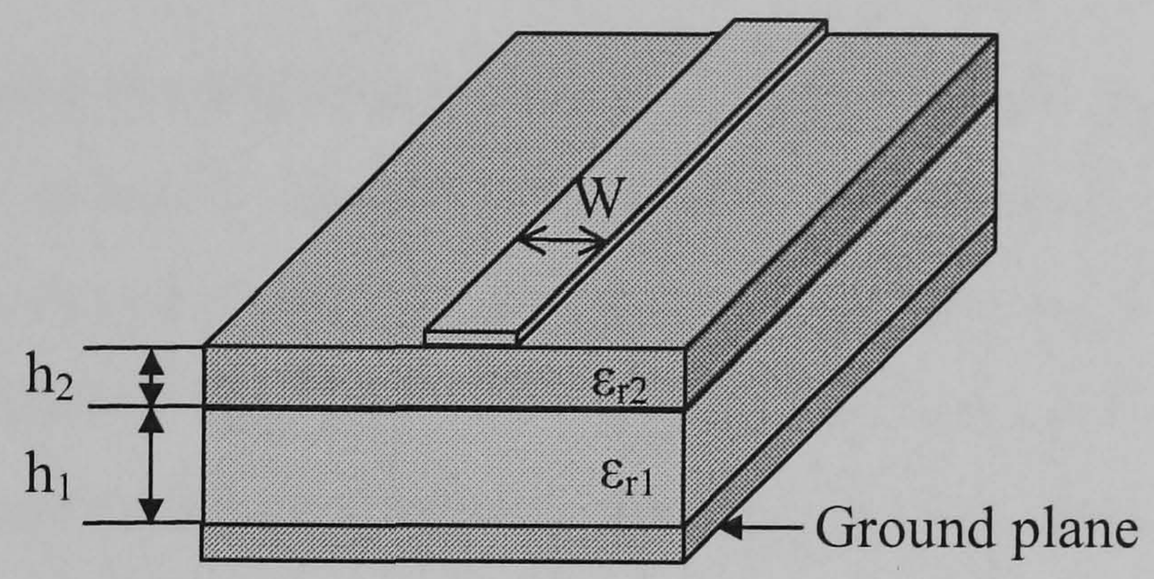

(a)

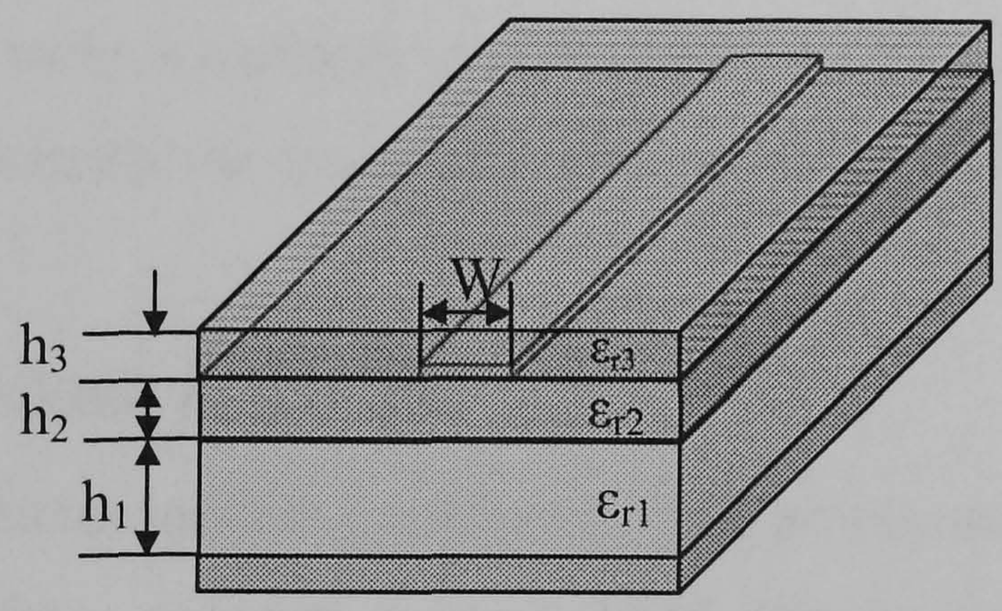

(b)

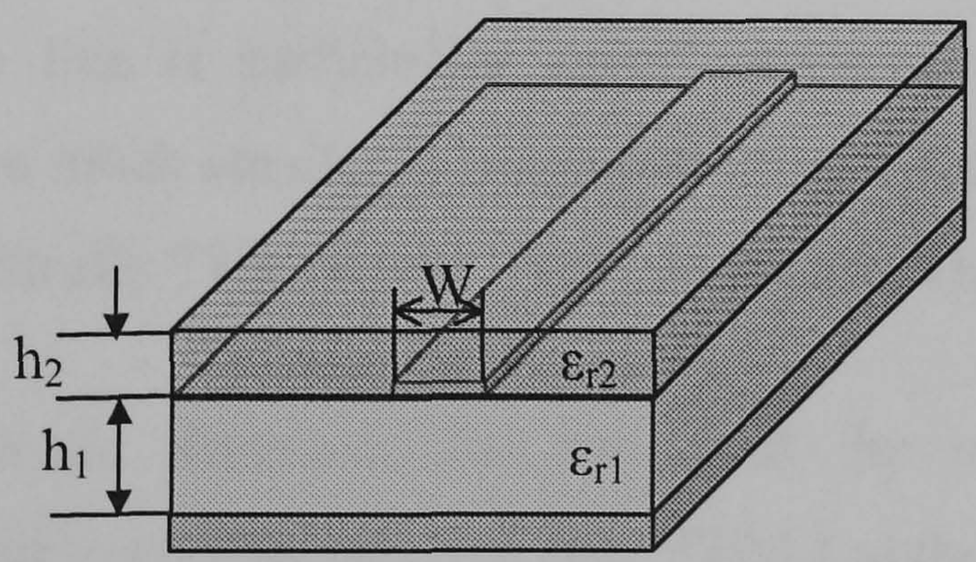

(c)

Figure 3.1: Multilayer microstrip line configurations

3.4 Analytical Methods and CAD Tools

The substrate used in multilayer microstrip structures may contain several layers of dielectric with different dielectric constants and thicknesses. Thus, multilayer microstrip lines exhibit special performance. However, in contrast to conventional single layer microstrip line, where the design techniques are well documented in the literature, there are no design equations available for multilayer structures to date.

The analysis of multilayer microstrip lines is aimed at determining the characteristic impedance and propagation constant, comprising phase velocity and attenuation constant. The various methods of microstrip analysis may be divided into two main approach [2]: namely the quasi-static approach and full wave analysis.

3.4.1 Quasi-Static Approach

Any two-conductor lossless transmission line arrangement placed in a homogeneous dielectric medium supports a pure TEM (transverse electromagnetic) mode of propagation. If the two-conductor transmission line has an inhomogeneous dielectric, the dominant mode is of a hybrid nature, i.e., it has both transverse and axial components of the electric and magnetic fields. However, if the maximum cross-section of the line is sufficiently small compared to the wavelength, the axial components are much smaller in magnitude than the transverse components and the waves are practically TEM waves. These waves are referred to as quasi-TEM waves.

In the quasi-static approach, the nature of the mode of propagation in the transmission line is considered to be pure TEM and the microstrip characteristics are calculated from the electrostatic capacitance of the structure. It is found that this analysis is adequate for designing circuits at low microwave frequencies where the strip width and the substrate thickness are much smaller than the wavelength in the dielectric material.

3.4.1.1 Quasi-Static Transmission Line Analysis Program – LINPAR

LINPAR (Matrix Parameters for Multiconductor Transmission Lines) is a computer program for the numerical evaluation of the quasi-static matrices representing multiconductor transmission lines embedded in multilayer dielectrics [3].

The technique used in the program is based on an electrostatic analysis. In this analysis, the primary (quasi-static) matrix parameters are first evaluated. These parameters are the matrix [L] of per-unit-length inductances, the matrix [C] of per-unit-length capacitances, the matrix [R] of per-unit-length resistances, and the matrix [G] of per-unit-length conductance. From these parameters, the secondary transmission line parameters namely the characteristic impedance, $Z_{0,}$ and the phase velocity, $\upsilon_{p,}$ can be obtained. The analysis includes conductor surface losses and dielectric losses. Compared with full wave analysis, quasi-static analysis is simple and quick. The calculated inductance and capacitance per unit length also provide an intuitive understanding of the behavior of multilayer microstrip lines and coupled lines.

3.4.2 Fullwave Analysis

As the microstrip configuration is not capable of supporting a pure TEM mode, small longitudinal components of both the electric and magnetic fields need to be present to satisfy boundary conditions at the dielectric-air interface. These hybrid modes supported by the microstrip cannot be fully described in terms of static capacitances and inductances. Therefore, one has to consider time-varying electric and magnetic fields and solve the wave equation subject to appropriate boundary conditions. Field analysis of the microstrip without invoking any quasi-static approximations is known as full wave analysis. Full wave analysis is carried out by directly solving electromagnetic equations to determine the propagation constant and characteristic impedance rather than the capacitance evaluated in quasi-static analysis.

Full wave analysis takes into account all modes of propagation. This includes both

the TE- and TM-modes that constitute the hybrid mode present in microstrip. Thus full wave analysis is more rigorous, but analytically more complex. An important outcome of the full wave analysis is information about the dispersive nature of the microstrip line. This includes the variation of characteristic impedance, Z_0, and phase velocity (or effective dielectric constant, ε_{reff}) with frequency.

3.4.2.1 Numerical Methods

Electromagnetic (EM) simulation involves the solution of Maxwell's equations with the boundary conditions imposed by the particular RF or microwave structure being considered. Most commercially available EM simulators use numerical methods to obtain the solution. There are a lot of different numerical methods, but generally speaking, they can be categorized as Time-Domain (TD) and Frequency-Domain (FD) EM methods.

All the EM phenomena are governed by Maxwell's equations. Maxwell's Equations are a set of partial differential equations describing the relationships between electric field, magnetic field, and the material properties of the medium. So, by obtaining a solution of Maxwell's equations, we can predict the EM behavior of the DUT (Device Under Test). Maxwell's Equations can be written in the Time-Domain or Frequency-Domain. Correspondingly, there are FD and TD methods to solve FD and TD Maxwell equations.

The difference between FD and TD analyses is mainly in the methodology used in the solution of the FD and TD equations. There are many techniques that can be used. For example, in the frequency-domain, there are the Finite-Element Method (FEM), the Finite-Difference Method (FDM), and the Integral Equation Method (IE). Similarly, in the time-domain, there are the Finite-Difference Time-Domain Method (FD-TD) and the Finite-Element Time-Domain Method (FE-TD). Different methods have very distinctive characteristics and limitations. Ansoft's High Frequency Structure Simulator (HFSS) adopts the Finite Element Method to solve the FD

Maxwell's Equations. Zeland's IE3D adopts the Integral equation Method to solve FD Maxwell's Equations while Remecon's X-FDTD uses the Finite-Difference Time-Domain method to solve the TD Maxwell's Equations. Each of these methods has its own advantages and disadvantages and is suitable for a particular class of problems. However, it is not our intention here to present these methods, we will concentrate on the appropriate choice and utilization of the EM simulators.

3.4.2.2 Types of EM Simulator

Nowadays, there are a number of EM simulators available. Knowing the basic theory and the correct use of an EM solver for high frequency design is the key to realistic evaluation of circuit performance. There are two types of EM simulator, classified according to the number of spatial dimensions that they can handle: these are full 3-D EM simulators and 2.5-D planar EM simulators.

A key feature when comparing the suitability of different software for a particular application is the computational effort required. In principle, the greater the computational effort the more comprehensive the simulator performance. Three-dimensional simulators that can analyze arbitrary conductor structures require the highest computational effort. They can provide a powerful tool that is able to simulate any arbitrary-shaped structure, taking into consideration all possible EM effects. Arbitrary 3-D simulators (such as Ansoft's HFSS^{TM}) mainly use finite elements to compute 3-D fields and the associated conductor currents. On the other hand, 2.5-D simulators require less computational effort and mainly use the method of moments (like Agilent's Momentum^{TM}) to compute 3-D fields, but only allow 2-D conductors and currents on planar layers. In other words, 3-D simulation is a full three dimensional analysis which includes both 3-D fields and 3-D currents, while 2.5D analysis includes full 3-D fields, but only 2-D currents. Thus, 2.5-D analysis doesn't allow vertical current. Agilent's Momentum^{TM} is an example of a 2.5D planar EM simulator. Further classification between 3-D and 2.5-D solvers exists, with their classification dependent on how they handle vertical currents between different

layers [4].

3.4.2.3 A 2.5-D Planar Electromagnetic Field Solver – Momentum™

Agilent's Momentum™ is based on a numerical discretization technique called the *method of moments*. This technique is used to solve Maxwell's electromagnetic equations for planar structures embedded in a multilayered dielectric substrate. Agilent's Momentum™ is well suited to the analysis of multilayer structures [5] and is used to characterize various multilayer microstrip structures investigated in this study.

The main features of Agilent's Momentum™ include:

Adaptive frequency sampling

Adaptive frequency sampling selects frequency samples automatically and constructs a rational fitting function to represent the data over the entire frequency range. Important performance details are modeled by sampling the response more often when the S-parameters are changing rapidly. This result in a higher-resolution S-parameter response while minimizing overall simulation time.

Automatic mesh (edge mesh)

Planar electromagnetic simulators represent the current in a pattern by subdividing the pattern into cells or patches. In the case where the current is highly localized, such as in a microstrip transmission line, or microstrip coupled-line, where most of the current is at the conductor edges, a dense mesh of cells is required to accurately represent the current. With the edge mesh feature, a denser row of cells can be placed along the edges of the conductor. This more accurately represents the current while minimizing simulation time through an efficient sampling algorithm.

As CAD has become an integral part of modern microwave circuit design, correct

choice and use of EM simulators is a crucial aspect of the design. The method of analysis of various multilayer structures using full wave simulator will be discussed in the appropriate chapters.

3.5 Advanced Thick-Film Technology

Unlike low frequency circuits, the design of microwave circuits is inseparable from the fabrication technique, which influences the achievable circuit performance. Also, the increased use of microwave hybrid circuits for wireless communication systems has made low cost a significant factor, and designers must be aware of the cost implications of their designs and choice of fabrication technique.

Thin-film technology is a well-established technology for fabricating microwave circuits. However, while thin-film deposition provides high accuracy, it is an expensive technology. The significant advantages of thick-film technology are low cost and the capability for mass production. But in the past, conventional thick-film processes suffered from poor line resolution and high losses, and thus were unable to compete with thin-film technology for high performance microwave circuitry.

Traditionally, thick-film processing is a print and fire technology. Screen-printed conductors generally have surface and edge roughness. Conductor gap and line widths better than 100 microns are rarely achievable in a production environment. Thick-film dielectrics are always composites and many are ground solid particles buried in a glass matrix. This means that they have a tendency to print and fire in a way that does not give the ideal smooth surface needed at microwave frequencies. All these make traditional thick-film processes unsuitable for microwave applications.

However, recent rapid progress in novel thick-film materials and advanced thick-film circuit patterning techniques has brought improvements that allow current thick-film technology to satisfy the performance requirements for microwave circuits [6-8].

3.5.1 Material

A new advanced ceramic-based technology using thick-film conductors and dielectric from Heraeus was used to fabricate the multilayer circuits investigated in this study. The excellent geometrical properties result from a combination of novel materials and processing, give line widths down to 10 microns. This technology overcomes the problems of conventional thick-film circuitry, and allows the fabrication of high-density circuits and packages with microwave quality. The technology consists of a gold thick-film conductor and a borosilicate-based thick-film dielectric.

3.5.1.1 Thick-Film Conductor

KQ500 is a cadmium free, gold conductor paste developed for producing ultra-high density interconnections using a combination of screen-printing and etching. This material uses the very latest developments in sub-micron gold powder technology in combination with a special printing vehicle to produce extremely dense fired films with very smooth fired finishes. These properties enable the production of conductor geometries as fine as 10 microns (0.4 mils).

Typical Fired Properties:

Lines/Spaces Resolution:

25 micron lines and spaces (10 micron lines and 15 micron spaces possible on suitable substrates using optimized processing conditions)

Fired Thickness:

4 to 5 microns (recommended); 10 microns (maximum)

Fired Surface Finish:

Ra < 0.4 microns on 96% Alumina with surface finish of 0.6 microns.

Resistivity:

< 3.0 milliohms/square at 10 microns thickness

3.5.1.2 Thick-Film Dielectric

KQ115 is photoimageable dielectric. The new photoimageable material allows for the use of processes that yield finer geometry than possible with standard printing processes.

The typical fired properties are:

Dielectric Constant:

3.9 (Measured up to 20 GHz)

Fired Thickness:

10-12 microns per layer (3 separately fired layers are recommended to avoid pinhole through the final layer)

Loss Factor:

$1x10^{-4}$ at Low Frequency, $<4 \times 10^{-4}$ at 20 GHz

Via Resolution:

75 microns (50 microns or better possible under suitable processing conditions)

3.5.2 Patterning techniques

Photo patterning techniques, including photo sensitive patterning technique and photo defining (or etching) process have been used to produce circuit geometries better than that normally possible when using conventional thick-film techniques. These new techniques offer improved line resolution and line geometry, which result in enhanced circuit performance. The fabrication processes of screen-printing, photosensitive patterning and etching, which may be used in the fabrication of multilayer microwave structures, are briefly summarized below.

3.5.2.1 Screen Printing Process

Screen printing is the deposition of thick-film pastes through a mesh screen. The screen is typically manufactured from stainless steel mesh, but can be made from other types of materials such as polyester.

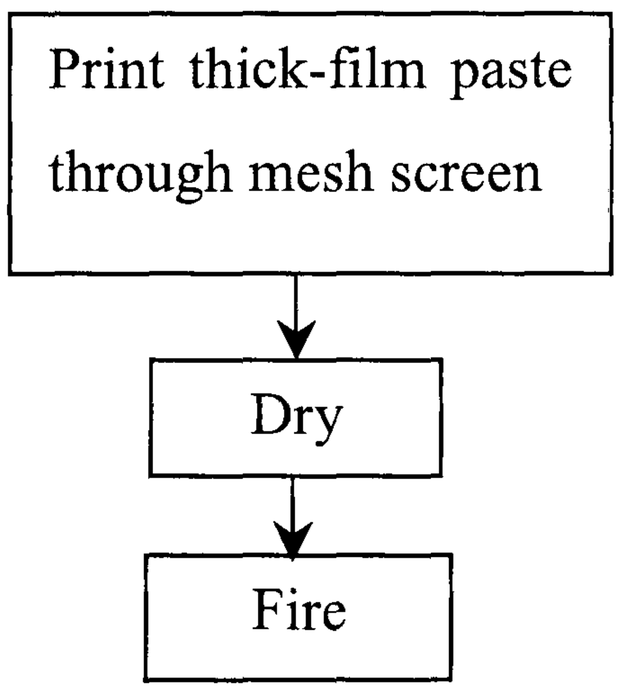

Figure 3.2: Flow chart of the screen print process

Figure 3.2 shows a flow chart of the screen printing process. The screen printing process is well established and simple. Advantages include high volume capability, low processing cost and the ability to use standard processing equipment. A significant limitation is that line resolution is generally greater than 100 microns. In addition, the surface of the printed line can be rough and edges scalloped. Scalloped

edges and rough surfaces are a source of loss in RF circuits.

3.5.2.2 Photo Sensitive Process

The photo sensitive process is also referred to as photo-imaging. For this process, the thick-film paste contains a photo-initiator, which is sensitive to ultra violet (UV) light. The photo-initiator cross-links the polymer, making it resistant to washing solvents. The first stage in the printing process is that an oversized area of paste is screen printed on the substrate. The paste is then dried and a pattern is imaged into the paste with a photo- negative mask and using an ultra violet light source. The pattern is then washed and fired. Figure 3.3 is a flow chart of the photo sensitive process.

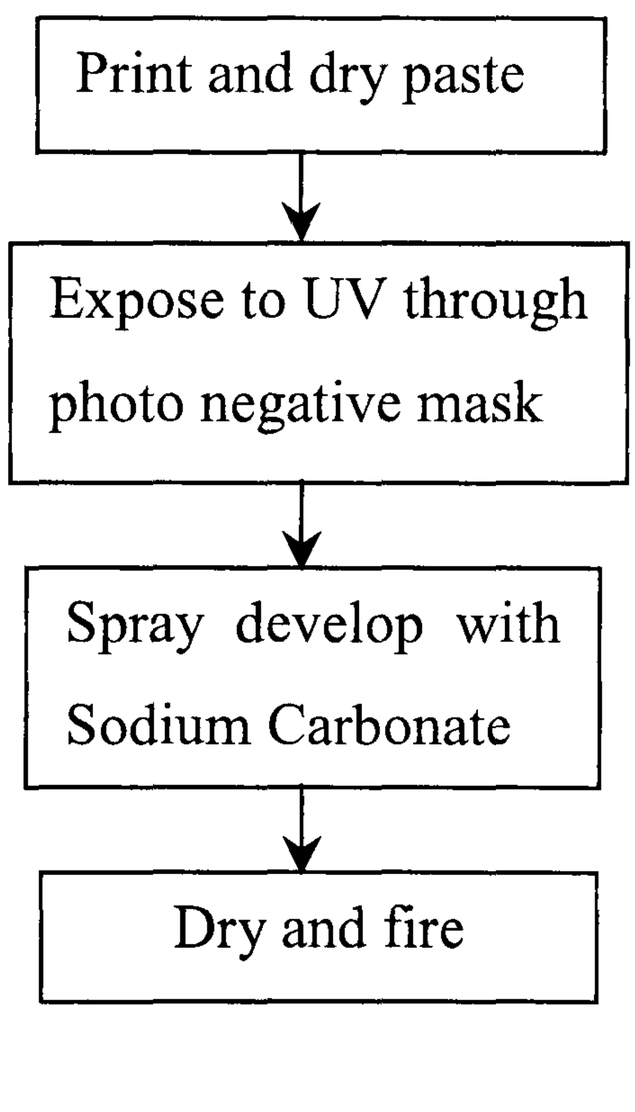

Figure 3.3: Flow chart of the photo sensitive process

Some benefits of the photo sensitive patterning technique are fine resolutions of at least 2 mils (50 microns), much better than screen printing, and also improved edge definition.

3.5.2.3 Photo Definable Process

The third patterning technique is the photo defining or etching process. Like the photosensitive process, a ground plane of thick-film paste is screen printed on the desired areas of the substrate. However for this process, the paste is fired before patterning. A photo resist is then applied to the fired film and exposed to an ultra violet light source, through a photolithographic mask. The circuit is then etched using, for example an iodine/potassium iodide solution for gold conductors. Finally, the photo resist is stripped, leaving the desired pattern. Figure 3.4 shows a flow chart of the photo defining process.

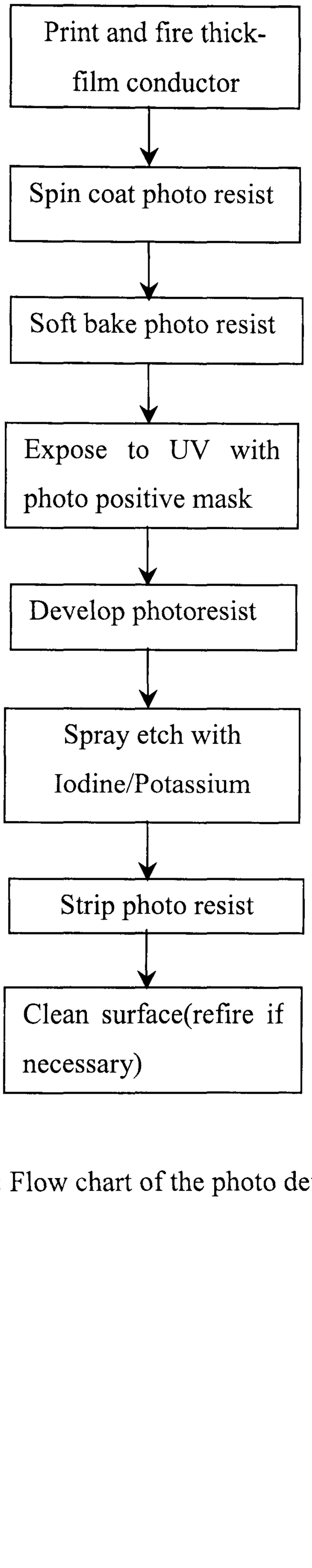

Figure 3.4: Flow chart of the photo defining process

3.5.2.4 Comparison

Table 3.1 shows a comparison of the resolution achievable using the three processes described above. Of the three patterning techniques, the best line resolution is achieved using the photo defining process. Both the photo sensitive patterning technique and photo defining technique offer better line resolution than screen printing, although, higher processing costs may result from additional equipment and more costly materials in these two processes.

For the screen printable paste, the error in the line width, Δw, (the difference between designed and actual line width), is larger for the smaller sized line (50 microns) than the larger lines (125μm). This suggests that screen-printing is still a viable technique for applications with line widths greater than 5 mils. But for narrower line applications, a photo processing technique will produce more precise line widths.

Figure 3.5 compares the line loss performance for a 50Ω line fabricated on 96% Alumina using both direct printing and etching technique. The etched line was fabricated using Heraeus KQ500 gold and the printed line was fabricated using KQ550 gold. It can be seen that, up to 8GHz, the printed line and etched line have similar line loss, while at higher frequencies, extra loss is exhibited in the printed line. This is mainly due to the uneven edges resulting from a direct printing process. This suggests that the low cost printing technique can provide reasonable microwave quality at low microwave frequencies, while in the high microwave frequency range, etching must be used to give better quality.

Table 3.1: Line resolution comparison [9]

	Designed line width (μm)	Actual line width (μm)	Line width error (μm)
Screen printable Ag	50	70	+20
	125	130	+5
Screen printable Au	50	66	+16
	125	130	+5
Photo imageable Ag	125	123	-2
	50	48	-2
Etchable Au	50	50	0
	125	125	0
Etchable Ag	50	50	0
	125	125	0

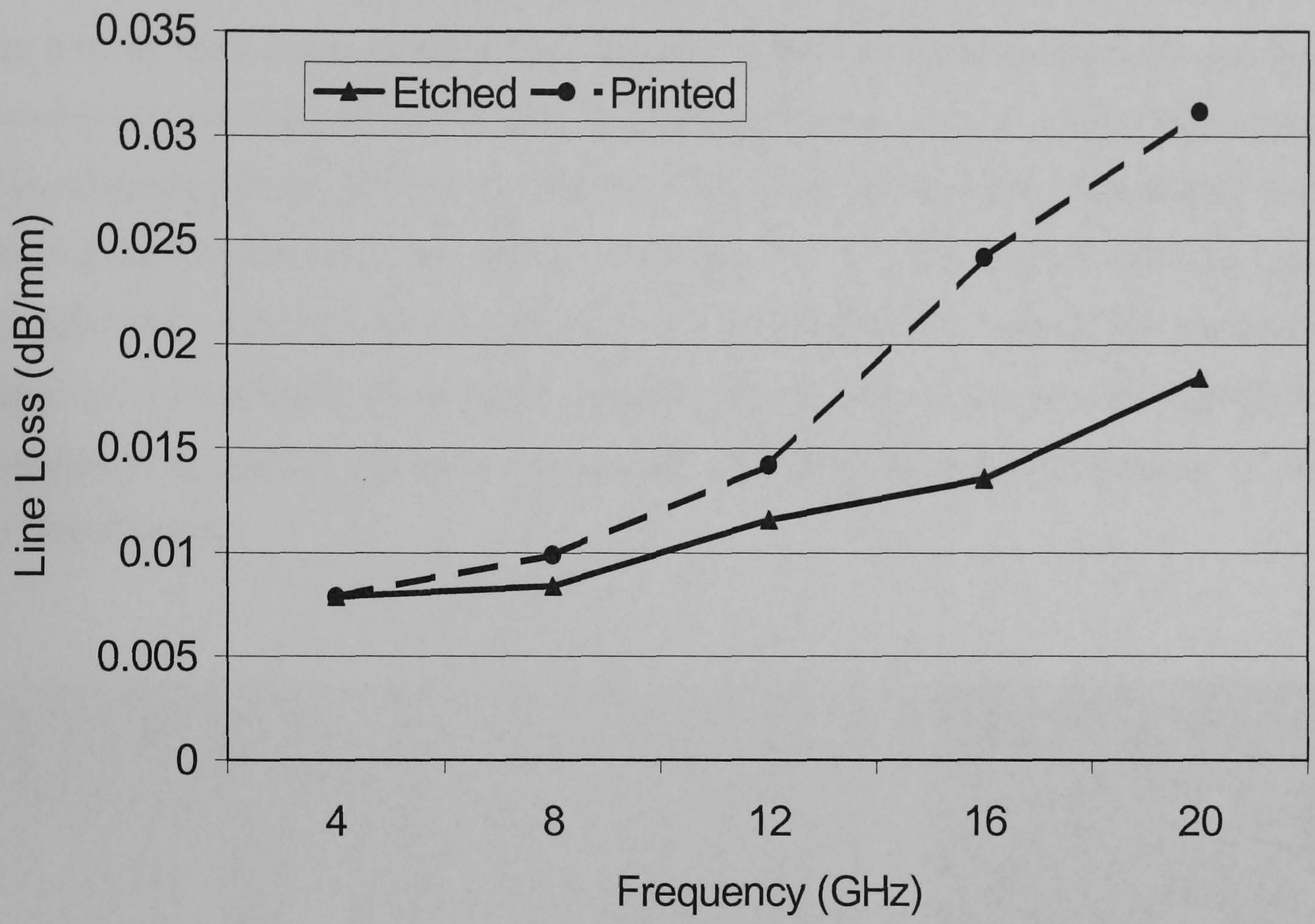

Figure 3.5: Measured loss in a gold 50Ω line on 96% Alumina

3.6 Multilayer Thick-Film Process

Thick-film technology is, by its nature, well compatible with the fabrication of multilayer structures. According to different requirements (such as line width, line spacing, cost) different patterning techniques can be used to fabricate the successive dielectric and conductor layers in a multilayer structure. Actually, by using a multilayer structure, the requirement for a very narrow gap in a single layer component to achieve strong coupling can be overcome, as tight coupling can be easily achieved by overlapping two conductor tracks on different layers.

In the multilayer thick-film process, firstly, the bottom signal conductor is printed onto an Alumina base and etched-back to give the correct line width and quality. In our process three layers of thick-film dielectric (10μm thickness per layer) were then successively printed and fired to give the final thickness of 30μm. Using three layers also minimised the possibility of pinholes. The dielectric should only be printed over the required region so as not affect the integration of other devices onto the same Alumina base. Finally the top conductor track was printed and etched. The conductor lines had a fired thickness of 5μm. A mask aligner (Figure 3.6) is important in the multilayer thick-film process as it is used to obtain accurate registration of the different layers.

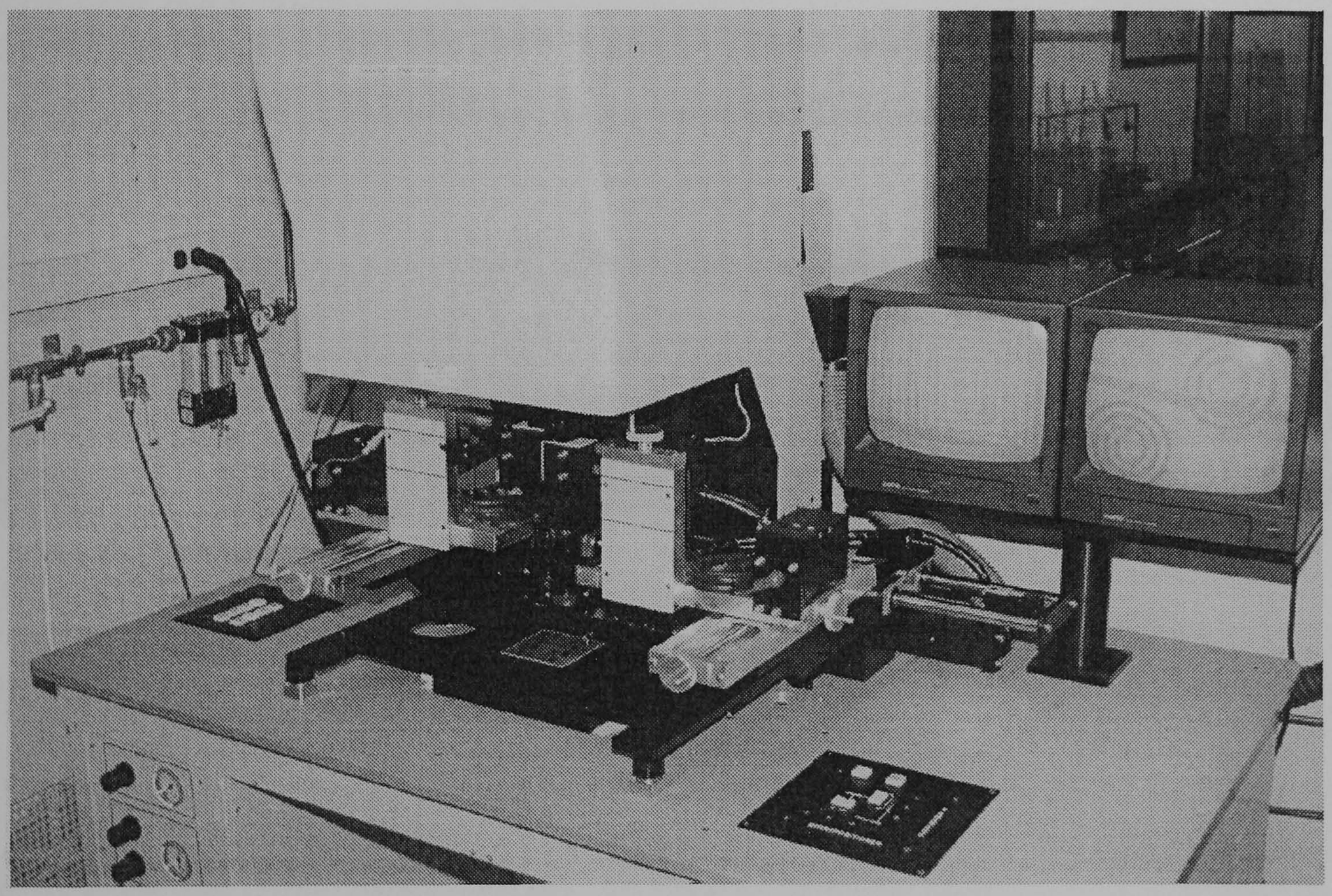

Figure 3.6: Mask aligner

3.7 Line Characterization

The characteristic impedance and effective dielectric constant of three multilayer microstrip lines (Figure 3.1) were calculated using Momentum™. The sensitivity analysis for each type of the multilayer line was also performed, and this provided useful information on the crucial aspects of the design and fabrication of various multilayer microwave structures.

3.7.1 Characterisation of multilayer microstrip line (I)

Multilayer microstrip line on top of two-layer dielectric as shown in Figure 3.1(a) was studied using Agilent's Momentum™. Figure 3.7 shows the current distribution along the line. It is seen that there is greater current intensity near the edges. Thus, edge mesh (Figure 3.8) is enabled during the simulation to achieve accurate results.

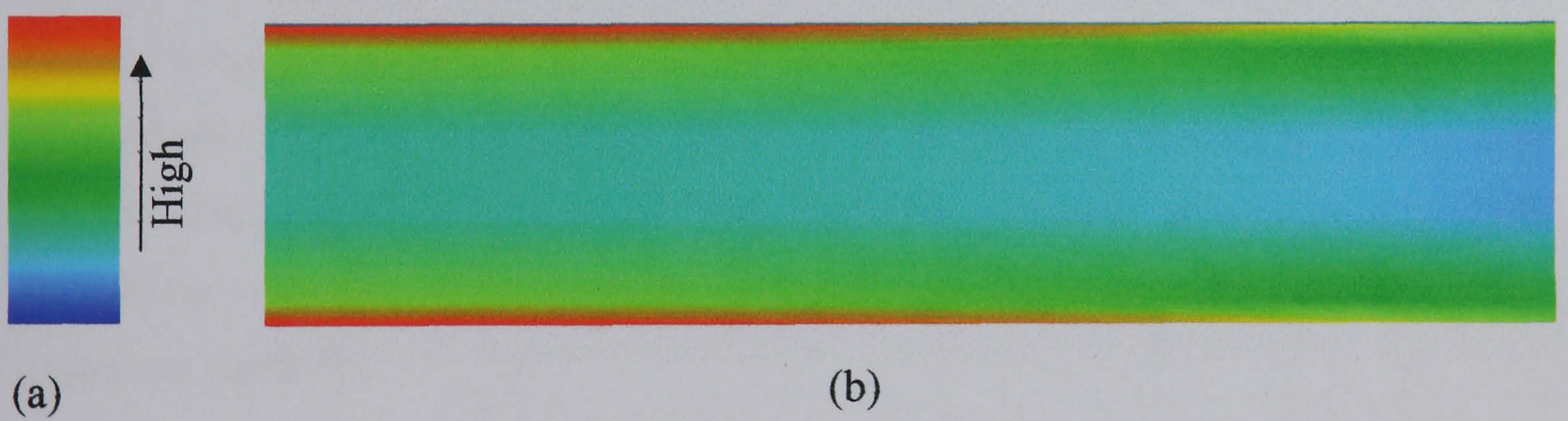

Figure 3.7: Current distribution along a multilayer transmission line.
(a) scale, (b) strip

Figure 3.8: Edge mesh of transmission line

Figure 3.9 shows the characteristic impedance Z_0 and effective dielectric constant ε_{reff} versus line width for printed thick-film dielectric layers, having thickness of 0μm, 30μm, 60μm and 90μm, respectively.

As seen from the graph, the characteristic impedance increases with the increasing thick-film dielectric thickness (h_2), whereas ε_{reff} decreases with the increasing of h_2. For a small value of h_2, the change in the Z_0 and ε_{reff} values is large with respect to h_2 =0. It is noted that the inclusion of the thick-film dielectric layer, despite this layer being very thin, significantly affects the characteristic impedance of the conductor on top of the two dielectric layers. For example, when h_2=0 (which is equivalent to standard Alumina substrate), the characteristic impedance for the line that has the width of 50μm is 114Ω. However, with the inclusion of thick-film dielectric layer (h_1 =100 μm), the characteristic impedance of the line with the same width is 156Ω (this represents an increase in the characteristic impedance of around 37%). This shows that by using a thin layer of thick-film dielectric, the microstrip line impedance can be increased. This is an important feature as it enables the realisation of very high characteristic impedance lines on high dielectric constant substrates. The high impedance capability of this structure is suitable for the implementation of low-loss matching networks.

For information, the dispersion of a 50Ω multilayer line is shown in Figure 3.10.

The effects of uncertainties in the printed dielectric layer's thickness and dielectric constant values on the effective dielectric constant and characteristic impedance are given in Table 3.2.

As mentioned earlier, a multilayer line can also be analyzed under quasi-static conditions, which is only accurate enough at lower frequencies but which provides a simple and quick analytical method. For comparison, the characteristic impedance and effective dielectric constant for a multilayer line has been calculated using both

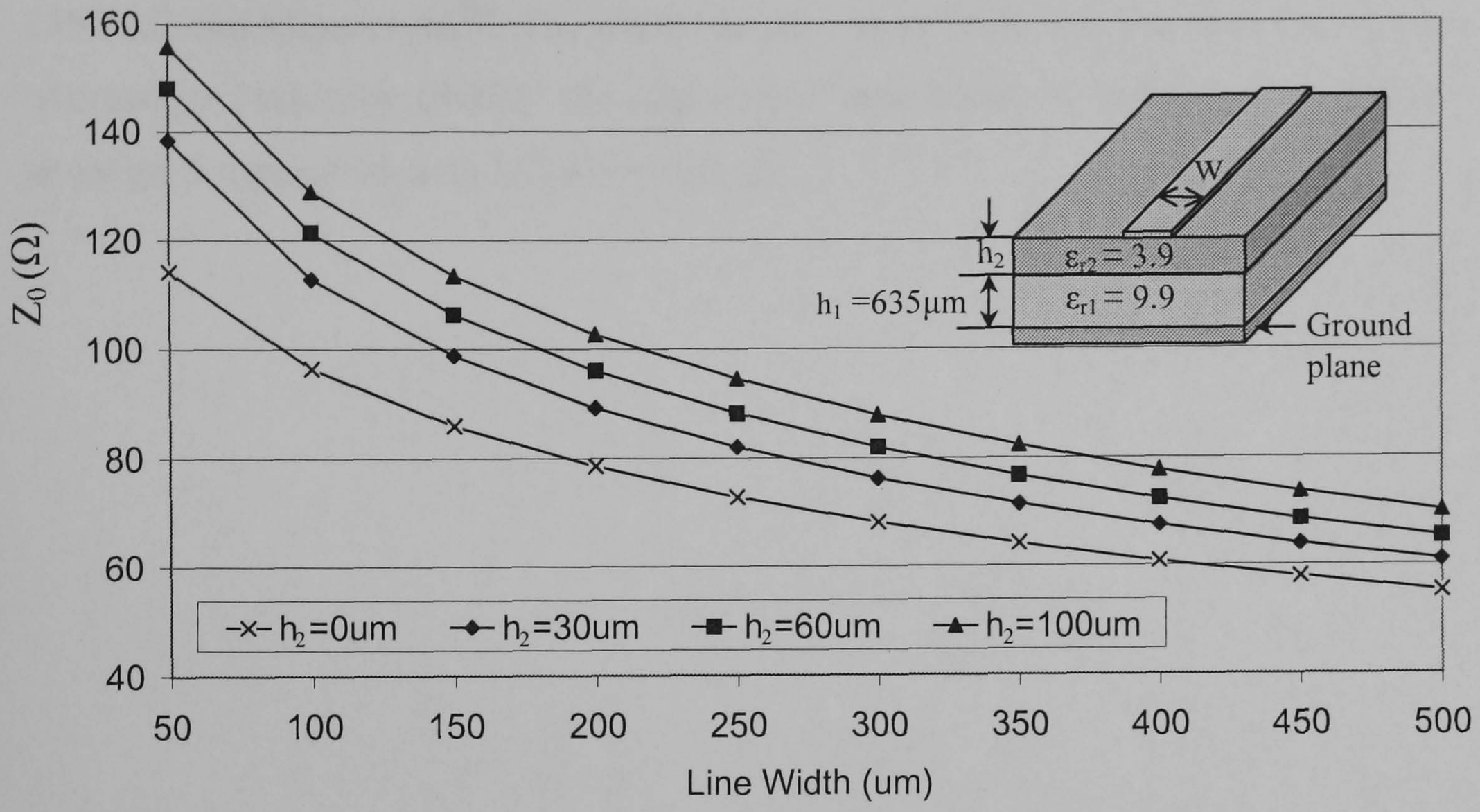

(a)

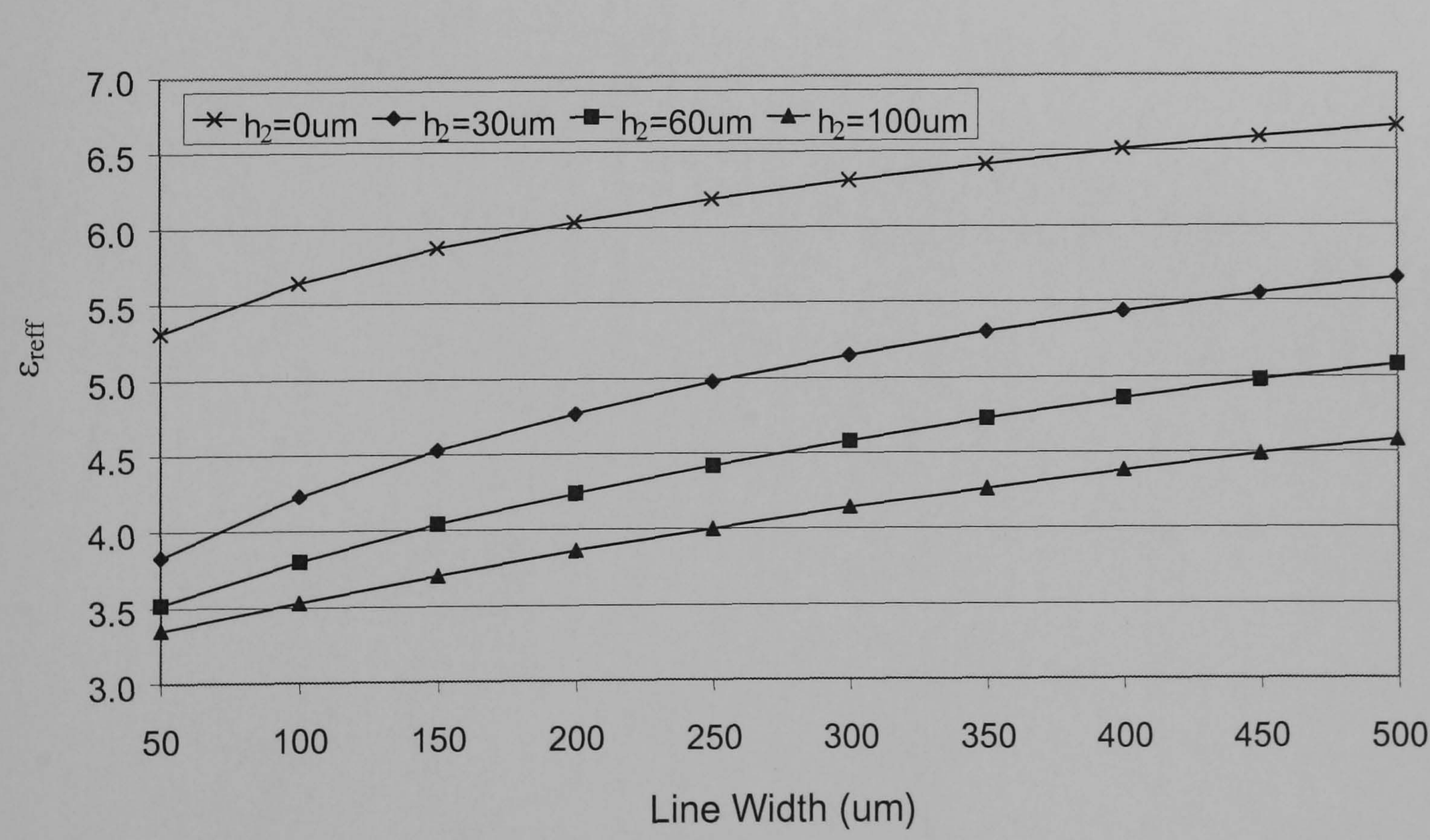

Figure 3.9 Calculated Z_0 and ε_{reff} versus line width for various values of h_2 at 6GHz.

LINPAR and Momentum™. The results are shown in Table 3.3. It is seen that at low microwave frequency (6GHz) the quasi-static assumption is valid and the results show good agreement with full wave analysis.

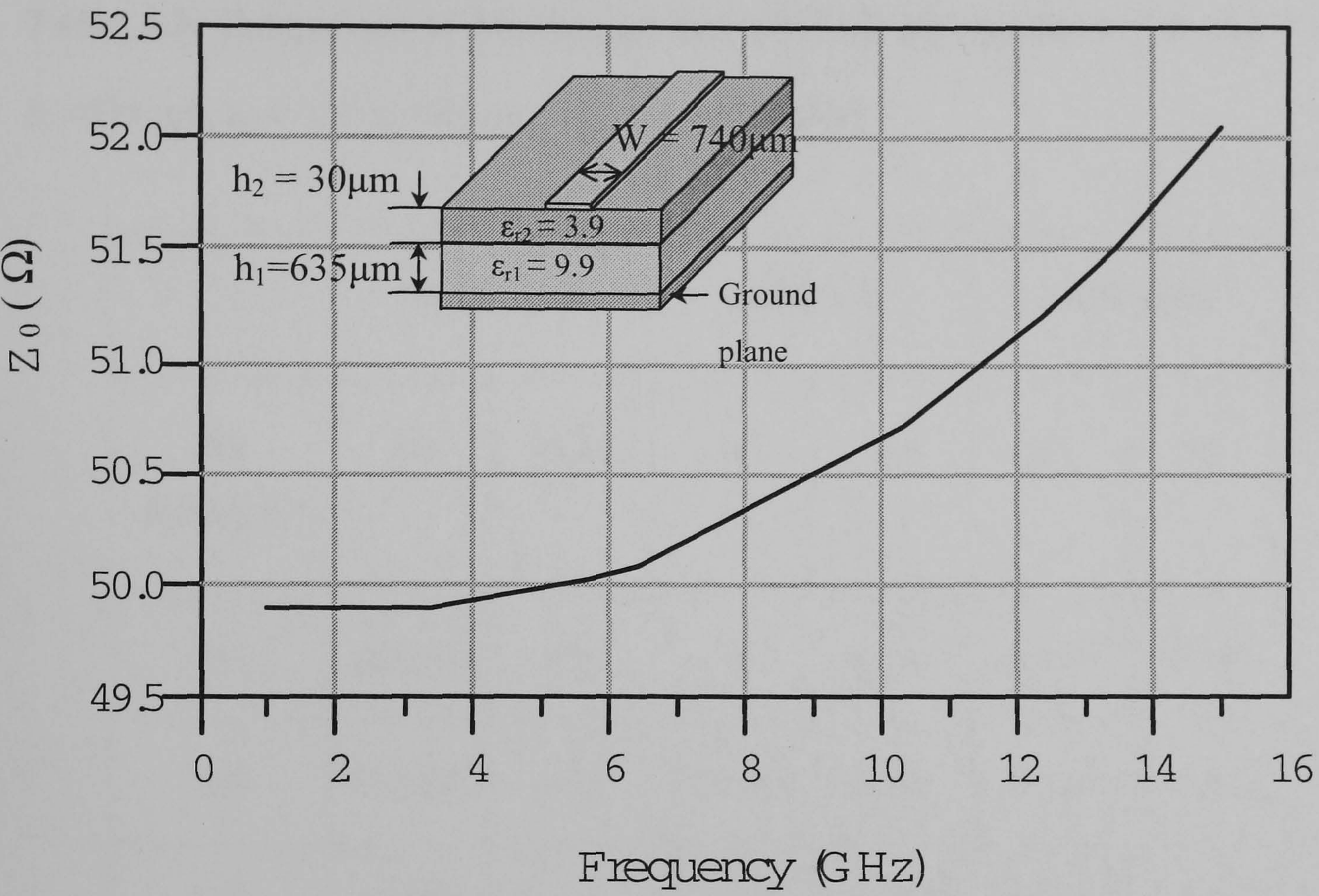

Figure 3.10: Dispersion of a 50Ω multilayer line.

Table 3.2: Sensitivity analysis of a 50 Ω multilayer microstrip line at 6GHz

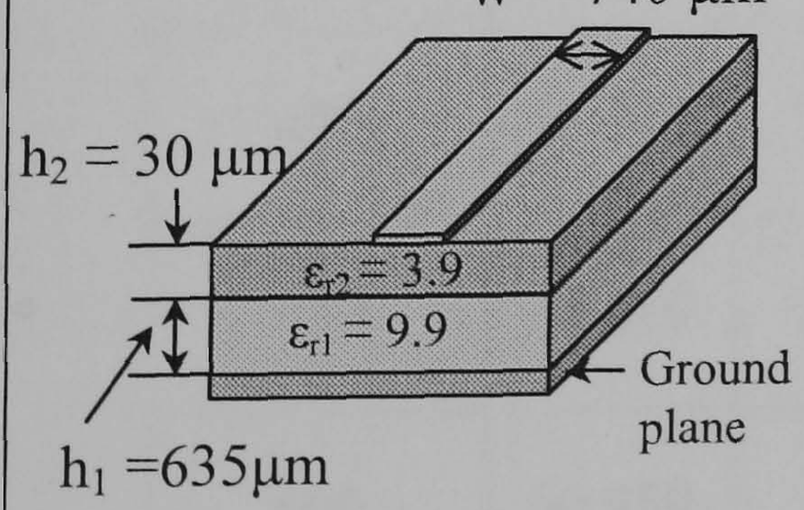		Uncertainty in thick-film dielectric layer	
		$\Delta\varepsilon_{r2}$ = +10%	Δh_2 = +10%
	$\Delta\varepsilon_{reff}$	+1.70	-1.00
	ΔZ_0 (Ω)	-0.73	+0.75

Table 3.3: Comparison of Momentum and LINPAR for multilayer line (ε_{r1} = 9.9, h_1=635 μm, ε_{r2} = 3.9, h_2=30 μm , calculated at 6GHz)

	Momentum		LINPAR		Difference	
line width(μm)	Z_0	ε_{reff}	Z_0	ε_{reff}	Z_0	ε_{reff}
50	138.395	3.83	138	4.146	0.395	-0.316
100	112.877	4.23	112.7	4.518	0.177	-0.288
150	98.808	4.53	98.39	4.785	0.418	-0.255
200	89.264	4.77	88.75	4.979	0.514	-0.209
250	82.112	4.98	81.69	5.113	0.422	-0.133
300	76.314	5.15	75.94	5.243	0.374	-0.093
350	71.552	5.3	71.23	5.35	0.322	-0.05
400	67.523	5.43	67.32	5.432	0.203	-0.002
450	64.019	5.55	63.83	5.521	0.189	0.029
500	60.959	5.65	60.79	5.6	0.169	0.05

3.7.2 Characterization of multilayer microstrip line (II)

Using the same method, characterization of the multilayer line as shown in Figures 3.1 (b) and (c) were performed and the results are shown in Figure 3.11 and 3.12. The common feature of these two structures is that they all have a thin layer of dielectric above the conductor as an overlay. Compared with the results presented in Figure 3.9, it is seen that when the thin layer of the dielectric is above the conductor track, it has less effect on the line characteristics compared to when the thin dielectric is below the conductor. These results show that the dielectric has different effect on the transmission lines, when it is above the dielectric and under the dielectric. The dispersion effect is shown in Figure 3.13. Table 3.4 shows the sensitivity analysis results.

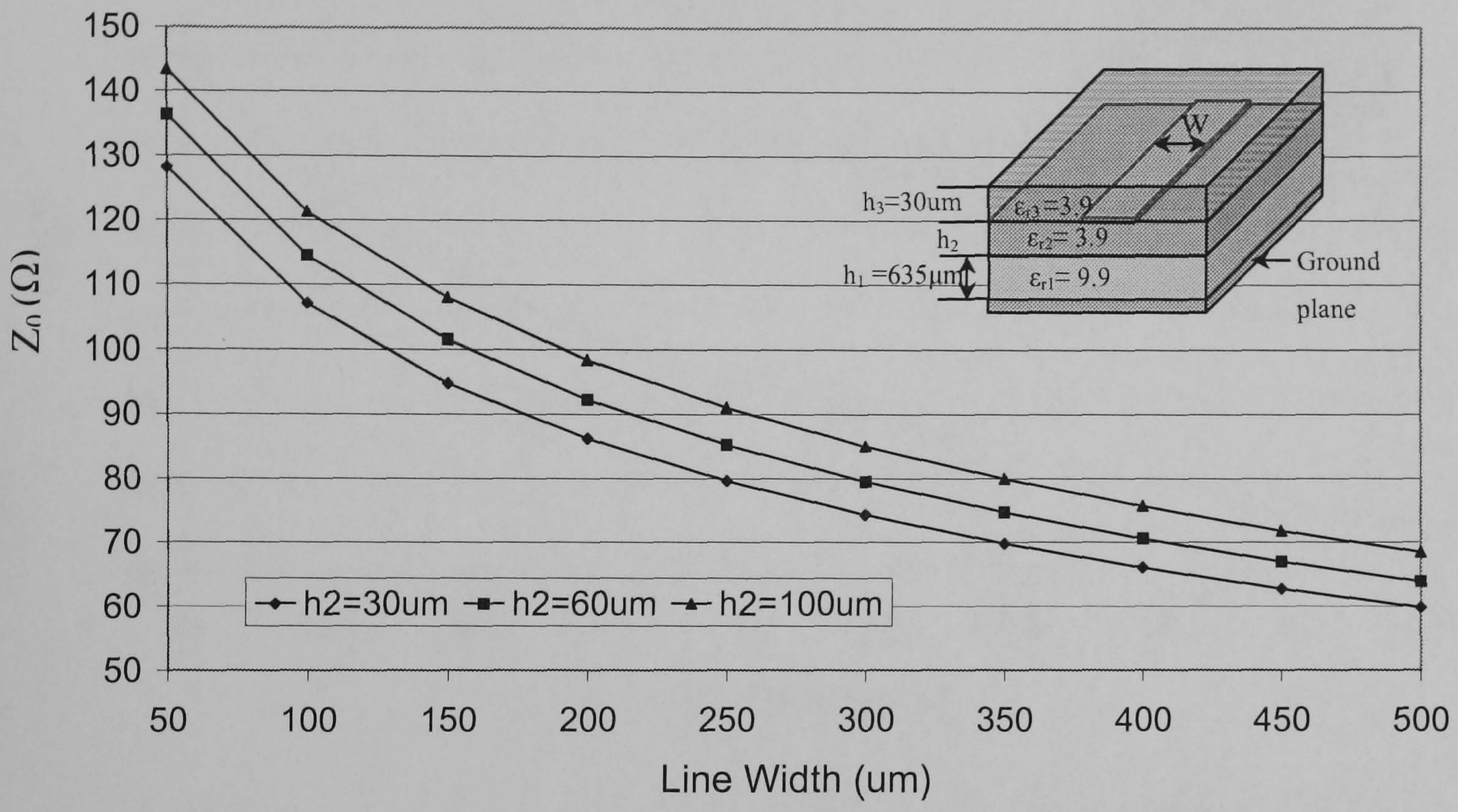

(a)

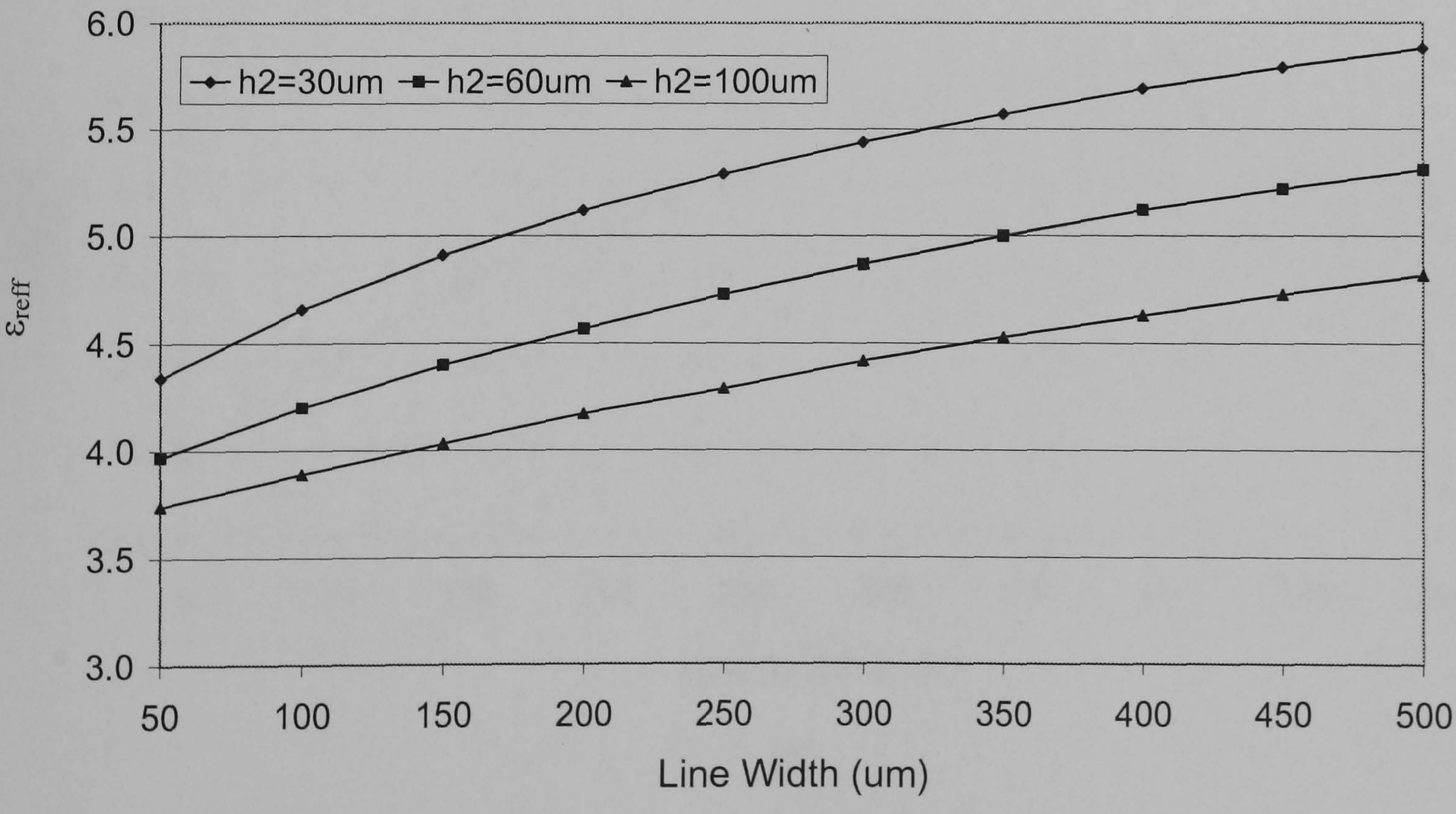

(b)

Figure 3.11 Calculated Z_0 and ε_{reff} for various values of h_2 and W at 6GHz.

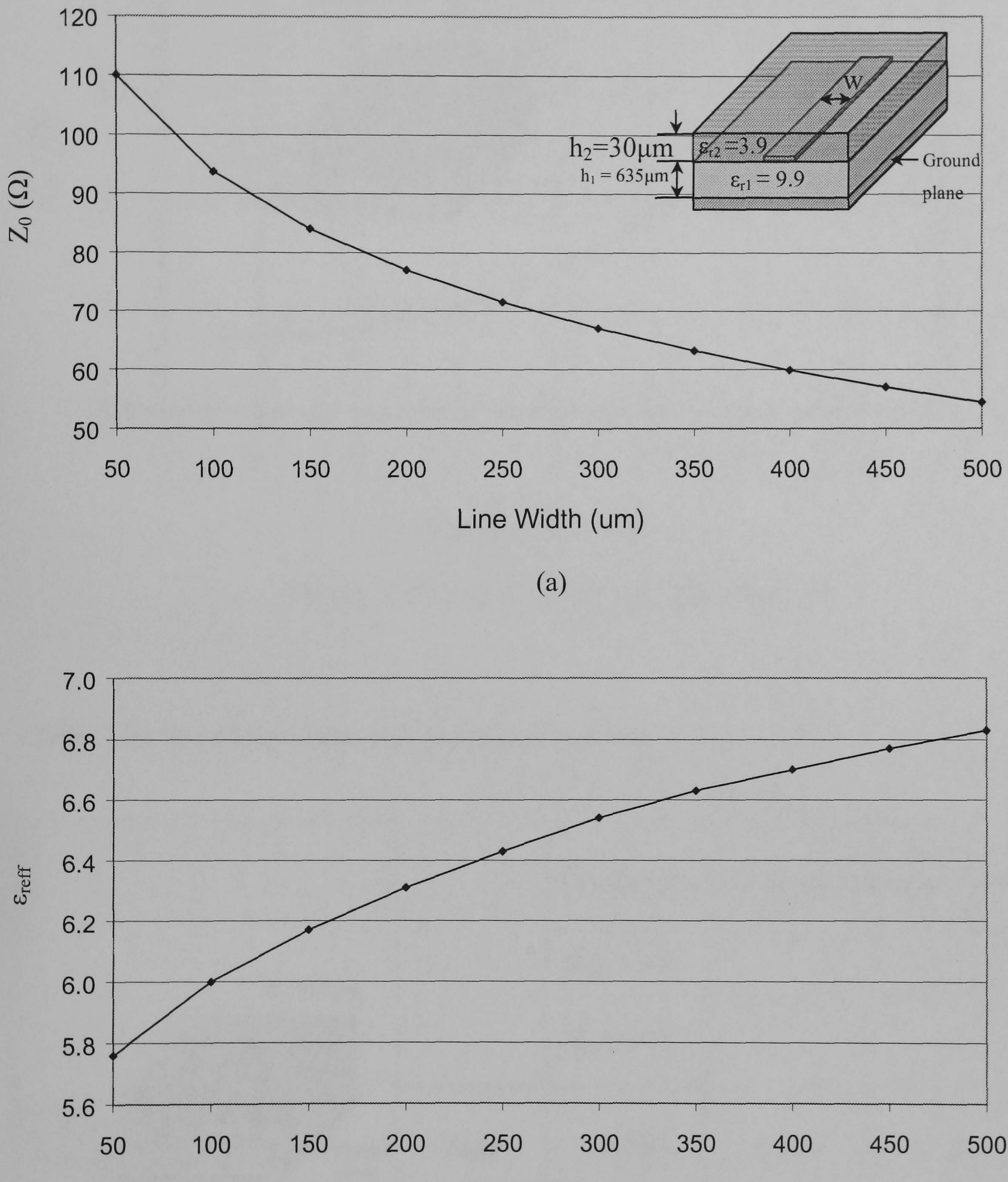

Figure 3.12 Calculated characteristics of a multilayer line at 6Hz. (a) Z_0, (b) ε_{reff}

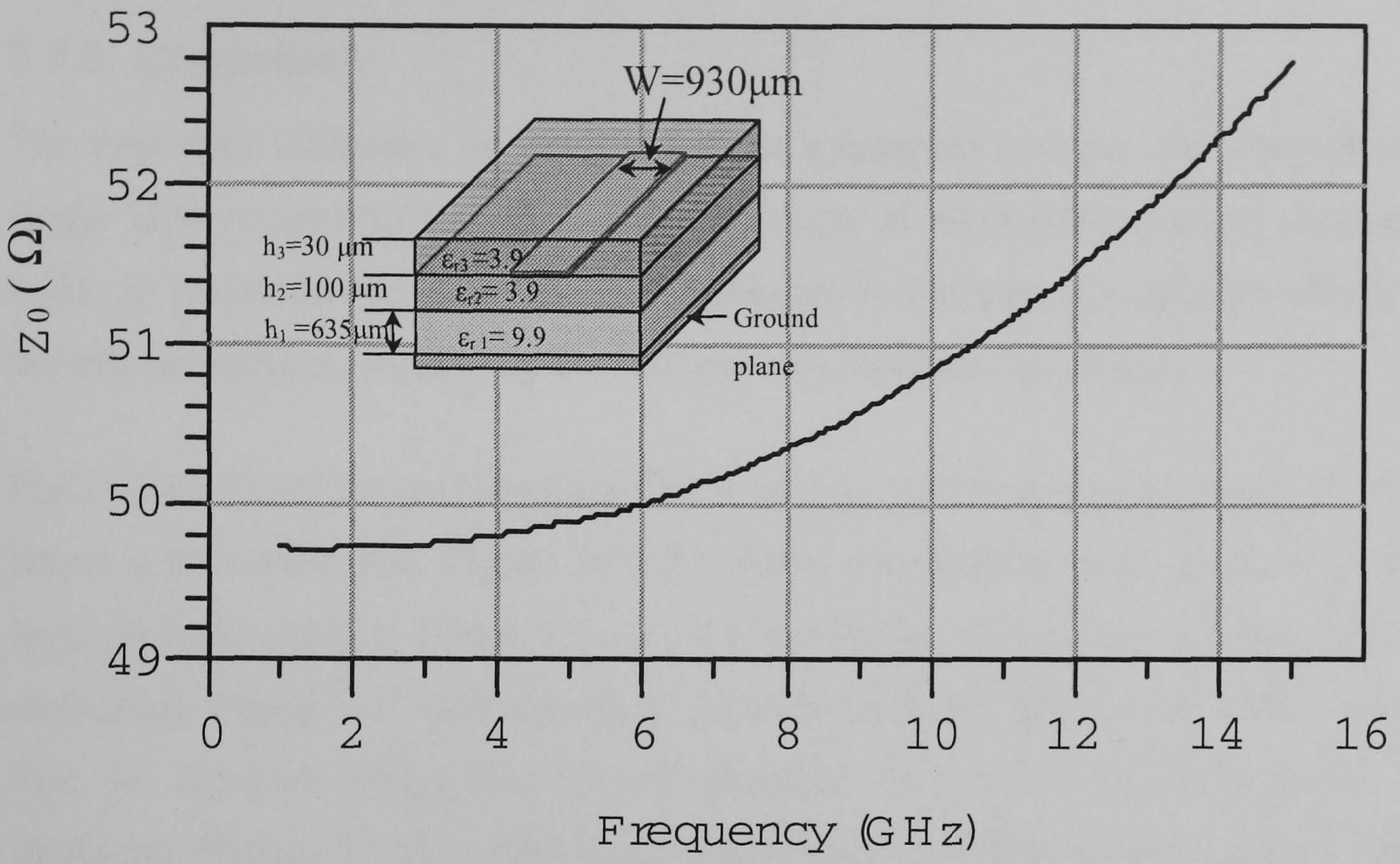

Figure 3.13: Dispersion of a 50Ω multilayer line.

Table 3.4: Sensitivity analysis of a multilayer microstrip line at 6GHz

		Uncertainty in thick-film dielectric layer		
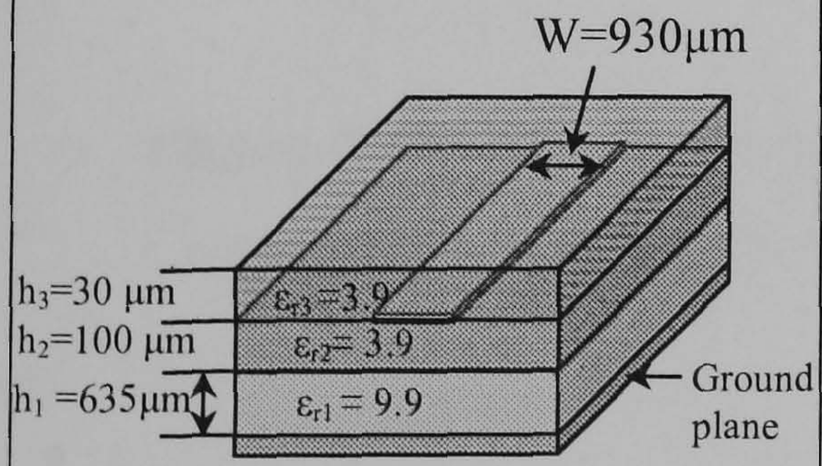		$\Delta\varepsilon_{r2}$=+10% $\Delta\varepsilon_{r3}$=+10%	Δh_2 = +10%	Δh_3= +10%
	$\Delta\varepsilon_{reff}$	+3.73%	-2.00%	+0.19%
	ΔZ_0 (Ω)	-1.83%	+1.60%	-0.10%

3.7.3 Comparison

The important difference between multilayer microstrip structure and conventional single layer microstrip structure is the inclusion of extra dielectric and conductor layers in the multilayer structure. It is interesting to compare the different effects on the line performance caused by the inclusion of extra dielectric layers.

Figure 3.14 shows the cross-sectional view of three typical structures. Figure 3.14 (a) shows a microstrip line. Figure 3.14 (b) shows a conductor track on top of a two-layer dielectric, and in Figure 3.14 (c) is a conductor track buried between the two dielectrics. Figure 3.15 summarized the characteristics of these lines. It can be seen that the situation where the printed dielectric layer is immediately under the conductor (Figure 3.14(b)), despite this layer being very thin, it significantly affects the characteristic impedance. Also, we see that the dielectric overlay (Figure 3.14 (c)) has much less effect on the performance of the transmission line.

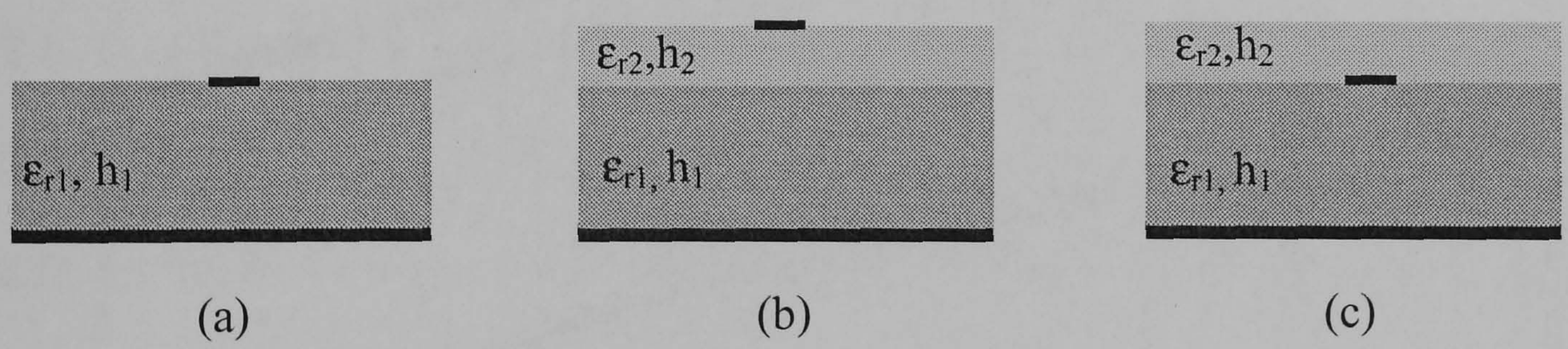

Figure 3.14: Cross sections of the basic structures. (a) Microstrip Line. (b) Conductor track on top of two-layer dielectric. (c) Buried conductor track.

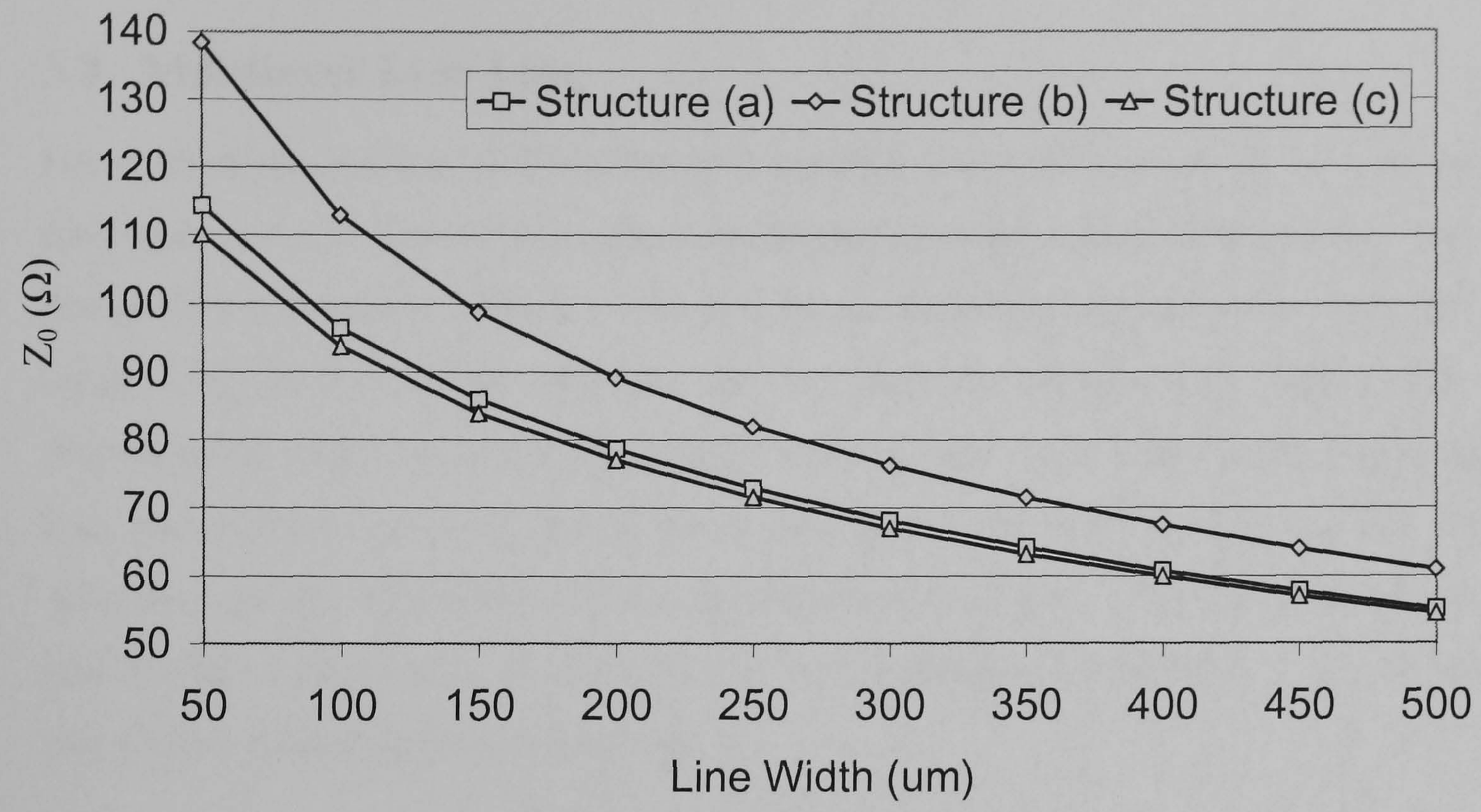

(a)

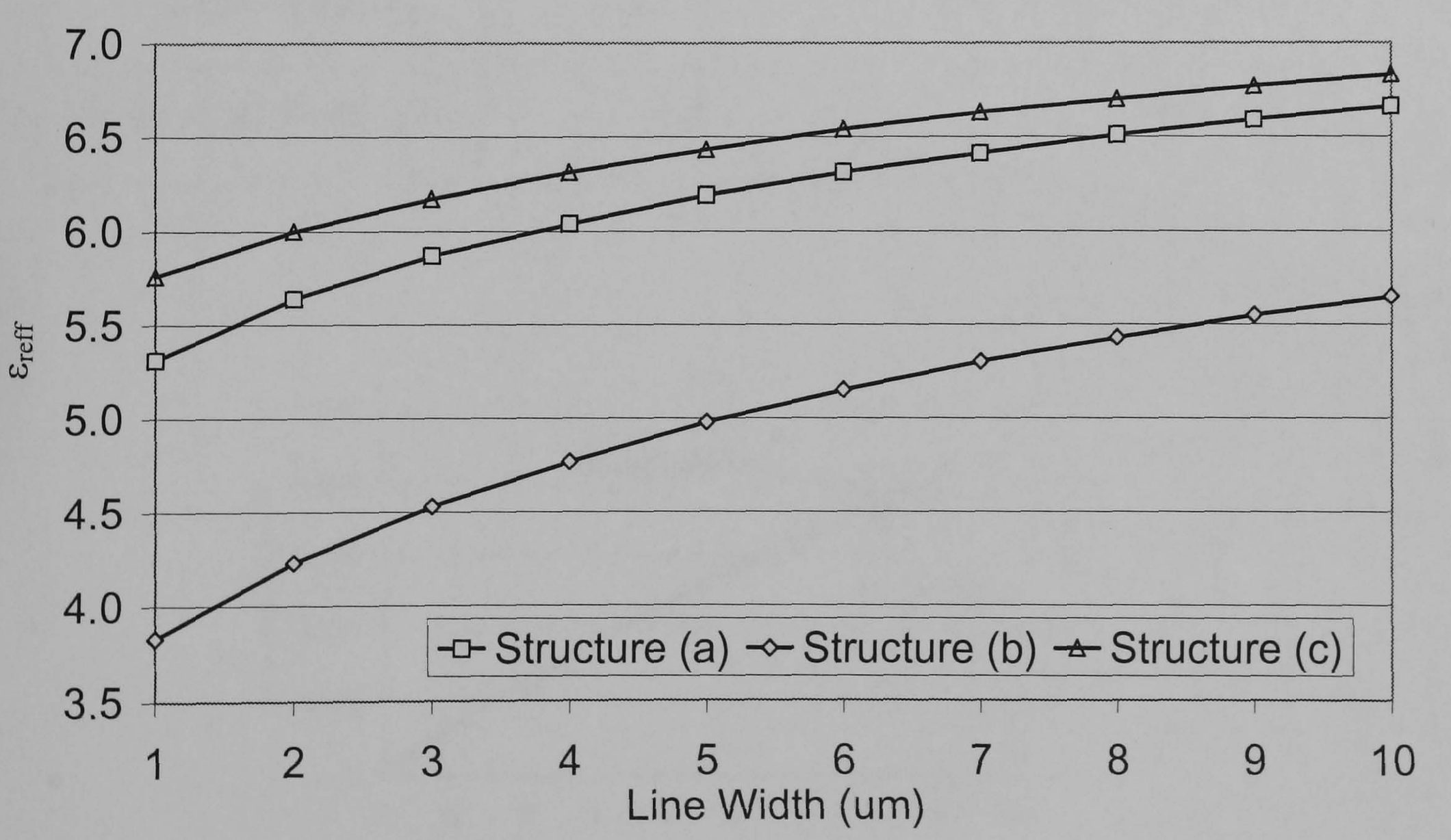

(b)

Figure 3.15: Comparison of the line characteristics for different structures shown in Figure 3.14. (ε_{r1}=9.9, h_1=635μm, ε_{r2}=3.9, h_2=30μm)

3.8 Multilayer Line Loss

For comparison, both a 50Ω multilayer microstrip line, which is on top of 2 layers dielectric, and a 50Ω microstrip line were fabricated using a thick-film process. The design data is shown in Table 3.5. The line loss of these two structures was measured using a HP 8510 network analyzer and the data are compared in Figure 3.16. Although the inclusion of the thick-film dielectric layer may cause extra dielectric loss, the width of the 50Ω line is wider than that of a microstrip line directly on Alumina, and this effectively reduces the bulk conductor loss. It can be seen that the loss of the multilayer line on top of the 2-layer dielectric is essentially the same as that for the microstrip line on Alumina.

Table 3.5: Fabrication data for a 50Ω line. (ε_{r1}= 9.9, h_1=635 μm; ε_{r2}= 3.9, h_2=30 μm)

Type of structure	Microstrip	Strip on two layers dielectric
Width of 50Ω line (μm)	604	735

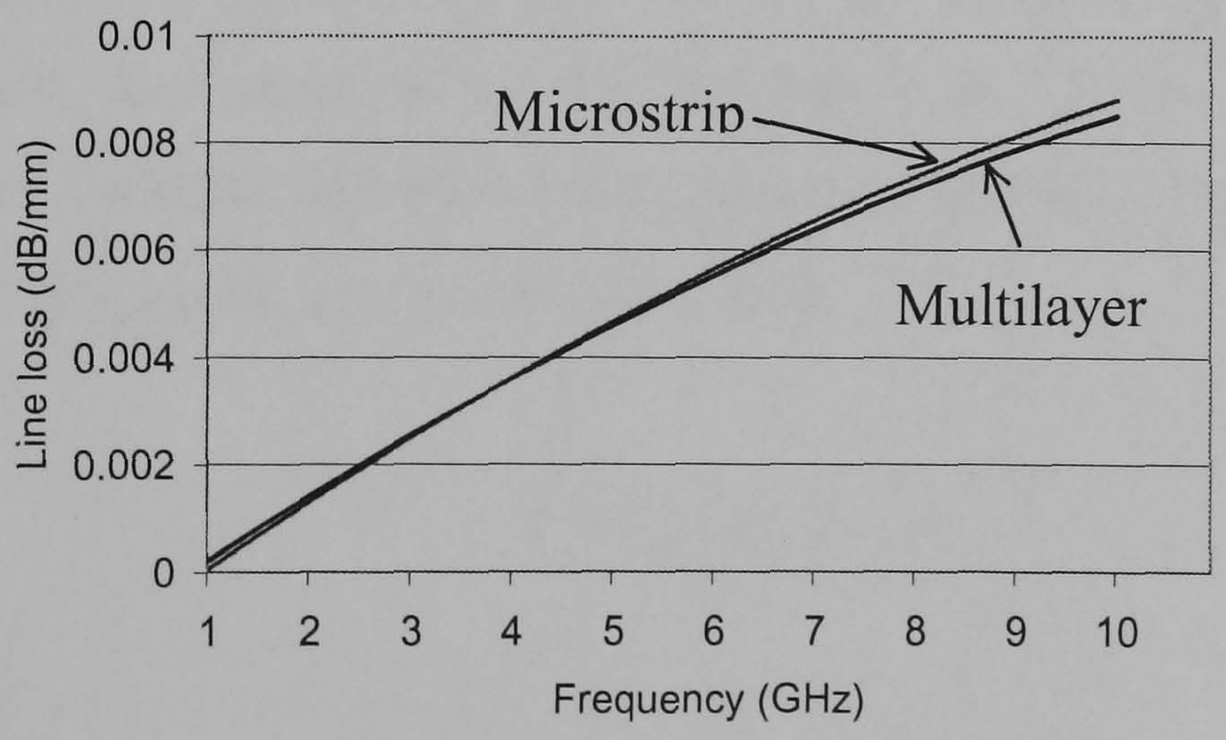

Figure 3.16: Measured line loss

3.9 Relative Permittivity of Multilayer Substrate

The relative permittivity of the multilayer substrate is important in the design of the multilayer structure. In the previous sections, electromagnetic analysis was used to obtain this data. It is important to examine the accuracy of the EM calculation. Test structures were built to evaluate the relative effective dielectric constant (ε_{reff}) of multilayer microstrip lines.

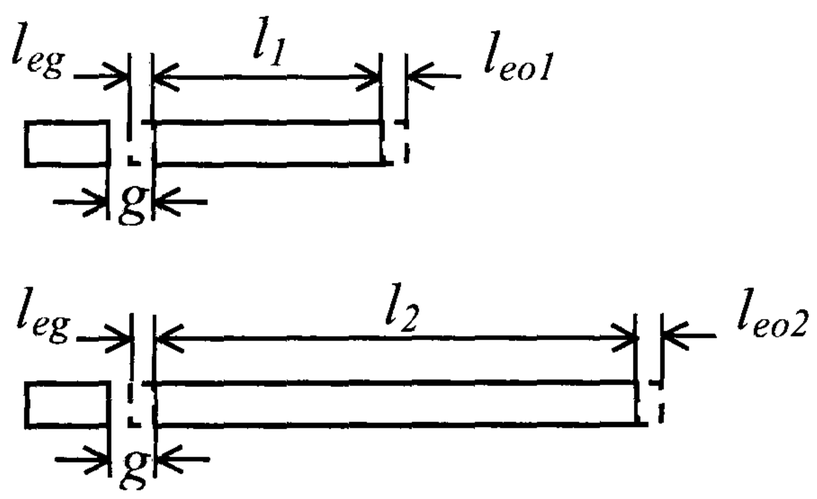

Figure 3.17: One-port line resonators

Figure 3.17 shows a pair of line resonators for practically evaluating ε_{reff}. By using two resonators of different lengths we can compensate for the open-end effects at both ends of the resonator [10]. To maintain the same resonant frequencies for the two structures, the lengths of the two resonators are chosen so that $l_2 \approx 2l_1 \approx \lambda_g$. The resonators are loosely coupled to have minimum loading effect. Knowing the length and resonant frequency, ε_{reff} can be calculated.

$$l_1 + l_{eg} + l_{eo1} = \frac{\lambda_{g1}}{2}$$

$$l_2 + l_{eg} + l_{eo2} = \lambda_{g2}$$

As l_{eo1} and l_{eo2} are both independent of resonator length, so we can assume that $l_{eo1} = l_{eo2}$. Thus

$$l_2 - l_1 = \lambda_{g2} - \frac{\lambda_{g1}}{2}$$

$$\varepsilon_{eff}(f) = \left(\frac{c}{\lambda_{g1} f_1}\right)^2 = \left(\frac{c}{\lambda_{g2} f_2}\right)^2$$

$$\varepsilon_{reff}(f) = \left(\frac{c(2f_1 - f_2)}{2f_1 f_2 (l_2 - l_1)}\right)^2$$

where f_1 and f_2 are the resonant frequency of resonator 1 and 2, respectively. c is the velocity of light.

Note that to measure the resonant frequency of the line resonator, a coupling gap is used to couple energy in and out of the resonator. Ideally the gap is expected to be as large as possible to eliminate the loading effect which may cause error in the measurement. On the other hand, if the gap is made too large, there may not be enough energy to be coupled into the line resonator. Therefore the resonance may not be strong enough to be observed. A compromise size of the gap has to be made which makes the resonance strong enough to be measured while minimising the loading effect.

EM simulation has been performed that shows the effect of the gap on the resonance. As seen from Figure 3.18, with the increasing of the gap distance, the resonant frequency tends to a consistent value. However, when the gap distance is increased to 500μm, the resonance is hardly to be observed. So a gap of 400μm was used in the experiment.

Measured and simulated data for ε_{reff} are summarized in Table 3.6. It can be seen that the measured data are in good agreement with the theoretical results.

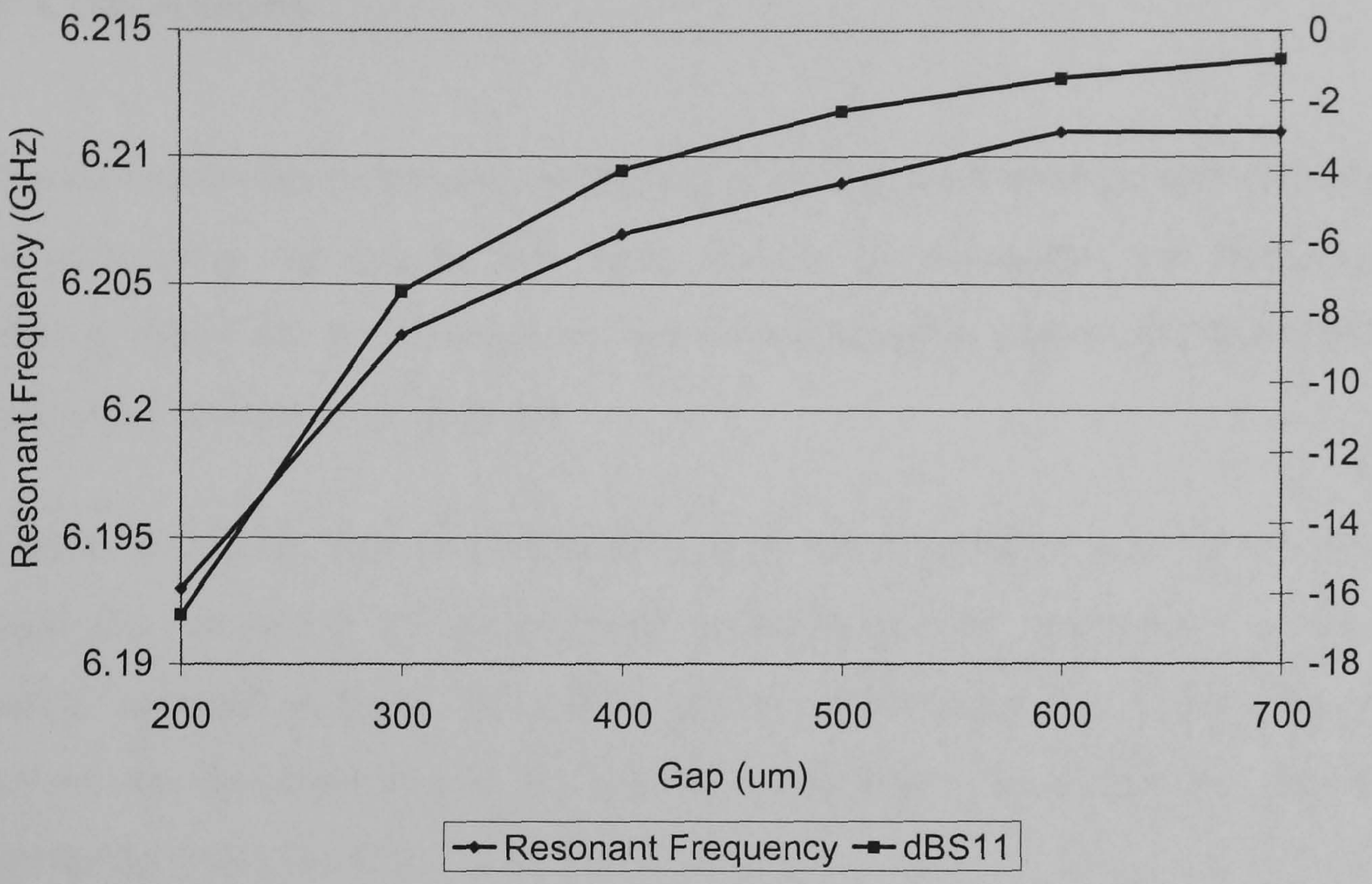

Figure 3.18: Resonant frequency versus the gap

Table 3.6: ε_{reff} of multilayer microstrip line

(ε_{r1}=9.9, h_1=635μm, ε_{r2}=3.9, h_2=30μm)

Line Width (μm)	Measured ε_{reff}	Calculated ε_{reff}	Frequency (GHz)
760	5.97	6.13	9

3.10 Conclusions

Advanced thick-film technology including new high performance material and new photo-processing techniques has been shown to overcome the limitations of traditional thick-film technology and provides a feasible process for the fabrication of multilayer microwave structures.

The study has shown that the characteristics of microstrip using a two-layer dielectric beneath the conductor are dramatically affected by the insertion of a thin, low dielectric constant material. The effect is more pronounced for narrow line widths. However, the characteristics of the line with a dielectric overlay are less affected by the presence of the overlay.

Multilayer structures will clearly provide more design flexibility for microwave components. In particular, the ability of multilayer structures to provide close conductor coupling will improve the performance of coupled-line components such as couplers and filters. Also, the realisation of high impedance lines, that is important in the design of matching networks for mixers and amplifiers, through the inclusion of an additional thin layer of thick-film dielectric under the line is a significant and useful technique.

3.11 References

[1] *KQ115 Application Notes*, Heraeus Inc.

[2] Gupta, K. C., Garg, R., Bahl, I. And Bhartia, P., *Microstrip lines and slotlines*, Artech House, 1996.

[3] Djordjevic, A. R., Bazdar, M. B., Sarkar, T. K. and Harrington, R. F., *LINPAR for Windows: Matrix Parameters for Multiconductor Transmission Lines, Software and User's Manual, Version 2.0*, Artech House, 1999.

[4] Robertson, I. and Lucyszyn, S., *RFIC and MMIC design and technology*, The Institute of Electrical Engineers, London, 2001.

[5] *Hp Momentum User's Manual*, HP.

[6] Barnwell P. and Wood J., "Advanced thick film technology - the new generation", *Proceeding of 11th European Microelectronics Conference*, Venice, May 1997.

[7] Barnwell, P., Wood, J. and Reynolds, Q., 'A microwave circuit fabrication technology using an advanced thick-film materials system', *Proc. E MIT'98 - Second International Conference on Emerging Microelectronics and Interconnection Technologies*, Bangalore, India, pp.399-404, February, 1998.

[8] Dziurdzia, B., Nowak, S., Ciez, M., Gregorczyk, W., Thust, H. and Polzer, E., 'Low cost high performance microwave structures fabricated by advanced thick film technique', *Microelectronics International*, Vol. 16, No. 3, pp.46-53, 1999.

[9] Tredinnick,M., Barnwell, P. G. and Malanga, D., 'Thick film line patterning - a definitive discussion of the alternatives', *2001 International Symposium on Microelectronics, Baltimore*, pp676-681, Oct. 2001.

[10] Edwards, T. and Steer, M., *Foundations of interconnect and microstrip design*, John Wiley & Sons, Ltd, 2000.

Chapter 4

Multilayer End-Coupled Bandpass Filters

4.1 Summary

A multilayer approach has been successfully applied to the design of end-coupled bandpass filters in order to achieve broad bandwidth. The design procedure has been developed and verified through experimental results. A 40% bandwidth has been achieved which shows a very significant improvement over conventional single layer structures, where the bandwidth achievable is normally less than 5%.

4.2 Introduction

The general configuration of an end-coupled microstrip bandpass filter [1-2] is

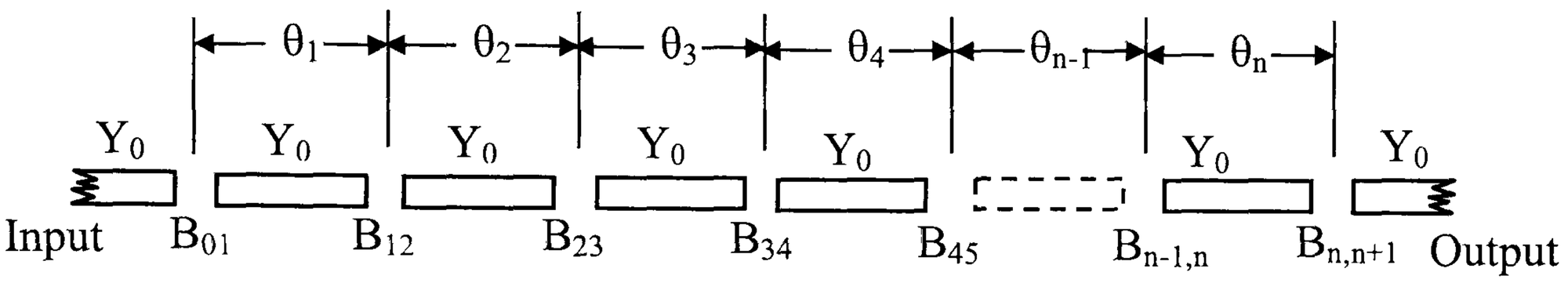

Figure 4.1: General layout for an end-coupled microstrip bandpass filter (Y_0: the characteristic admittance of the line; θ_n: the electrical length of the resonator; $B_{n,n+1}$: susceptances of the gaps)

illustrated in Figure 4.1. Each open-end microstrip resonator is approximately a half guided wavelength long at the midband frequency of the bandpass filter. The coupling between resonators is across the gap between adjacent open ends. This configuration of filter provides a simple physical structure that can be easily fabricated. No discontinuities, other than capacitively coupled-gaps, occur in this circuit. Conventionally, these filters have been utilised in single layer configurations for relatively narrow bandwidth (around 5%) applications. For a medium or wide bandwidth (>10%), the required capacitive coupling between resonators becomes so strong that this cannot be obtained by classical photolithographic techniques, since the gap spacing is very small, possibly less than 10μm. This exceeds the capability of standard wet etching processes. However, this limitation can be overcome in a multilayer structure, by overlapping the two track ends, with a dielectric separator, thus achieving strong capacitive coupling.

Clearly the multilayer overlap is a crucial component in the design of multilayer end-coupled filter and this must be characterized through electromagnetic simulation. To

achieve good design efficiency, a design procedure has been developed, where a combination of EM computation and circuit simulation is used in the filter design. The new method has been verified by the design, fabrication and measurement of several multilayer end-coupled filters.

4.3 Design Theory

The top view of an end-coupled bandpass filter in multilayer format is illustrated in

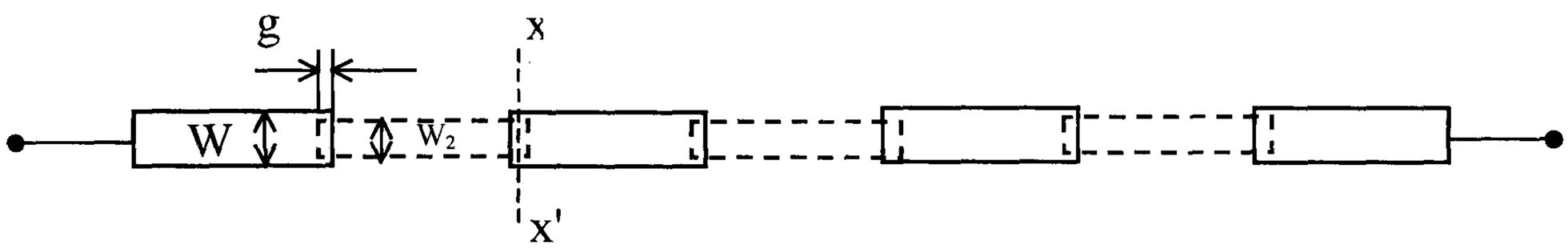

Figure 4.2: Top view of a multilayer end-coupled bandpass filter

Figure 4.2. The adjacent resonators are positioned on different layers with a certain amount of overlap so as to achieve the required strong coupling. Note that the widths of the top and buried conductors are of different widths, so they will have the same characteristic impedance. In a similar manner to the representation of gaps in single layer structures, the multilayer overlap can be represented by inverters, which are of the form in Figure 4.3 [1].

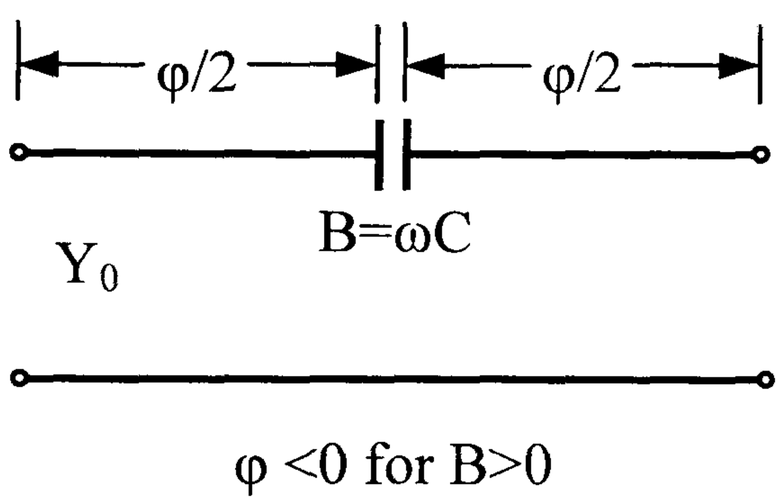

$$J = Y_0 \tan\left|\frac{\varphi}{2}\right|$$

$$\varphi = -\tan^{-1}\frac{2B}{Y_0}$$

$$\left|\frac{B}{Y_0}\right| = \frac{J/Y_0}{1-(J/Y_0)^2}$$

Figure 4.3: Multilayer overlap represented by J inverter

Assuming the multilayer overlap acts as perfect, series-capacitance discontinuities, the design equations of the filter under consideration are then given by [1]:

For the first coupling structure:

$$\frac{J_{01}}{Y_0} = \sqrt{\frac{\pi\delta}{2g_0g_1}} \tag{4.1}$$

for the intermediate coupling structures:

$$\left.\frac{J_{j,j+1}}{Y_0}\right|_{j=1}^{n-1} = \frac{\pi\delta}{2\sqrt{g_j g_{j+1}}} \tag{4.2}$$

For the final coupling structure:

$$\frac{J_{n,n+1}}{Y_0} = \sqrt{\frac{\pi\delta}{2g_ng_{n+1}}} \tag{4.3}$$

where g_0, g_1 ... g_n are the elements of a ladder-type lowpass prototype with a normalised cut-off frequency equal to 1 and δ is the fractional bandwidth of a bandpass filter, defined as: $\delta = (f_2 - f_1)/f_0$. $J_{j,j+1}$ are the characteristic admittances

of J-inverters and Y_0 is the characteristic admittance of the microstrip line.

The susceptances $B_{j,j+1}$ are evaluated from:

$$\frac{B_{j,j+1}}{Y_0} = \frac{\frac{J_{j,j+1}}{Y_0}}{1-\left(\frac{J_{j,j+1}}{Y_0}\right)^2} \tag{4.4}$$

$$\theta_j = \pi - \frac{1}{2}\left[\tan^{-1}\left(\frac{2B_{j-1,j}}{Y_0}\right) + \tan^{-1}\left(\frac{2B_{j,j+1}}{Y_0}\right)\right] \tag{4.5}$$

where $B_{j,j+1}$ and θ_j are evaluated at centre frequency f_0. Note that the second term on the right hand side of (4.5) represents the absorption of the negative electrical lengths of the *J*-inverters associated with the *j*th half-wavelength resonator.

In the case of the multilayer configuration, the capacitances required are formed by the multilayer overlap. The overlap is chosen to give the same transmission coefficient (dBS21) as the corresponding capacitance in the single layer structure. However, the phase shift caused by the multilayer overlap is different from that obtained from the ideal capacitance. A correction of the resonator length is then needed to compensate for this difference. In other words, the resonator lengths depend not only upon the microstrip wavelength, but also on the phase shift performance due to the multilayer overlaps. Thus the length of the resonator, excluding the effective overlap length, is given by the following expression:

$$\theta_j = \pi - \frac{1}{2}\left[(\pi - Phase(S21)_{j-1,j}) + (\pi - Phase(S21)_{j,j+1})\right] \tag{4.6}$$

where $Phase(S21)_{j-1,j}$ and $Phase(S21)_{j,j+1}$ are the phase shift caused by the multilayer overlap at both ends of the resonator.

It is seen from the above design theory that the multilayer overlap is an essential element in the design of multilayer end-coupled filters. The overlap is chosen to give required coupling capacitances for the desired bandwidth. Also, its phase shift should be included into the calculation of the length of the resonator so as to give the correct working frequency. In the single layer format, closed form expressions for microstrip gaps can be used to determine the gap dimensions. However, for the multilayer overlap, there is no closed form expression available, as the structure is rather more complex. Consequently, EM analysis on the multilayer overlap has to be carried out to provide the required design information.

4.4 Characterization of Multilayer Overlap

As we have seen, in the design of multilayer end-coupled filters the coupling gaps between resonators are of prime importance. Figure 4.4 shows both the top view and cross sectional view of multilayer overlap. To date, there is no equivalent circuit expression available to represent this situation. Thus EM simulation (using HP

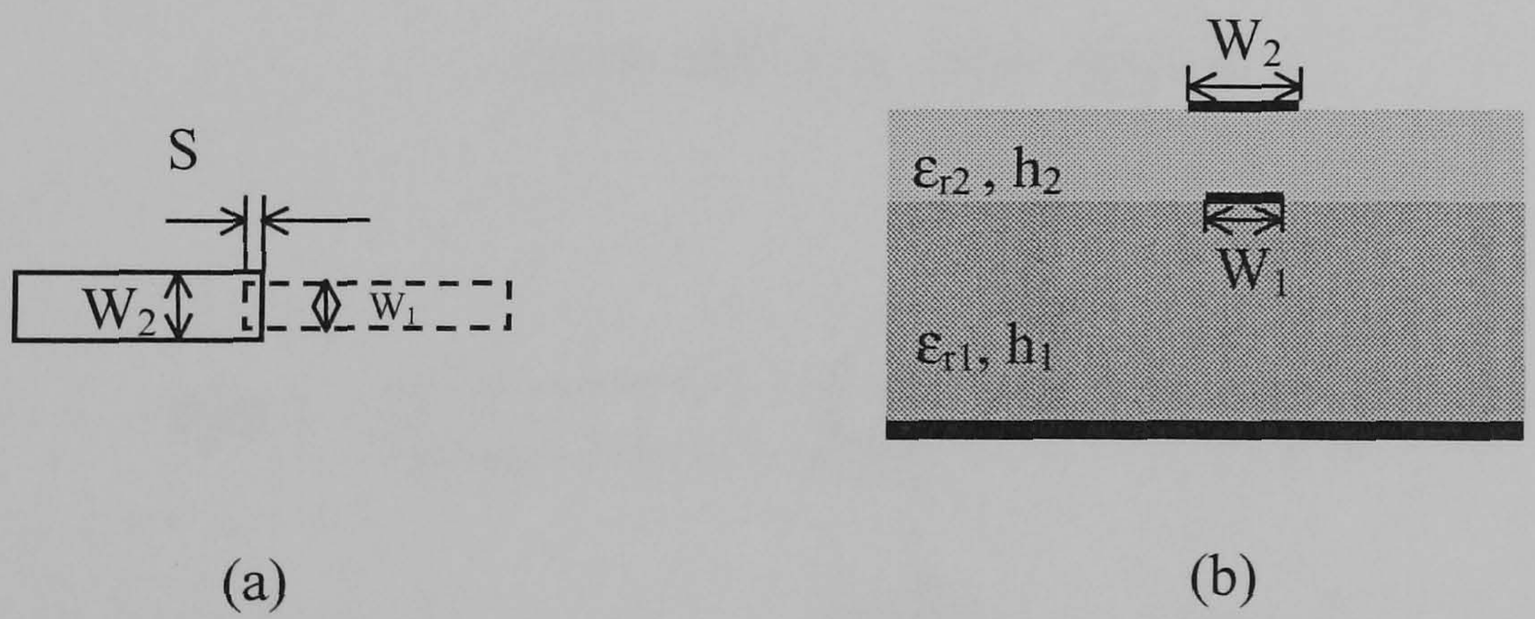

Figure 4.4: The layout of a multilayer overlap. (a) Top view. (b) Cross-sectional view

Momentum) has been used to characterise this structure. As very dense charge exists in the vicinity of the relatively small overlapping area, appropriate utilization of the EM simulator is critical for accurate characterization.

4.4.1 Applying Reference Offset

When simulating multilayer overlap using the EM simulator, we have to allow for some feedline length on either side of the overlapping region of interest in order for the fundamental mode to settle. This is the same concept as that used in the practical hardware measurement of small discontinuities. Figure 4.5 (a) shows a multilayer overlap with feedline at both ends for simulation.

In Figure 4.5 (a), S-parameters will be extracted from the simulation based on the positions of port 1 and port 2. This simulation will yield accurate results as the necessary feedlines have been included, but the results will also contain the extra line

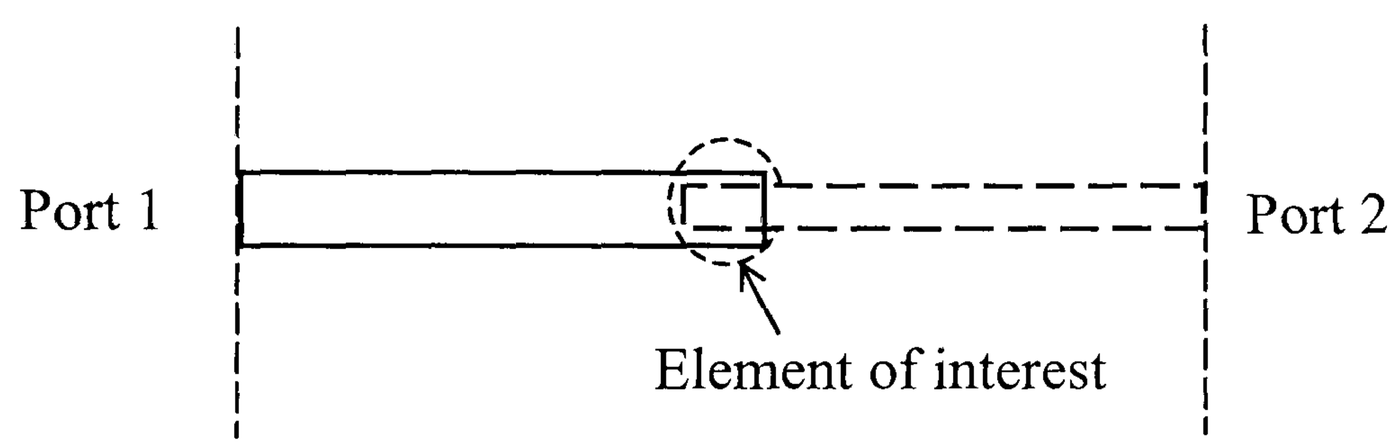

(a) no reference offset applied

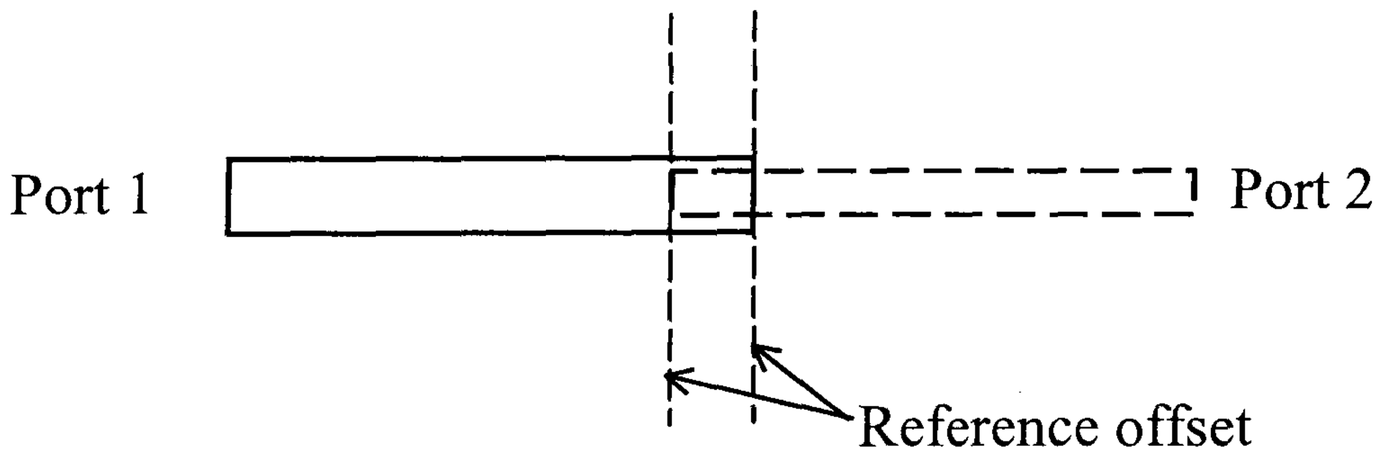

(b) reference offset applied

Figure 4.5: Illustrating the concept of reference offset

lengths. To de-embed the overlap, reference offsets [3] can be applied to the two ports in HP Momentum as shown in Figure 4.5 (b). Although the circuit has been analyzed with the long feed lines, reference offset shifting allows the software to produce the S-parameters as if port 1 and port 2 were positioned at the reference offsets. Then the S-parameters obtained are only the S-parameters for the short discontinuity. During the analysis, the impedance and propagation constant are calculated for the ports, based on their physical location in the circuit. With this knowledge of the impedance, propagation constant, and the distance of de-embedding, the software can cancel out the extra lengths of line from the S-parameter results, by compensating for the loss and phase shifts of those lines. The net result is a set of S-parameters, calculated as if the extra line lengths were not there. Thus the effect of the extra feed lines has been mathematically eliminated from the S-parameter solution.

4.4.2 Mesh for a Single Object

Meshing is an important basic concept in using an EM simulator. The accuracy of EM simulation largely depends on the correct settings for the mesh.

A mesh is a grid-like pattern of triangles and rectangles and each triangle or rectangle is a cell. Rectangular cells are applied to most of the geometry. But for curved or non-rectangle objects, triangles are used to complete the mesh. The current within each cell is computed and any coupling effects in the circuits are identified during simulation. From these calculations, S-parameters are then calculated for the entire circuit. Normally, it is not necessary to set up mesh parameters; default parameters will be suitable for general analysis. However, in the case of the multilayer overlap, which may carry a dense charge, suitable mesh parameters and correct methodologies to set the mesh are important. Good understanding of how the EM simulator works is important to be able to apply denser mesh to the structure correctly.

Figure 4.6 compares different mesh settings for a multilayer overlap. For clarity, only the mesh on one track is shown. The same mesh pattern is applied to the other track. In Figure 4.6 (a) and (b), the same mesh parameters are applied to both the access line and the multilayer overlap. Figure 4.6 (b) has denser mesh compared with Figure 4.6 (a) with the intention of giving more accurate results.

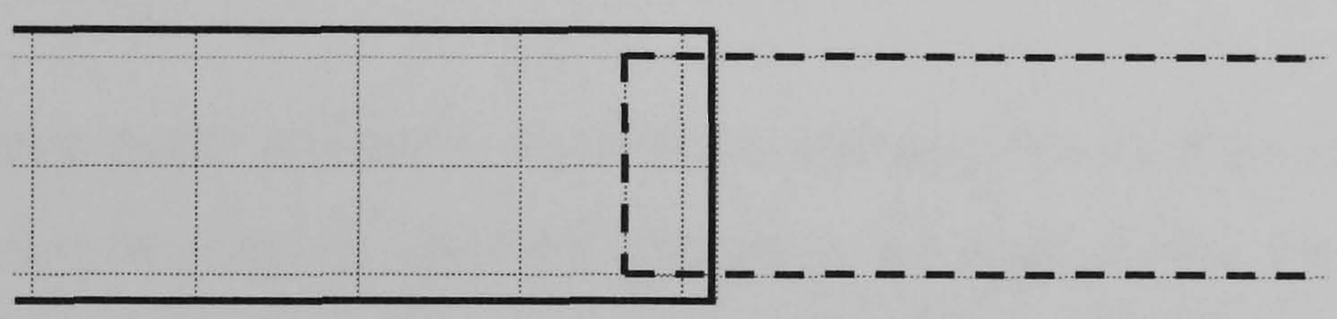

(a)

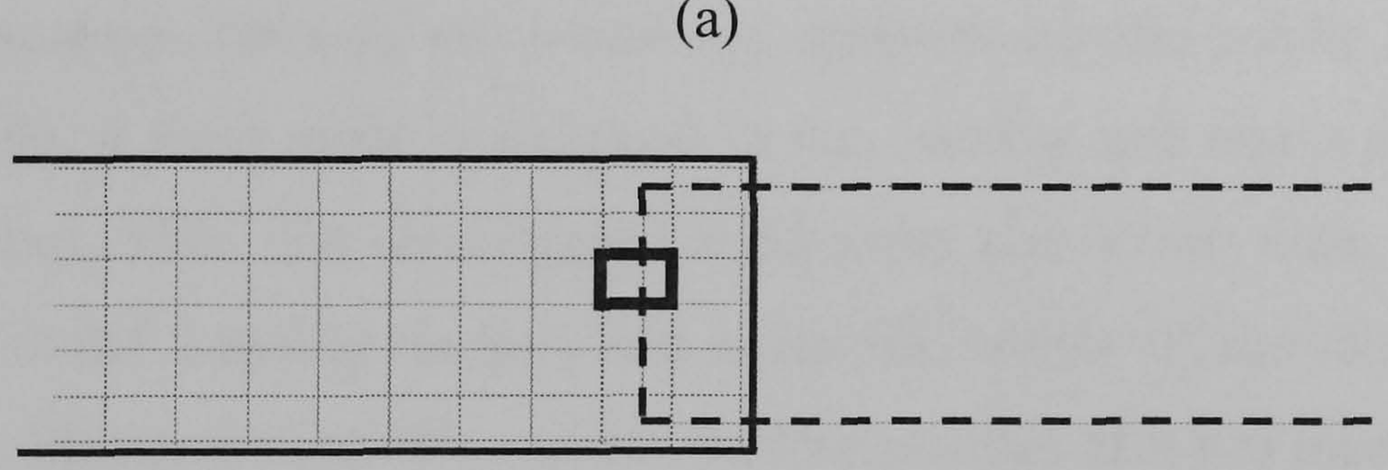

(b)

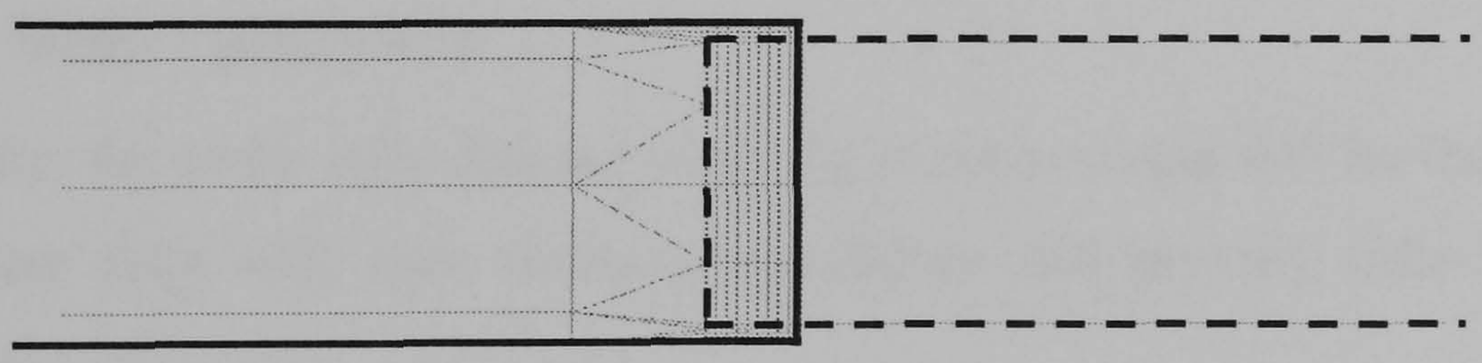

(c)

Figure 4.6: Different mesh settings

However, there are two problems that exist with these kinds of mesh settings. Firstly, if a finer mesh has been applied to the whole structure, including the access lines, the

computation time will be significant. Secondly, and most importantly, the mesher can create cells that will cross the border of the overlapping region. For example, for the highlighted cell shown in Figure 4.6 (b), half of the cell would have a high charge density where the overlap is present, and another half is in low charge density area where there is no overlap. But the EM computation performed by HP Momentum assumes each cell is with a constant charge density, the simulator would approximate the strongly-varying charge in the cell with a constant and this can cause large errors in the simulation.

To overcome these problems, instead of treating the overlap and access line as a whole device, they can be meshed separately. To achieve this, the overlap and access lines are regarded as separate objects and drawn separately in the layout window of HP Momentum. Through this technique, different meshes can be applied to different objects. So, a finer mesh is assigned to the overlap area and a normal mesh to the access lines. This will significantly reduce the simulation time. More importantly, this can avoid creating meshes that cross the border of the discontinuity. This is shown in Figure 4.6 (c). We can see that the overlap area has much denser mesh and there is no mesh across the border.

4.4.3 Mesh Parameters

Logically, the more cells that are used, the more accurate will be the simulation. But too many cells will slow down a simulation and provide little improvement in accuracy.

EM simulation tools can accurately model a wide range of RF/microwave structures and can be more efficiently used if the user is aware of the sources of error. One principal error, that is common to most all the numerical methods, is due to the finite cell or mesh size. These EM simulators divide an RF/microwave structure into subsections or cells with 2D or 3D meshing, and then solve Maxwell's equations within these cells. Larger cells yields faster simulations, but at the expense of larger

errors. Errors are diminished by using smaller cells, but at the cost of longer simulation times. It is important to learn if the errors in the simulation are due to mesh-size errors. This can be done by repeating the EM simulation using different mesh sizes and comparing the results, which is known as a convergence analysis.

In order to determine a suitable cell size for the simulation of multilayer overlap, a number of simulations were carried out using different mesh sizes. Figure 4.7 shows the simulated dBS21 and Phase S21 of a 200 μm multilayer overlap at 6GHz with

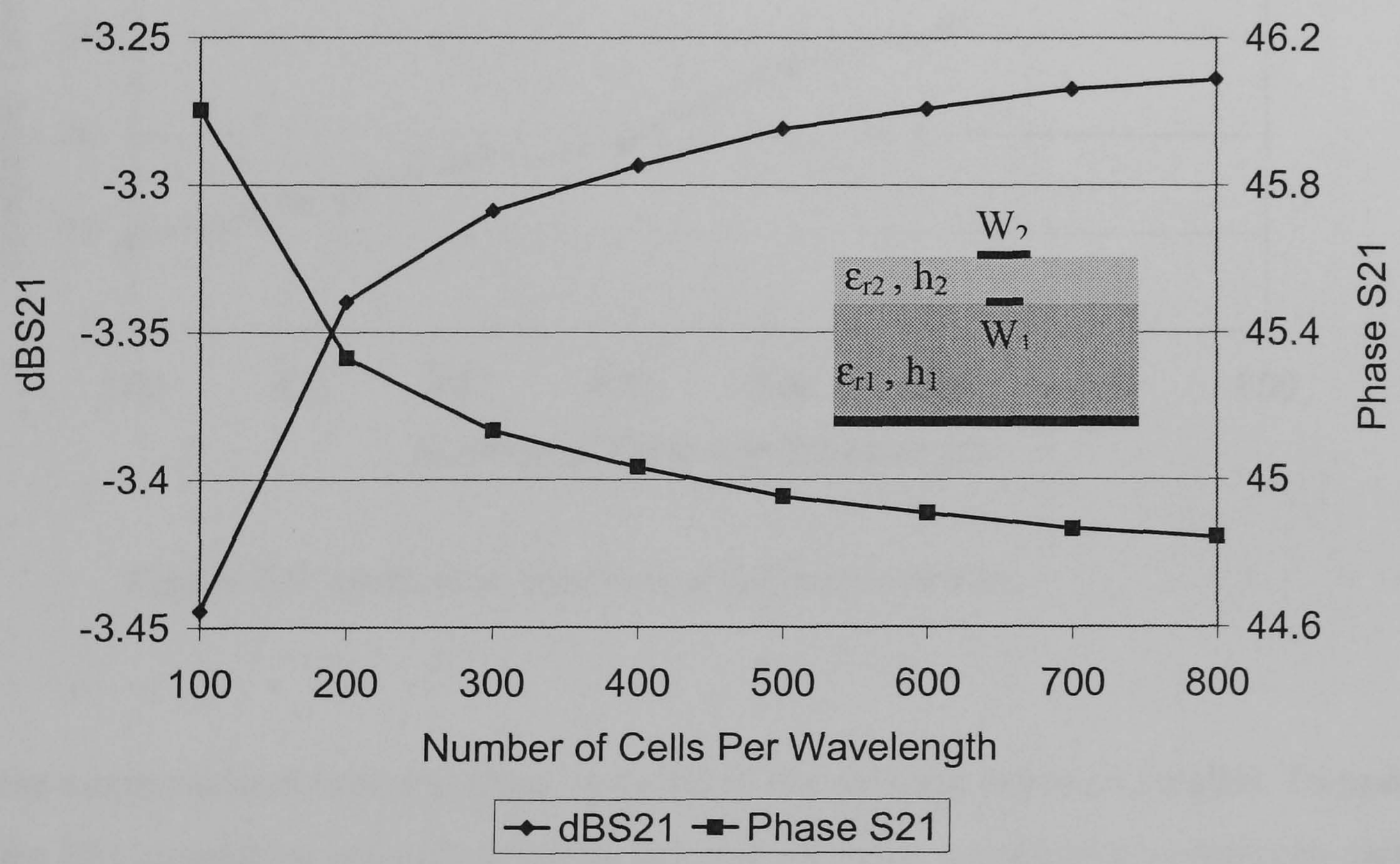

Figure 4.7: Simulation of 200μm multilayer overlap with different cell size at 6GHz (ε_{r1}=9.8, h_1=635μm, ε_{r2}=8, h_2=28μm, W_1=605μm W_2=680μm)

different mesh size. The transmission line mesh cells are fixed at 10 cells width. Figure 4.8 shows the required simulation time versus different cell size. It is seen when the mesh cells covering the overlap are 100 per wavelength, the simulation results are far from convergence and consequently would lead to an incorrect

prediction. However, as the cell size becomes smaller, the simulation results approach convergence ones and show no significant changes when the number of cells per wavelength reaches 500. However, as can be seen from Figure 4.8, which shows the required simulation time versus different number of cells per wavelength,

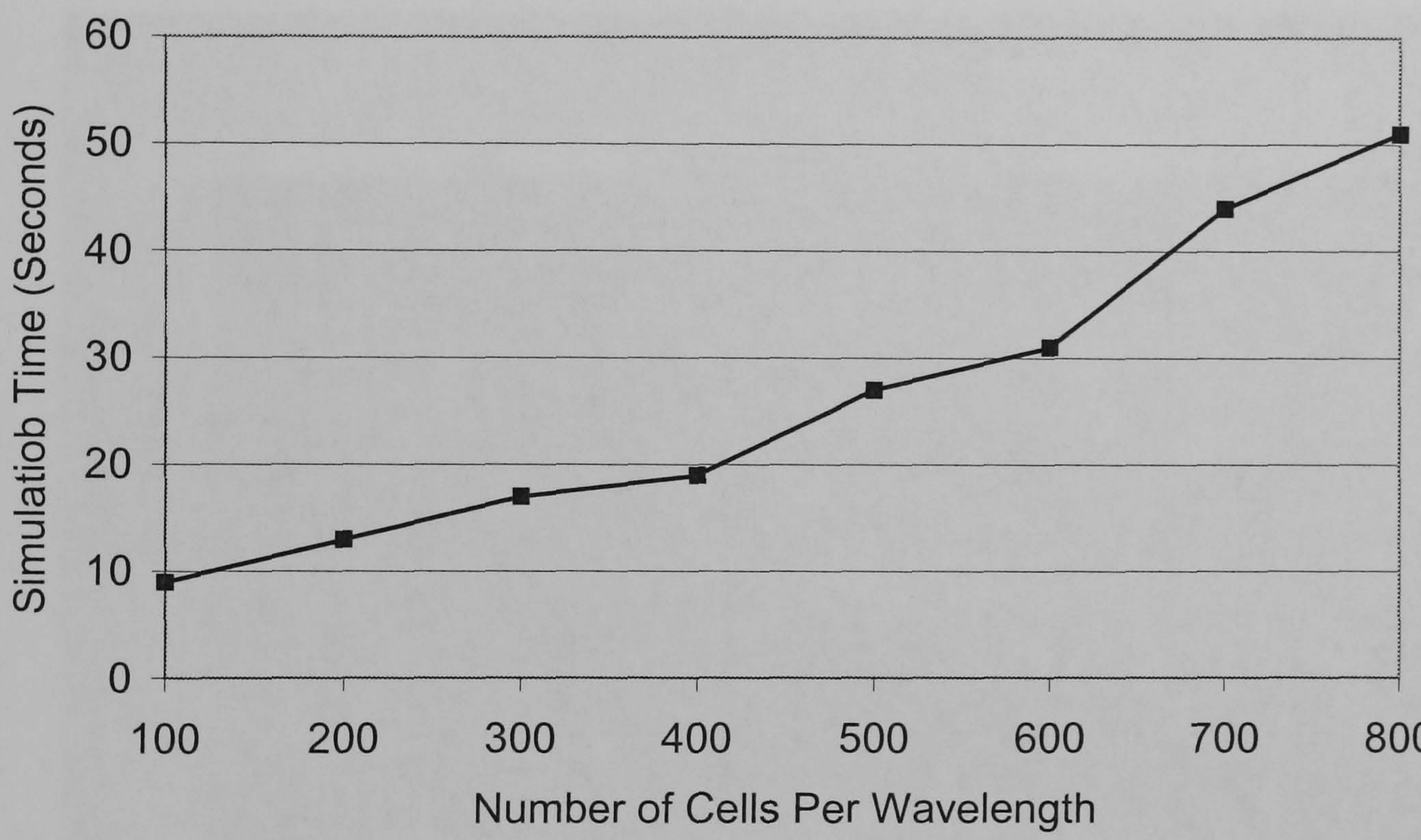

Figure 4.8: simulation time versus different cell size

the computational time increases very fast as the cell size becomes smaller. To make the EM simulation not only accurate but also efficient, a compromise between mesh size and accuracy has to be established.

4.5 Simulation Results

The S parameters of multilayer overlaps were calculated at the proposed centre frequency of the filter using HP Momentum (Figure 4.9), following the simulation techniques suggested in the previous sections.

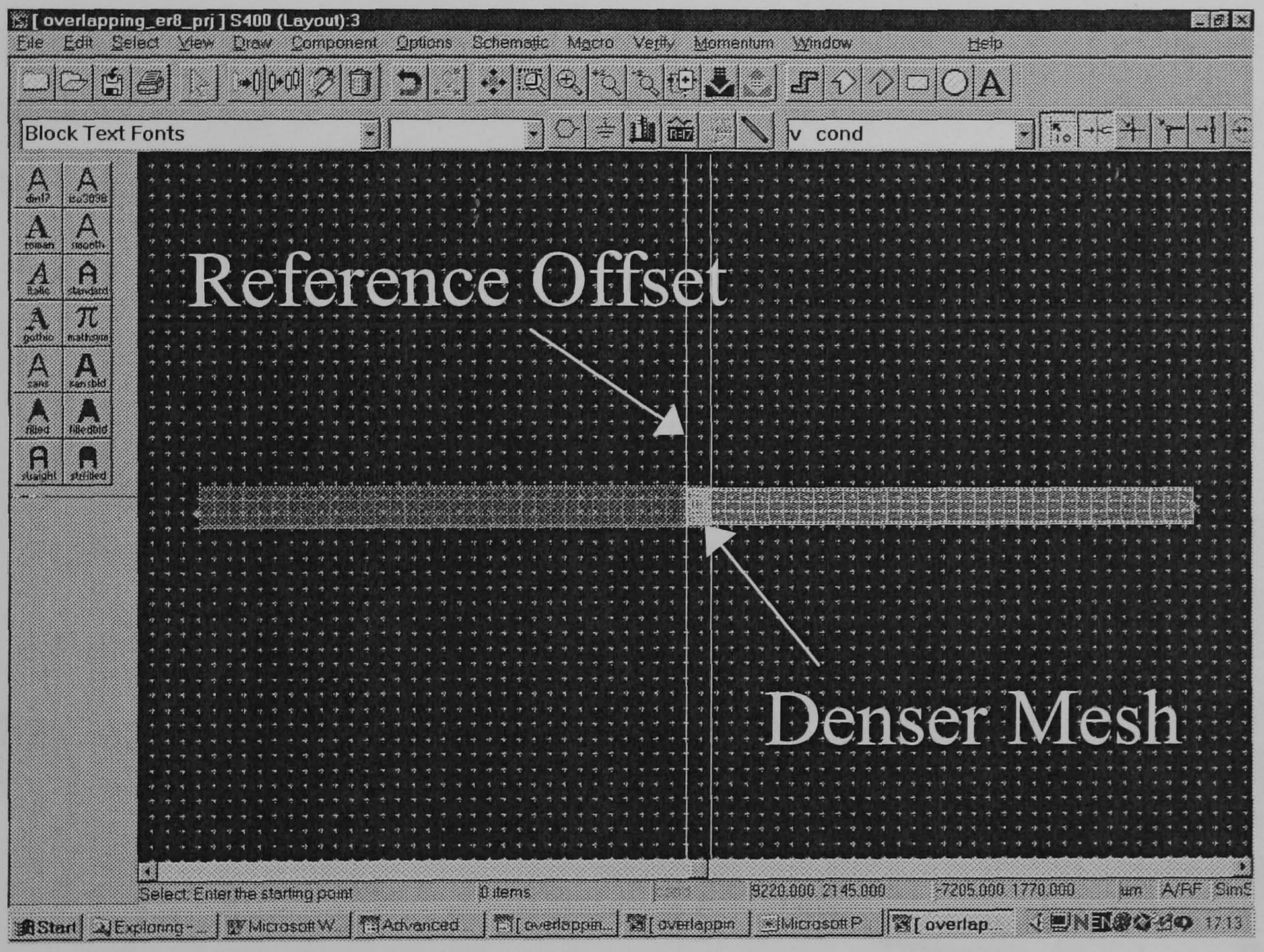

Figure 4.9: Simulation of multilayer overlap using HP Momentum

The dependence of the transmission performance with different overlap size when the thick-film dielectric layer has dielectric constant of 3.9 and thickness of 30μm is shown in Figure 4.10. Figures 4.11 and Figure 4.12 show the calculated transmission performance at 6GHz and 10GHz, for multilayer overlaps using the parameters for a thick-film dielectric that has a dielectric constant of 8 and a thickness of 28μm. The calculation is only performed for these two particular thick-film dielectric materials

because they were the materials available for this study. The characteristic impedance of the resonators is 50Ω and the corresponding width of the multilayer lines is obtained using the method described in Chapter 3.

It is seen that a very wide range of coupling coefficients is possible depending on the amount of overlap, giving the chance to design filters with wider bandwidth.

The graphs obtained here are very useful and will be used in the design of multilayer end-coupled filters for the determination of appropriate gap dimensions to achieve the required bandwidth.

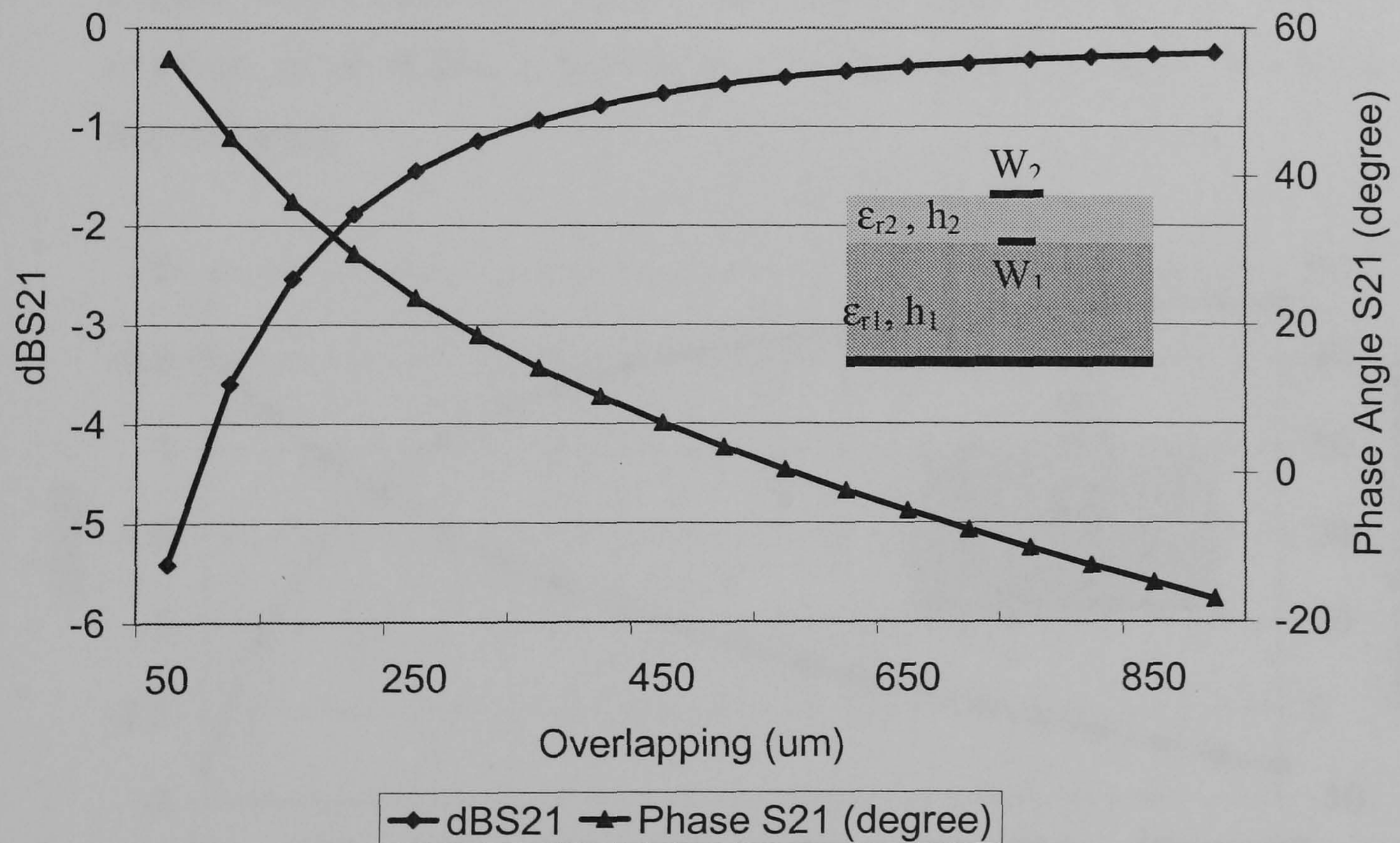

Figure4.10: Calculated dBS21 and phase angle of S21 of multilayer overlaps at 10GHz.(ε_{r1}=9.8, h_1=635μm, ε_{r2}=3.9, h_2=30μm,W_1=600μm, W_2=730μm)

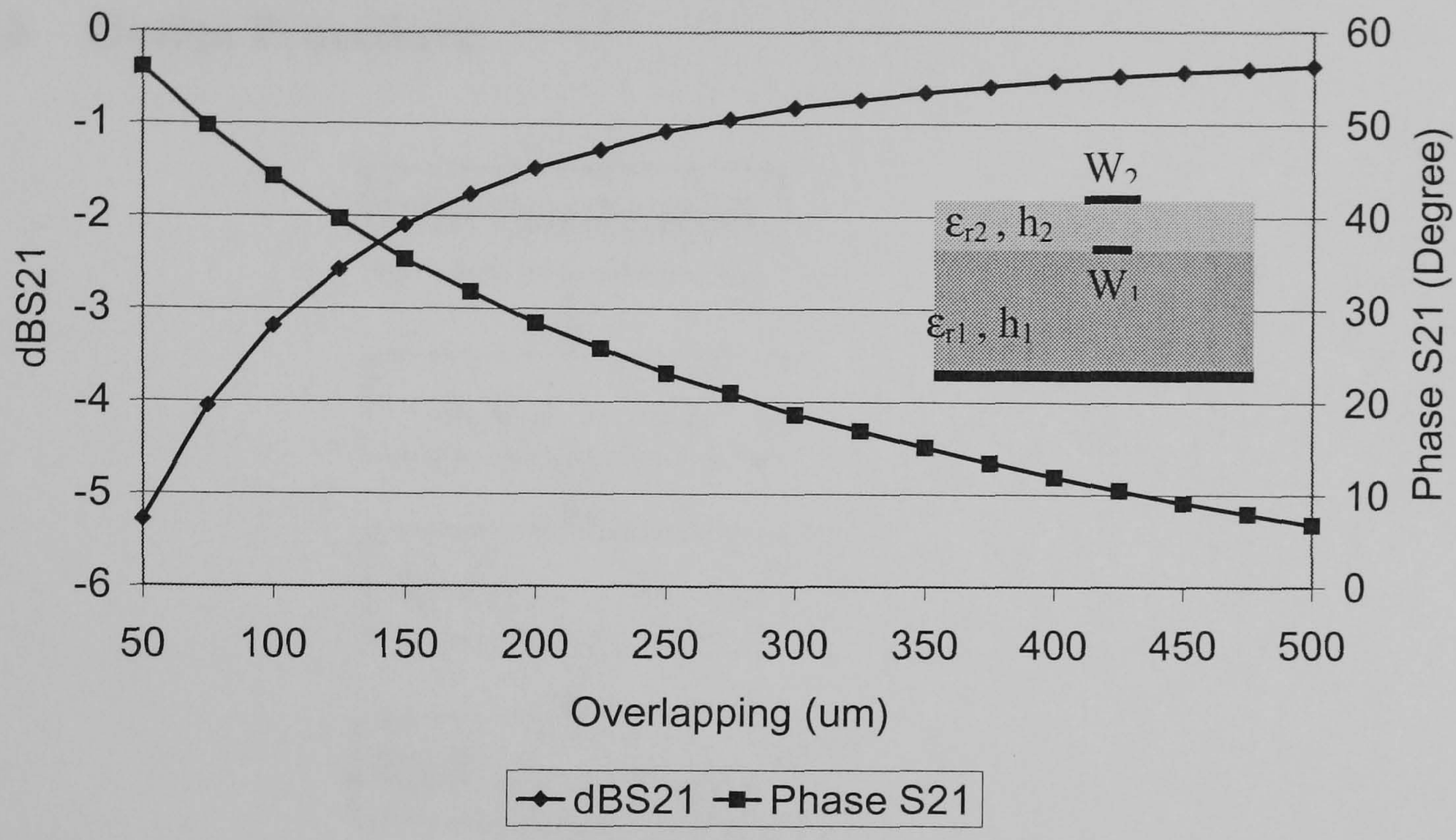

Figure 4.11: Calculated dBS21 and phase angle of S21 of multilayer overlaps as at 6GHz. (ε_{r1}=9.8, h_1=635μm, ε_{r2}=8, h_2=28μm, W_1=605μm W_2=680μm)

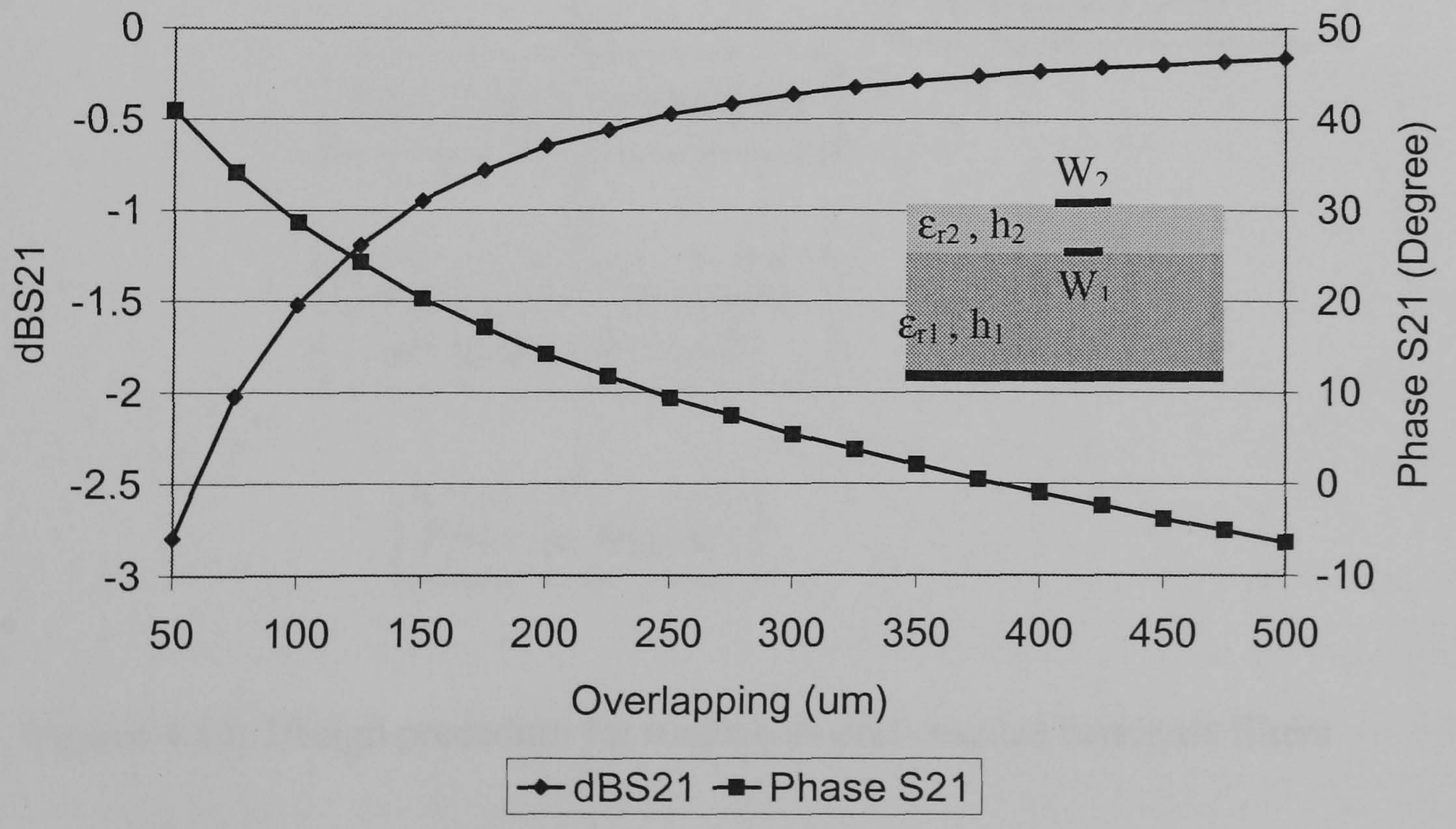

Figure 4.12: Calculated dBS21 and phase angle of S21 of multilayer overlaps at 10GHz. (ε_{r1}=9.8, h_1=635μm, ε_{r2}=8, h_2=28μm, W_1=605μm W_2=680μm)

4.6 Design Procedure

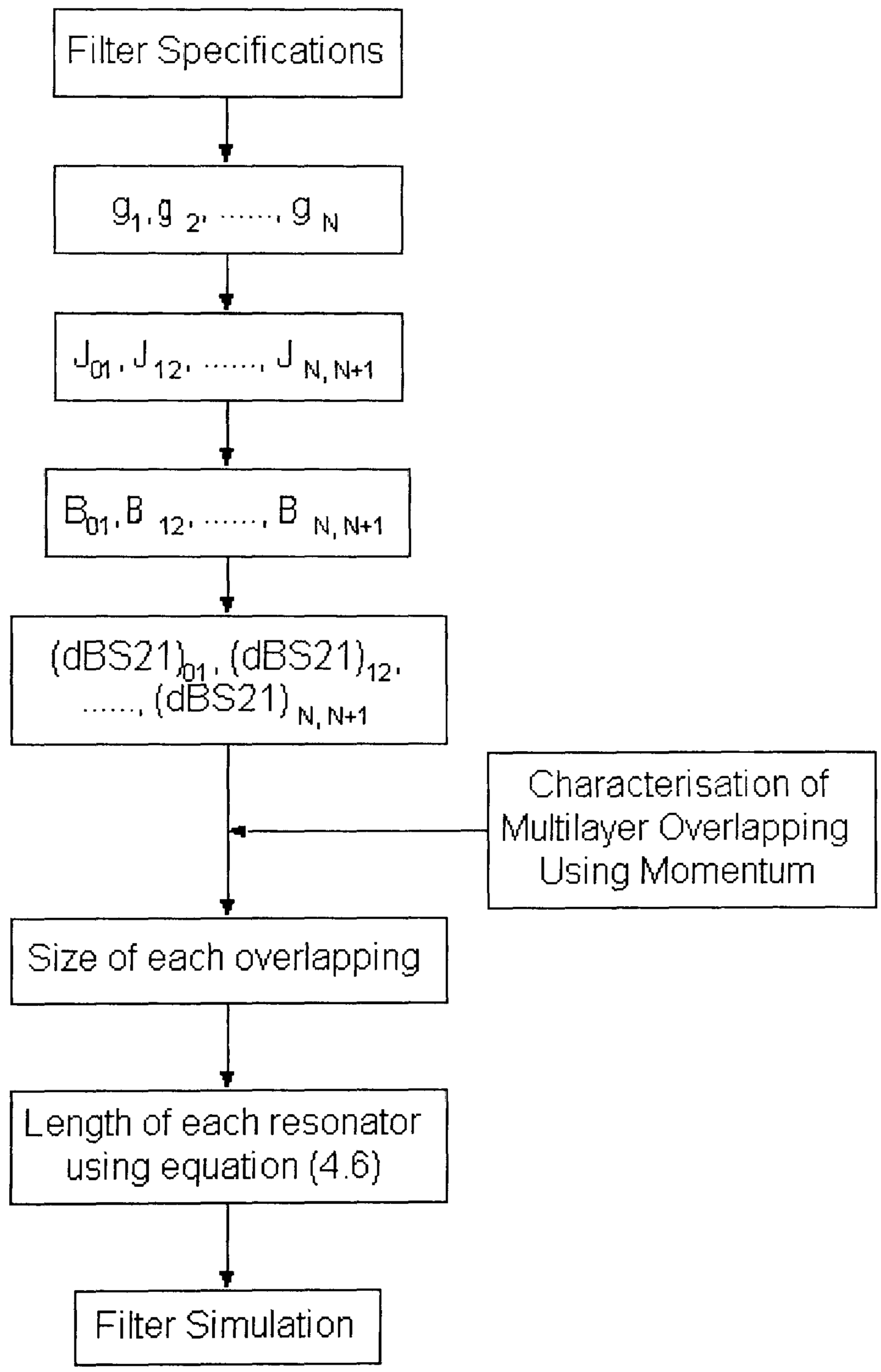

Figure 4.13: Design procedure for multilayer end-coupled bandpass filters

The overall design procedure developed for multilayer end-coupled bandpass filters is summarized in Figure 4.13. This procedure can be divided into four parts:

1. Evaluation of the susceptance for each coupling gap. This is the same as for a single layer structure.

2. Characterization of multilayer overlap using EM calculation. This is a crucial part of the design of multilayer end-coupled filters.

3. Determination of the physical dimensions of the filter including the width of the resonator, the amount of overlap and the length of the resonator.

4. Simulation of the filter.

EM simulation of the whole filter would be tremendously time-consuming as the length of the overall filter is of around three wavelengths. Thus a combination of EM simulation and circuit simulation has been used to simulate multilayer end-coupled filters as discussed in the following section.

4.7 Filter Simulation

Figure 4.14 shows the general layout of a multilayer end-coupled filter, where W_1 and W_2 are the widths of the top and bottom resonators, respectively. S_0, S_1, S_2 and S_3 are the multilayer coupling overlaps between each resonator, and they have geometric symmetry about the centre of the filter structure. l_1, l_2, ... l_6 are the lengths of the resonators. They also exhibit symmetry. Note that the resonators on different layers have different physical lengths, although they have the same electrical length.

To illustrate the procedure, the design of a particular filter is considered. A multilayer end-coupled bandpass filter is to be designed to have a fractional bandwidth (δ) of 35%, with a centre frequency (f_0) of 6GHz. A six-pole (n=6) Chebyshev lowpass prototype with 0.1 dB passband ripple is chosen. The filter specifications are summarized in Table 4.1. The physical dimensions of the filter are shown in Table 4.2. The detailed calculation procedure of the filter will be presented in the next section. The simulation methodology for the filter is the main interest in

the current section.

After obtaining the physical dimensions of the filter, it is necessary to simulate the filter so as to verify the design before the fabrication.

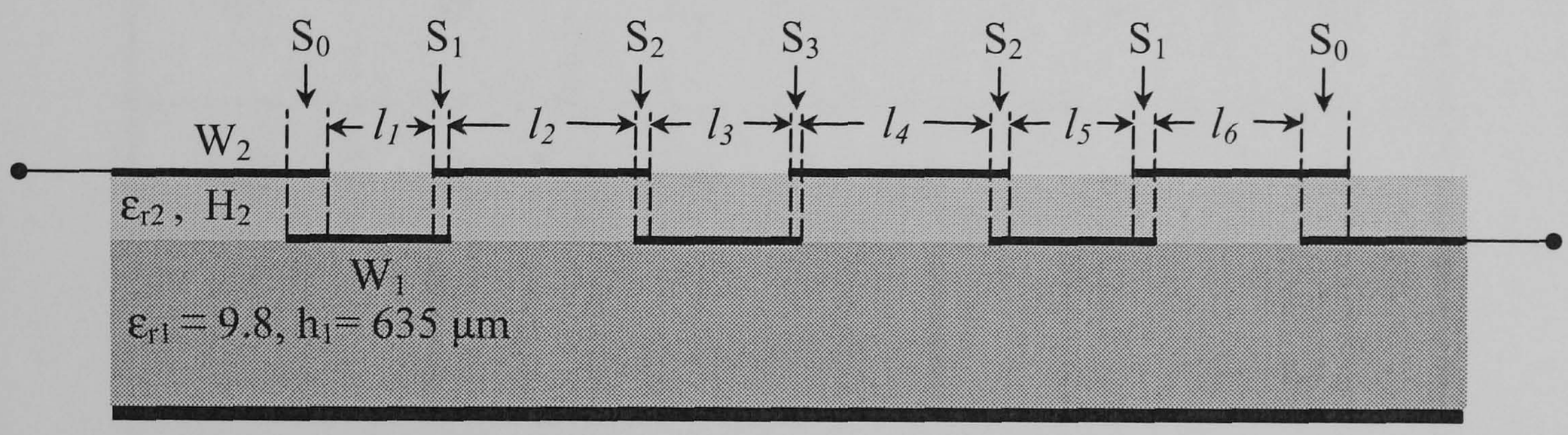

Figure 4.14: The layout of a multilayer end-coupled filter

Table 4.1: Specifications of a multilayer end-coupled filter

Design Frequency	Bandwidth	Ripple	ε_{r1}	h_1	ε_{r2}	h_2
6 GHz	35%	0.1 dB	9.8	635μm	8	28 μm

Table 4.2: Geometrical dimensions of a filter(unit: μm)

Line Width		Multilayer Overlap			
W_1	W_2	S_0	S_1	S_2	S_3
680	605	450	120	65	60
Resonator Length					
l_1	l_2	l_3	l_4	l_5	l_6
6018	7403	7503	7754	7163	6220

Ideally, the most accurate and straightforward simulation method for a filter of this kind would be to use an EM simulator such as HP Momentum to simulate the whole structure. Figure 4.15 shows the layout of the filter in the HP Momentum layout window. The red tracks are the resonators in the top conductor layer and the yellow

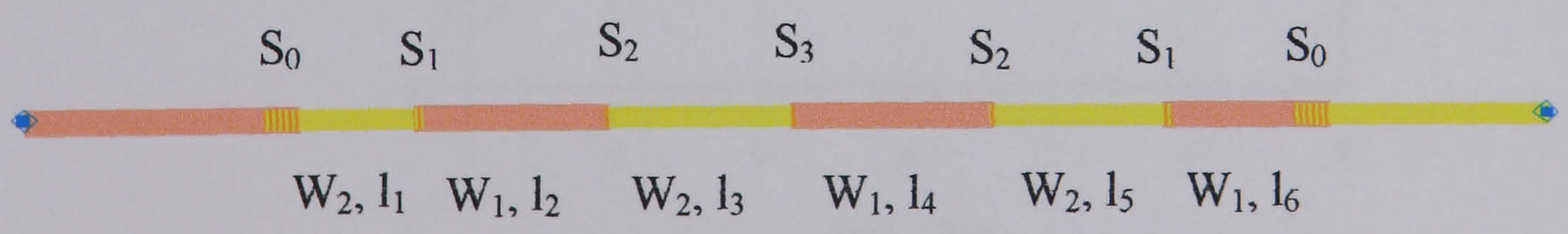

Figure 4.15: Simulation of a multilayer end-coupled filter using HP Momentum

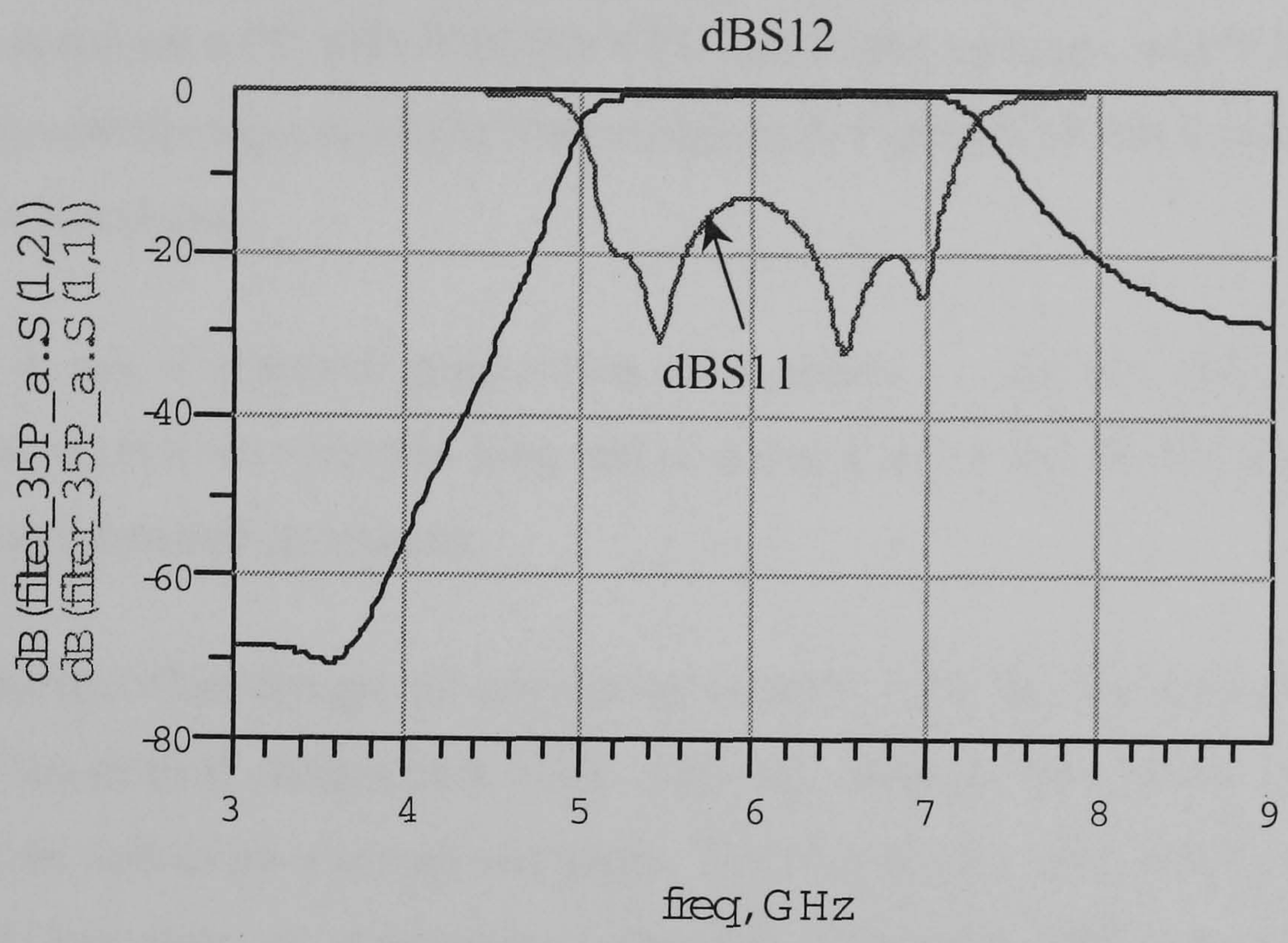

Figure 4.16: Filter response simulated using EM simulator

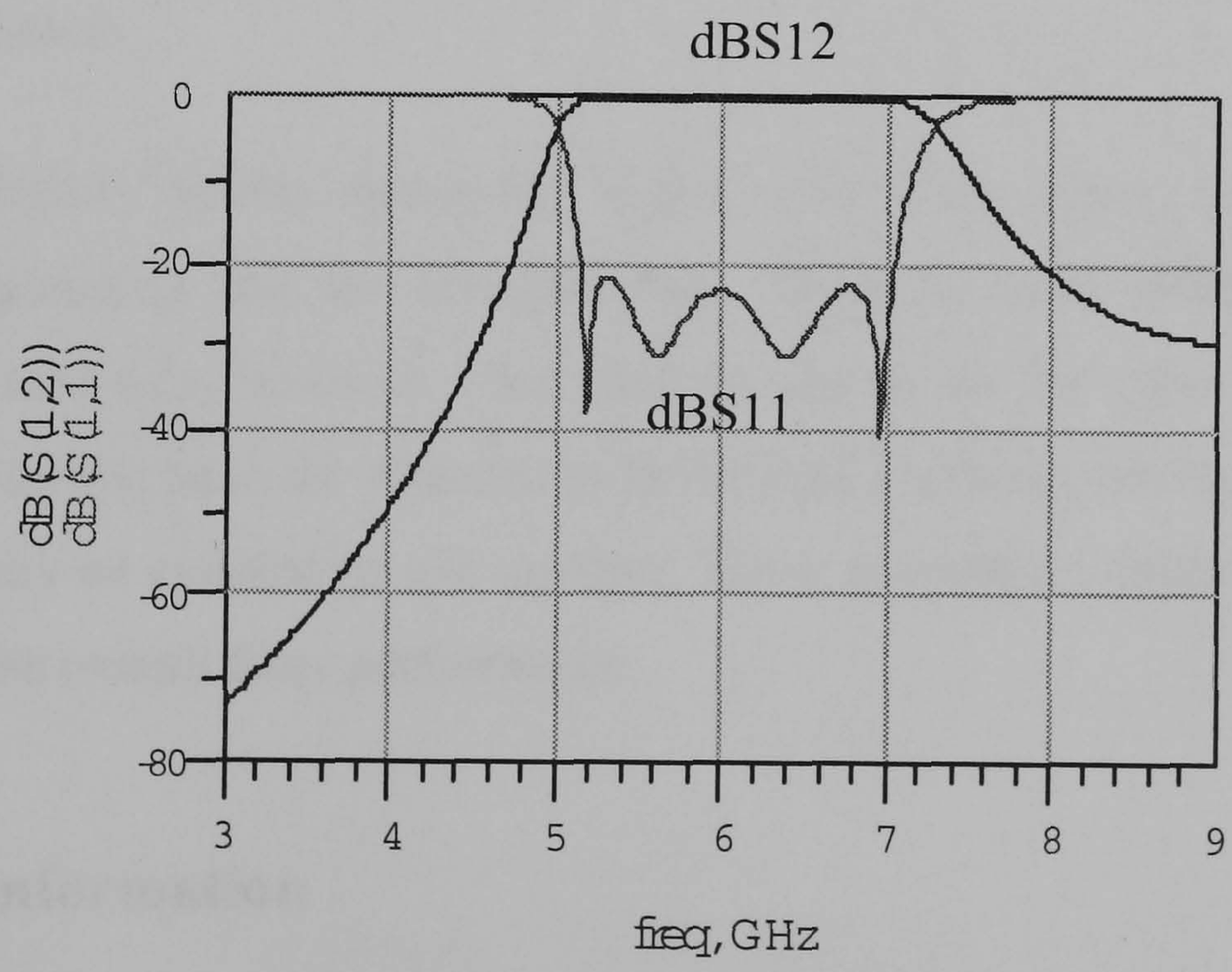

Figure 4.17: Filter response simulated using circuit simulator

lines show the resonators, which are positioned in the bottom conductor layer. The simulation is run on a PC with 800MHz CPU and 256M memory, and Windows NT 4.0. The simulated response of the filter is shown in Figure 4.16 and it took 36 hours to finish the simulation.

Clearly it is not a practical proposition to simulate a complete filter structure, because it is several wavelengths long and contains a lot of non critical sections that do not warrant detailed simulation.

To speed up the filter design, an alternative solution is to use the EM simulator to just model the critical components of the structure, such as the multilayer overlaps, that cannot be solved by a circuit simulator. These critical components can then be represented by their S parameters, obtained from the EM simulation, and implemented into the circuit simulator. The whole circuit is then simulated using a circuit simulator, thus achieving good design efficiency. The simulated results for the filter using this approach are given in Figure 4.17. It only takes 10 to 20 seconds to obtain the simulation results, once the multilayer overlaps have been characterized using EM simulation.

The two simulation results essentially agree with each other, especially the bandwidth performance and the insertion loss. There is some difference in the magnitude of return loss, however. This may be due to the fact that in the circuit simulation, the various parts are assumed to be isolated elements, but in the real filter structure they may be coupled to one another. These unwanted couplings may have some effect on the overall filter performance.

4.8 Design Information

As an example of the design approach that has been used, a multilayer end-coupled bandpass filter has been designed and the detailed design procedures and data are presented in this section.

The filter specification was:

fractional bandwidth: $\delta = 0.4$ (40%)

centre frequency: $f_0 = 10$GHz

Chebyshev response with 0.1 dB passband ripple

A six-pole (n=6) lowpass prototype was chosen whose element values are:

g_0	g_1	g_2	g_3	g_4	g_5	g_6	g_7
1	1.1681	1.4039	2.0562	1.517	1.9029	0.8618	1.3554

J parameters are calculated using Equations (4.1) to (4.3):

J_{01}	J_{12}	J_{23}	J_{34}
0.01466	0.00982	0.0074	0.00712

The susceptances associated with the J-inverters are calculated using Equation (4.4):

B_{01}	B_{12}	B_{23}	B_{34}
0.03174	0.01292	0.00856	0.00814

The corresponding dBS21 values for each multilayer overlap are listed in the table below:

$(dBS21)_{01}$	$(dBS21)_{12}$	$(dBS21)_{23}$	$(dBS21)_{34}$
-0.411	-2.038	-3.733	-3.991

For multilayer microstrip implementation, we used substrate having the following data:

ε_{r1}	h_1	ε_{r2}	h_1
9.8	635μm	8	28 μm

The line width for microstrip half-wavelength resonators is chosen to give a characteristic impedance, Z_0, of 50Ω for good matching performance and simplicity The widths and guide wavelengths are obtained through the analysis described in Chapter 3:

W_1	W_2	λ_{g1}	λ_{g2}
680	605	11534 at 10GHz	11160 at 10GHz

Unit: μm

Using the graph obtained in Section 4.5, the size of the multilayer overlaps can be determined and these are listed below, along with the phase shifts through the multilayer overlaps:

Overlap	S_0	S_1	S_2	S_3
Size (μm)	345	75	30	25
Phase shift	-2.3°	34.2°	47.5°	49.4°

The electrical lengths of the half-wavelength resonators after absorbing the negative electrical lengths attributed to the J-inverters are determined by using Equation (4.6),

and the physical length of each section can be calculated using the information on the guided wavelength in the multilayer structure that was obtained previously.

Resonator Length					
l_1	l_2	l_3	l_4	l_5	l_6
106°	131°	138°	138°	131°	106°
3286 μm	4197 μm	4278 μm	4421 μm	4061 μm	3396 μm

Now we have all the physical dimensions required for the design of a multilayer end-coupled filter. The simulated response of the filter is shown in Figure 4.18. It is seen that the filter has bandwidth of 40% with a centre frequency at 10 GHz, and this meets the specification.

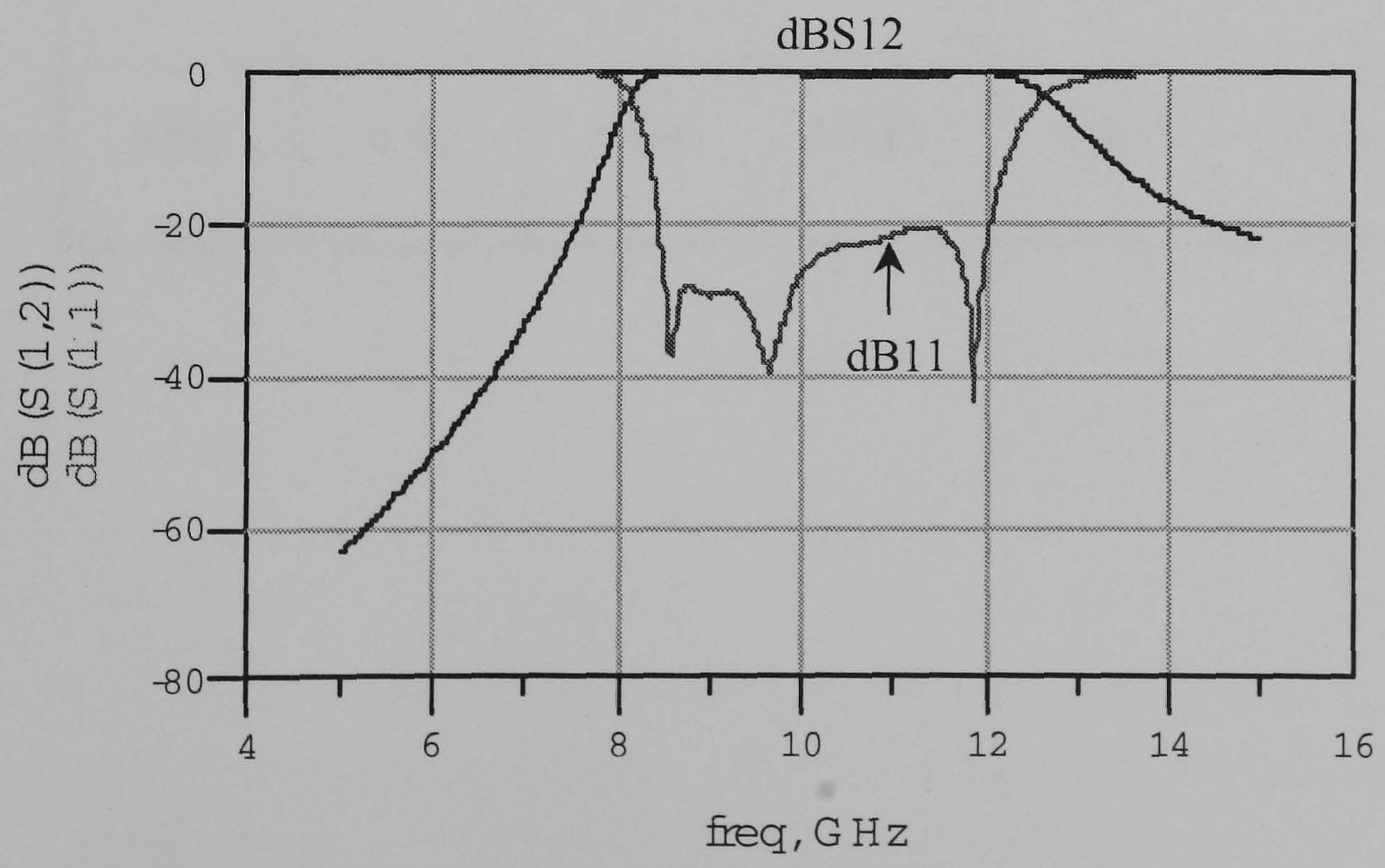

Figure 4.18: Simulated performance of 40% filter centred at 10 GHz

Using the same procedure, a 30% filter was designed using the same multilayer substrate. The design data are listed in Table 4.3, and Figure 4.19 shows the simulated results.

Table 4.3: Design data for a 30% filter (unit: μm)

Line Width		Overlap			
W_1	W_2	S_0	S_1	S_2	S_3
680	605	185	30	8	7
Resonator Length					
l_1	l_2	l_3	l_4	l_5	l_6
122°	143°	148°	148°	143°	122°
3782	4582	4588	4742	4433	3909

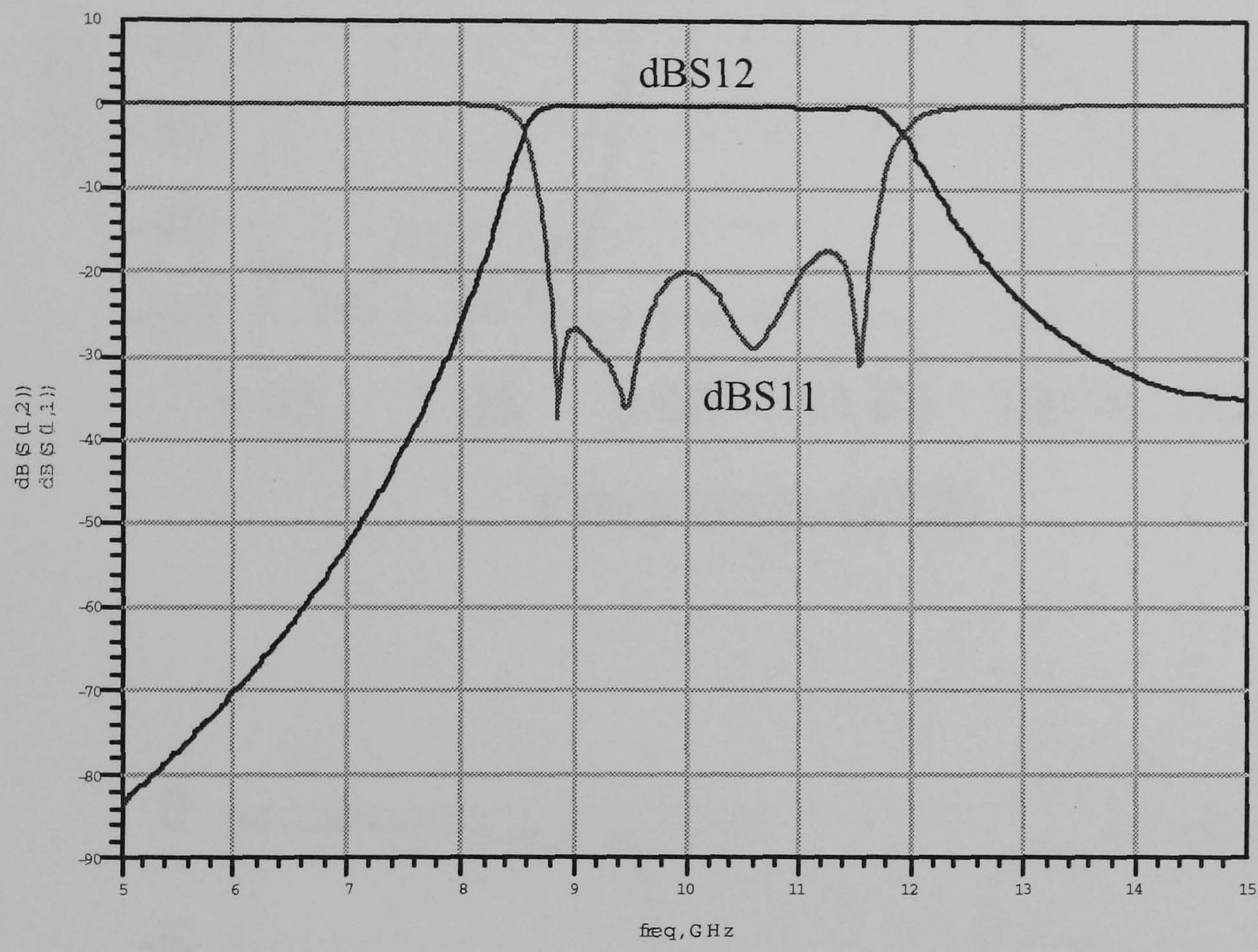

Figure 4.19: Simulated response of a 30% filter

4.9 Test Results

The filters were fabricated using the thick-film process that was described earlier. For testing, each filter was mounted in a Wiltron Universal Test Fixture, and this was connected to a HP 8510 Vector Network Analyzer. Figures 4.20 and 4.21 show the measured results for the multilayer end-coupled filter with the bandwidth of 30% and 40% respectively. Very broad bandwidths have been successfully achieved, and this is a significant improvement over filters fabricated using a single layer structure.

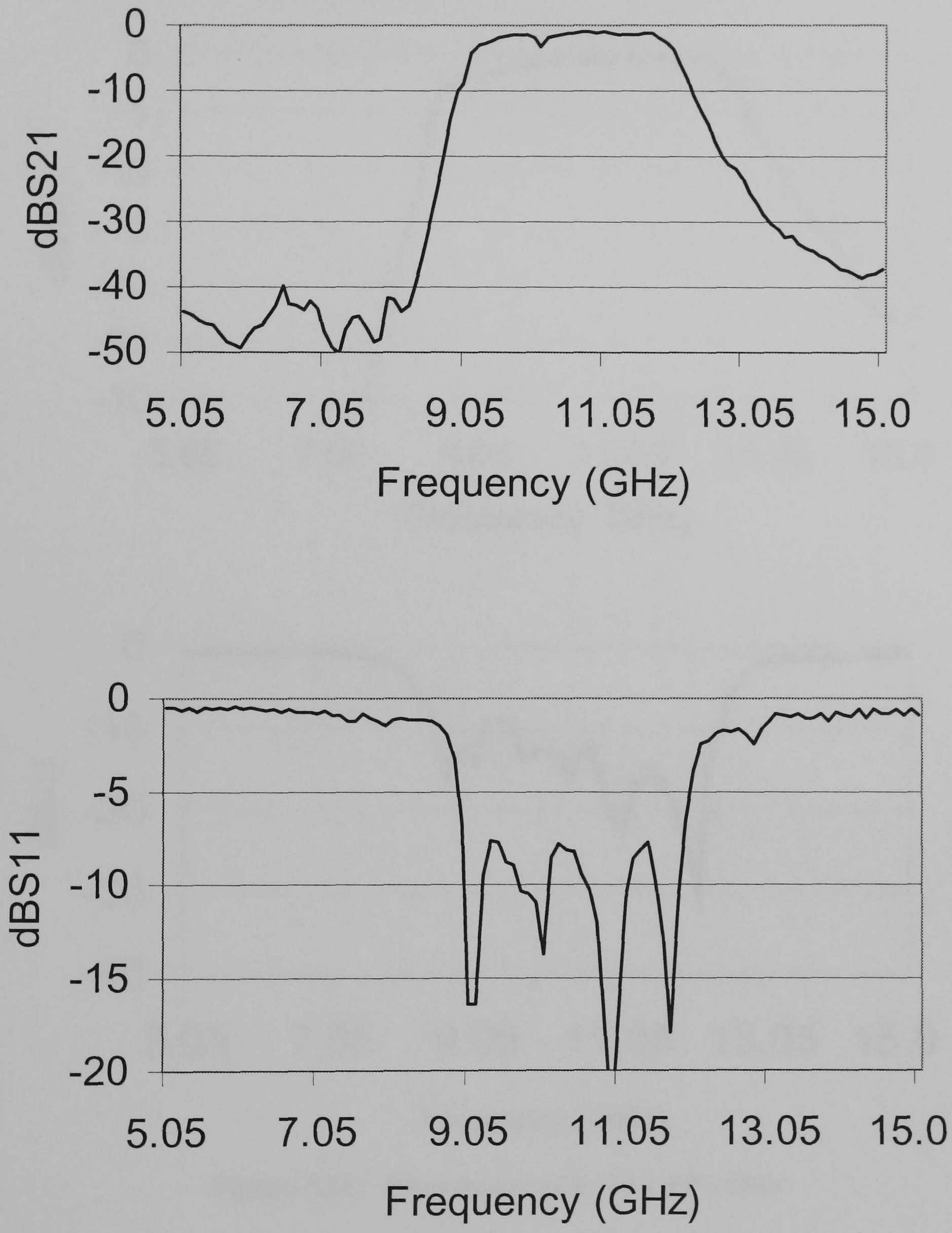

Figure 4.20: Measured results for a 30% filter

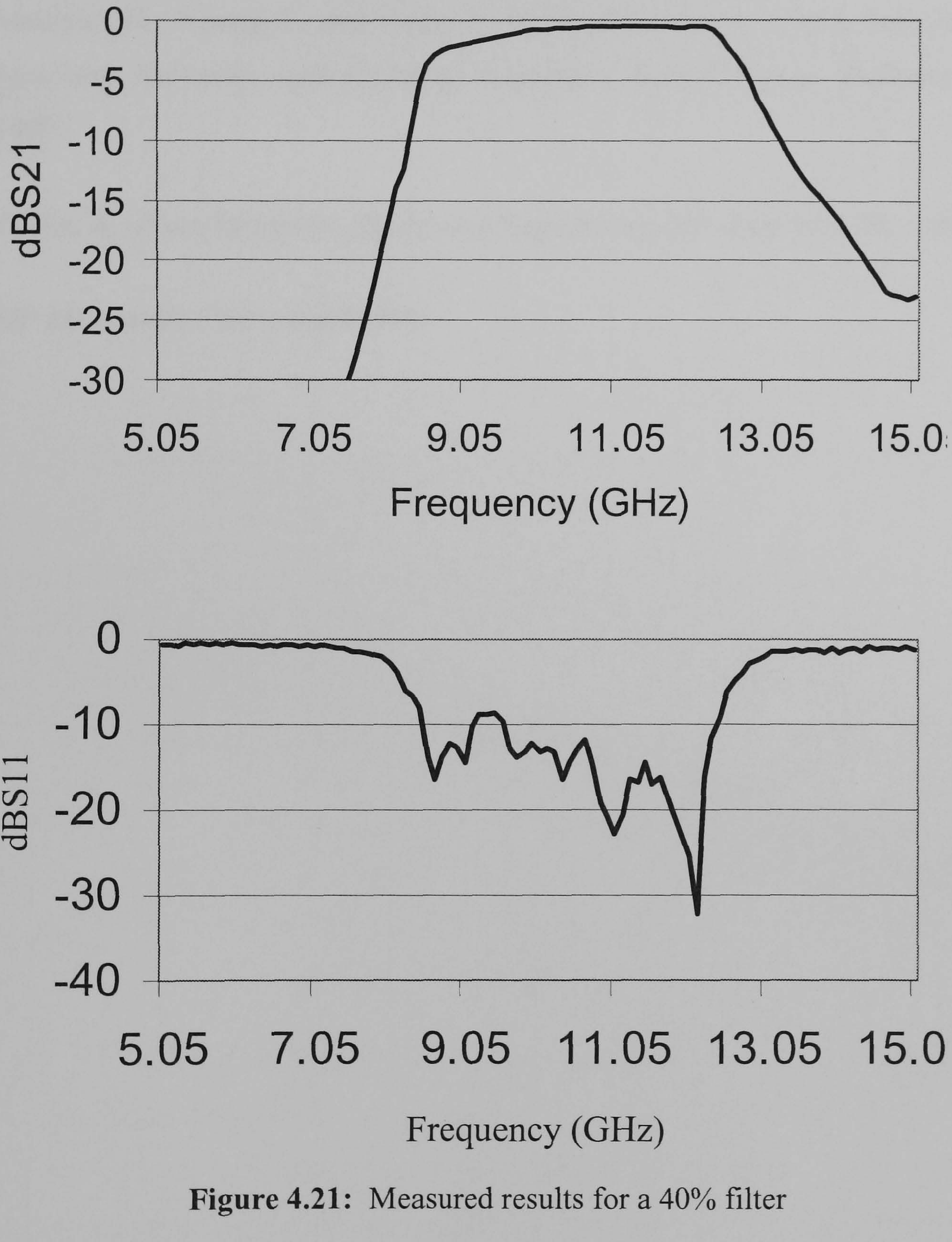

Figure 4.21: Measured results for a 40% filter

4.10 References

[1] Matthaei, G., Young, L. and Jones, E. M. T., *Microwave Filters, Impedance – Matching Networks, and Coupling Structures*, Artech House, Dedham, MA, 1990.

[2] Collin, R., *Foundations for Microwave Engineering*, McGraw-Hill, Inc. 1992

[3] *HP Momentum User's Guide*, HP.

Chapter 5

Broadband Multilayer DC Blocks and Coupled-line Bandpass Filters

5.1 Summary

A quarter wavelength two-port coupled-line section forms the basic building block in the design of coupled-line filters and DC blocks. In this chapter the concept of the multilayer structure is applied to the two-port coupled-line section so as to achieve stronger coupling between the two coupled-lines and hence broaden the bandwidth of the device. Novel, octave band DC blocks have been designed, fabricated and tested using a new multilayer format. The tight coupling required between the coupled-lines was realized by overlapping these lines in a multilayer structure. Very good agreement was obtained between measured and simulated data. Multilayer techniques have also been applied to the design of coupled-line bandpass filters where an 80% bandwidth has been achieved.

5.2 Multilayer DC Blocks

5.2.1 Circuit Configuration

Microstrip DC blocks are convenient circuit components because they permit the isolation of the bias DC voltages while acting as a bandpass filter for microwave signals. In RF and microwave circuits, a 3-dB backward-wave coupled-line section with open circuit terminations can be used instead of a series capacitor to form series DC block [1-4]. This overcomes the problems of surface mounting the capacitor, and also eliminates the parasitics associated with lumped components at microwave frequencies. With the traditional single layer microstrip arrangement, that uses two closely spaced coupled-lines, correct RF-DC isolation can only be obtained over a

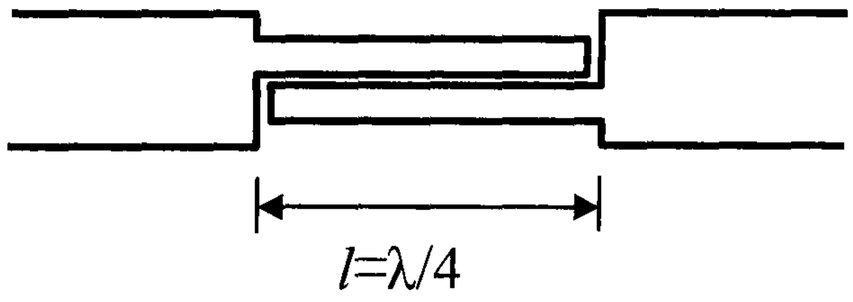

Figure 5.1: Physical layout of a DC block

small frequency range due to the requirement for a very small gap (often less than 20μm) between the coupled-lines. The physical layout of this type of component is shown in Figure 5.1.

Using a multilayer structure, a new form of DC block has been designed, where the tight coupling is achieved by overlapping conductors on different dielectric layers. Figure 5.2 shows the cross-sectional and planar views of the new structure.

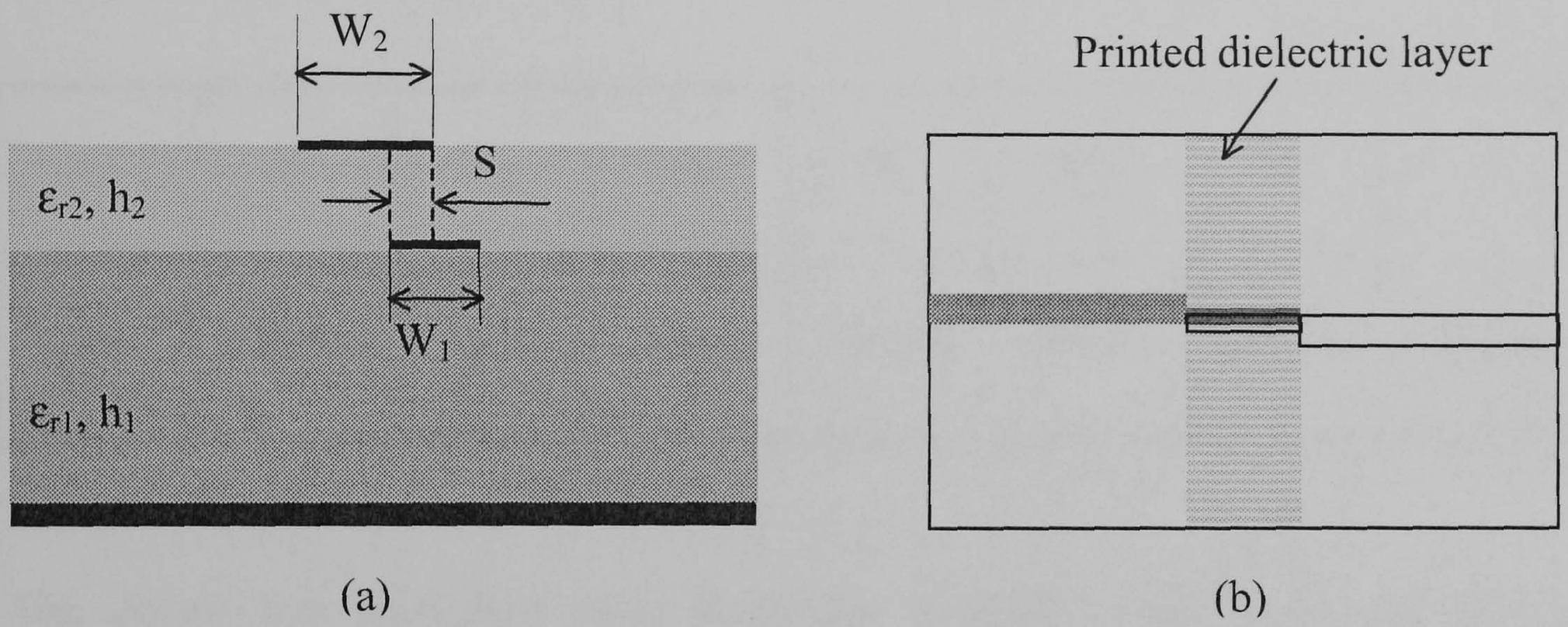

Figure 5.2: Two-layer DC block (a) Cross-sectional view; (b) Top view

5.2.2 Circuit Design and Fabrication

Design equations for symmetrical coupled-lines are well documented in the literature [5]. A multilayer coupled-line section is an asymmetric structure as the two lines are located on different layers and thus have different electric performance. The electromagnetic analysis method, as discussed in Chapter 3, can be applied to the design of multilayer DC blocks.

The amount of overlap is set to a certain value. The widths of the two coupled-lines are then optimized to give good matching performance at the two ports. The substrate information and the physical dimension for the DC block are listed in Table 5.1. The widths of the top and bottom conductor tracks are different. This is to compensate for the changes to the even and odd mode impedance caused by the introduction of the printed dielectric. The top conductor has a wider width than the

bottom conductor as the relative permittivity for the top conductor is lower than that for the bottom conductor, again according to the results obtained in Chapter 3. The length of the coupled region was a quarter-wavelength, as in the traditional edge-coupled, single layer circuit.

Table 5.1: Design data for a DC block centred at 6GHz (ε_{r2}=3.9)

ε_{r1}	h_1	ε_{r2}	h_2	W_1	W_2	S	*l*
9.9	635 μm	3.9	30μm	380μm	300μm	180μm	5080μm

The device was fabricated using thick-film conductors and a standard etching process.

5.2.3 Test Results and Discussion

Measured responses are shown in Figure 5.3. Over an octave band, the worst case measured VSWR and insertion loss were about 1.4 and 0.2 dB, respectively. Very good agreement between the measured and simulated data was obtained.

With the multilayer arrangement, it has been possible to achieve very high coupling between overlap transmission lines over a wide operating frequency range, thus eliminating the need for fine lines and small gaps. The errors caused by poor registration and variations in the dielectric thickness between the two coupled conductors have been examined. The results are shown in Figure 5.4. It can be seen from this data that registration errors of ±10μm and dielectric thickness variations of ±3μm have very little effect on the circuit responses. Normal manufacturing processes can usually be maintained within these error bounds.

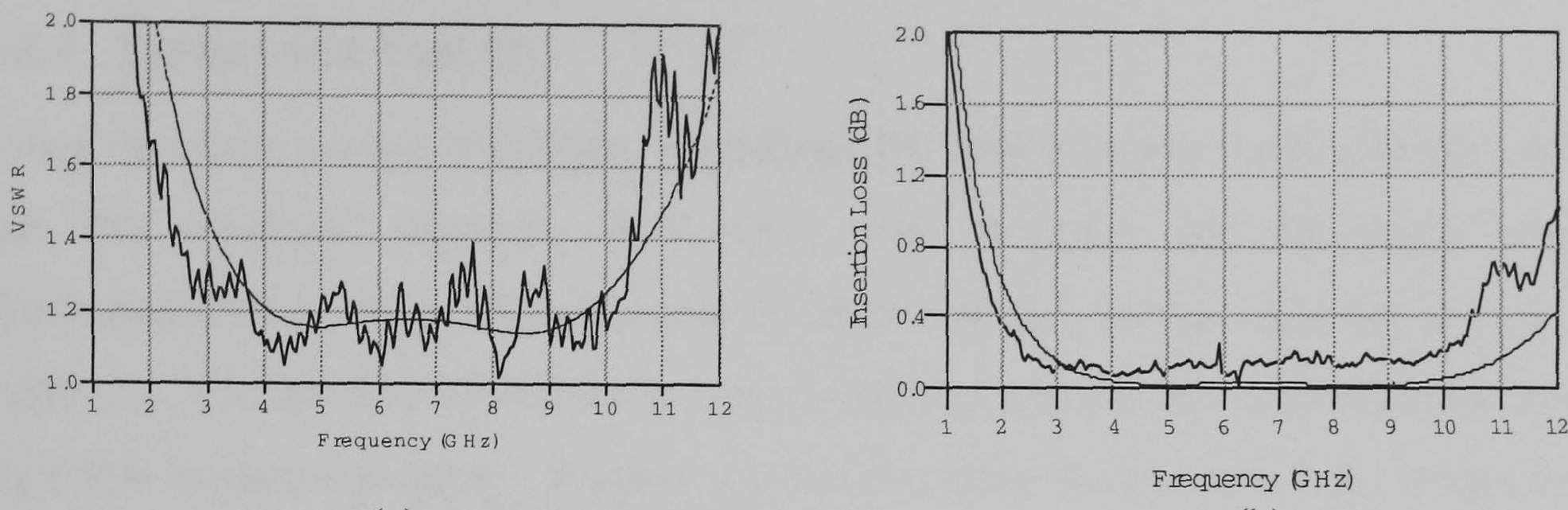

(a) (b)

Figure 5.3: Measured responses of DC block. (a) VSWR. (b) Insertion loss
——— Measured, ——— Simulated.

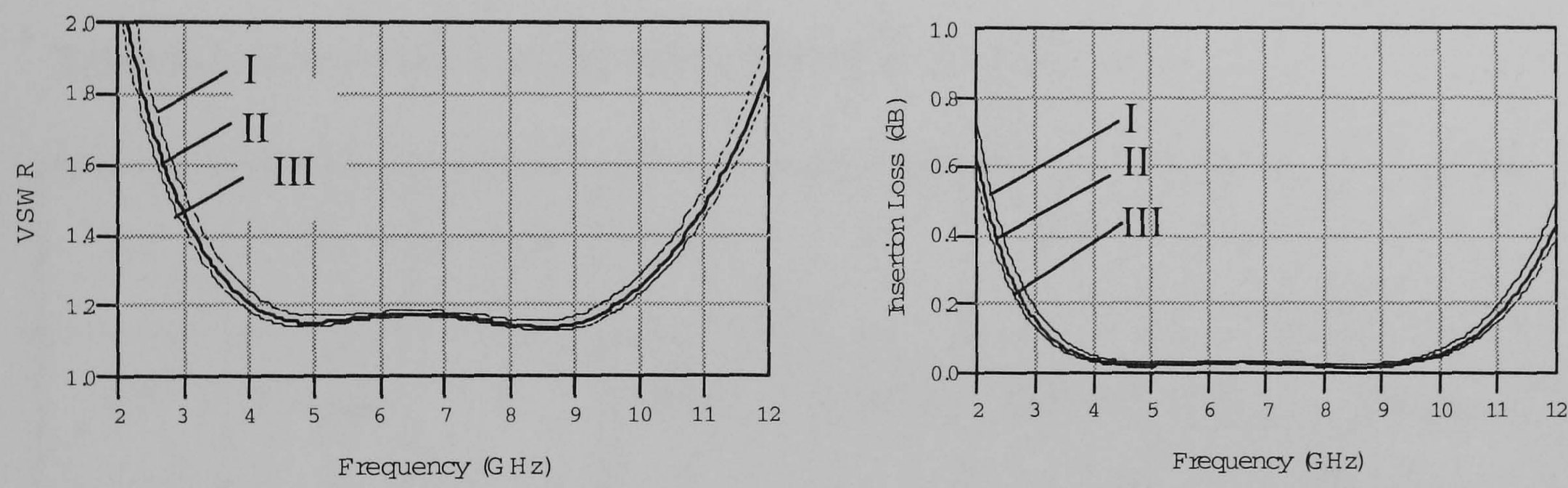

(a) Simulated responses of DC block with different thickness of the printed dielectric layer (I --- 30μm, II --- 27 μm, III --- 25 μm.)

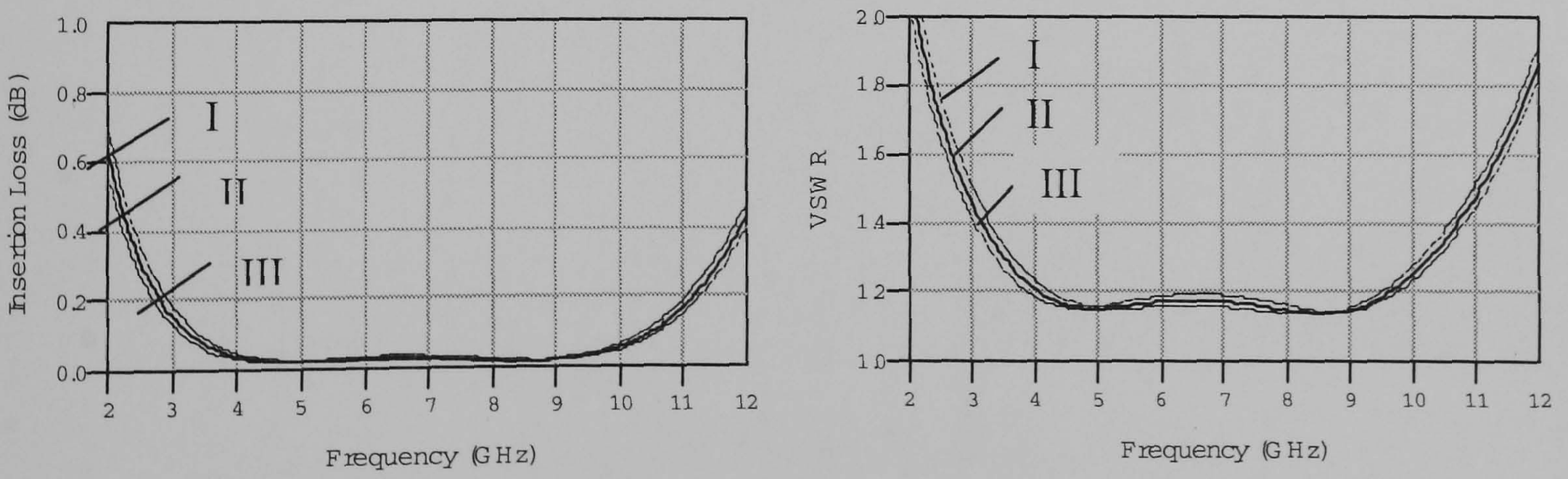

(b) Simulated responses of DC block with different amounts of overlapping, S. (I --- 200μm, II --- 210μm, III --- 220μm.)

Figure 5.4: Simulated responses showing the effect of fabrication tolerances

5.2.4 Design and Test (II)

Using the same design technique, multilayer DC blocks using thick-film dielectric that has dielectric constant of 8 were also designed and fabricated using photoimageable materials maufactured by Hibridas Ltd. Design data are shown in Table 5.2. Several DC blocks have been fabricated and the measured results show good fabrication consistency. Figures 5.5 and 5.6 show the measured performance of two DC blocks. In the frequency range of 2 to 12 GHz, the return loss is better than 15 dB and the insertion loss is around 0.16 to 0.3 dB. Up to 140% bandwidth has been achieved with very low insertion loss due to the novel multilayer structure which gives very strong coupling between the coupled-lines.

Table 5.2: Design data for a DC block centred at 7GHz (ε_{r2}=8)

ε_{r1}	h_1	ε_{r2}	h_2	W_1	W_2	S	*l*
9.8	635 μm	8	28μm	450μm	350μm	300μm	4000μm

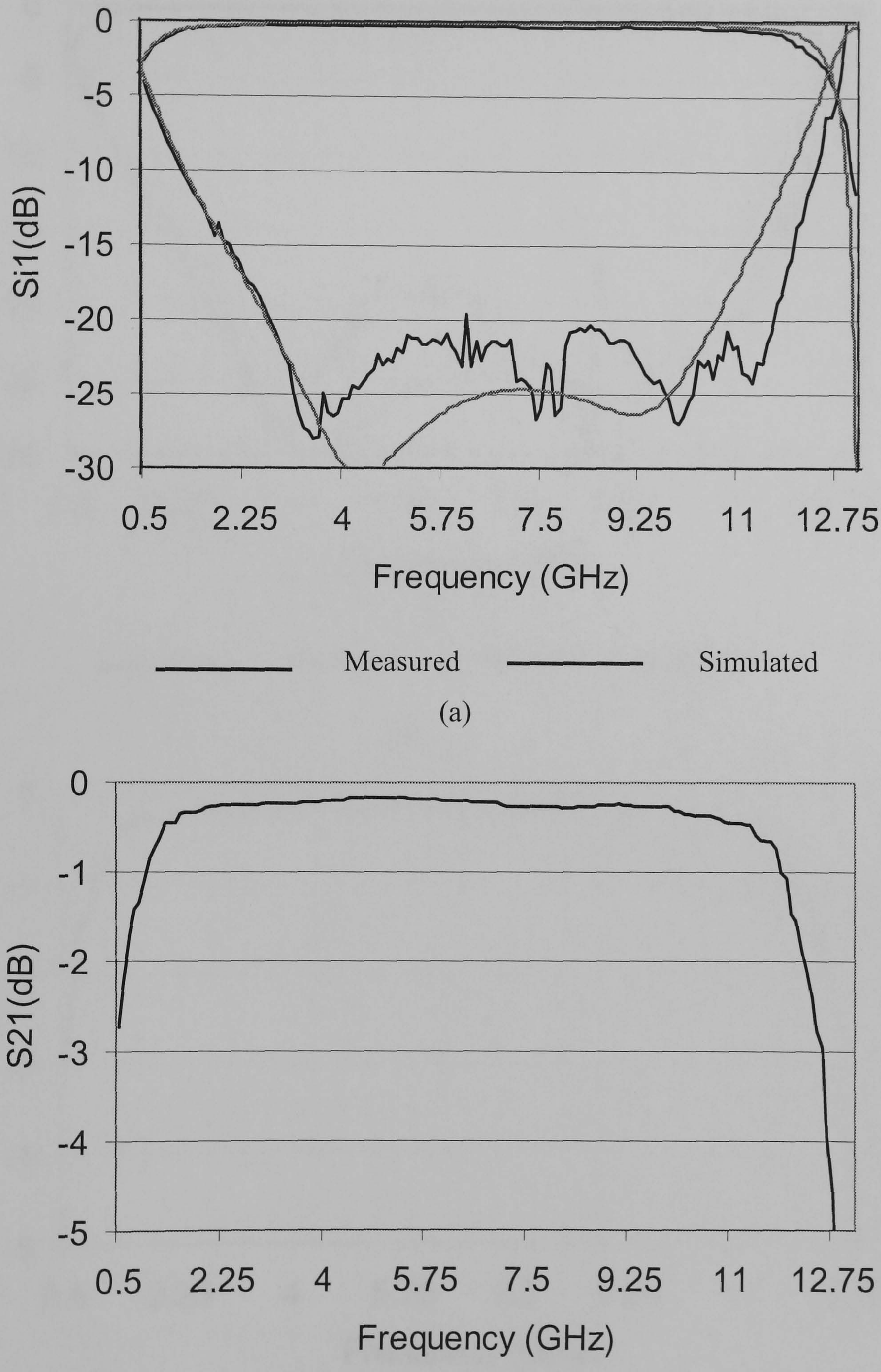

Figure 5.5: Measured results for DC block#1 (a) Comparison of measured and simulated data, (b) shows measured dBS21 in more detail.

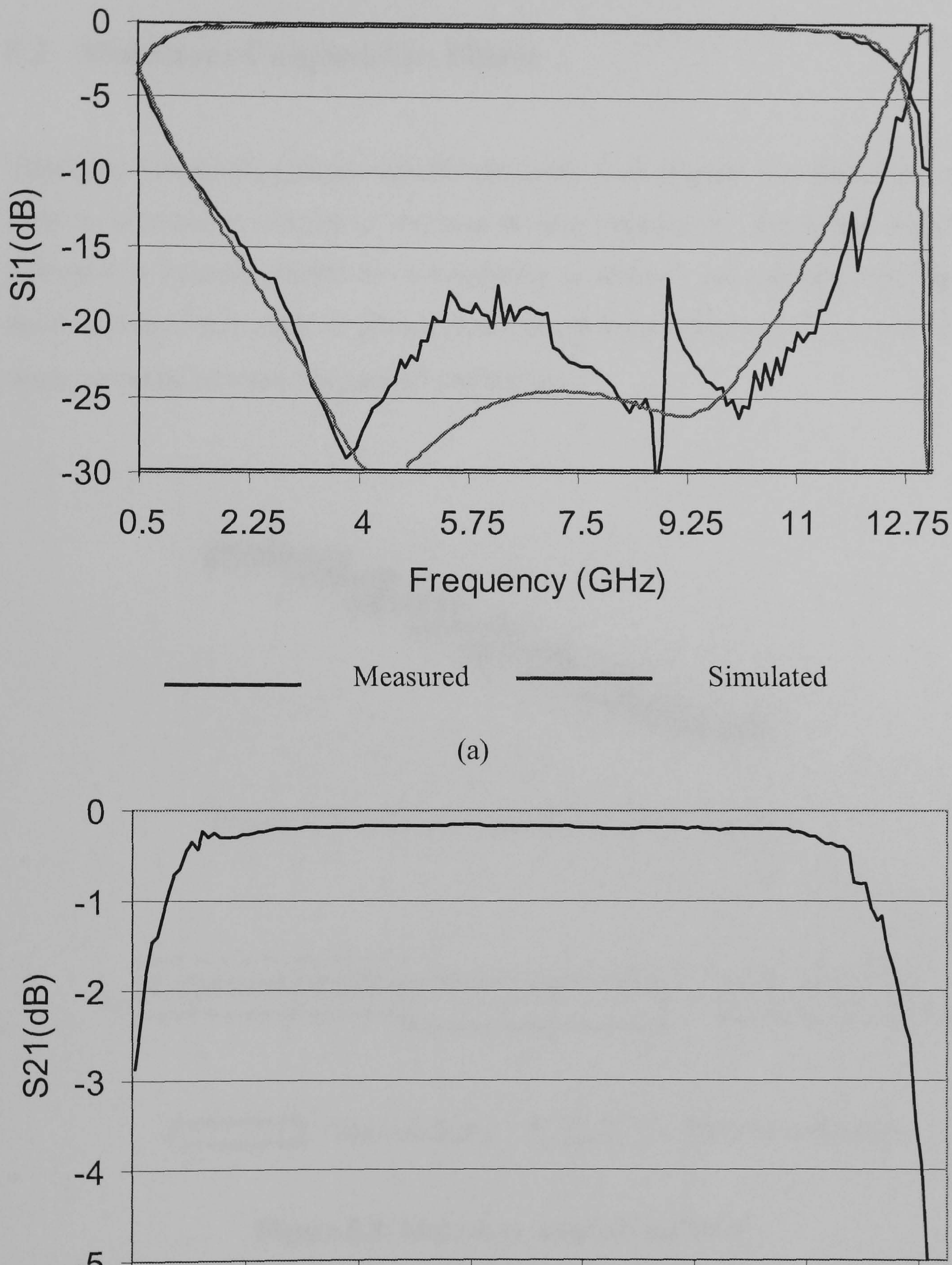

(a)

(b)

Figure 5.6: Measured results for DC block#2 (a) Comparison of measured and simulated data, (b) shows measured dBS21 in more detail.

5.3 Multilayer Coupled-line Filters

Bandpass filters using edge-coupled microstrip lines (Figure 5.7) have been widely used in microwave circuits in the past several decades [6]. Each half wavelength resonator is located parallel to its neighbour to achieve the required coupling. One shortcoming of this class of filters is the limited bandwidth (~15%) imposed by the weak coupling between the parallel conductors.

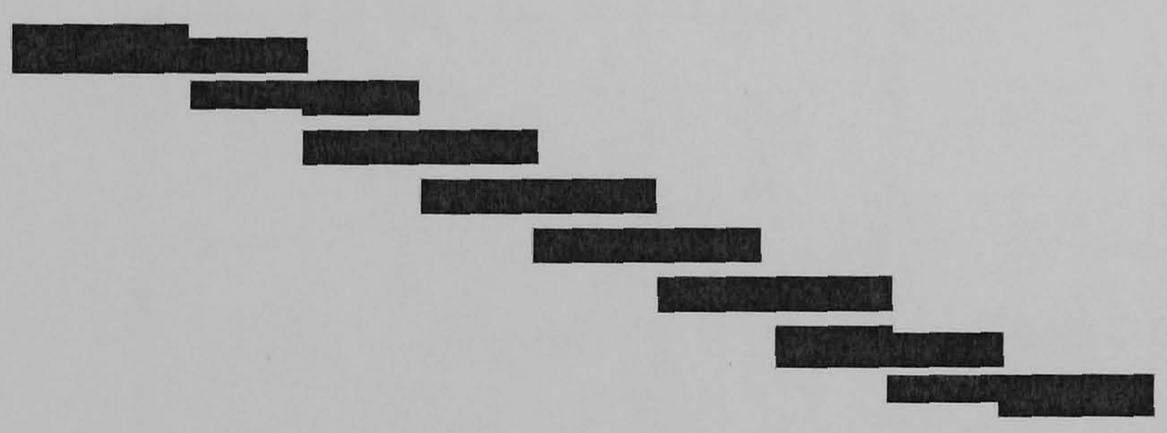

Figure 5.7: Microstrip parallel coupled-line filter

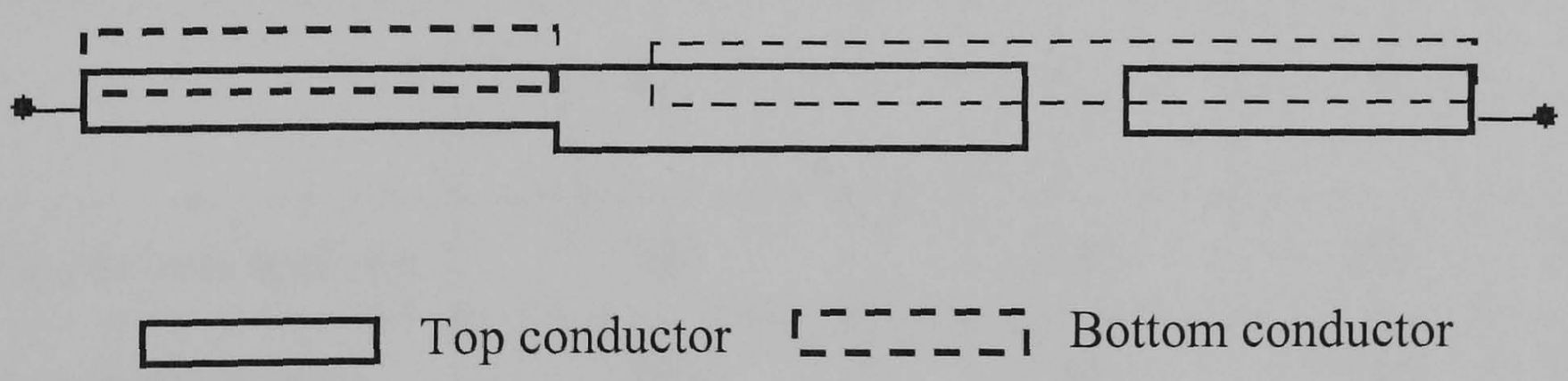

Figure 5.8: Multilayer coupled-line filter

Recently, multilayer structures have been employed in the design of coupled-line filters for broader bandwidth [7-9]. Figure 5.8 shows a 3 section coupled-line filter in a multilayer format. The coupled-lines are positioned in different layers with overlapping to provide the strong coupling that is required. Multilayer coupled-line filters using different thick-film dielectrics have been designed. The intention is to

investigate the potential for achieving broad bandwidth using a multilayer structure.

5.3.1 Design Example (I)

A 3 section multilayer coupled-line filter was designed. The substrate information is listed in Table 5.3, and Table 5.4 shows the physical dimensions of the filter. The simulated response (Figure 5.9) shows that very broad bandwidth (80%) can be achieved using multilayer structure.

Table 5.3 : Substrate information

ε_{r1}	h_1	ε_{r2}	h_2
9.8	635 μm	8	28μm

Table 5.4: Physical dimension of a 3 section multilayer coupled-line filter

	W_1	W_2	S	*l*
The first and end sections	300	180	50	3300
The second section	390	310	310	2100

Unit: μm

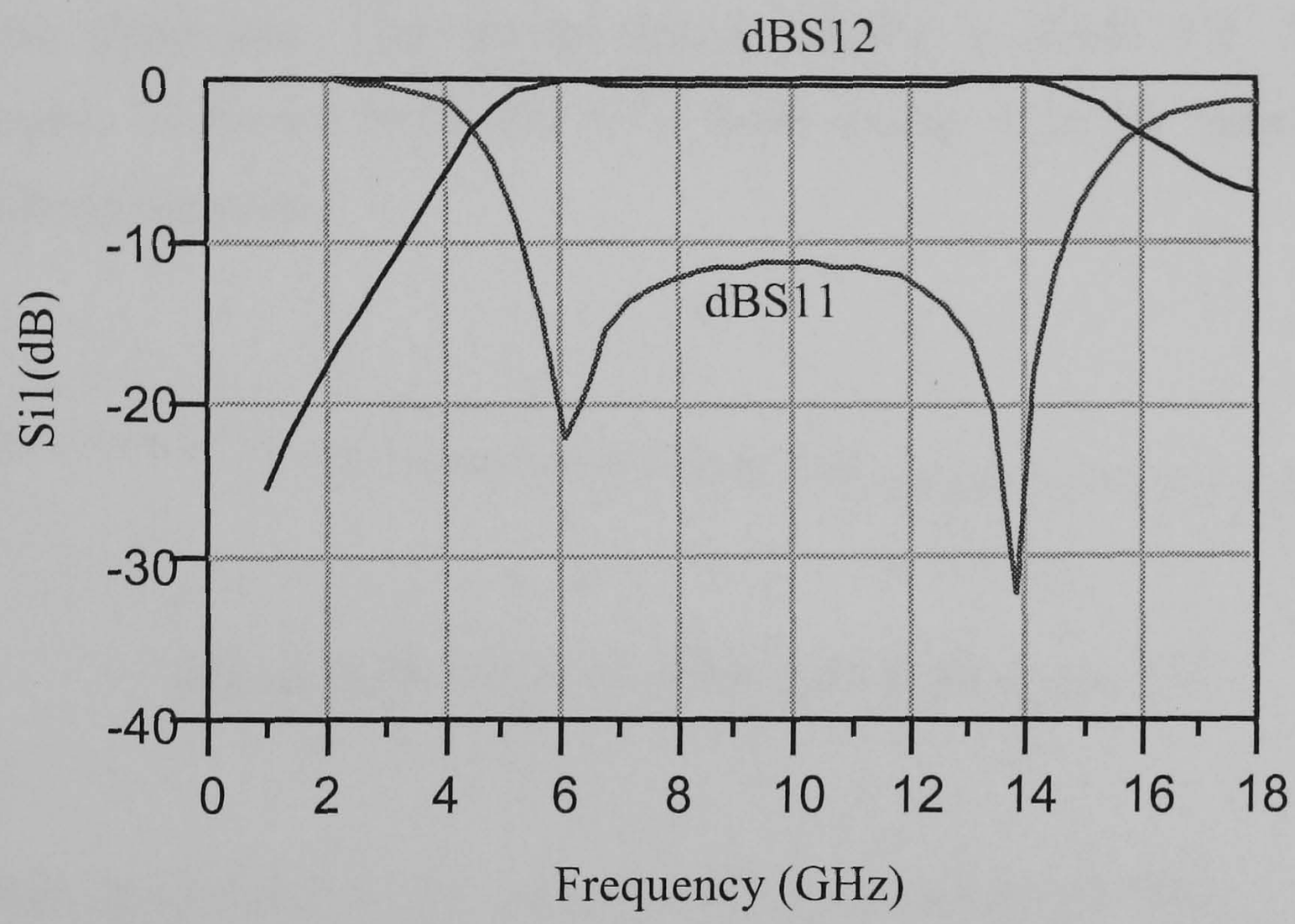

(a)

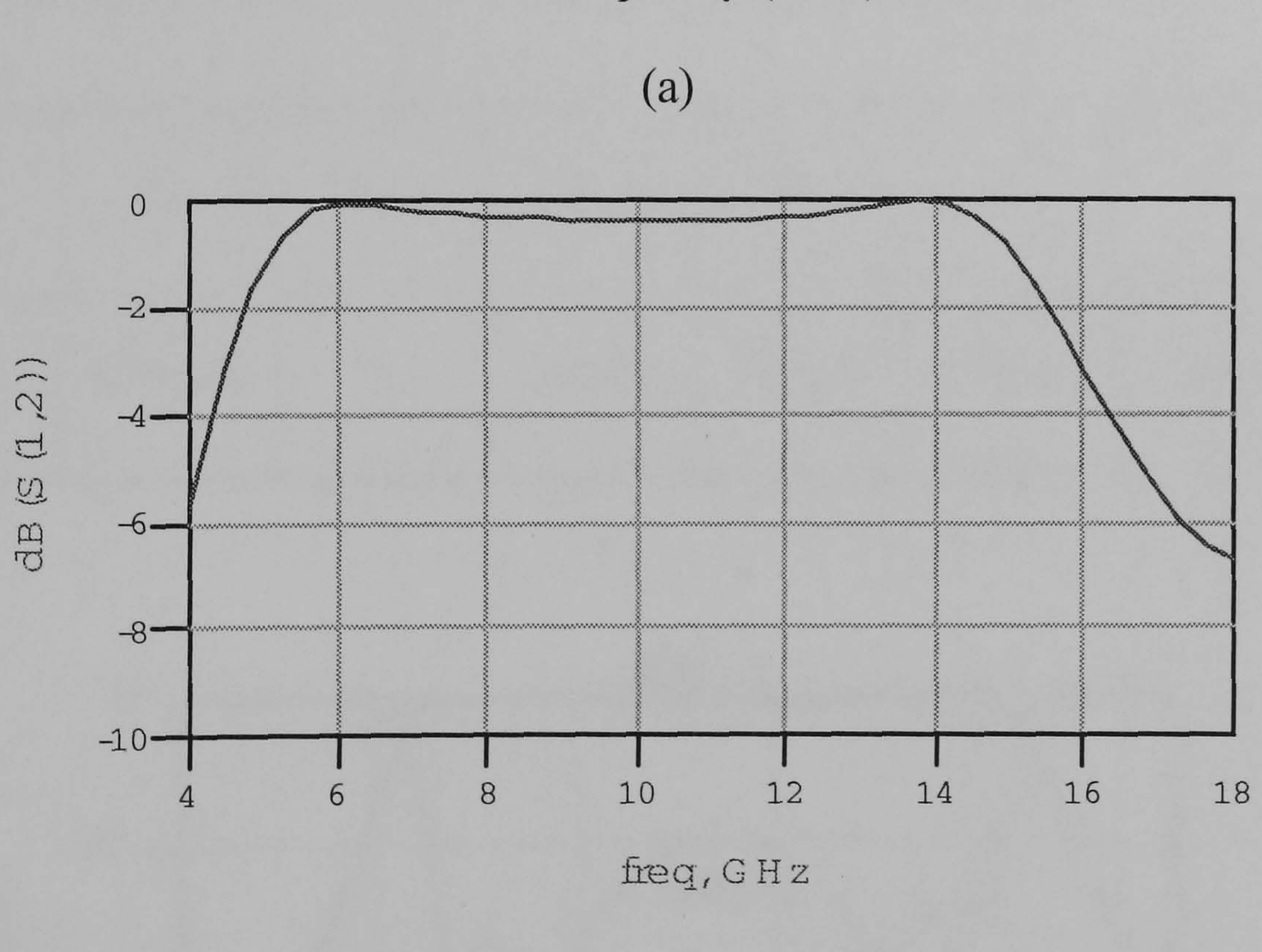

(b)

Figure 5.9: Simulated result for a multilayer coupled-line filter (a) dBS21 and dBS11, (b) details of dBS21.

5.3.2 Design Example (II)

A 5 section multilayer coupled-line filter (Figure 5.10) is designed. Each section has the same dimension. The design data is shown in Table 5.5. The simulated performance is shown in Figure 5.11, from where it can be seen that an 80% bandwidth is obtained.

Figure 5.10: 5 section multilayer coupled-line filter

Table 5.5: Design data for a 5 section multilayer coupled-line filter

ε_{r1}	h_1	ε_{r2}	h_2	W_1	W_2	S	l
9.8	635 μm	8	28μm	200μm	150μm	0μm	4000μm

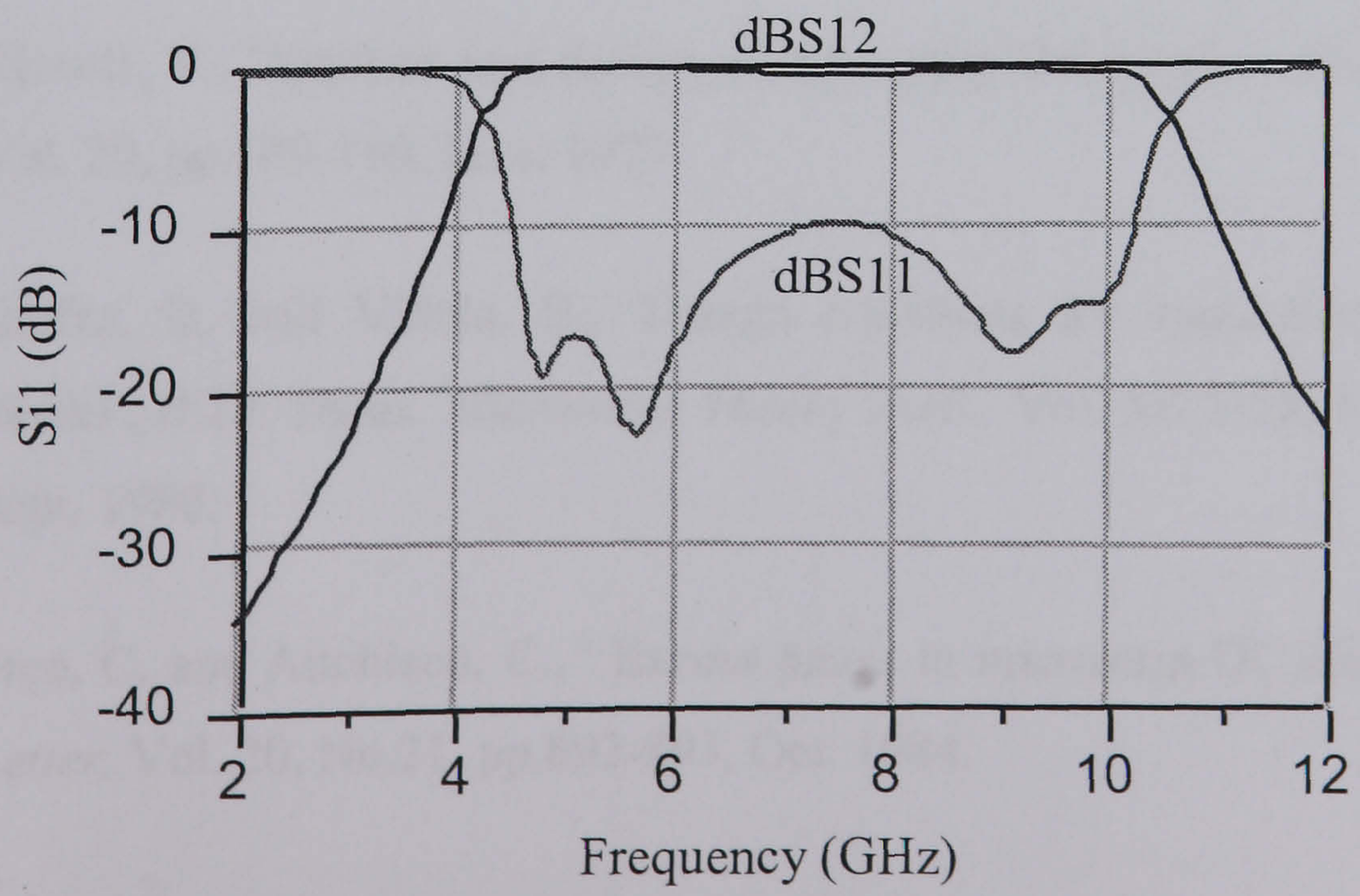

Figure 5.11: Simulated response of a multilayer filter

The multilayer coupled-line filters, whose design is given above, were fabricated using a thick-film process. However, there were significant registration errors between the layers in the fabricated component. Consequently the expected performance was not achieved, and no measure data are presented for this component.

5.4 Conclusions

Excellent results were obtained for DC blocks fabricated in a multiplayer format. In particular, very wide bandwidth was obtained combined with low insertion loss. These results demonstrate clearly the usefulness of the multilayer structure for obtaining strong conductor coupling and overcoming the need to fabricate fine gaps.

Furthermore, the simulation results for band-pass filters show that the multilayer approach can profitable be applied to other structures, where tight conductor coupling is a critical requirement.

5.5 References

[1] LaCombe, D. and Cohen, J., 'Octave-band microstrip dc blocks', *IEEE Trans. Microwave Theory Tech.,* vol. MTT-20, pp. 555-556, Aug. 1972.

[2] Rizzoli, V., 'Analysis and design of microstrip DC blocks', *Microwave Journal,* Vol. 20, pp.109-110, June. 1977.

[3] Kajfez, D. and Vidula, B., 'Design equations for symmetric microstrip DC blocks', *IEEE Trans. Microwave Theory Tech.,* Vol. MTT-28, No.9, pp.974-981, Sept. 1980.

[4] Free, C. and Aitchison, C., ' Excess phase in microstrip DC blocks', *Electronics Letter,* Vol. 20, No.21, pp.892-893, Oct. 1984.

[5] Gupta, K. C., Garg, R., Bahl, I. And Bhartia, P., *Microstrip lines and slotlines*, Artech House, 1996.

[6] Cohn, S., 'Parallel coupled transmission line resonator filters,' *IRE Trans. Microwave Theory Tech.*, vol. MTT-6, No.2, pp. 223-232, Apr. 1958.

[7] Wolfgang Schwab and W. Menzel, "On the design of planar microwave components using multilayer structures," *IEEE Trans. Microwave Theory Tech.*, Vol.40 No.1, pp67-71, Jan. 1992.

[8] Choonsik Cho and K. C. Gupta, "Design Methodology for Multilayer Coupled-line Filters", *IEEE MTT-S Digest Int. Microwave Symp. Dig.*, pp785-788, 1997.

[9] R. Lutz, A. Tripathi, Y. Seo, and V. Tripathi, "Design Considerations for Embedded passives, " *Wireless Communications Conference*, pp.181-186, 1997.

Chapter 6 Multilayer Directional Couplers

6.1 Summary

In this chapter the multilayer approach that has been developed in earlier sections is applied to the design of directional couplers. A simple arrangement, where overlapping conductors are separated by a dielectric layer, provides large coupling factors, without the need for rigorous manufacturing tolerances.

For the first time, the properties of multilayer coupled lines using a range of different thick-film dielectrics are examined using their coupled-mode parameters. Design curves for multilayer coupled lines are obtained, that provide important information in the design of multilayer directional couplers.

A practical design strategy for multilayer directional couplers is developed, which overcomes the problem of excessive computation that is normally associated with the electromagnetic optimization of multilayer circuit designs. The methodology has been verified through the design and measurement of wide bandwidth 2dB and 3dB directional couplers that were fabricated using multilayer, thick-film technology.

6.2 Introduction

The general configuration of the multilayer directional coupler considered is shown in Figure 6.1. The two conductors are positioned in different layers above a common ground plane with a certain amount of overlap, denoted by S. The widths of the bottom and top conductor tracks are W_1 and W_2, respectively. Port definitions are

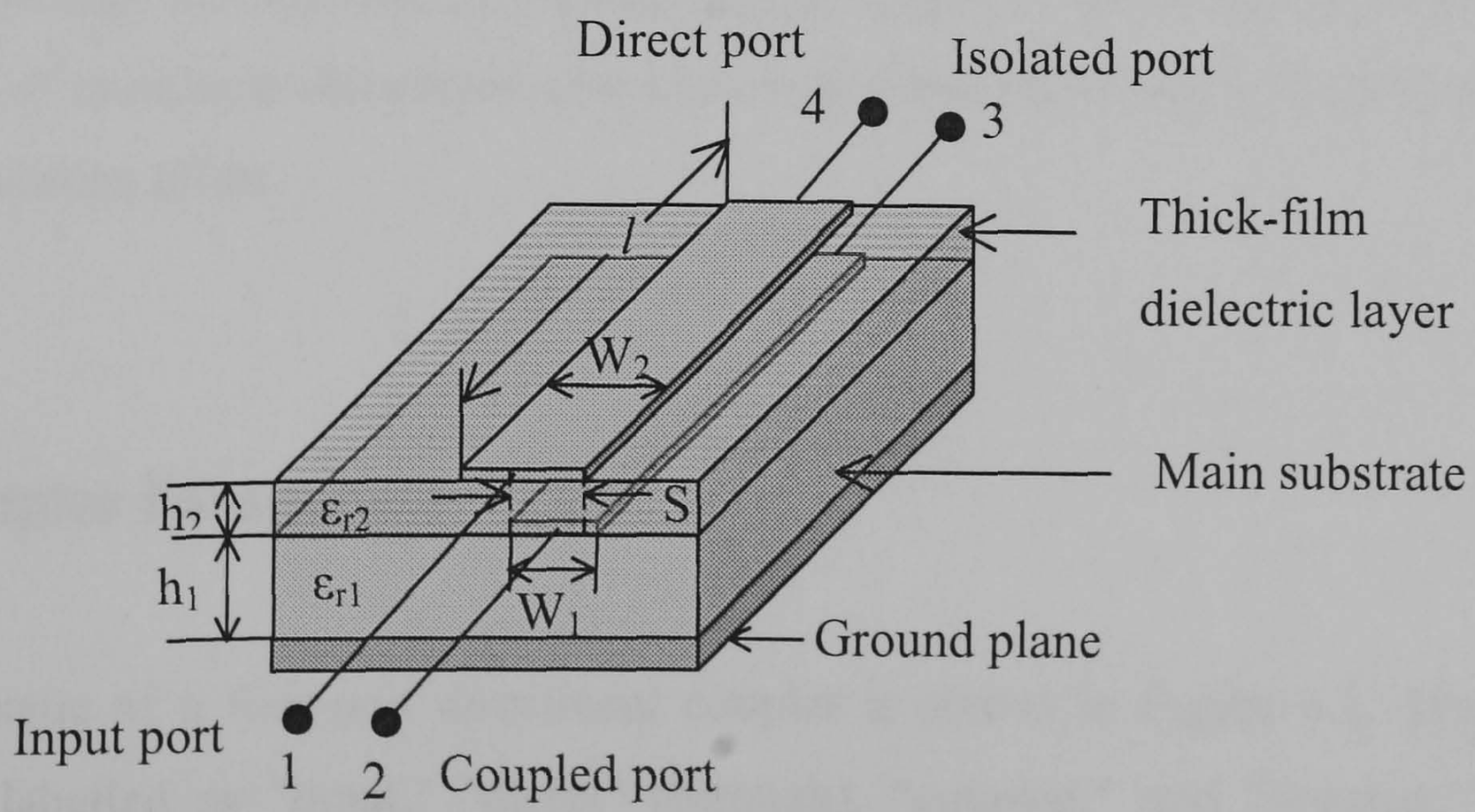

Figure 6.1: The configuration of a two-layer directional coupler.

also shown in this figure.

The principal advantage of this structure is that very strong coupling can be easily achieved without the need for fine gap lithography as occurs in the more common single-layer coupler. The strong coupling is obtained by overlapping the two transmission lines, which are separated with a thin layer of printed thick-film dielectric.

The coupling mechanism between the two conductor lines is more complicated than in the case of single layer coupling, and the synthesis equations for conventional single layer structures are no longer applicable. This causes the major drawback to the design of multilayer directional couplers, where electromagnetic (EM) analysis has to be employed to optimize the structure of this kind.

It is recognized that the choice of the initial design parameters is thus crucial if the EM optimization process is not to be unduly time-consuming and expensive. To achieve this, we firstly examine the properties of coupled lines using different thick-film dielectrics using their coupled-mode parameters. This enables us to quantify the influence of thick-film dielectric on the performance of the coupled lines, and find a link between the physical dimensions of the coupled lines and the performance of the coupler. Through this approach a practical design method is developed that facilitates the design of multilayer directional couplers of optimum performance with minimum EM computation effort.

6.3 Coupler Parameters

The schematic of a four-port directional coupler is shown in Figure 6.2. The four ports are labelled as "input," "direct" (through), "coupled," and "isolated." Two important parameters that characterize a directional coupler are its coupling and

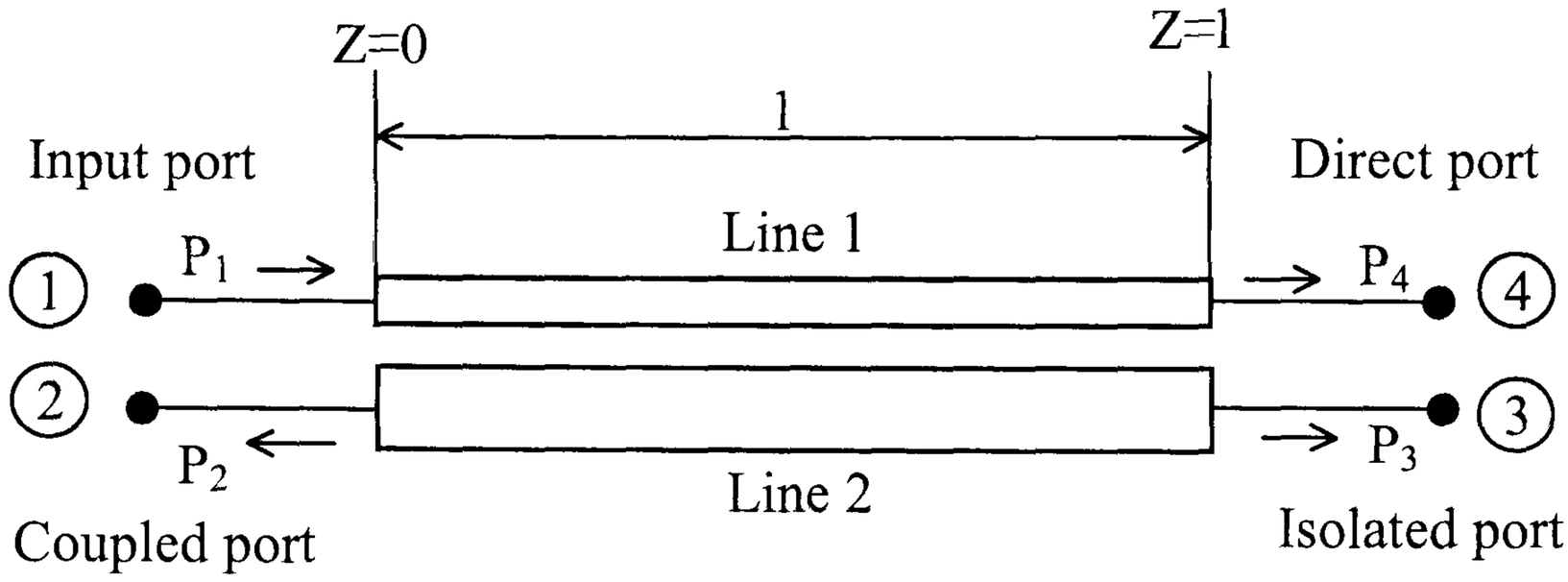

Figure 6.2: Schematic of a four-port directional coupler

directivity, as defined below:

$$\text{Coupling (dB)} = 10\log\frac{P_1}{P_2}$$

$$\text{Directivity (dB)} = 10\log\frac{P_2}{P_3}$$

where P_1 is the power input at port 1, and P_2, P_3, P_4 are the power outputs at ports 2, 3 and 4, respectively. All the ports are assumed to have matched terminations. In the ideal case there is no output power at port 3, although in practice a small amount of power is always coupled to this port due to the unequal velocities of propagation of the odd and even modes.

If the coupling and directivity are known, the isolation of the coupler can be determined. The isolation is defined as

$$\text{Isolation (dB)} = 10\log\frac{P_1}{P_3}$$

The design of multilayer directional couplers involves finding the optimum overlap, S, the widths of the bottom and top conductor track W_1 and W_2, the length of the coupled region, *l*, to achieve required coupling with good matching and isolation

performance in the desired frequency range.

6.4 Methods of Analysis of Multilayer Coupled lines

Figure 6.3 shows the cross sectional view of a multilayer coupled line, where the two conductors are located in different layers. The dielectric substrate has a different effect on the characteristic impedance and propagation constant of the top and bottom conductors. Thus multilayer coupled lines are, by nature, asymmetrical.

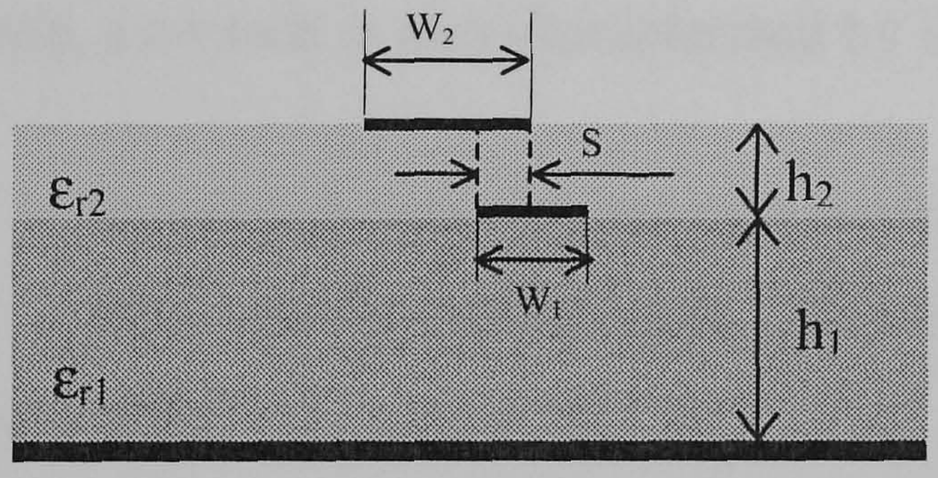

Figure 6.3: Cross-sectional view of multilayer coupled lines

The coupling between symmetrical coupled lines can be determined in terms of the phase velocities and characteristic impedances of the well-known even and odd modes. When the coupled lines are asymmetrical, as in the case of multilayer coupled lines, the even and odd mode theory is no longer applicable, and the coupling mechanism is more complicated. Traditionally, two approaches have been used to study the coupling between asymmetric coupled lines, involving, respectively, normal-modes and coupled-modes.

6.4.1 Normal mode theory

A set of two coupled lines can support two fundamental, independent modes of propagation, called normal modes. For asymmetrical coupled lines, the two normal modes of propagation are know as the *c* and π modes as defined by Tripathi [2] and obtained from solving the *V-I* equations.

A *c* mode is characterized by four parameters:

γ_c : the propagation constant of *c*-mode;

Z_{c1} and Z_{c2} : the *c*-mode characteristic impedance of line 1 and line2, respectively;

R_c : the ratio of *c*-mode voltages on the two lines.

Similar to the *c*-mode, a π-mode is also characterized by four parameters:

γ_π : the propagation constant of π-mode;

$Z_{\pi 1}$ and $Z_{\pi 2}$: the π-mode characteristic impedance of line 1 and line2, respectively;

R_π : the ratio of π-mode voltages on the two lines.

The relations between characteristic impedances Z_{c1}, Z_{c2}, $Z_{\pi 1}$ and $Z_{\pi 2}$ and ratio parameters R_c and R_π are found to be:

$$\frac{Z_{c2}}{Z_{c1}} = \frac{Z_{\pi 2}}{Z_{\pi 1}} = -R_c R_\pi \tag{6.1}$$

Therefore, a total of six quantities (i.e., γ_c, γ_π, Z_{c1}[or Z_{c2}], $Z_{\pi 1}$[or $Z_{\pi 2}$], R_c, and R_π) are required to characterize asymmetrical coupled line. It is not necessary to specify both Z_{c1} and Z_{c2}, as they are related by (6.1). The same holds for $Z_{\pi 1}$ and $Z_{\pi 2}$.

For symmetrical coupled lines, R_c =1 and R_π =-1, and normal modes are known as even and odd modes. Thus, symmetrical coupled lines are completely characterized

by four parameters: the even- and odd-mode characteristic impedances of any line (as both lines are identical) and the even- and odd-mode phase constants.

The normal mode provides an exact method for analysis of coupled lines. However, the task of determining normal-mode parameters is very complicated.

6.4.2 Coupled mode theory

In the coupled mode approach, the wave propagation is expressed in terms of four well-known forward and backward power waves: a_+, b_+ and a_-, b_-, respectively. The coupled mode theory leads to explicit expressions showing how individual waves are modified in the presence of coupling because of mutual capacitances and inductances. This approach, therefore, provides an insight into the mechanism of coupling. This theory also leads to an important result for the condition of quasi-ideal coupling.

The principle of coupled-mode analysis is restated in the following section and serves to introduce coupled-mode parameters and the necessary notations used in the design of multilayer directional coupler.

6.5 Coupled-Mode Analysis [3]

A coupled pair of transmission lines and their equivalent circuit are shown in Figure 6.4. The behavior of two lossless coupled transmission lines is described by the following set of differential equations:

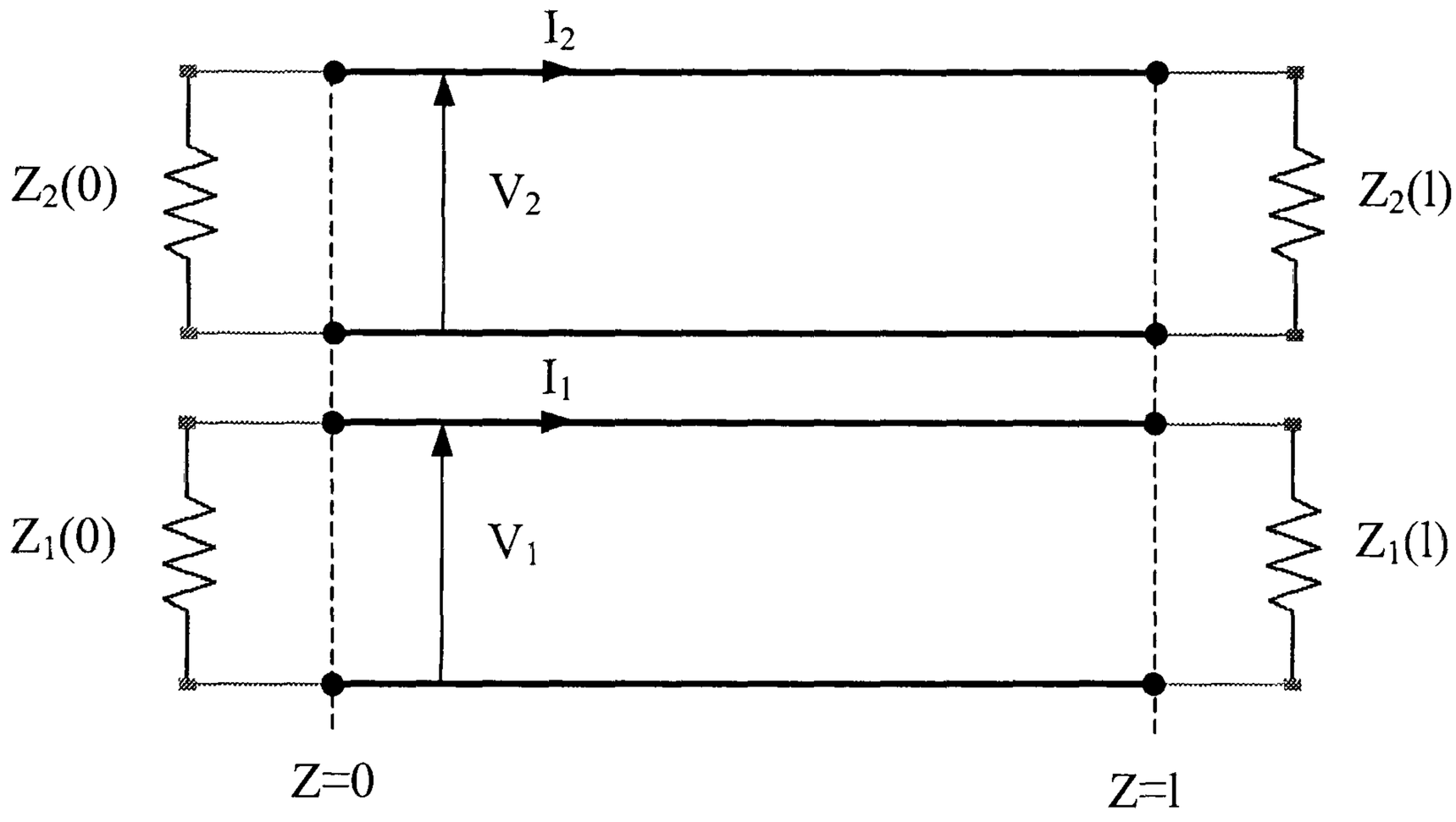

(a)

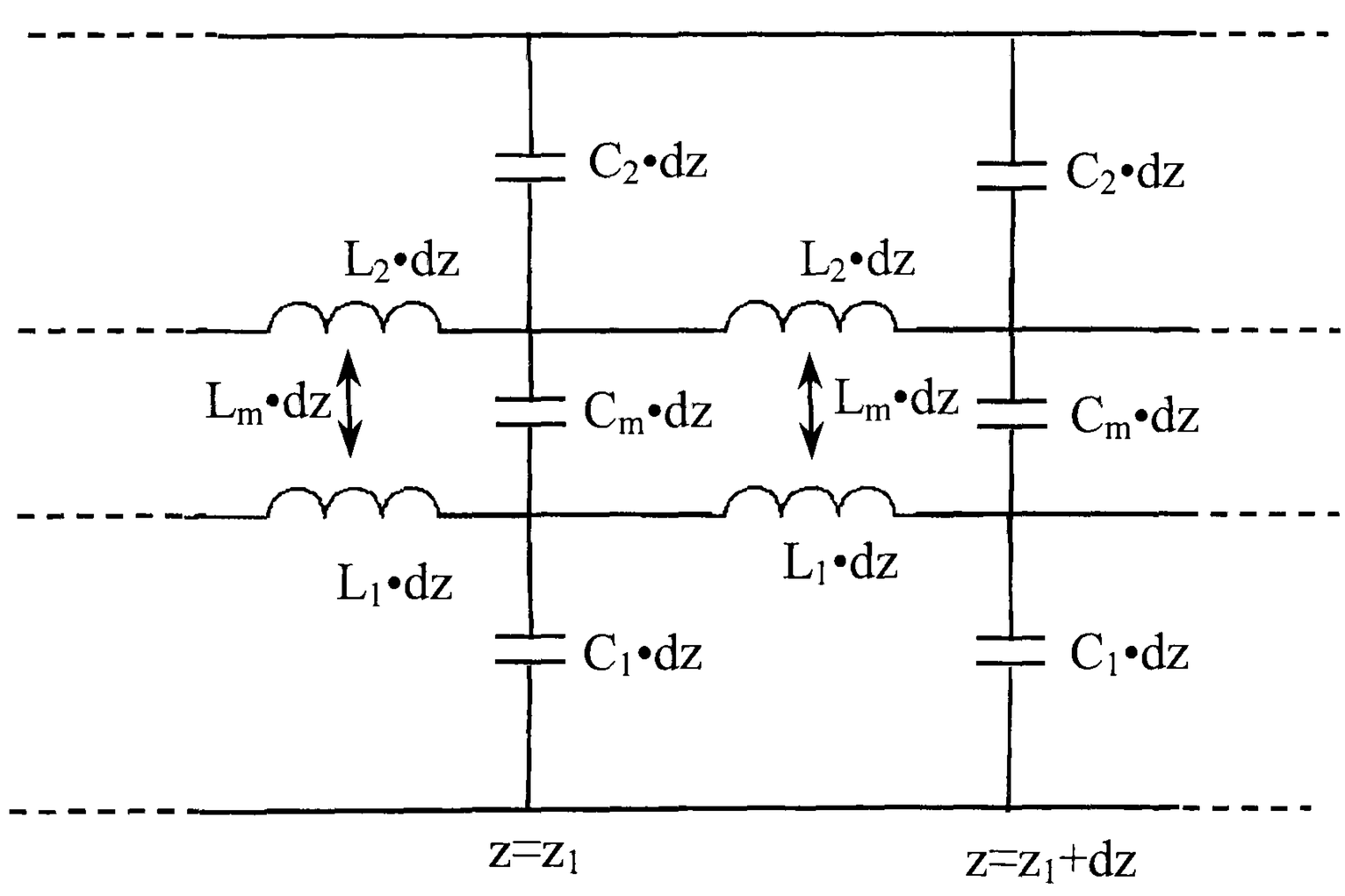

(b)

Figure 6.4: (a) Coupled transmission lines. (b) Lumped equivalent circuit of coupled asymmetrical transmission lines of differential length of dz.

$$\frac{\partial V_1(z,t)}{\partial z}+L_1\frac{\partial I_1(z,t)}{\partial t}+L_m\frac{\partial I_2(z,t)}{\partial t}=0 \tag{6.2}$$

$$\frac{\partial I_1(z,t)}{\partial z}+C_1\frac{\partial V_1(z,t)}{\partial t}-C_m\frac{\partial V_2(z,t)}{\partial t}=0 \tag{6.3}$$

$$\frac{\partial V_2(z,t)}{\partial z}+L_2\frac{\partial I_2(z,t)}{\partial t}+L_m\frac{\partial I_1(z,t)}{\partial t}=0 \tag{6.4}$$

$$\frac{\partial I_2(z,t)}{\partial z}+C_2\frac{\partial V_2(z,t)}{\partial t}-C_m\frac{\partial V_1(z,t)}{\partial t}=0 \tag{6.5}$$

where $V_i(z,t)$ and $I_i(z,t)$ denote the voltage and current, respectively, on line i(i=1,2) as a function of distance z along the transmission line and time t. L_j and C_j (j=1,2) are the self-inductance and self-capacitance per unit length of line j in the presence of line k(k=1,2, $k\neq j$), and L_m, C_m are the mutual inductance and mutual capacitance per unit length, respectively.

More specifically, self and mutual inductance and capacitance parameters are the elements of inductance and capacitance matrices [**L**] and [**C**], where

$$[L]=\begin{bmatrix}L_{11} & L_{12}\\ L_{21} & L_{22}\end{bmatrix}=\begin{bmatrix}L_1 & L_m\\ L_m & L_2\end{bmatrix} \tag{6.6}$$

$$[C]=\begin{bmatrix}C_{11} & C_{12}\\ C_{21} & C_{22}\end{bmatrix}=\begin{bmatrix}C_1 & -C_m\\ -C_m & C_2\end{bmatrix} \tag{6.7}$$

The four forward and backward power waves on a pair of coupled transmission lines (Figure 6.5) , namely: a_+, b_+ and a_-, b_-, which are also known as the coupled modes, are defined by:

$$a_{\pm} = \frac{1}{2\sqrt{Z_1}}(V_1 \pm Z_1 I_1) \tag{6.8}$$

$$b_{\pm} = \frac{1}{2\sqrt{Z_2}}(V_2 \pm Z_2 I_2) \tag{6.9}$$

where $Z_i = \sqrt{L_i / C_i}$ is the characteristic impedances of uncoupled lines, and L_i and C_i are the self-inductances and self-capacitances per unit length of line i in the presence of the other (i =1,2).

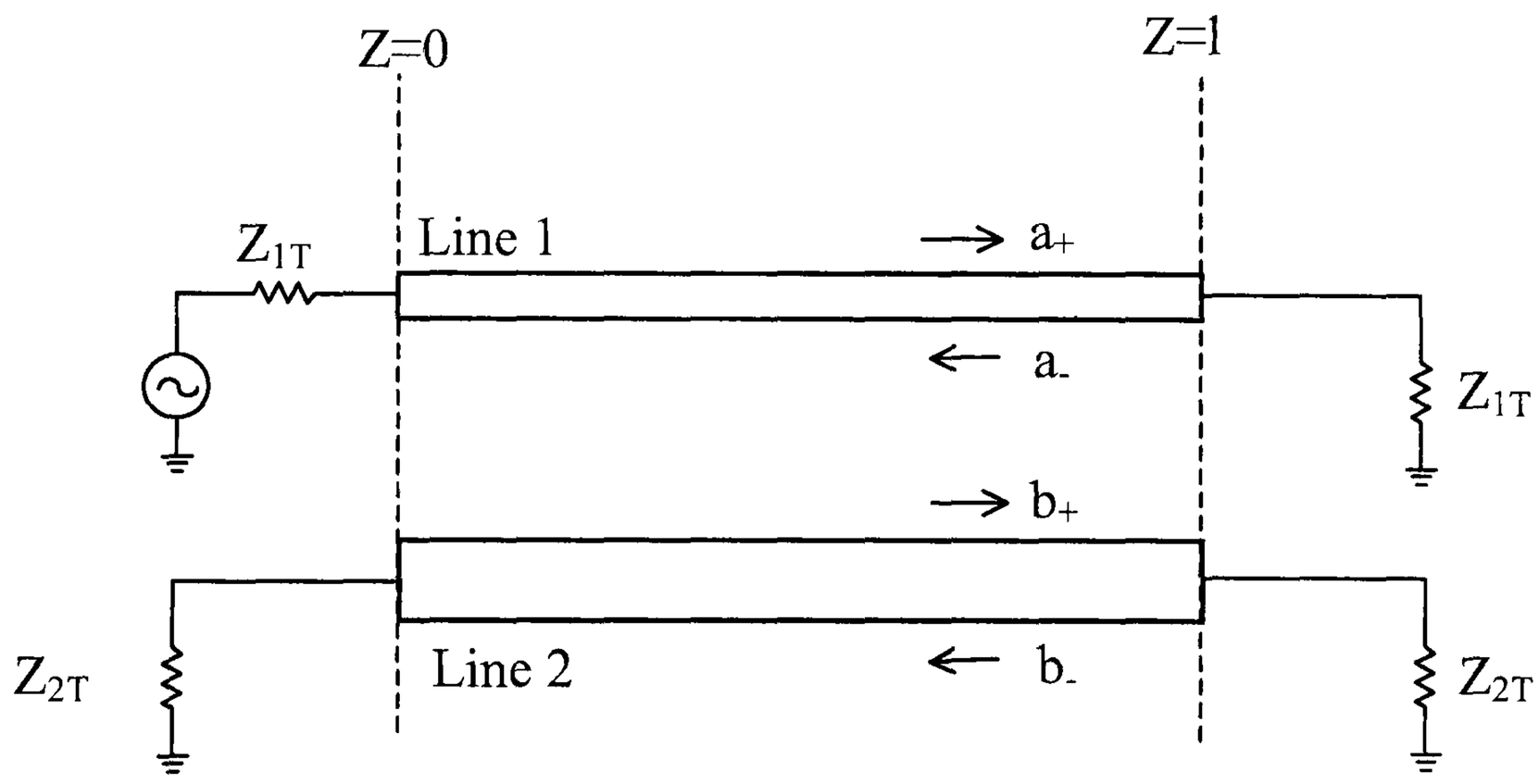

Figure 6.5: Modes on a pair of coupled transmission lines.

Substitution of the definitions of (6.8) and (6.9) in (6.2) through (6.5), and assuming the impedance and coupling along the transmission lines are constant with distance, gives the following set of coupled-mode equations:

$$\left(\frac{\partial}{\partial z} \pm j\beta_1\right) a_{\pm} = -j\sqrt{\beta_1\beta_2}\left[\left(\frac{k_L \mp k_C}{2}\right) b_{+} - \left(\frac{k_L \pm k_C}{2}\right) b_{-}\right]$$

and

$$\left(\frac{\partial}{\partial z} \pm j\beta_2\right) b_{\pm} = -j\sqrt{\beta_1\beta_2}\left[\left(\frac{k_L \mp k_C}{2}\right) a_{+} - \left(\frac{k_L \pm k_C}{2}\right) a_{-}\right] \tag{6.10}$$

where

$$\beta_i = \omega\sqrt{L_i C_i} \qquad (i = 1,2), \qquad k_L = L_m / \sqrt{L_1 L_2}, \qquad k_C = C_m / \sqrt{C_1 C_2}.$$

k_L and k_C are known as inductive and capacitive coupling coefficient, respectively.

Assuming a lossless propagating wave of the form $Ae^{j(\omega t - \beta z)}$ ($\omega = 2\pi f$, f = frequency, β = phase propagation constant) results in four normal modes of the coupler, two with positive eigenvalues and two with negative ones, corresponding to a pair of modes propagating in each direction. The eigenvalues are $\pm\beta_c$ and $\pm\beta_\pi$, where β_c and β_π are given by:

$$\beta_r = \beta_0\sqrt{1 \pm \delta}, \qquad (r = c \ \ or \pi). \tag{6.11}$$

where

$$\beta_0 = \sqrt{\frac{\beta_1^2 + \beta_2^2}{2} - \beta_1\beta_1 k_L k_C} \tag{6.12}$$

and

$$\delta = \sqrt{1 - \left(\frac{\beta_1^2\beta_2^2}{\beta_0^4}\right)(1 - k_L^2)(1 - k_C^2)} \tag{6.13}$$

6.6 Conditions for Ideal Coupling

An important outcome of coupled-mode analysis in the design of high-performance directional couplers has been made by the proof [4] that the asymmetric coupled line coupler is ideally matched and perfectly isolated at all frequencies if

$$k_L = k_C \tag{6.14}$$

and

$$Z_{Ti} = Z_i = \sqrt{\frac{L_i}{C_i}}, \qquad i = 1,2 \tag{6.15}$$

where

$k_L = \dfrac{L_m}{\sqrt{L_1 \cdot L_2}}$ the inductive coupling coefficient;

$k_C = \dfrac{C_m}{\sqrt{C_1 \cdot C_2}}$ the capacitive coupling coefficient;

$Z_{Ti}, \quad i = 1,2$ the characteristic impedances of the terminating lines;

$Z_i, \quad i = 1,2$ the characteristic impedances of uncoupled lines;

$L_1, L_1, L_m,$ and C_1, C_2, C_m the self and mutual inductances and capacitances (per unit length) of the firstand second line in the presence of the other per unit length.

This statement is valid for the quasi-static approximation previously discussed.

6.7 Evaluation Software for Primary Matrix Parameters

As we have seen in previous sections, coupled-mode parameters are essential for evaluating the properties of multilayer microstrip coupled lines. These parameters (Z_1, Z_2, K_L and K_C) can be obtained through the evaluation of primary (quasi-static) matrix parameters, namely the matrix [L] of per-unit-length inductances, and the matrix [C] of per-unit-length capacitances. LINPAR (Matrix Parameters for Multiconductor Transmission Lines) is a computer program for the numerical evaluation of the quasi-static matrices for multiconductor transmission lines embedded in multilayer dielectrics [5].

The program can analyze arbitrary multiconductor transmission lines (with up to 32 signal conductors), of arbitrary cross section. The dielectric can be homogeneous or piecewise homogeneous. The program can analyze lossless lines or incorporate bulk and surface conductor losses and lossy dielectrics. It has a set of built-in multiconductor transmission line structures, that are frequently encountered in practice. These built-in structures are :

- Microstrip lines and coupled microstrip lines with zero-thickness conductors,
- Microstrip lines and coupled microstrip lines with finite-thickness conductors,
- Suspended-substrate striplines and coupled suspended-substrate striplines,
- Transmission lines and coupled transmission lines with rectangular conductors,
- Striplines and coupled striplines,
- Broadside-coupled lines,
- Coplanar waveguides and coupled coplanar waveguides,
- Arbitrary multilayer planar structures.

LINPAR numerically evaluates the primary matrix parameters based on an electrostatic analysis. The capacitances are found from the charge on the conductors in the presence of dielectrics, while the inductances are found from the charges when the problem is solved with all dielectric constants equal to the free-space value. The computation time is quick. For example, it only takes around 5 seconds for calculating a pair of multilayer coupled lines. In the following section, the primary matrix parameters are calculated using LINPAR software so as to evaluate the coupled-mode parameters for multilayer coupled lines.

6.8 Basic Behaviour of Multilayer Microstrip Coupled Lines

There are several parameters involved in the description of multilayer coupled lines. It is important to understand the basic behavior of each element so that computation can be simplified based on some physical phenomena. To understand the relationship between coupled-mode parameters (Z_1, Z_2, K_L and K_C) and the geometrical parameters of the multilayer coupled line (W_1, W_2, S), the coupled-mode parameters of a multilayer coupled line versus the gap/overlap are calculated and shown in Figure 6.6. The corresponding microstrip width is chosen such that each single line has characteristic impedance of 50Ω. In other words, two 50Ω lines are placed in different layers with a certain separation. We are looking at the change in the coupled mode parameters when theses two lines are brought close to each other. Note that in the figure, a negative value for the gap corresponds to an overlap. From Figure 6.6 we can see that K_L and K_C increase with the decrease of the gap (or increase of the overlap). Meanwhile, Z_1 and Z_2 decrease when the two lines come closer. This suggests that with the increase of the overlap, the coupling will be increased, and to maintain good match, the line width needs to be decreased.

Figure 6.7 shows the change of coupled mode parameters when the width of a single line is changed. It is seen that the change of the width of a single line will only have a significant effect on the characteristic impedance of the line itself, whilst the characteristic impedance of the other line and the coupling coefficients basically

remain unchanged. The significance of this feature is that in the design of multilayer coupled lines, the design procedure can be simplified by optimizing the width of a single line to achieve required impedance for the line itself. This greatly reduces the complexity of the optimization process.

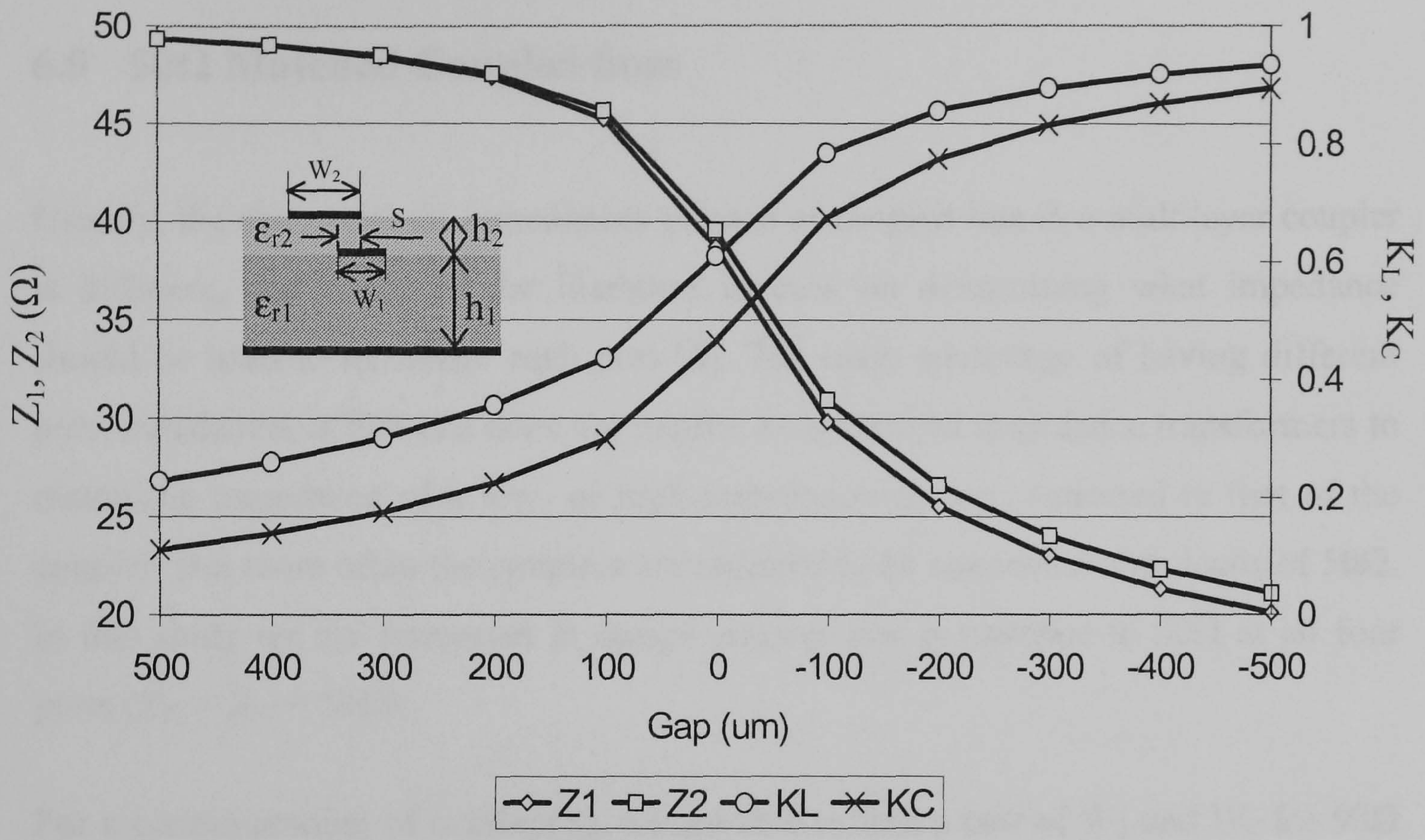

Figure 6.6: Behaviour of multilayer coupled lines showing the effect of the gap/overlap. (W_1=590μm, W_2=730μm, ε_{r1}=9.9, h_1=635μm, ε_{r2}=3.9, h_2=30μm)

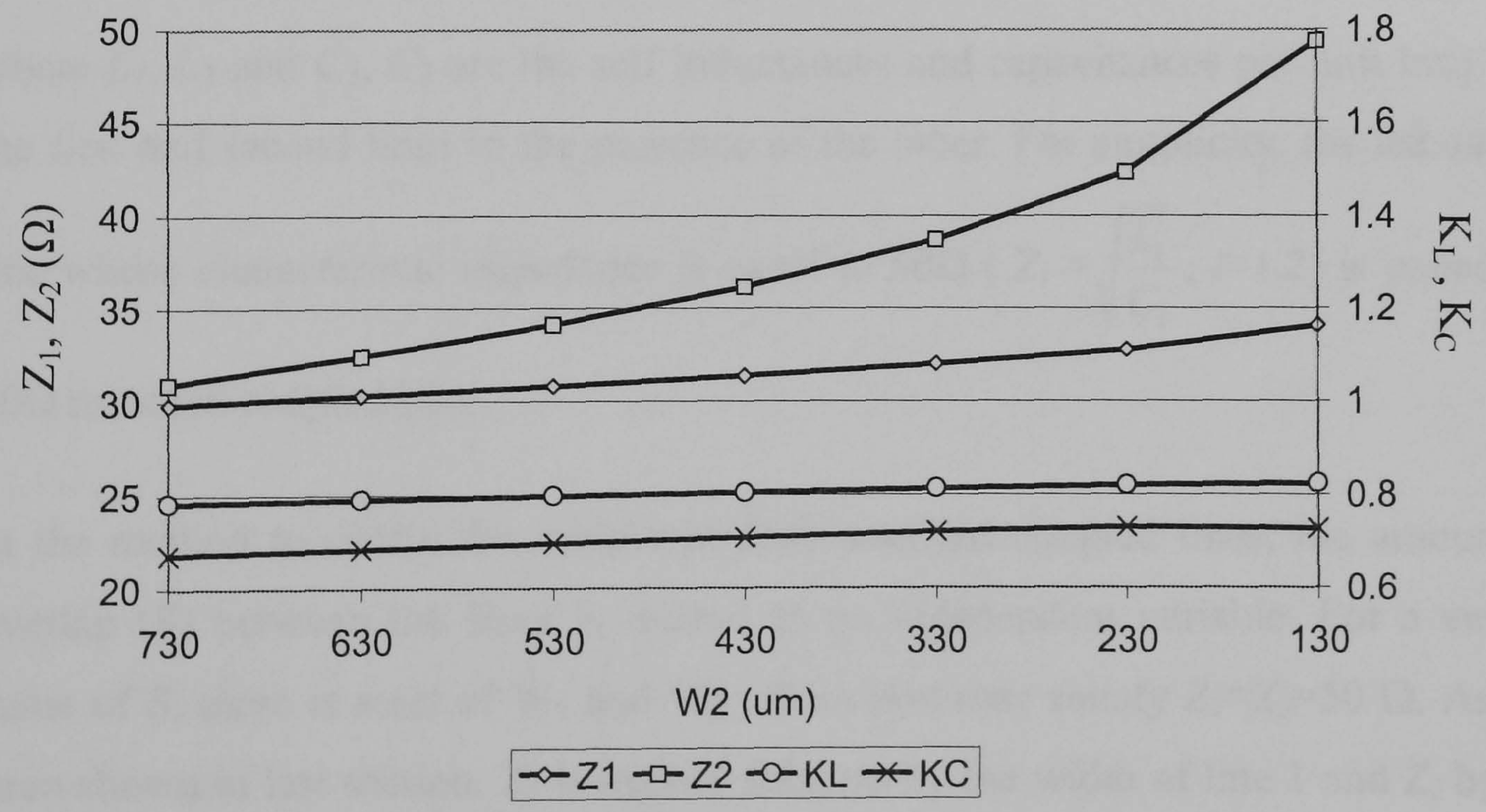

Figure 6.7 : Behaviour of multilayer coupled lines showing the effect of W_2 (W_1=590μm, S=-100μm, ε_{r1}=9.9, h_1=635μm, ε_{r2}=3.9, h_2=30μm)

6.9 50Ω Matched Coupled lines

Usually, the characteristic impedances of each uncoupled line in a multilayer coupler is different, and much of the literature focuses on determining what impedance should be used to terminate each port [6]. The main advantage of having different port impedances is that one does not require an additional impedance transformers to match the impedance of a low- or high-impedance device connected to that of the coupler. But more often the couplers are required to be connected with loads of 50Ω. In this study we are interested in design coupler that is matched to 50Ω at all four ports ($Z_{T1} = Z_{T2} = 50\Omega$).

For a certain amount of overlap(S), we are able to find a pair of W_1 and W_2 for 50Ω matched coupled lines, namely:

$$\sqrt{\frac{L_1}{C_1}} = \sqrt{\frac{L_2}{C_2}} = 50\Omega$$

where L_1, L_2 and C_1, C_2 are the self inductances and capacitances per unit length of the first and second lines in the presence of the other. For simplicity, the uncoupled line whose characteristic impedance is equal to 50Ω ($Z_i = \sqrt{\frac{L_i}{C_i}}$, i=1,2) is called the 50Ω matched coupled line.

In the method to obtain the widths of 50Ω matched coupled lines, the amount of overlap (S) between the lines is treated as an independent variable. For a certain value of S, there is a set of W_1 and W_2 values that may satisfy Z_1=Z_2=50 Ω. As has been shown in last section, Z_1 is mainly affected by the width of line 1 and Z_2 by the width of line 2. Basically the wanted values of W_1 and W_2 for 50Ω matched coupled lines can be obtained by adjusting the widths of the two lines separately.

The widths of 50Ω matched coupled lines versus the amount of overlap, S, for

various values of dielectric constant are plotted in Figure 6.8, along with the corresponding values of k_L and k_C. The base substrate used is Alumina, with ε_{r1}=9.9 and a thickness, h_1, of 635μm. The analysis is carried out for some typical printed thick-film dielectrics that have dielectric constants between 4 and 10. The thickness for the printed thick-film dielectric layer is assumed to be 30μm (achieved by three prints with each print of 10μm thickness), which is a practical situation for most thick-film processes.

It is seen from Figure 6.8, that the values of k_L and k_C for 50Ω matched coupled lines vary monotonically as the value of the dielectric constant (ε_{r2}) of the printed thick-film dielectric layer is increased. For a low dielectric constant (e.g ε_{r2}=4), $k_L > k_C$ and the difference between the two is of the order 0.07-0.12. As ε_{r2} is increased a point is found such that $k_L = k_C$, as shown in Figure 6.8(c). With further increase in ε_{r2}, i.e. high dielectric constant, $k_L < k_C$. Figure 6.9 shows that the change in the thickness of the printed thick-film dielectric has a relatively small effect on the inductive and capacitive coupling coefficients. This suggests that the difference between the inductive and capacitive coupling coefficient is mainly affected by the material used. Thus, if the material can be chosen freely, it may be possible to equalise k_L and k_C, so as to achieve a quasi-ideal coupler. However, in reality, the materials available to the designer are often limited, that means most often designers have to carry out designs under non-ideal conditions. Thus it is imporatnt to provide a design technique for multilayer microstrip couplers to achieve optimal performance under non-ideal conditions.

It also can be seen from Figure 6.8, that with an increase in the amount of overlap between the two lines, the width of the two coupled lines needs to be decreased to maintain the 50Ω match. The upper conductor track is always wider than the lower one. This is consistent with the conclusion obtained in Chpater 3 that the upper conductor has a lower effective relative permittivity because of the presence of the thick-film dielectric layer. This futher suggests that in the design of multilayer microstrip devices, in order to ensure the device is matched to 50Ω at all ports, the

upper conductor track need to be wider than the lower one. This is a useful design guide for multilayer microstrip circuit design.

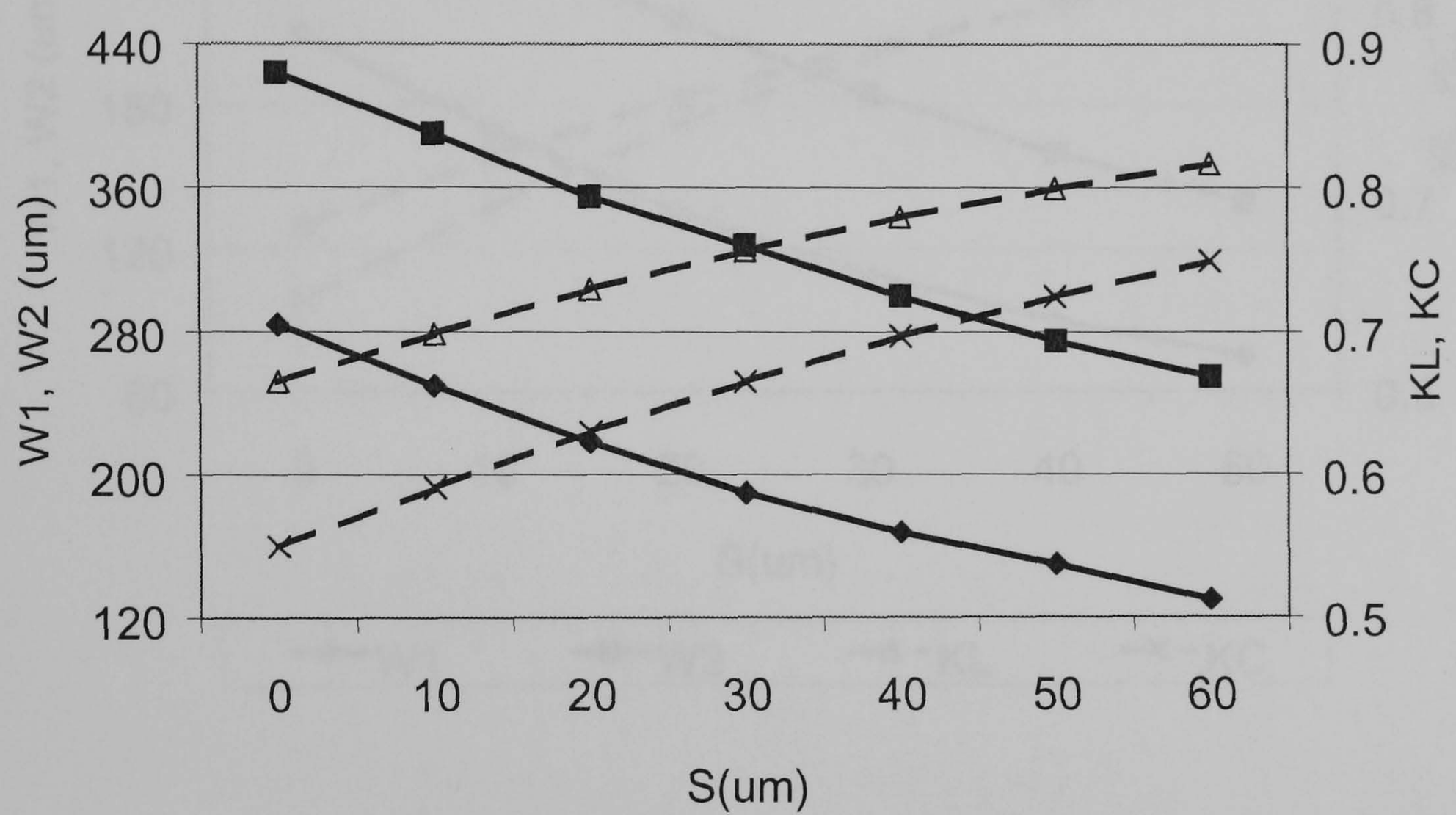

(a) ε_{r2}=4, h_2=30μm, ε_{r1}=9.9, h_1=635μm

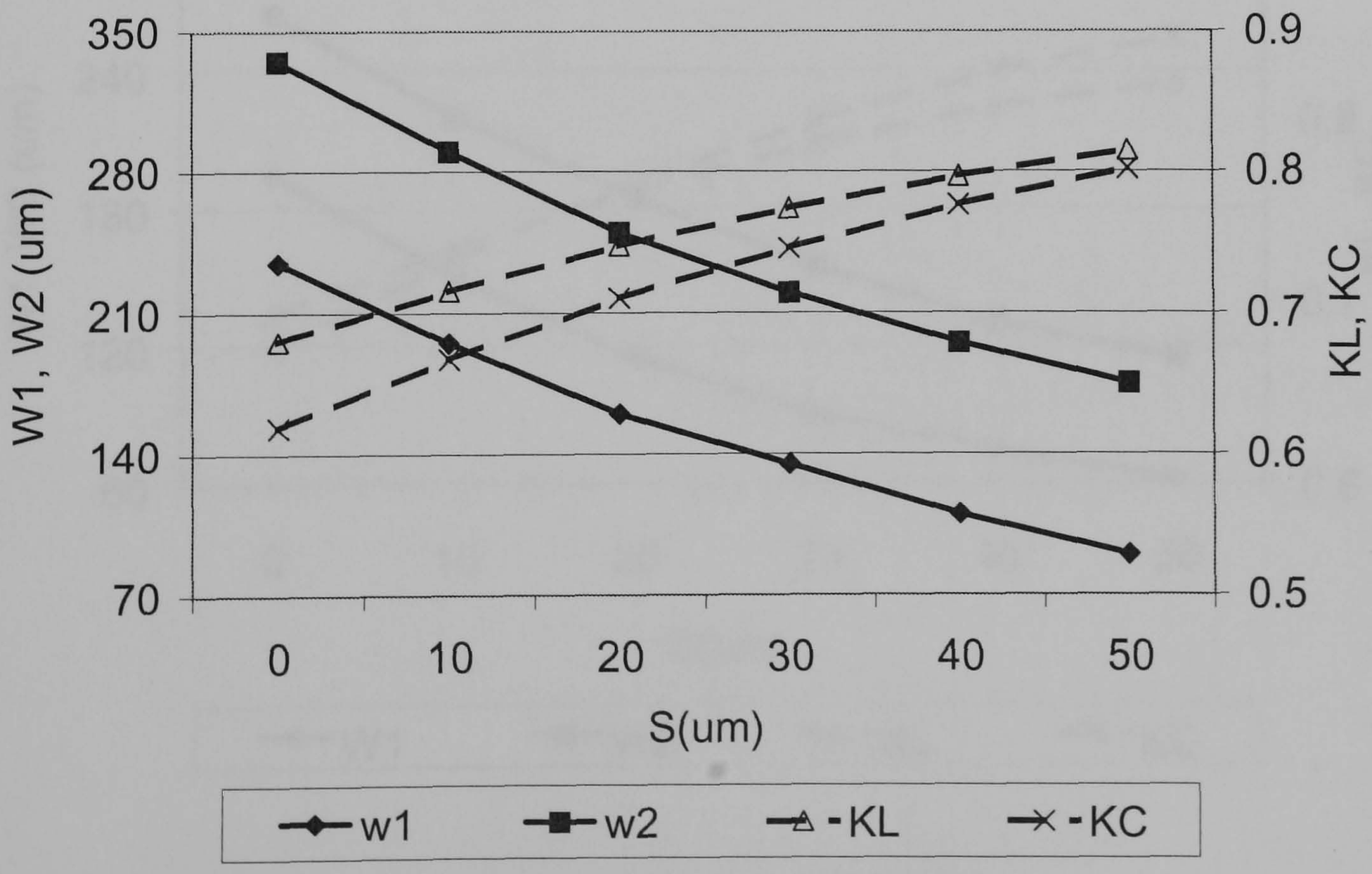

(b) ε_{r2}=6, h_2=30μm, ε_{r1}=9.9, h_1=635μm

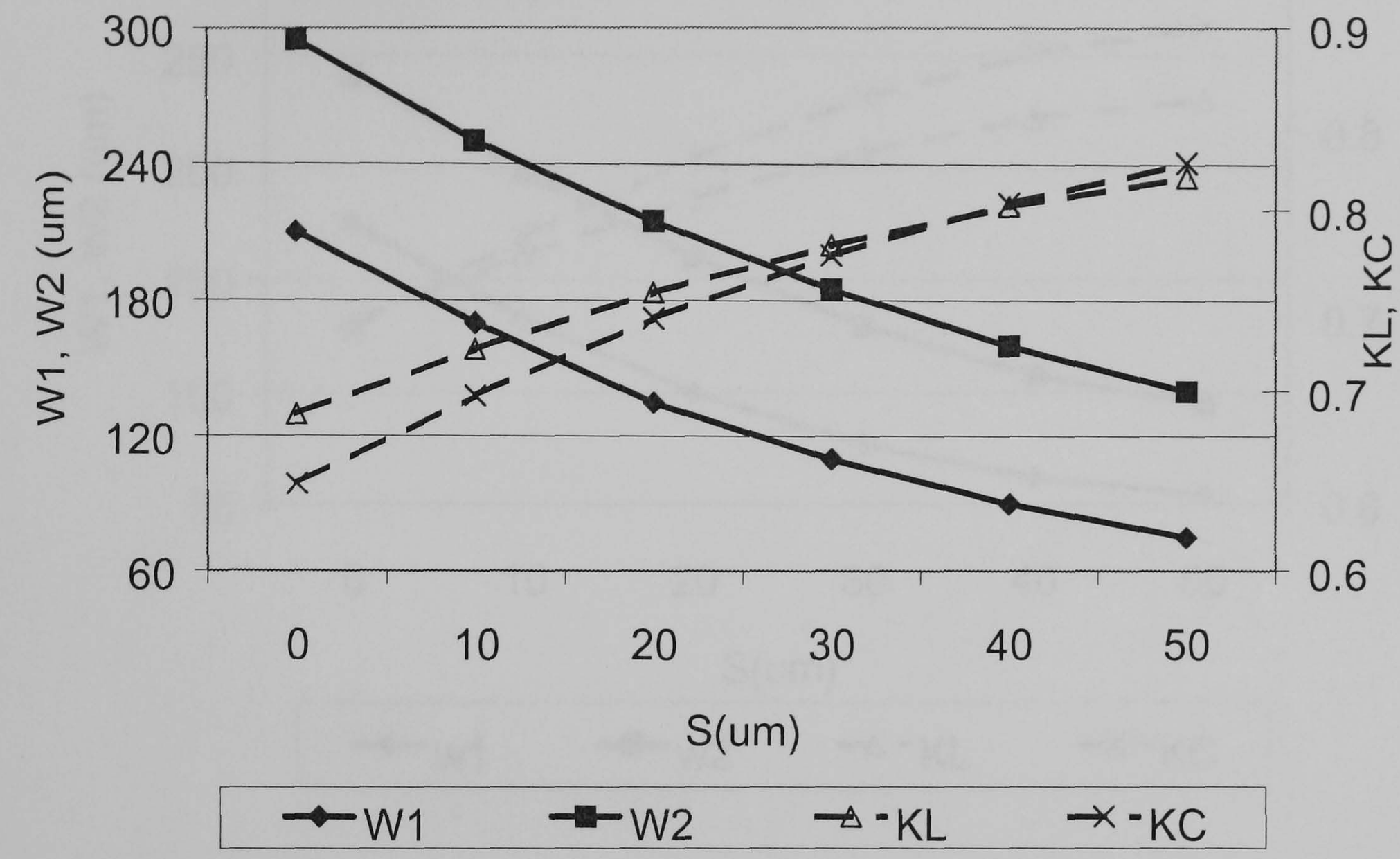

(c) ε_{r2}=7, h_2=30μm, ε_{r1}=9.9, h_1=635μm

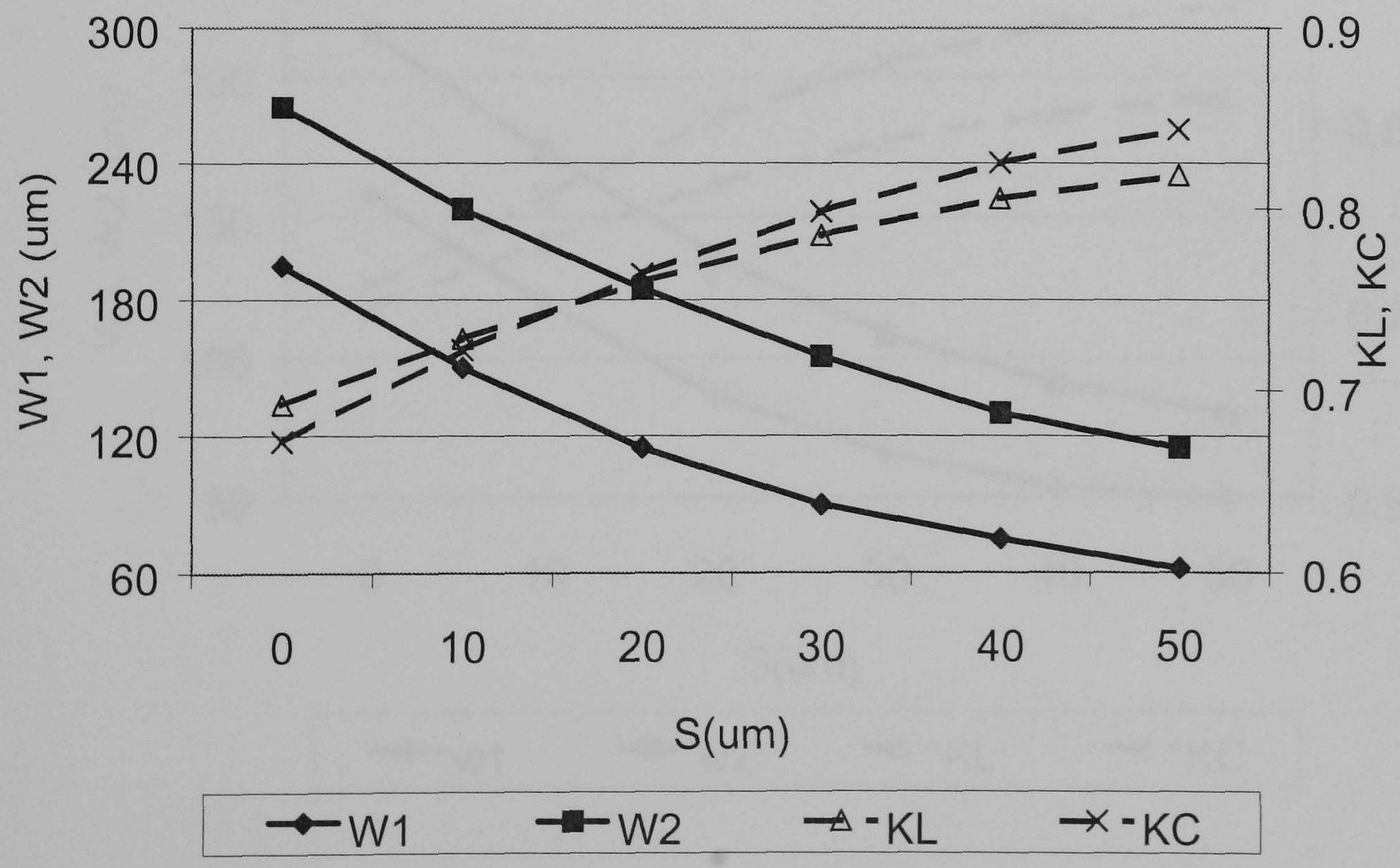

(d) ε_{r2}=8, h_2=30μm, ε_{r1}=9.9, h_1=635μm

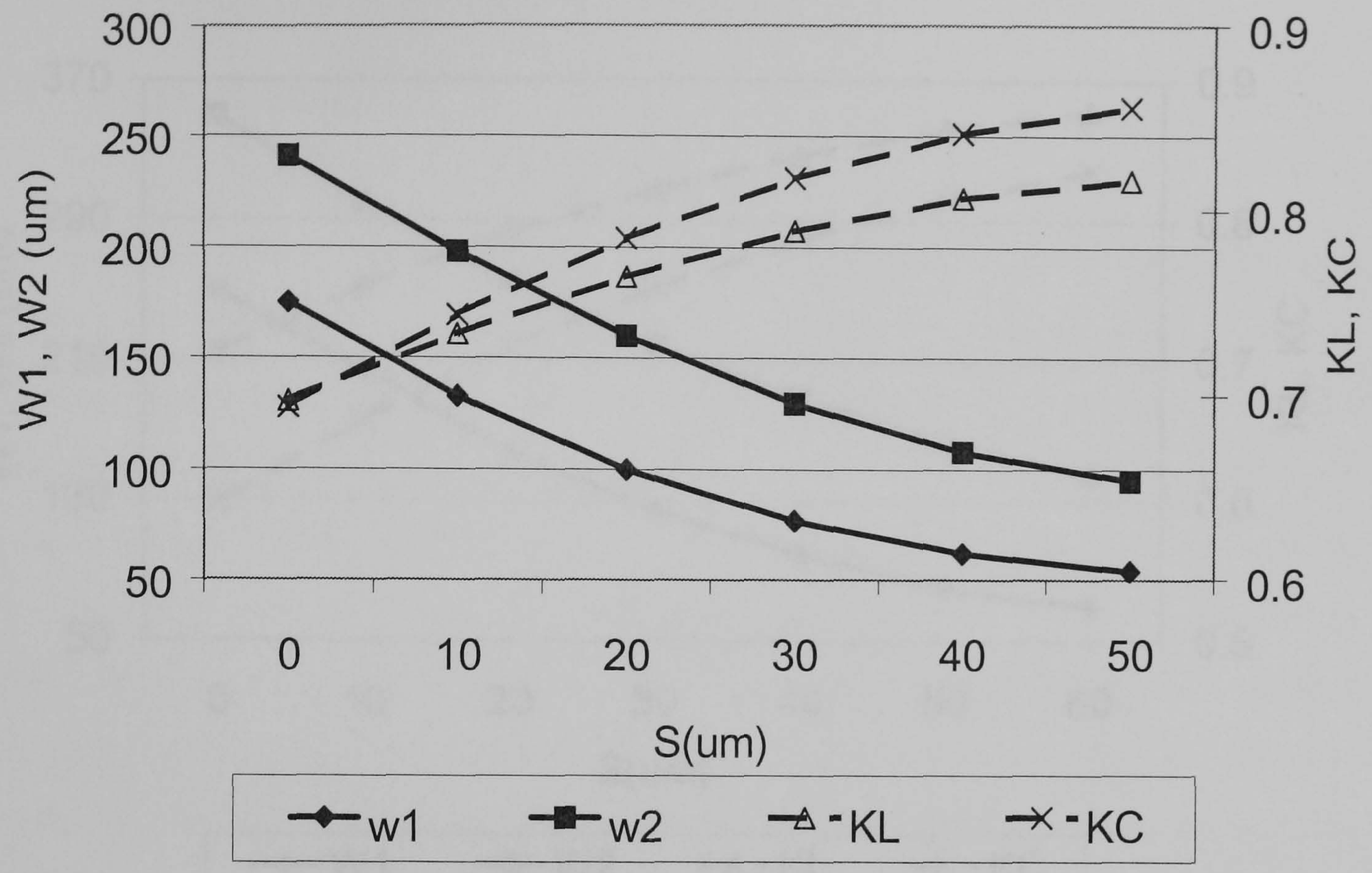

(e) ε_{r2}=9, h_2=30μm, ε_{r1}=9.9, h_1=635μm

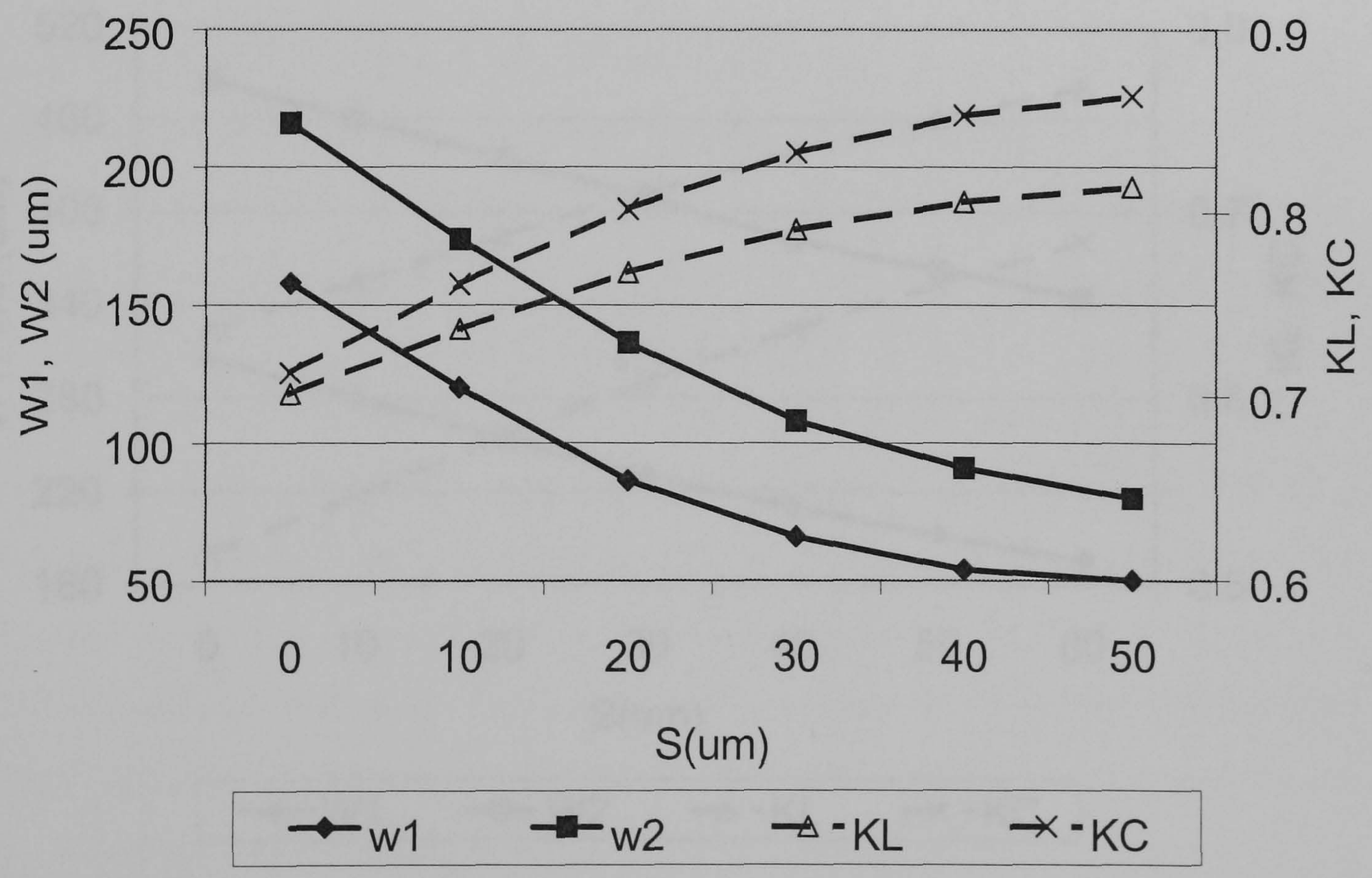

(f) ε_{r2}=10, h_2=30μm, ε_{r1}=9.9, h_1=635μm

Figure 6.8: W_1,W_2,K_L and K_C for 50Ω matched coupled lines showing the influence of S

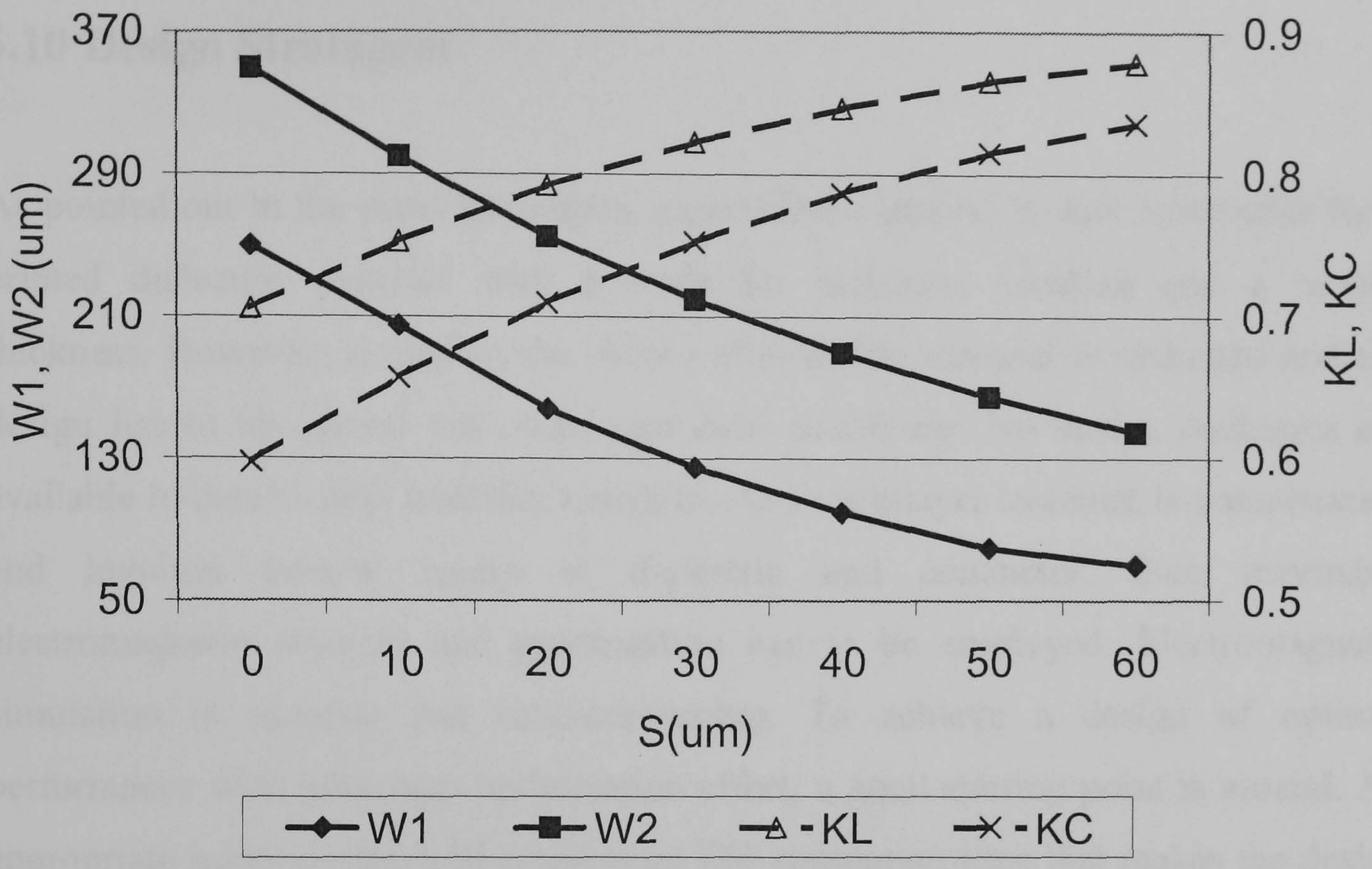

(a) ε_{r2}=4, h_2=20μm, ε_{r1}=9.9, h_1=635μm

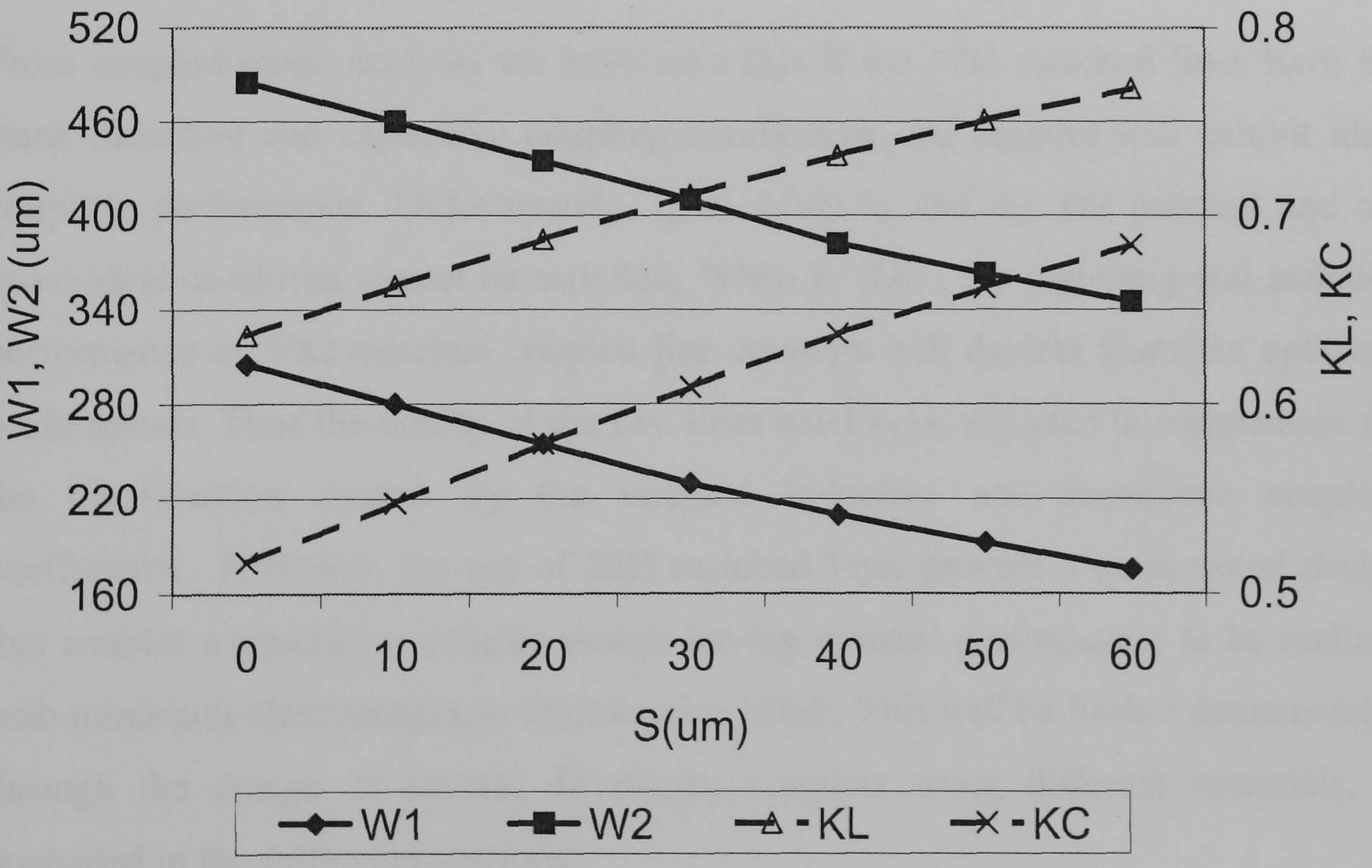

(b) ε_{r2}=4, h_2=40μm, ε_{r1}=9.9, h_1=635μm

Figure 6.9: W_1, W_2, K_L and K_C for 50Ω matched coupled lines showing the influence of h_2

6.10 Design Stratagem

As pointed out in the previous section, quasi-ideal coupling is only achievable for a printed dielectric material with a particular dielectric constant and a certain thickness. However, in reality, the choice of available material is restricted and the design has to be carried out under non-ideal conditions. No design equations are available to date to deal with this situation. As a multilayer structure is complicated, and involves several layers of dielectric and conductor, then inevitably electromagnetic analysis and optimization has to be employed. Electromagnetic simulation is accurate but time-consuming. To achieve a design of optimal performance with minimum optimization effort, a good starting point is crucial. An appropriate initial design will cause extra EM simulation time that makes the design more expensive. More importantly, the optimal performance may not be achievable, as the optimization may not converge.

From coupled-mode analysis we have seen that if the 50Ω matched lines have the same inductive and capacitive coupling coefficients, the coupler will exhibit ideal coupling performance. Unfortunately, quite often k_L and k_C are unequal and the quasi-ideal condition cannot be satisfied. When $k_L \neq k_C$, the matching and isolation performance of 50Ω matched coupled line couplers will deviate from the optimum performance. Thus the widths of the two lines need to be adjusted to compensate for the deterioration caused by the unequal inductive and capacitive coupling coefficients. However, the use of 50Ω matched lines provide a good initial design that enables a multilayer coupler design having optimal performance to be realized with minimum electromagnetic optimization effort. This will be further demonstrated through the design of several directional couplers using different materials, as presented in the following sections.

The design procedure is thus as follows. First the amount of overlap is chosen as an independent parameter. Using the graphs shown in Figure 6.8, we select W_1 and W_2 corresponding to the desired value of S. Starting with these initial parameters, we

wish to minimize the reflection coefficient at each port. Good matching at the four ports is always closely related to good isolation and directivity. As the matching performance at port 1 will mainly be affected by line 1 and the matching performance at port 2 will mainly be affected by line 2, the optimization of each line can be carried out separately. The change in the line width will not significantly change the coupling, as this is mainly determined by the amount of overlap (S). The length of the coupler is also obtained through EM optimization.

6.11 Design Examples

Using the design stratagem described in the previous section, 3dB multilayer directional couplers using thick-film dielectrics with the dielectric constant of 4,7,8 and 9, have been designed. The design data and simulated responses of these multilayer directional couplers are shown in Tables 6.1 through 6.4, and Figures 6.10 through 6.13, respectively. The couplers all designed with an Alumina base substrate having a dielectric constant of 9.9, and a thickness of 635μm.

In the design of 3dB multilayer directional couplers, the amount of overlap is first chosen to give the required coupling (3dB). The widths of 50Ω matched coupled line obtained in Section 6.9 (Figure 6.8), are used as the initial design data for the coupler. By adjusting the width of the two coupled lines, 3dB coupling with good matching and isolation performance has been achieved, as shown in Figures 6.10 through 6.13. Compared with single coupled line coupler, multilayer coupler overcomes the limited coupling (8dB), as discussed earlier. Tight coupling (3dB) is achieved over a broad bandwidth, without the need for fabricating a very fine gap.

It is worth mentioning that through the design and simulation of 3dB multilayer couplers using materials having different dielectric constants, it can be seen that the optimal coupler performance is affected by the material used. As already observed

from Figure 6.9, the material with relative dielectric constant of 4 results in a large difference between k_L and k_C. Correspondingly, the optimal performance using this material is less than other material. However, still, it is a good performance. Best performance is achieved when using dielectric of 7. This is a significant result: it shows that there is an optimum value of the dielectric constant of the printed dielectric layer. This is information not previously reported in the literature.

Table 6.1: Design data for a multilayer 3dB coupler at 6GHz when ε_{r2}=4

ε_{r2}	h_2	W_1	W_2	S	*l*
4	30 μm	200μm	230μm	70μm	5250μm

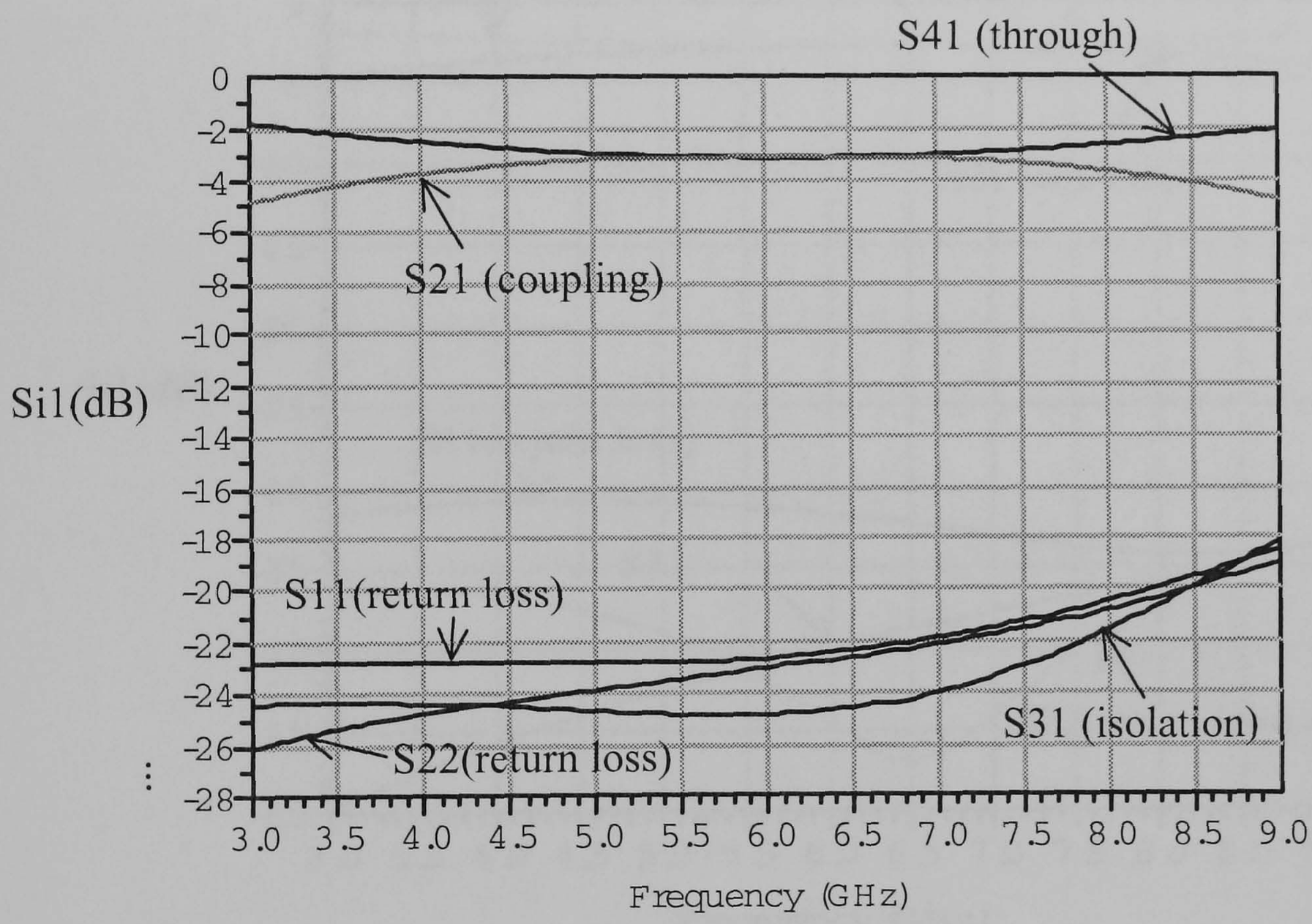

Figure. 6.10: Simulated response of a 3dB multilayer directional coupler.
(ε_{r1}=9.9, h_1=635μm, ε_{r2}=3.9, h_2=30μm)

Table 6.2: Design data for a multilayer 3dB coupler at 6GHz when $\varepsilon_{r2}=7$

ε_{r2}	h_2	W_1	W_2	S	*l*
7	30 μm	135μm	180μm	50μm	4400μm

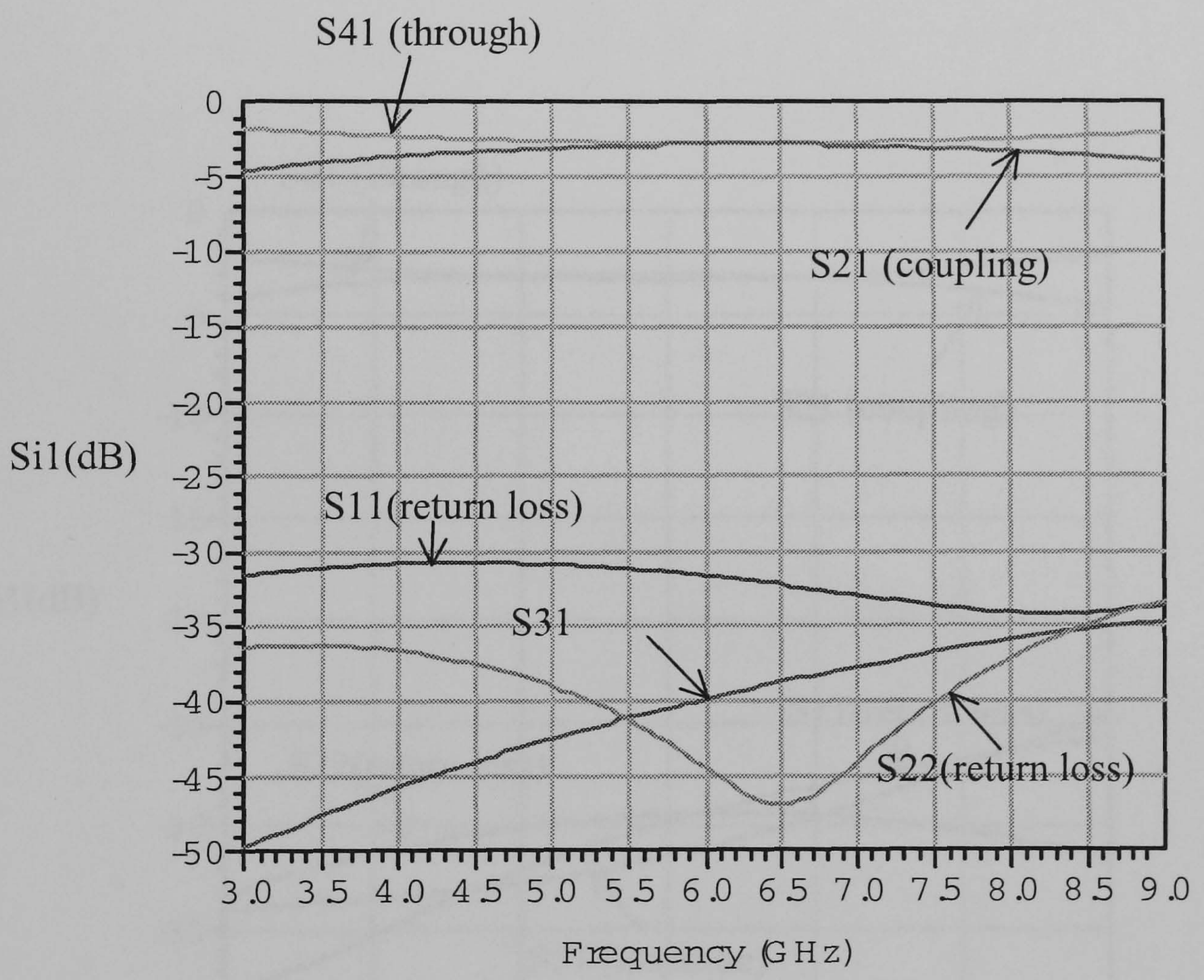

Figure 6.11: Simulated response of a 3dB multilayer directional coupler. ($\varepsilon_{r1}=9.9$, $h_1=635\mu m$, $\varepsilon_{r2}=7$, $h_2=30\mu m$)

Table 6.3: Design data for a multilayer 3dB coupler at 6GHz when $\varepsilon_{r2}=8$

ε_{r2}	h_2	W_1	W_2	S	l
8	28 μm	100μm	180μm	50μm	4500μm

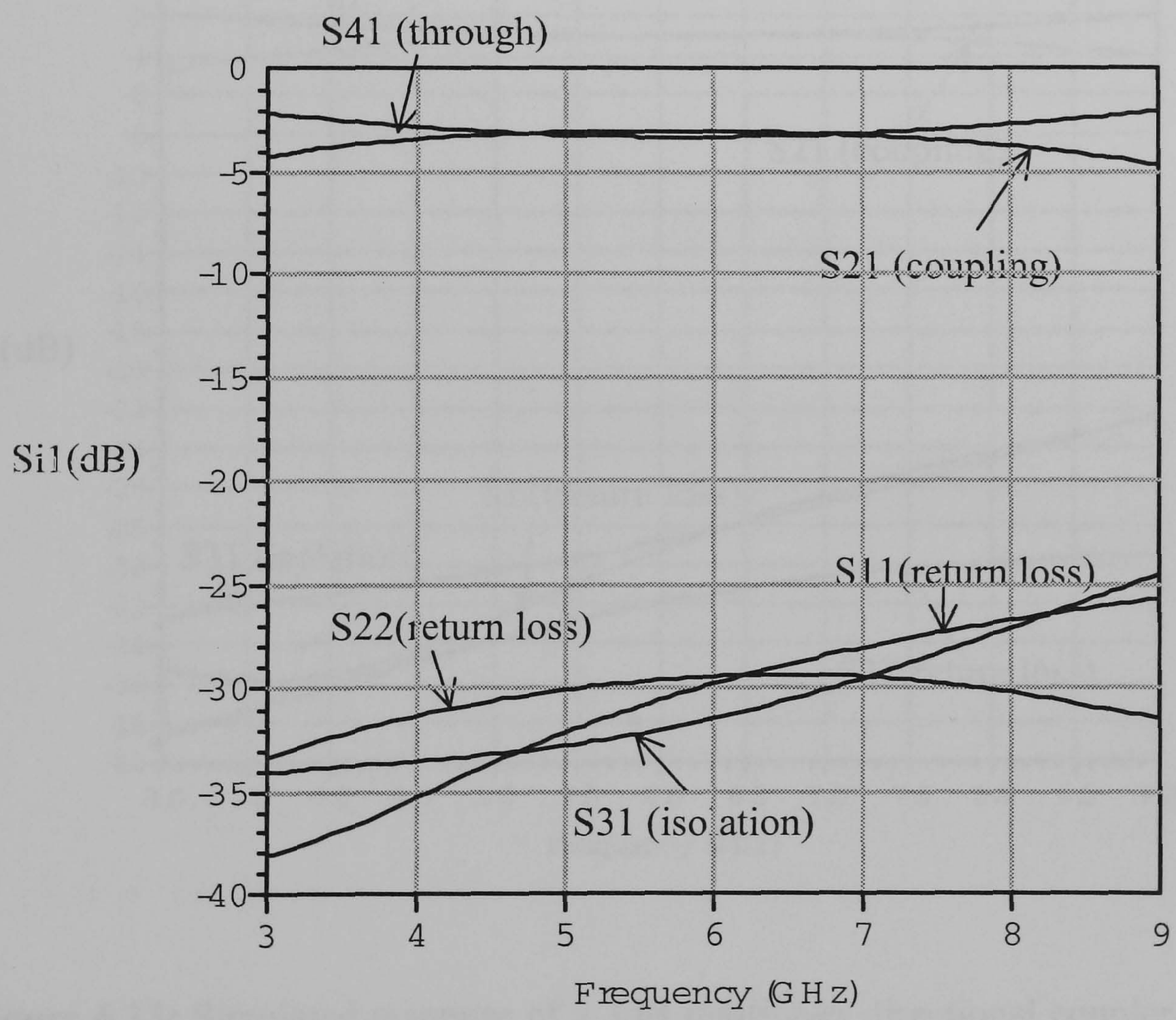

Figure 6.12: Simulated response of a 3dB multilayer directional coupler. ($\varepsilon_{r1}=9.8$, $h_1=635\mu m$, $\varepsilon_{r2}=8$, $h_2=28\mu m$)

Table 6.4: Design data for a multilayer 3dB coupler at 6GHz when ε_{r2}=9

ε_{r1}	h_1	W_1	W_2	S	*l*
9	30 μm	100μm	230μm	40μm	4200μm

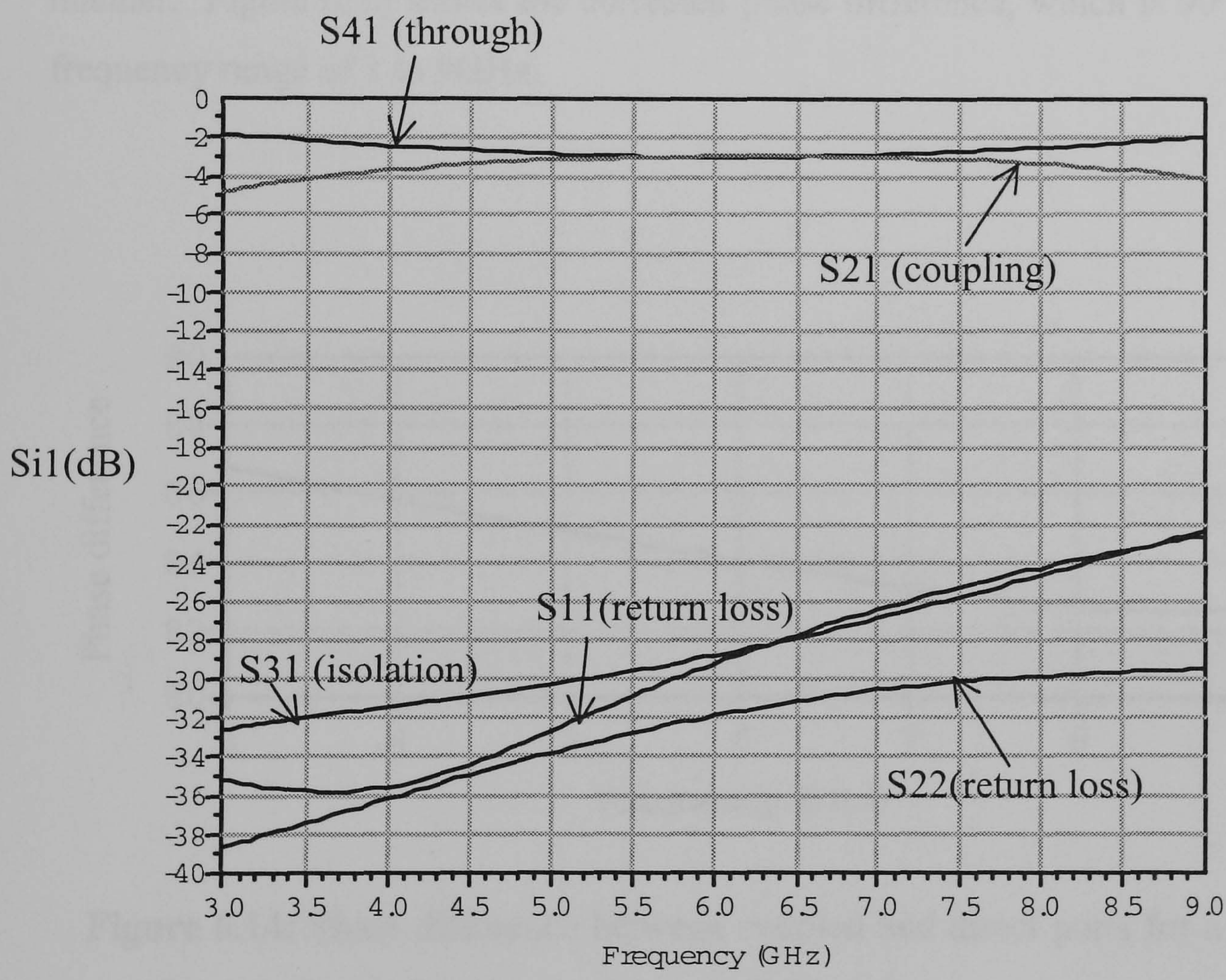

Figure 6.13: Simulated response of a 3dB multilayer directional coupler. (ε_{r1}=9.9, h_1=635μm, ε_{r2}=9, h_2=30μm)

6.12 Phase Compensation

The phase difference between the coupled port and through port of a coupler (the corresponding design data of the coupler is shown in Table 6.1) is plotted in Figure 6.14. The phase difference is $85.4^{o}\pm1.7^{o}$. It is noted that the phase diverges linearly. This suggests that a length of transmission line could be added for correction (Figure 6.15). The electrical length of the added line can be calculated in a straightforward manner. Figure 6.16 shows the corrected phase difference, which is $90^{o}\pm0.2^{o}$ in the frequency range of 3 to 9GHz.

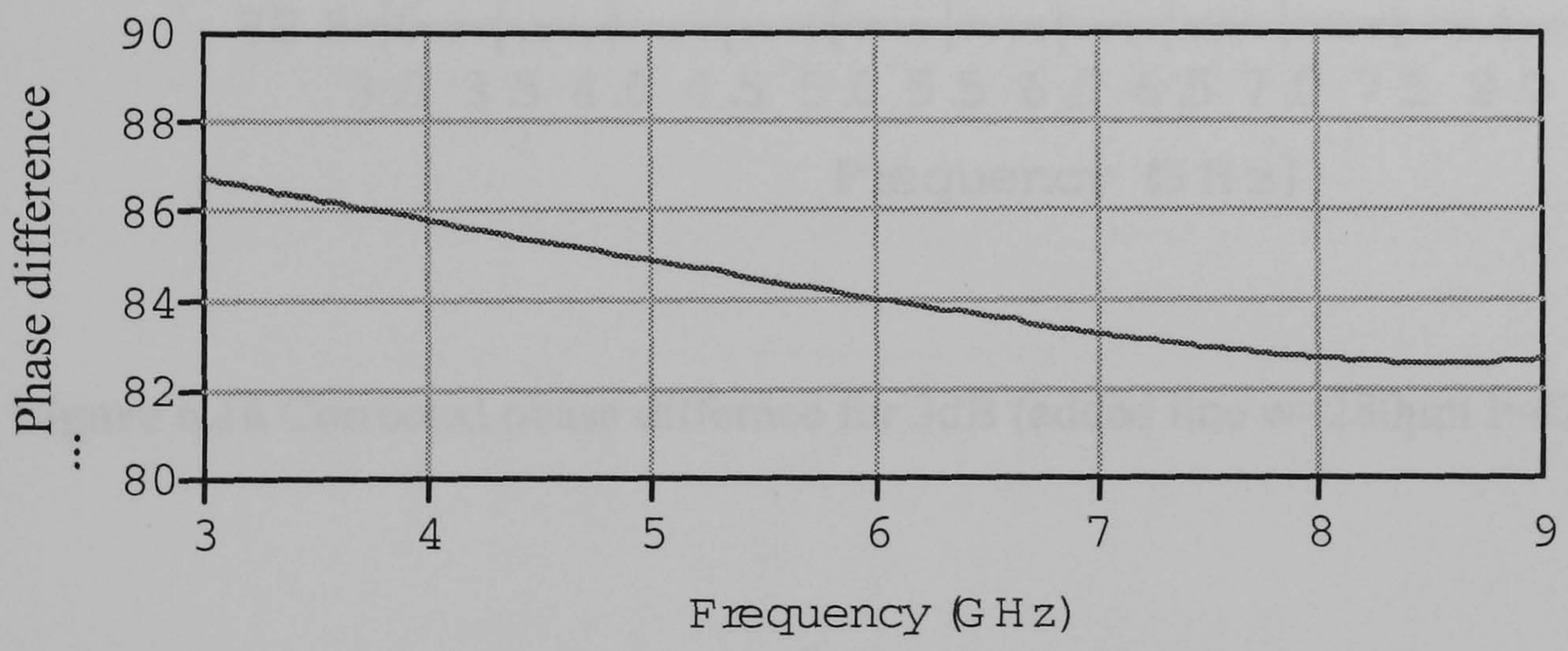

Figure 6.14: Phase difference between coupled and direct ports for a 3dB coupler (coupler design data is shown in Table 6.1)

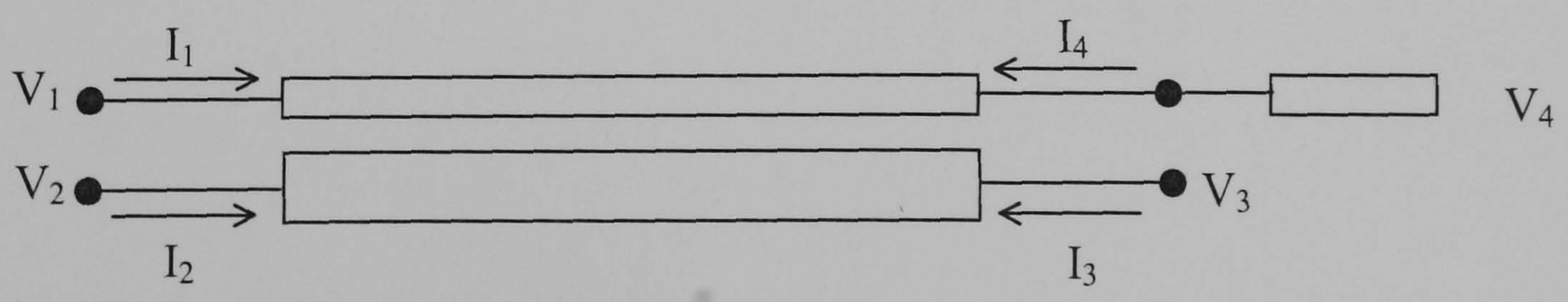

Figure 6.15: Diagram showing an additional length of line added for phase correction.

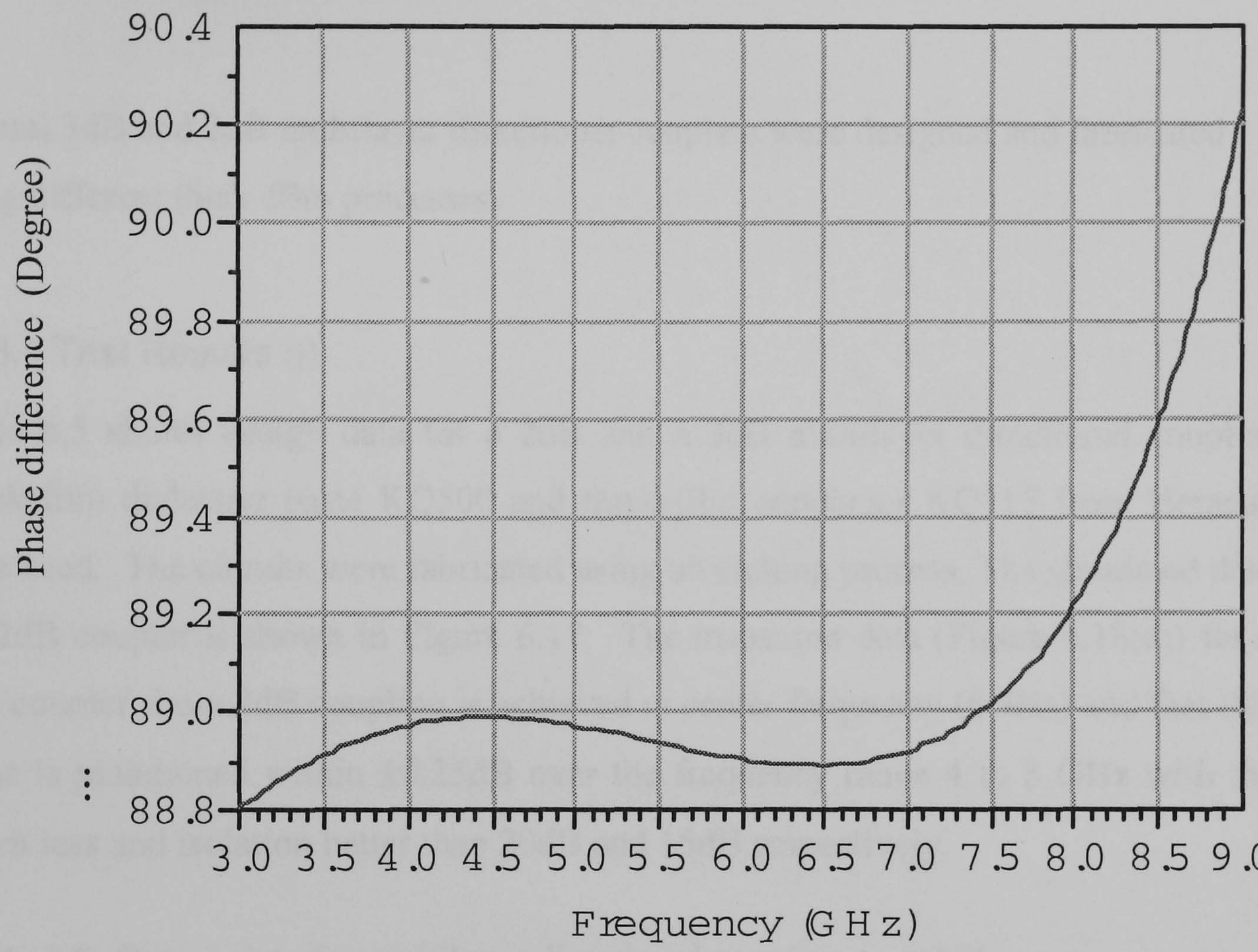

Figure 6.16 Corrected phase differnce for 3dB (added line w=280μm l=420μm)

By adding the correction line, the phase difference has been significantly reduced, while the coupling and directivity are essentially unchanged.

6.13 Test Results

Several 3dB and 2dB multilayer directional couplers were designed and fabricated using different thick-film processes.

6.13.1 Test Results (I)

Table 6.5 shows design data for a 2dB and a 3dB multilayer directional coupler. Thick-film dielectric paste KQ500 and thick-film conductor KQ115 from Heraeus were used. The circuits were fabricated using an etching process. The simulated data for 2dB coupler is shown in Figure 6.17. The measured data (Figure 6.18(a)) for a 2dB coupler show 2dB coupling is achieved at center frequency (6GHz) and that this value is maintained within ±0.25dB over the frequency range 4 to 8 GHz with the return loss and isolation better than 20dB and 15dB respectively.

Table 6.5: Design data for multilayer directional couplers (ε_{r1}=3.9)

Substrate			
ε_r	H	ε_{r1}	h_1
9.9	635μm	3.9	30μm
Physical dimension (μm)			
	W1	W2	S	1
2dB	140	190	100	5250
3dB	200	230	70	3260

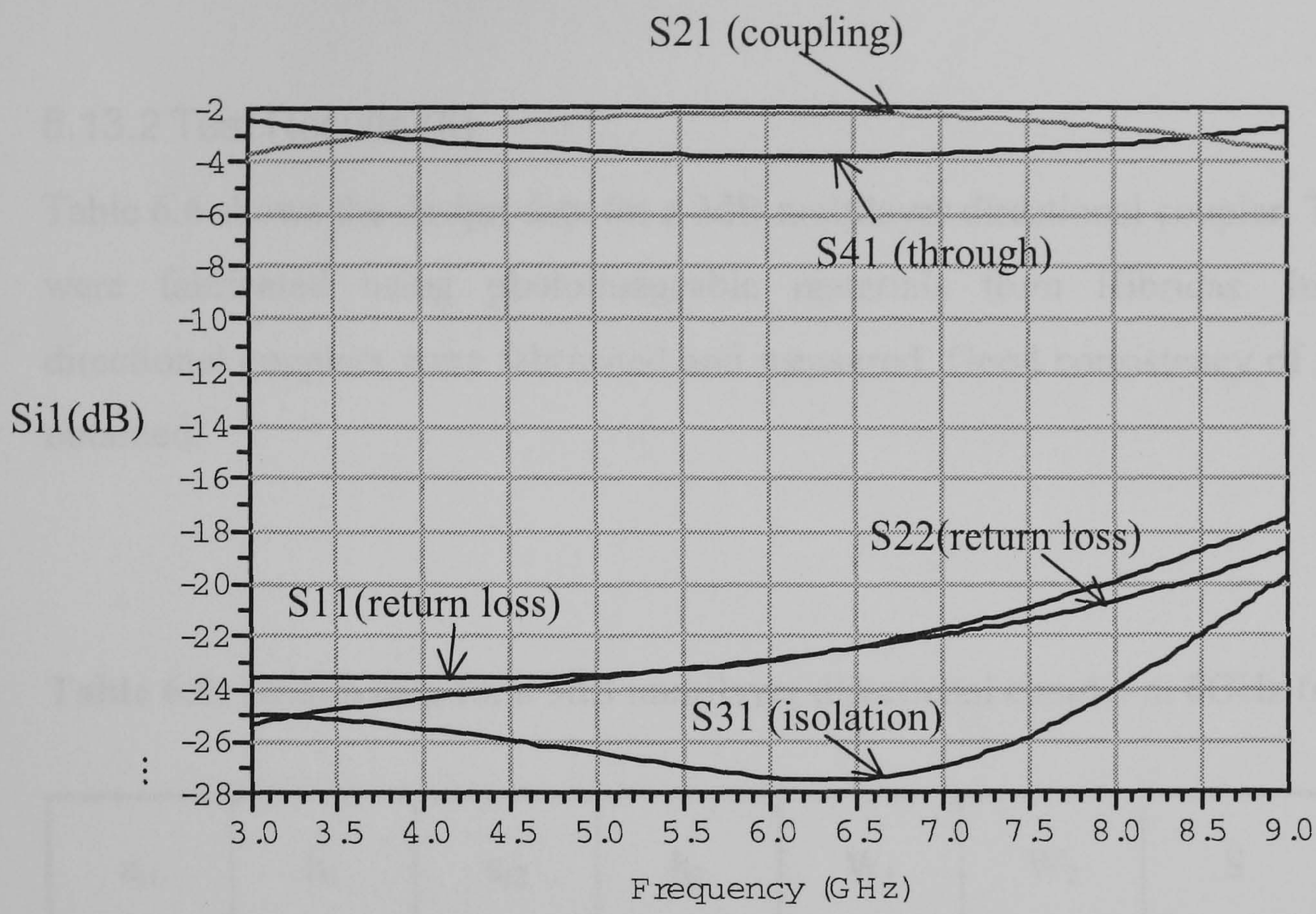

Figure. 6.17: Simulated response of a 2dB multilayer directional coupler at 6GHz. (ε_{r1}=9.9, h_1=635μm, ε_{r2}=3.9, h_2=30μm)

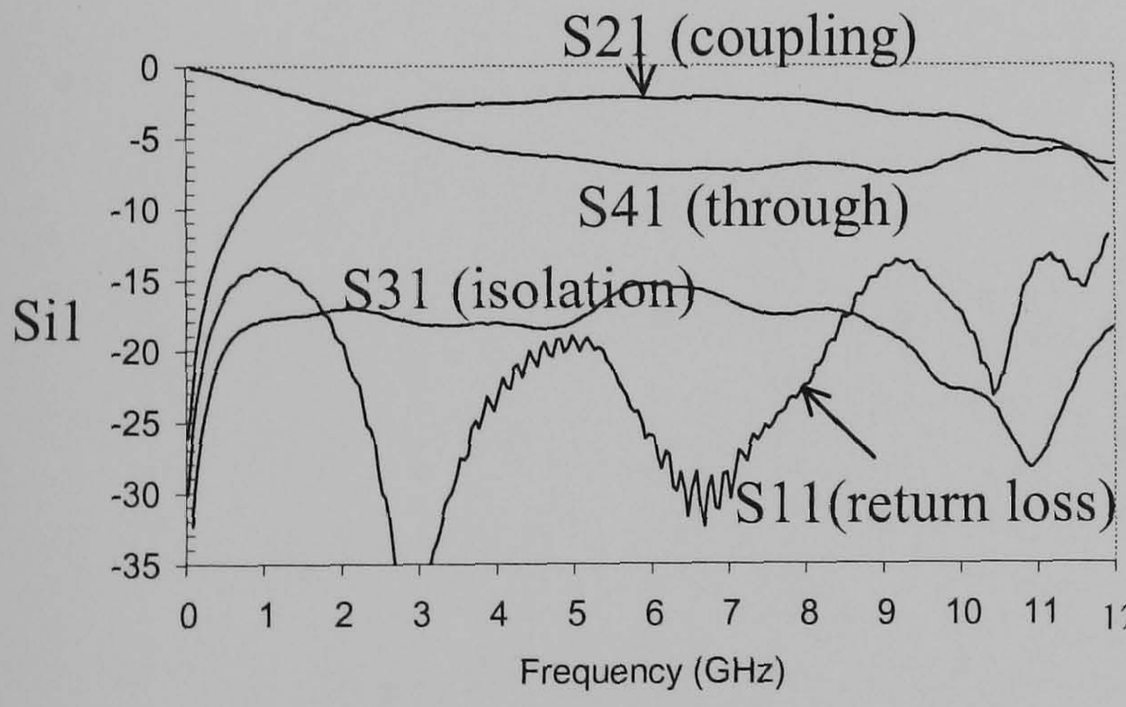

Figure 6.18(a): Measured response of a 2dB multilayer directional coupler.

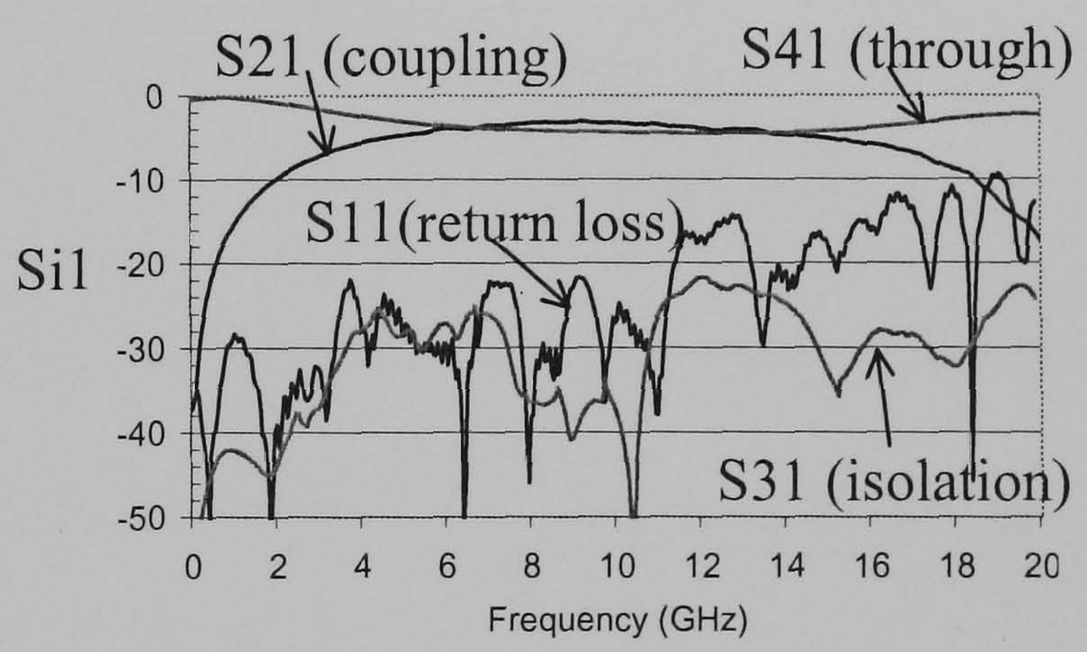

Figure 6.18 (b): Measured response of a 3dB multilayer directional coupler.

The measured performance for a 3dB coupler (Figure 6.18(b)) shows that 3dB coupling is achieved over a relative broad bandwidth (6-14GHz) with very promising isolation (better than 22dB) and good matching (return loss better than 15dB).

6.13.2 Test Results (II)

Table 6.6 shows the design data for a 3dB multilayer directional coupler. The circuits were fabricated using photoimageable materials from Hibridas. In all, four directional couplers were fabricated and measured. Good consistency of results was obtained.

Table 6.6: Design data for a 3dB multilayer directional coupler at 6GHz (ε_{r2}=8)

ε_{r1}	h_1	ε_{r2}	h_2	W_1	W_2	S	*l*
9.8	635 μm	8	28 μm	100μm	180μm	50μm	4500μm

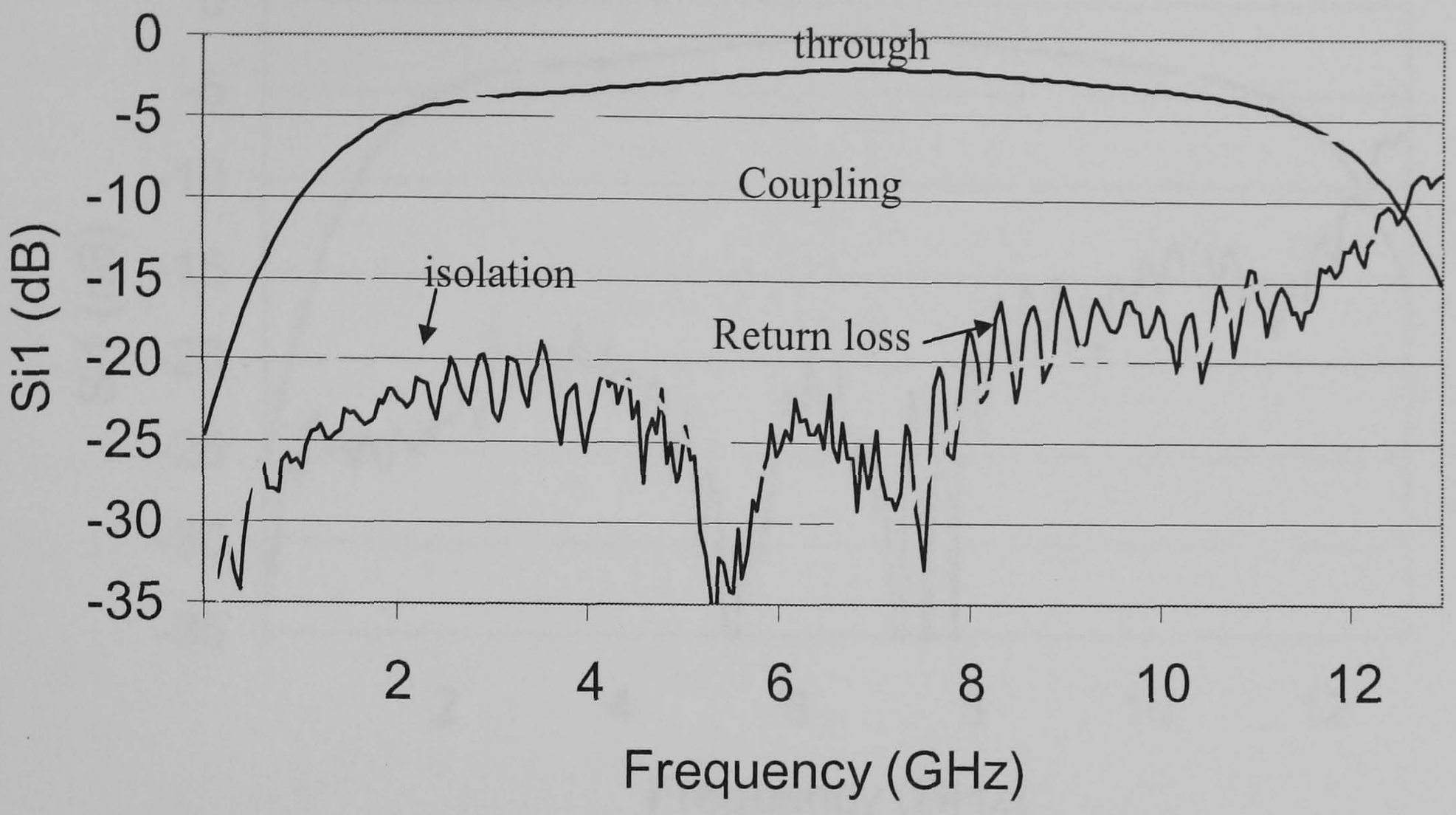

(a) 3dB coupler #1

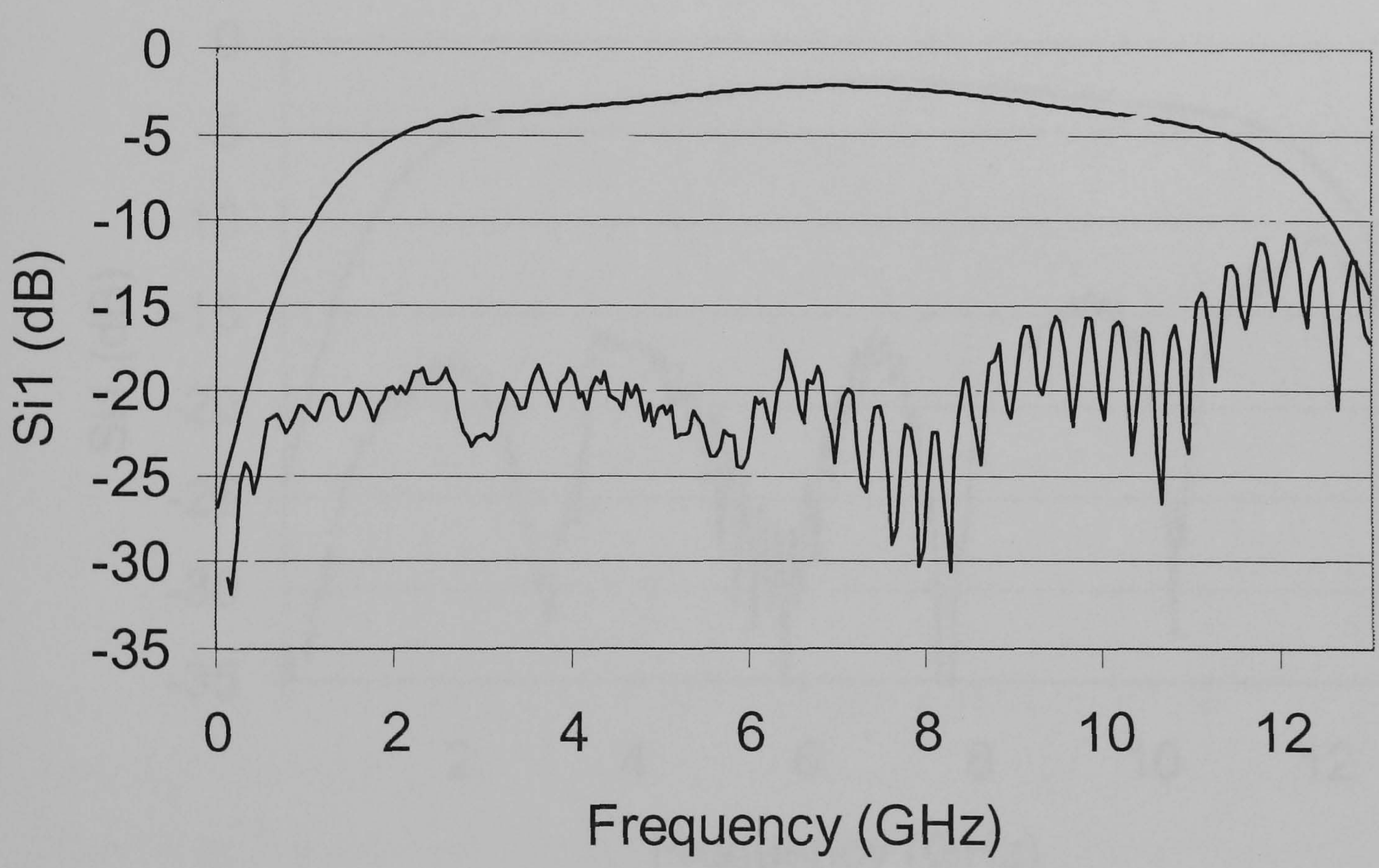

(b) 3dB coupler #2

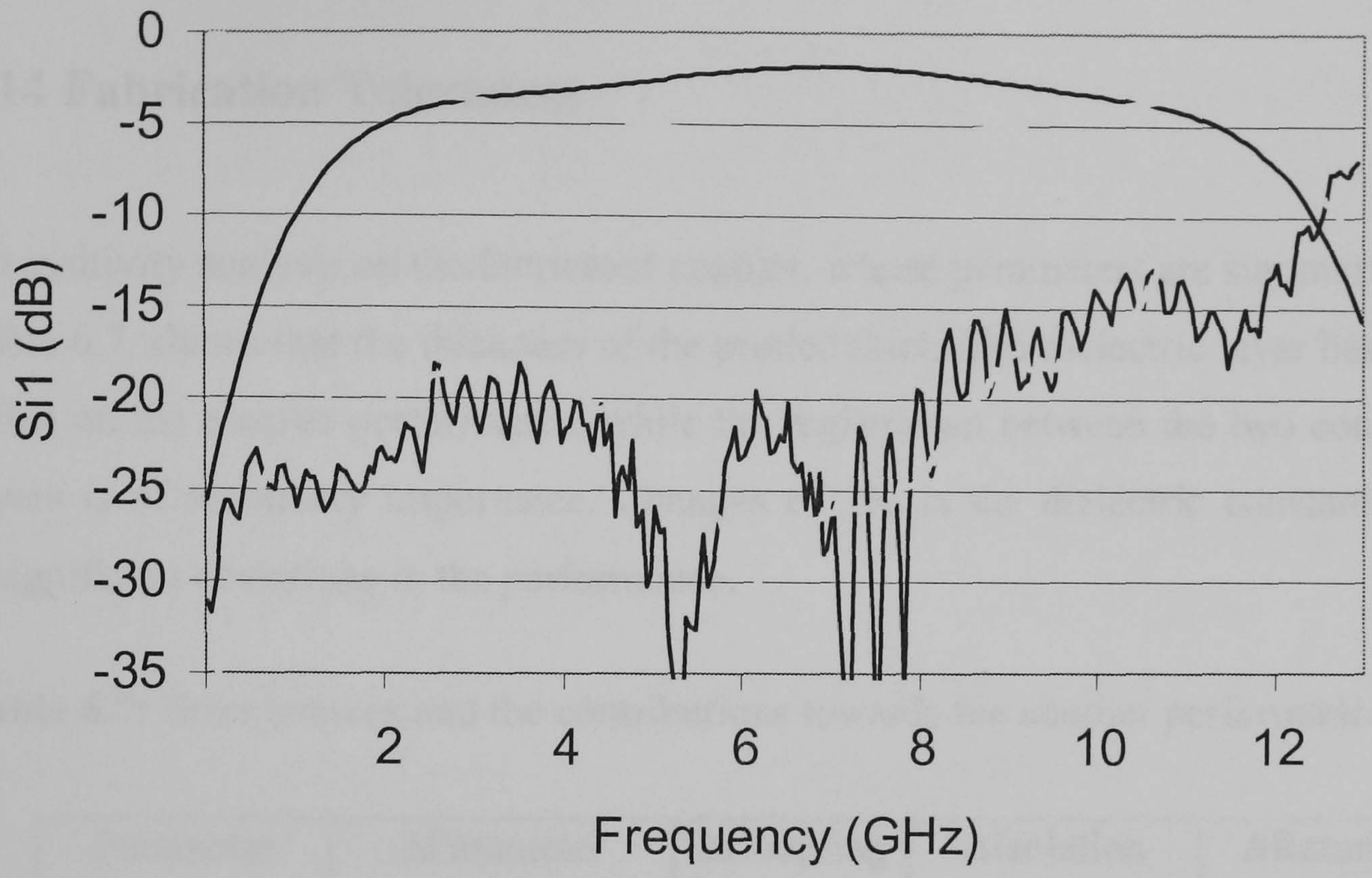

(c) 3dB coupler #3

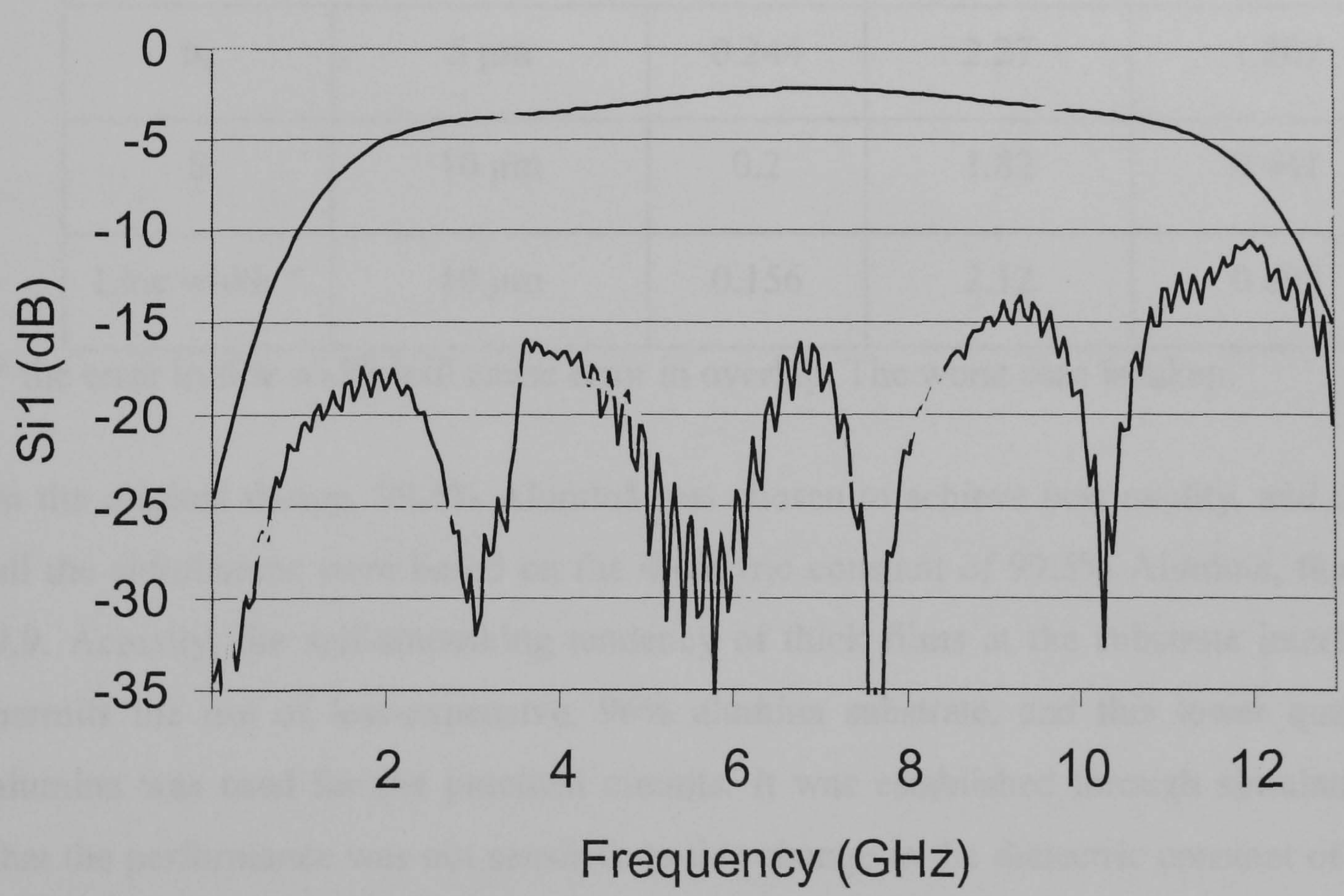

(d) 3dB coupler #4

Figure 6.19: Measured response of 3dB multilayer directional couplers

6.14 Fabrication Tolerances

A sensitivity analysis on the fabricated coupler, whose parameters are summarized in Table 6.7, shows that the thickness of the printed thick-film dielectric layer has most affect on the coupler performance, while the registration between the two conductor layers is of secondary importance. Changes of 5% in the dielectric constant cause insignificant deviations in the performance.

Table 6.7: Error sources and the contributions towards the coupler performance

Parameter	ΔParameter	ΔCoupling	ΔIsolation	ΔReturn loss
ε_{r1}	0.2	0.041	0.787	1.858
h_1	5 μm	0.244	2.27	1.207
S	10 μm	0.2	1.82	0.441
Line width *	10 μm	0.156	2.12	0.808

* the error in line width will cause error in overlap. The worst case is taken.

In the original design, 99.5% Alumina was chosen to achieve best quality, and thus all the simulations were based on the dielectric constant of 99.5% Alumina, that is 9.9. Actually, the self-smoothing tendency of thick films at the substrate interface permits the use of less-expensive, 96% alumina substrate, and this lower quality alumina was used for the practical circuits. It was established through simulation, that the performance was not sensitive to this change in the dielectric constant of the base substrate, i.e. the change in ε_r from 9.9 to 9.6.

6.15 Conclusions

A new design strategy for multilayer directional couplers has been developed and

validated through practical measurement. The technique offers a simple and practical approach to exploiting the design flexibility of three-dimensional microwave structures. Using this new technique, a measured coupling coefficient of 2dB has achieved. There was a good agreement between the predicted and measured data, with the coupler exhibiting a very wide bandwidth.

It has been shown that multilayer structure provides a simple geometry to realize large coupling factors without the need for rigorous manufacturing tolerances. Remarkably, if the dielectric constant of one of the layers can be freely chosen, ideal coupler performance is achievable. This provided new information on the optimum values for the dielectric constant of the printed dielectric that has not previously been reported in the literature. Even when the choice of dielectric constant is restricted, good results can still be obtained using the multilayer approach.

6.16 References

[1] J. Lange, 'Interdigitated stripline quadrature hybrid,' *IEEE Trans. Microwave Theory Tech.,* vol. MTT-17, pp. 1150-1151, Dec. 1969.

[2] Tripathi, V. K., ' Asymmetric coupled transmission lines in an inhomogeneous medium ', *IEEE Trans. Microwave Theory Tech.,* Vol. MTT-23, No.9, pp.734-739, Sept. 1975.

[3] Krage, M. K. and Haddad, G., ' characteristics of coupled microstrip transmission lines-I: coupled-mode formulation of inhomogeneous lines', *IEEE Trans. Microwave Theory Tech.,* Vol. MTT-18, No.4, pp.217-222, Apr. 1970.

[4] Sachse, K., ' The scattering parameters and directional coupler analysis of characteritically terminated asymmetric coupled translission lines in an inhomogeneous medium', *IEEE Trans. Microwave Theory Tech.,* Vol. MTT-38,

No.4, pp.417-425, Apr. 1990.

[5] Djordjevic, A. R., Bazdar, M. B., Sarkar, T. K. and Harrington, R. F., *LINPAR for Windows: Matrix Parameters for Multiconductor Transmission Lines, Software and User's Manual, Version 2.0*, Artech House, 1999.

[6] Tripathi, V. K. and Chin, Y. K., ' Analysis of the general nonsymmetrical directional coupelr with arbitrary terminations', *IEE Proc.,* Vol. 129, pt. H., pp. 360-362, 1982.

Chapter 7

Conclusions and Suggestions for Further Work

7.1 Conclusions

The original aim of this work, namely to develop a design methodology for multilayer microwave structures using thick-film technology, has been achieved. A variety of multilayer microwave structures such as multilayer end-coupled filters, DC blocks and directional couplers have been designed, fabricated and tested. Good agreement between the measured results and theoretical analysis has been achieved, that verifies the validity of the design methodology developed in this study.

A new slit cavity technique was developed for the measurement of thick-film dielectric materials in a two-layer format that enables the materials to be characterized accurately and easily. The method has been verified through measurement on several thick-film materials over X-band.

A new design procedure for multilayer end-coupled filters has been developed, that enables the designer to arrive at the physical dimensions of the multilayer structure, based on the given filter specification. This design technique combines the accuracy of electromagnetic (EM) analysis and efficiency of circuit simulation. A 40% filter bandwidth has been achieved experimentally, that shows a very significant improvement over conventional single layer structures, where the bandwidth achievable is normally less than 5%.

Excellent results were obtained for DC blocks fabricated in a multilayer format. In particular, very wide bandwidth was obtained combined with low insertion loss. These results demonstrate clearly the usefulness of the multilayer structure for obtaining strong conductor coupling and overcoming the need to fabricate fine gaps.

Furthermore, the simulation results for coupled-line bandpass filters show that the multilayer approach can profitably be applied to other structures, where tight conductor coupling is a critical requirement.

For the first time, the properties of multilayer coupled-lines using a range of different thick-film dielectrics are examined using their coupled-mode parameters. This provides greater insight into the behaviour of the device. Remarkably, it is found that if the dielectric constant of one of the layers can be freely chosen, ideal coupler performance is achievable. This has useful practical significance in terms of choosing the optimum values for the dielectric constant of the printed dielectric that has not previously been reported in the literature. However, even when the choice of dielectric constant is restricted, good results can still be obtained using the multilayer approach.

A new design strategy for multilayer directional couplers has been developed and validated through practical measurement. The technique offers a simple and practical approach to exploiting the design flexibility of three-dimensional microwave structures. Using this new technique, a measured coupling coefficient of 2dB has

achieved. There was a good agreement between the predicted and measured data, with the coupler exhibiting a very wide bandwidth.

Overall the work has led to the development of a potentially powerful design technique for multilayer thick-film microwave circuits. It has been shown that multilayer structures provide a simple geometry to realize large coupling without the need for rigorous manufacturing tolerances. The current work has also shown that multilayer structures, in conjunction with low-cost thick-film technology, offer the possibility to produce small size, low-cost high performance microwave circuits easily, and with high reliability.

7.2 Suggestions for Further Work

Whilst the original concepts of the work have been established, there are a number of aspects that warrant further investigation. In particular:

- To extend the concept of the slit cavity for measurement of lower loss materials
- To extend the design techniques developed in this study to multilayer coplanar waveguide structures

7.2.1 Slit circular cavity

The inclusion of the slits in a resonant rectangular cavity has been shown to be useful in improving the accuracy and repeatability of dielectric measurements, whilst providing a simple measurement procedure. Rectangular cavities have a simple geometry and are suitable for measuring materials with loss tangents of the order of 10^{-4}. For measurement of material with lower loss, a cylindrical cavity is more useful as it has much higher value of Q-factor.

For example, a rectangular cavity formed from X-band waveguide has an unloaded Q-factor of 5000 (TE_{10n} mode), whereas an overmoded circular cavity, of diameter 50mm, has an unloaded Q-factor of 50,000 (TE_{01n}mode). The TE_{01} mode is chosen because it exhibits a special attenuation property, whereby the attenuation decreases with increasing frequency. Thus very high Q-factors are possible at high frequencies. However, the use of overmoded circular waveguide has one drawback, namely that of identifying the correct resonances. This problem can be overcome by using helical waveguide, where the walls of the guide are formed from a helix of fine gauge (~40swg) enamelled copper wire. This wall structure does not impede the propagation of the TE_{01} modes, in which all the wall currents are circumferential, but attenuates (due the enamel coating between the turns of the helix) of all other modes because they have wall currents with axial components.

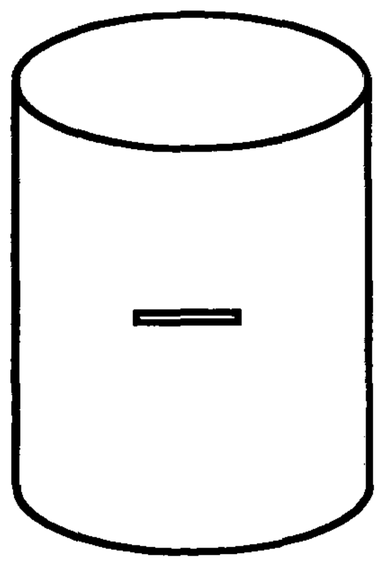

Figure 7.1: Circular waveguide with slit

Using the 'slit' concept, slits can be cut in the wall of circular waveguide as shown in Figure 7.1. A section of helical waveguide then can be attached to the slit circular waveguide to work as a mode filter as shown in Figure 7.2. In the measurement of low loss material in a two-layer format, the reference substrate is first inserted into the cavity through the slits, as shown in Figure 7.2 (a). Then the reference substrate is replaced by the two-layer sample (Figure 7.2(b)). The resonant frequency and Q-

factor are measured and used to compute the complex permittivity of the sample.

When the dielectric constant of the sample under test is known, the loss tangent of the sample can be evaluated straightway using perturbation theory. When both the determination of dielectric constant and loss tangent are required, the filling factor is needed and it can be obtained through electromagnetic field analysis as in the case of the slit rectangular cavity.

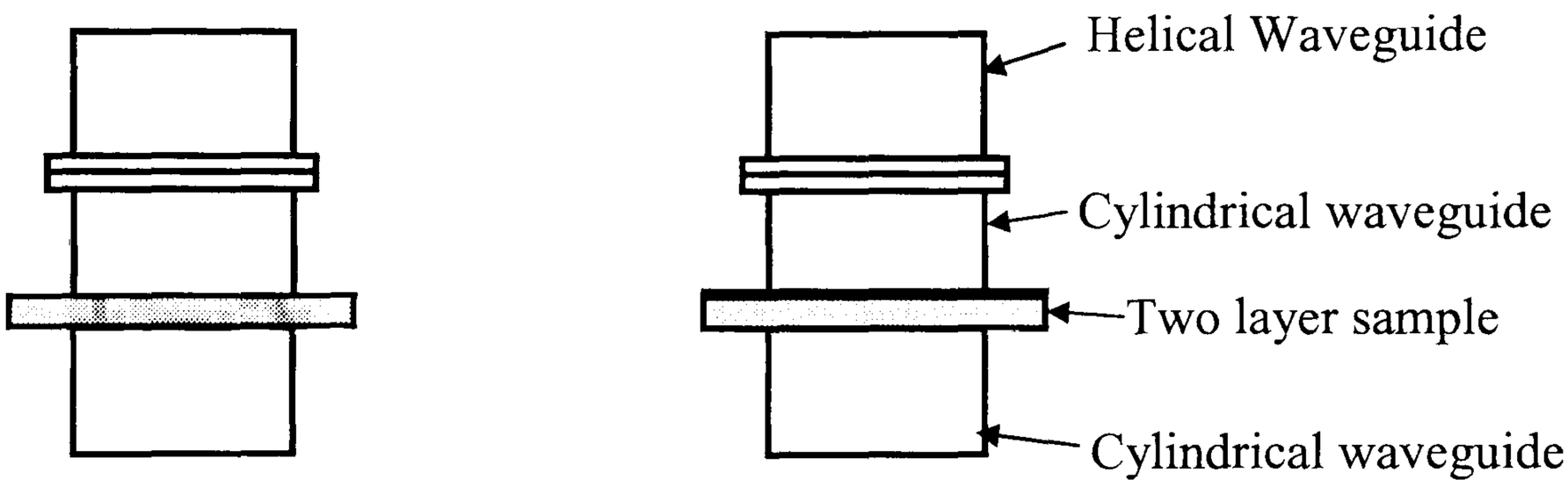

Figure 7.2: Reference cavity and perturbed cavity. (a) Cavity loaded with the reference substrate. (b) Cavity loaded with the two-layer sample.

7.2.2 Modelling of multilayer overlap

The multilayer overlap is a critical element in the design of multilayer end-coupled filters. It provides much stronger coupling than the comparable gap in a single layer gap. Whilst the design equations for single layer gaps are available in the literature, there is no equivalent circuit expression for multilayer overlaps. In this study, the S parameters for multilayer overlaps are obtained through EM simulation and incorporated into circuit simulator for simulation of the final circuits. It would be worthwhile to generate a circuit design equation for multilayer overlaps that will enhance the efficiency of circuit design. The equivalent circuit model of a multilayer

overlap can be obtained through modification of the equivalent circuit of single layer gap. The proposed circuit is shown in Figure 7.3.

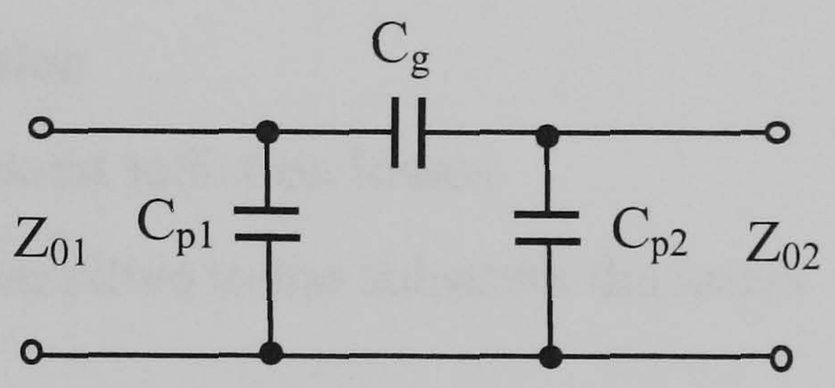

Figure 7.3: Equivalent circuit of a multilayer overlap

In this case the series capacitance (C_g) accounts chiefly for the overlapping field, whilst the grounded capacitances (C_{p1} and C_{p2}) account mainly for the fringing fields from the ends. The two ends are in different dielectric environments and consequently they are represented by different capacitances.

7.2.3 Multilayer coplanar structures

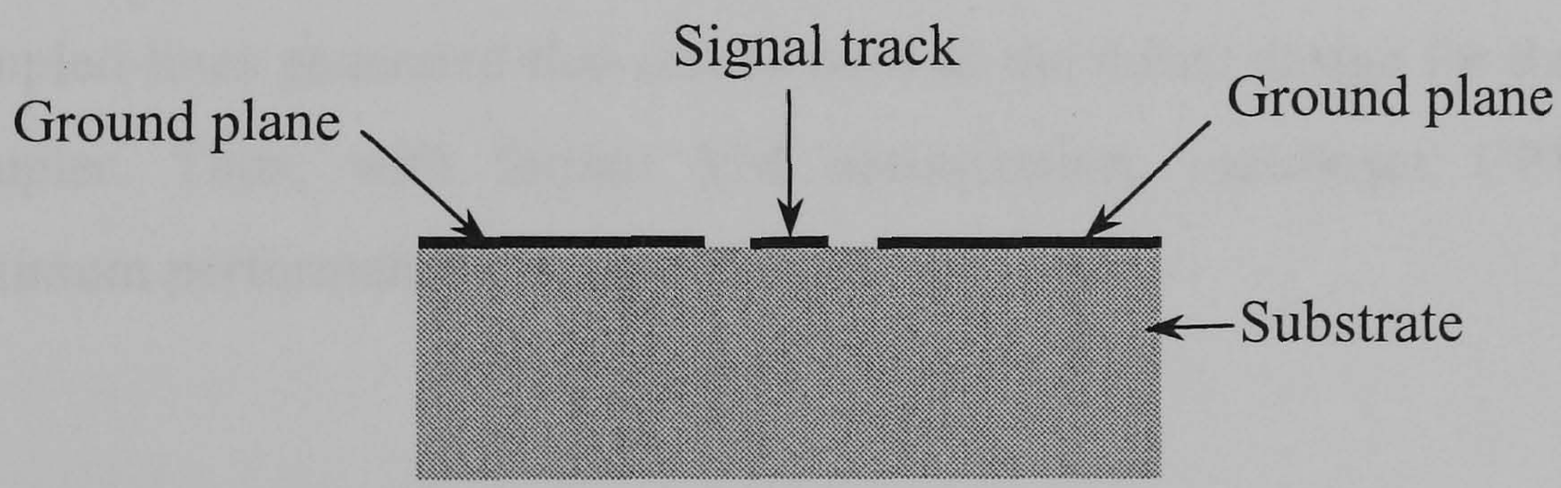

Figure 7.4: Structure of a coplanar waveguide (CPW)

Multilayer microstrip structures have been extensively investigated in this study.

Coplanar waveguide structures (Figure 7.4) have been attracting more attention recently due to some specific advantages over microstrip lines:

- Easier grounding of surface-mounted components.
- Lower fabrication costs
- Reduced dispersion
- May have decreased radiation losses
- Relatively less sensitive to the substrate thickness

The design techniques developed in this study can be further extended to the design of multilayer CPW structures.

To design multilayer CPW end-coupled filter, the multilayer CPW gap can be characterized using EM analysis. The design procedure developed in this study then can be employed to determine the physical dimensions of multilayer CPW end-coupled filter.

The design of multilayer CPW directional couplers can be approached in a similar way to that of the multilayer microstrip coupled-line. The performance of multilayer CPW coupled-lines can be studied using LINPAR and data for 50Ω matched CPW coupled-lines generated that can be used as the initial design for the multilayer CPW coupler. Thus, with further EM optimization, multilayer CPW couplers with optimum performance can be achieved.

Appendix A Publications

The following list of publications resulted from the work described in this thesis. For the convenience of the reader, scanned copies of the articles 1 to 3 are given in this appendix.

1. Tian, Z., Free, C., Aitchison, C., Barnwell, P. and Wood, J., 'Design of directional couplers using multilayer thick-film technology ', *2002 IEEE Radio and Wireless Conference (RAWCON2002)*, pp.261-264, Boston, USA, Aug. 2002.

2. Tian, Z., Free, C., Aitchison, C., Barnwell, P. and Wood, J., 'Multilayer thick-film microwave components and measurements ', *35th International Symposium on Microelectronics,* pp.394-399, Denver, USA, Sept. 2002.

3. Tian, Z. and Free, C., 'Measurement techniques for the evaluation of thick-film materials used in wireless applications", *Microelectronics International*, Vol. 18, Number 2, pp21-25, May. 2001.

4. Tian, Z., Free, C., Aitchison, C., Barnwell, P. and Wood, J., "Design of novel multilayer microwave coupled-line structures using thick-film technology," *Proceedings of 31st European Microwave Conference,* Vol. 1, pp. 395-398, London, Sept. 2001.

5. Tian, Z. Free, C. and Barnwell, P., 'The Influence of materials properties on the performance of microwave planar components", *Proceedings of 2001 International Symposium on Microelectronics*, pp161-166, Baltimore, Oct. 2001.

6. Free, C., Tian, Z. and Barnwell, P., 'Characterization and analysis of ceramic

interconnects at microwave frequencies with special emphasis on LTCC technology", *IMAPS Strasbourg*, March. 2001.

7. Tian, Z. and Free, C., 'Investigation of multilayer microwave structures and characterization of dielectric material", *Third Conference on Postgraduate Research in Electronics, Photonics, Communications and Software*, pp21-22, April 2001.

8. Free, C., Tian, Z. and Barnwell, P., 'Substrate characterization: simulation and measurement at high microwave frequencies', *Microelectronics International,* Vol. 18, No.1, pp. 32-34, January 2001,

9. Tian, Z. and Free, C., 'Micro technology measurement techniques for the evaluation of thick-film materials used in wireless applications', *European Conference on Wireless Technologies*, pp65-73, London, Jan. 2001.

10. Barnwell, P., Reynolds, Q., Free, C. and Tian, Z., 'LTCC systems for low GHz frequencies - a study of the critical properties and their measurement techniques', *European Conference on Wireless Technologies,* pp80-87, London, Jan. 2001.

11. Free, C., Pitt, K. and Tian, Z., 'The effects of overglazing on the performance of microwave thick-film circuits in the frequency range 8-18 GHz', *Proceedings of XXIV International Conference IMAPS-POLAND* pp101-106, Rytro, September 2000.

12. Free, C., Tian, Z. and Barnwell, P., 'Substrate characterization: simulation and measurement at high microwave frequencies', *Proceedings of the 33rd International Symposium on Microelectronics*, pp57-61, Boston, October 2000.

13. Free, C., Tian, Z., Barnwell, P., Robertson, I. And Aitchison, C., 'A new LTCC fabrication technology for a planar millimeter-wave circuits', *Proceeding of 1999 Asia-Pacific Microwave Conference*, pp962-965. Singapore, 1999.

14. Tian, Z., Free, C., Aitchison, C., Barnwell, P. and Wood, J., 'Multilayer thick-film microwave components and measurements ', to be published by *Microelectronics International.*

W3.4

Design of Directional Couplers Using Multilayer Thick-Film Technology

Zhengrong Tian
Middlesex University, Bounds Green Road, London N11 2NQ, UK
Tel: +44 208 411 2708, Fax: +44 208 411 6411 Email: T.Zhengrong@mdx.ac.uk

Charles Free, Colin Aitchison
School of Electronics, Computing and Mathematics, University of Surrey
Guildford GU2 7XH, UK
Tel: +44 1483 686 108, Email: C.Free@surrey.ac.uk

Peter Barnwell, James Wood
Heraeus Circuit Materials Division, 24 Union Hill Road, West Conshohocken
PA 19428, USA
Tel: +1 610 825 7810, Email: PBarnwell@4cmd.com

Abstract

The performance of multilayer directional couplers using a range of different thick-film dielectrics has been investigated. The properties of multilayer coupled lines are examined using their coupled-mode parameters. It is found that the optimum performance of multilayer directional couplers is largely affected by the thick-film dielectric used. A practical design strategy for multilayer directional couplers is developed, which overcomes the problem of excessive computation that is normally associated with the optimization of multilayer circuit designs. The methodology has been verified through the design and measurement of wide bandwidth 2dB and 3dB directional couplers that were fabricated using multilayer, thick-film technology.

Introduction

Multilayer thick-film technology offers a low-cost and compact solution for directional couplers to achieve tight coupling. These components overcome the problem of fabricating very small gaps between coupled lines in a traditional single layer structure [1]. In a multilayer component strong coupling is obtained by overlapping coupled lines, that are separated with a thin layer of printed thick-film dielectric. The presence of the thick-film dielectric layer not only acts as an insulator between the two conductor layers but, more importantly, it will influence the properties of the inductive and capacitive coupling coefficients of the coupled lines. To quantify this influence, the properties of coupled lines using different thick-film dielectrics have been examined using their coupled-mode parameters. It is found that the optimal performance of multilayer directional couplers is significantly affected by the properties of the thick-film dielectric layer. By choosing an appropriate dielectric constant for the thick-film dielectric, a wideband, quasi-ideal 3dB coupler can be realized.

The major drawback to the design of multilayer directional couplers is that straightforward, synthesis equations are not available in the literature. Electromagnetic (EM) analysis has to be employed to optimize the performance. The choice of the initial design parameters is thus crucial if this optimization process is not to be unduly time-consuming and expensive. In this paper we introduce a method for obtaining the initial design parameters for multilayer directional couplers, such that optimum performance can be achieved with minimum simulation effort.

Fabrication Data

The structure of a multilayer directional coupler studied is shown in Figure 1. The bottom signal conductor was printed onto an Alumina (ε_r=9.9, H=635μm) base and etched-back to give the correct line width and quality. Three layers of thick film dielectric (10μm thickness per layer) were then successively printed and fired to give the final thickness of 30μm. Using three layers also minimised the possibility of pinholes. The dielectric was only printed over the coupled region so as not to

0-7803-7458-4/02/$17.00 @ 2002 IEEE

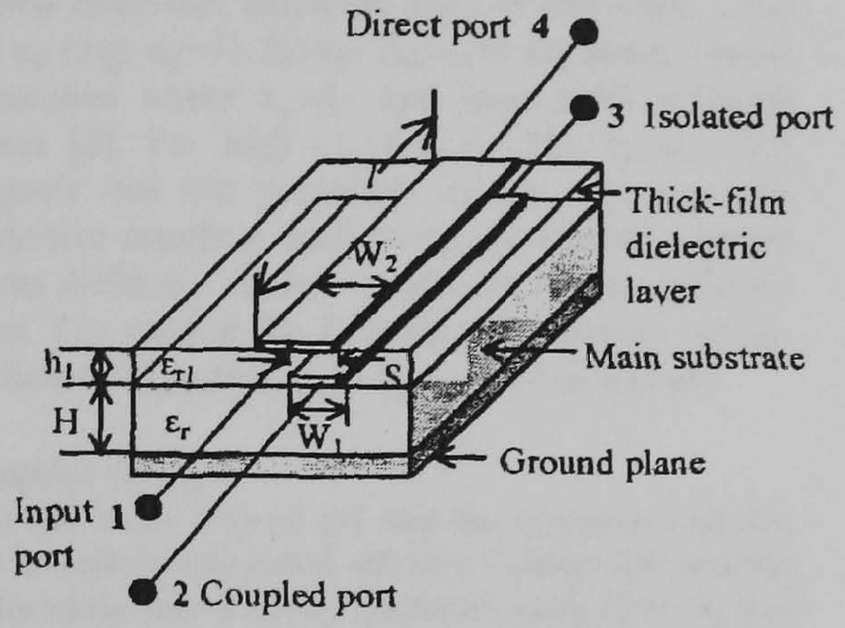

Fig. 1 *The configuration of a multilayer directional coupler*

affect the integration of other devices onto the same Alumina base. Finally the top conductor track was printed and etched. The conductor lines had a fired thickness of 5μm. A mask aligner was used to obtain accurate registration of the two conductor layers. Overlapping of the conductors as previously described provided the required close coupling between the signal paths.

Coupled Line Analysis

We are interested in designing couplers that are matched to 50Ω at all four ports. For a certain degree of overlapping, S. we were able to find, through quasi-static analysis, a pair of W_1 and W_2 values for 50Ω matched coupled lines, such that:

$$\sqrt{L_1/C_1} = \sqrt{L_2/C_2} = 50\Omega$$

where L_1, L_2 and C_1, C_2 are the self inductances and capacitances of the first and second lines in the presence of the other, per unit length. The widths of 50Ω matched coupled-line versus the overlapping (S) are plotted in Figure 2, along with corresponding k_L and k_C parameters, where:

$k_L = \dfrac{L_m}{\sqrt{L_1 \cdot L_2}}$ the inductive coupling coefficient;

$k_C = \dfrac{C_m}{\sqrt{C_1 \cdot C_2}}$ the capacitive coupling coefficient;

L_m and Cm are the mutual inductance and capacitance per unit length.

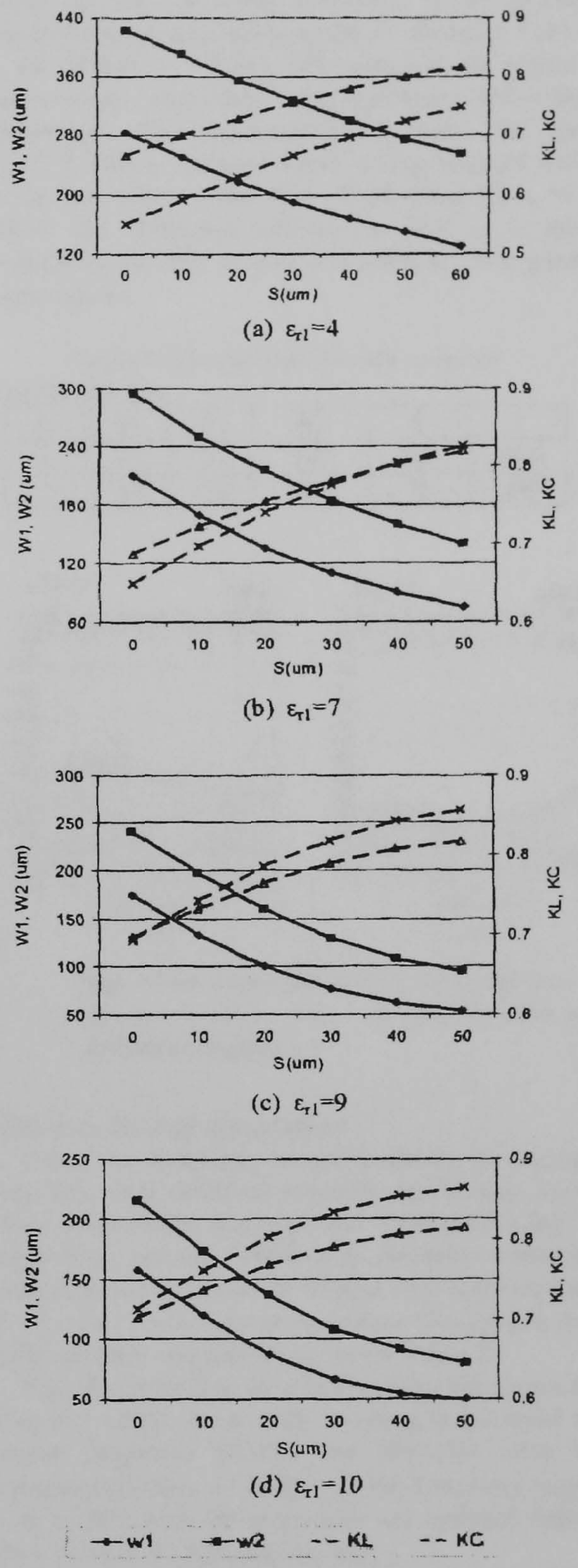

(a) ε_{r1}=4

(b) ε_{r1}=7

(c) ε_{r1}=9

(d) ε_{r1}=10

Fig. 2 W_1, W_2, k_L *and* k_C *for 50Ω matched coupled lines versus S. (a)* ε_{r1}=4, *(b)* ε_{r1}=7, *(c)* ε_{r1}=9, *(d)* ε_{r1}=10.

It can be seen in the graph that the performance of k_L and k_C for 50Ω matched coupled lines varies monotonically as the dielectric constant (ε_{r1}) of the printed thick-film dielectric layer is increased. . For low ε_{r1} (e.g. ε_{r1}=4). $k_L > k_C$. As ε_{r1} is increased a point is reached where $k_L = k_C$ and quasi-ideal coupling occurs [2]. For high ε_{r1} (e.g. ε_{r1}=10), $k_L < k_C$. This suggests that the properties of the inductive and capacitive coupling coefficients are mainly affected by the dielectric constant of the thick-film dielectric layer. The smaller the difference between k_L and k_C, the better the performance that can be achieved.

Coupler Design

It has been proved [2] that the asymmetric coupler that is correctly terminated can have a quasi-ideal coupling performance only if $k_L = k_C$. However, quite often k_L and k_C are different in the multilayer structure, as shown in Figure 2. When $k_L \neq k_C$, the matching and isolation performance of 50Ω matched coupled-line couplers will deviate from the optimum performance. Thus the widths of the two lines need to be adjusted to compensate for the deterioration caused by unequal values of k_L and k_C. However, 50Ω matched coupled-line couplers provide good initial design data that enable multilayer coupler designs having optimum performance to be realized with minimum EM computation effort.

The design procedure is thus as follows. Firstly, the amount of overlap (S) is chosen so as to give the desired coupling coefficients for 50Ω matched coupled-line couplers. Secondly, the line widths are adjusted to give the optimum matching and isolation performance. As the matching at port 1 will mainly be affected by line 1, and the matching at port 2 mainly affected by line 2, this simplifies the problem of optimization, where we optimize each line separately. Note that the change in the line width will not change the coupling significantly, as the coupling is mainly determined by the overlapping (S).

The length of the coupler is determined by:

$$l = \frac{1}{4} \frac{\lambda_0}{\sqrt{\varepsilon_{eff}}}$$

$$\sqrt{\varepsilon_{eff}} = \frac{1}{2}(\sqrt{\varepsilon_c} + \sqrt{\varepsilon_\pi})$$

where ε_c and ε_π are modal dielectric constants of the coupled lines and are evaluated through quasi-static analysis.

Using the physical dimensions of the 50Ω matched lines as a prototype design, we employed electromagnetic analysis to design 3dB couplers using various thick-film dielectrics. Some of the design data and simulation results are shown in Table 1 and Figure 3. These data represent the typical performance achievable using multilayer thick-film technology. The simulated results show that for ε_{r1}=7, k_L and k_C become equal, giving isolation and return loss values better than -30dB. Even for ε_{r1}=4, where the difference between k_L and k_C is not negligible, the 3dB coupler still exhibits very good perfromance.

Table 1. *Design data for 3dB couplers*

Length unit: μm

ε_{r1}	h1	W_1	W_2	S	*l*
7	30	135	180	50	4400
4	30	220	230	70	5250

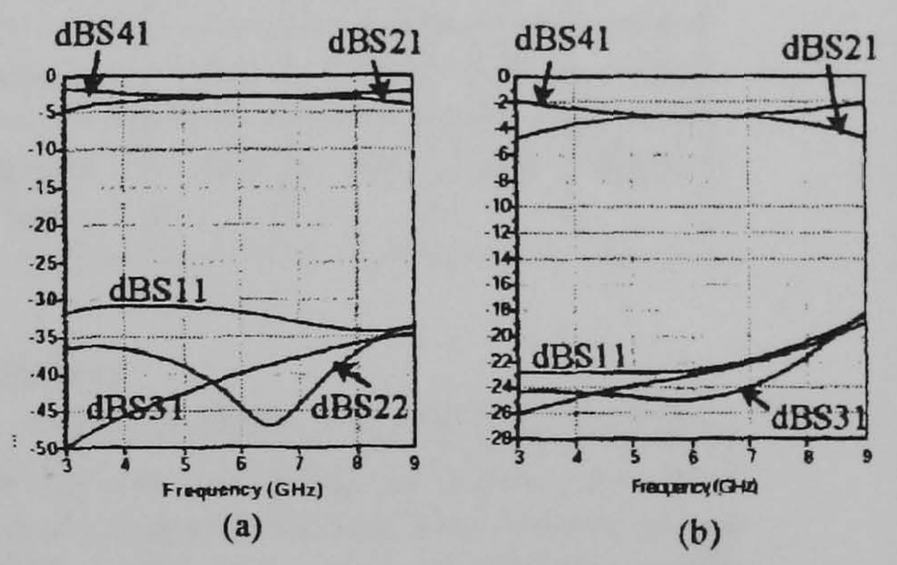

Fig. 3 *Simulated response for 3dB couplers. (a) ε_{r1} =7; (b) ε_{r1} =4. (the port notation is defined in Figure. 1)*

Test results and discussions

Using the technique described above, directional couplers with different coupling coefficients have been successfully designed and fabricated using a thick-film process. Thick-film dielectric material with dielectric constant of 3.9 and very low loss (tan $\delta < 4 \times 10^{-4}$) was used in this study. Design data for 2dB and 3dB couplers are shown in Table 2.

The measured data for a 2dB coupler are shown in Figure 4 which shows 2dB coupling is achieved at center frequency (6GHz) and that this value is maintained within ±0.25dB over the frequency range 4 to 8 GHz with the return loss and isolation better than 20dB and 15dB respectively.

The measured performance of a 3dB coupler (Figure 5) shows that 3dB coupling is achieved over a relative broad bandwidth (6-14GHz) with very

promising isolation (better than 22dB) and good matching (return loss better than 15dB).

Table 2. *Design data for multilayer couplers*

Substrate			
ε_r	H	ε_{r1}	h_1
9.9	635μm	3.9	30μm
Physical dimension (μm)			
	W1	W2	S	l
2dB	140	190	100	5250
3dB	200	230	70	3260

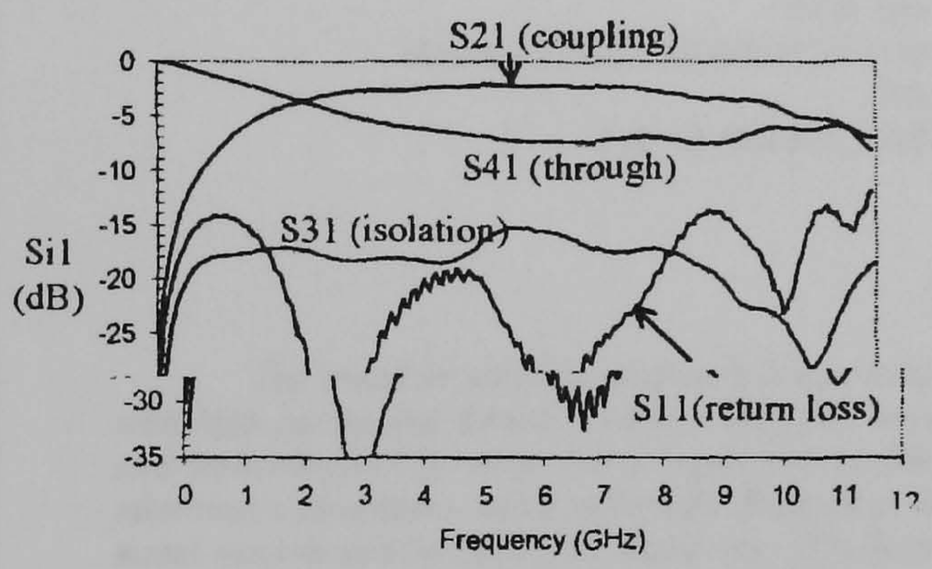

Fig. 4 *Measured response of a 2dB multilayer directional coupler. (the port notation is defined in Figure. 1)*

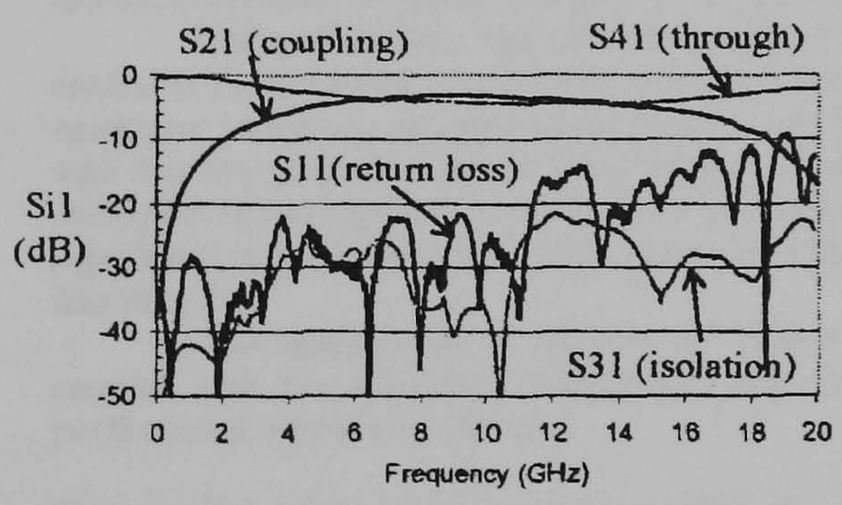

Fig. 5 *Measured response of a 3dB multilayer directional coupler. (the port notation is defined in Figure. 1)*

A sensitivity analysis on the fabricated coupler was carried out and the results are summarized in Table 3. It is shown that the coupler performance is most sensitive to the thickness of the printed thick-film dielectric layer. The registration between the two signal conductor layers is of secondary importance.

Table 3. *Error sources and the contributions towards the coupler performance*

Parameter	ε_{r1}	h_1	S	Line width
ΔParameter	0.2	5 μm	10 μm	10 μm
ΔCoupling	0.041	0.244	0.2	0.156
ΔIsolation	0.787	2.27	1.82	2.12
ΔReturn loss	1.858	1.207	0.441	0.808

Conclusions

The study has shown that multilayer thick-film technology can provide high performance microwave directional couplers, that offer a combination of tight coupling and very wide bandwidth, whilst maintaining good matching and isolation. Moreover, the technology offers the capability for mass-producing low-cost, compact microwave components. A new design strategy for multilayer directional couplers has been developed and validated through practical measurement. The technique offers a simple and practical approach to exploiting the design flexibility of three-dimensional microwave structures.

References

1. Z. Tian. C. Free. P. Barnwell, J. Wood and C. Aitchison, "Design of novel multilayer microwave coupled-line structures using thick-film technology," *Proceedings of 31st European Microwave Conference*, Vol. 1, pp. 395-398, London, 2001.
2. Sachse, K., ' The scattering parameters and directional coupler analysis of characteristically terminated asymmetric coupled transmission lines in an inhomogeneous medium', *IEEE Trans. Microwave Theory Tech.*, Vol. MTT-38, No.4, pp.417-425, Apr. 1990.

2002 International Symposium on Microelectronics

Multi-Layer Thick-Film Microwave Components and Measurements

Zhengrong Tian
Middlesex University, Bounds Green Road, London N11 2NQ, UK
Tel: +44 208 411 2708, Fax: +44 208 411 6411 Email: T.Zhengrong@mdx.ac.uk

Charles Free, Colin Aitchison
School of Electronics, Computing and Mathematics, University of Surrey
Guildford GU2 7XH, UK
Tel: +44 1483 686 108, Email: C.Free@surrey.ac.uk

Peter Barnwell, James Wood
Heraeus Circuit Materials Division, 24 Union Hill Road, West Conshohocken
PA 19428, USA
Tel: +1 610 825 7810, Email: PBarnwell@4cmd.com

Abstract

The trend in wireless and mobile communications for broader bandwidth microwave circuitry, coupled with high packaging density and low cost fabrication has triggered investigations of new circuit configurations and technologies that meet these requirements. We have addressed these issues through the study of multilayer microwave structures using advanced thick-film technology. The techniques described employ several layers of metal sandwiched by thick-film dielectric. This leads to an efficient solution for system miniaturization.

Characterization of 2-layer thick-film microstrip line has been carried out through electromagnetic computation and practical measurement, and this has established the basic database for designing multilayer thick-film microwave structures. It is also shown that the use of multilayer thick-film microstrip permits the realization of very high characteristic impedance lines on high dielectric constant substrates, without the need for very narrow lines. The high impedance capability of this structure is very attractive for the implementation of low-loss matching networks and passive components with enhanced bandwidth performance.

Strong coupling, that is often required in the design of microwave couplers and filters, is difficult to realize in conventional single layer structures, due to the requirements for very narrow gaps. However, by using multilayer structure, strong coupling can be easily obtained by overlapping conductor tracks in different layers, with less stringent geometrical requirements. A multilayer end-coupled microwave filter centered at 10GHz using thick-film technology has been designed and simulated. A 30% bandwidth has been achieved which shows a very significant improvement over conventional single layer structures, where the bandwidth achievable is normally less than 5%.

The significance of this work is that it shows that the multilayer approach to microwave structures, coupled with new thick-film technology, offers a viable and economic solution to achieving high-density, high-performance microwave circuits.

Key words: *Multi-Layer Microwave Circuits, Thick-Film Technology, Multi-layer Transmission Line, Multi-Layer Filter*

Introduction

Increased use of microwave hybrid circuits for wireless communication systems has made low cost a main theme in the development of circuits having advanced functions. The significant advantage of thick-film technology is the

combination of low cost and feasibility for mass production. Recent, rapid progress in novel thick-film materials and advanced thick-film circuit patterning techniques has brought improvements that allow current thick-film technology to reach beyond its previous limitations [1-2] and make it a good candidate for achieving low cost microwave circuits. However, like all the other fabrication techniques, the limitation on achievable fine line width and fine gap limits the performance of conventional microwave microstrip. It is shown in this paper that the need for fabricating fine line and fine gap can be effectively eliminated by using multilayer structures, thus alleviating the pressure on the fabrication process and improving the reliability.

Microstrip line with high impedance is often required in the design of matching networks for mixers and amplifiers. The characteristic impedance of a microstrip line with the width of 50μm on a standard 25mil Alumina substrate is 110Ω. If we insert a thin layer of low-dielectric constant thick film dielectric (with the dielectric constant of 3.9 and thickness of 30μm) under the line, the characteristic impedance can be increased to 138 Ω. This means an improvement of line impedance of around 25% can be obtained by using multilayer structure without increasing the difficulty of fabrication. The substrate used in multilayer microstrip structures may contain several layers dielectric having different dielectric constants and thickness. Thus multilayer microstrip lines will exhibit some special performance. In contrast to conventional single layer microstrip, where the design techniques are well documented in the literature, there are no design equations available for multilayer structures. Electro-magnetic analysis has been performed on multilayer microstrip lines to obtain the characteristic impedance and relative effective dielectric constant. These are essential data for designing various multilayer structures.

In the design of end-coupled band-pass microwave filters, very narrow coupling gaps are required to achieve wide bandwidth. Conventionally, these filters have been utilised in single layer configurations for relatively narrow bandwidth applications (about 5%). For a medium or wide bandwidth (>10%), the required capacitive coupling between resonators becomes so strong that the gaps, in a single layer structure, cannot be obtained by classical photolithographic techniques. However, in multilayer structure, by overlapping the end of the two tracks using a dielectric separation sheet, strong capacitive coupling can easily be obtained. The design and simulation of a multilayer end-coupled filter centred at 10GHz is presented in this paper.

Structure of Multilayer Microstrip Line

The configurations of the multilayer microstrip lines studied are shown in Figure 1. Figure 1(a) shows a conductor track on top of a two-layer dielectric. Figure 1(b) shows a conductor track buried between the dielectrics. ε_r and H are the dielectric constant and thickness of the Alumina base, which functions as the main supporting substrate. ε_{r1} and h_1 are the dielectric constant and thickness of the printed thick-film dielectric layer. Thick-film dielectric with low dielectric constant (3.9) and low loss factor (4×10^{-4}) were used for the investigations reported in this paper. The fired thickness of each thick-film dielectric could be between 9-12μm per layer. To avoid pinholes in the final thickness, normally 3 separately fired layers are recommended. The conductor could be either gold or silver, with a fired thickness of 4-5μm.

Thick-film technology, by its nature, is well compatible with the fabrication of multilayer

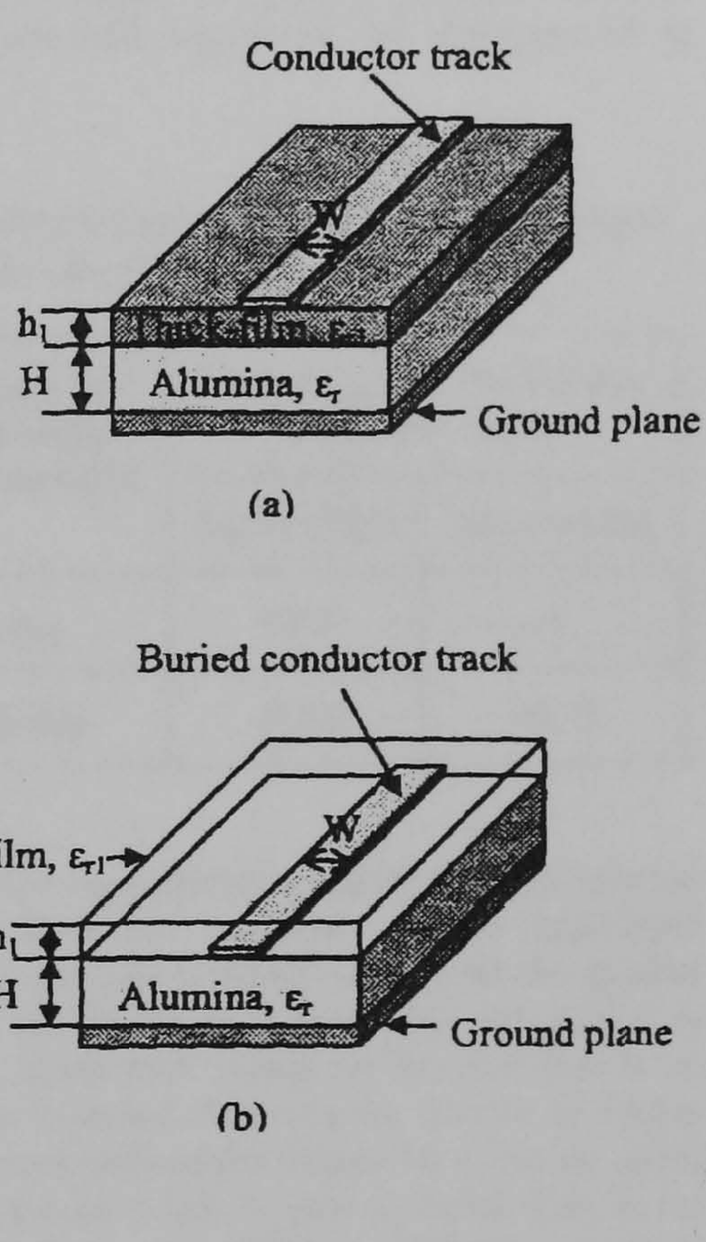

Figure 1: Structure of Multilayer Microstrip Line.
(a) Conductor track on two-layer dielectric.
(b) Buried conductor track.

structures. According to different requirements (line width, line spacing, cost, etc.) different patterning techniques can be used to fabricate the dielectric layer and conductor layer. Use of a mask aligner is necessary to achieve the correct registration between the different dielectric and conductor layers.

Line Characterization -Simulation

The analysis of multilayer microstrip line is aimed at determining the characteristic impedance and propagation constant (comprising phase velocity and attenuation constant). Full-wave analysis is used to characterise the multilayer microstrip lines.

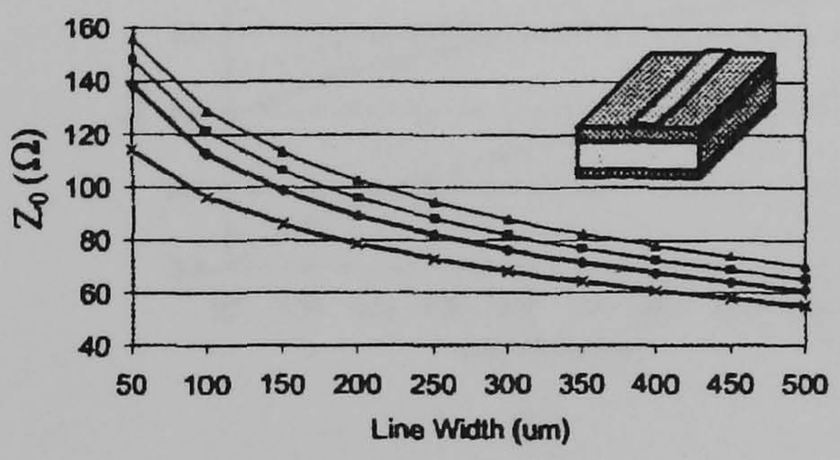

(a)

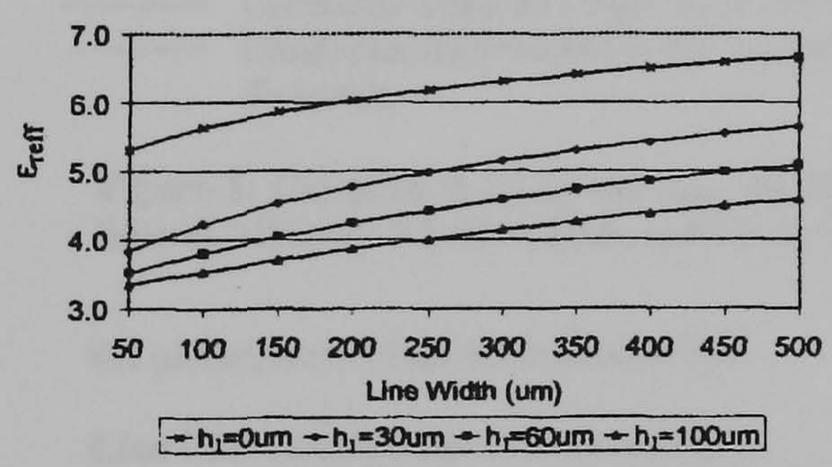

(b)

Figure 2: Calculated Z_0 and ε_{reff} versus line width for various values of h_1.(ε_r=9.9, H=635μm, ε_{r1}=3.9)

Figure 2 shows the characteristic impedance (Z_0) and effective dielectric constant (ε_{reff}) versus line width for multilayer microstrip line on top of two-layer dielectric, with the thickness of printed thick-film dielectric layer of 0μm, 30μm, 60μm and 100μm, respectively.

As can be seen from the graph, the characteristic impedance increases with an increase in the thick-film dielectric thickness (h_1), whereas ε_{reff} decreases with an increase in h_1. For a small value of h_1, the change in the Z_0 and ε_{reff} values is large with respect to h_1=0. It is noted that the inclusion of a thick-film dielectric layer under the conductor track, despite this layer being very thin, significantly affects the characteristic impedance of the conductor on top of the two dielectric layers. For example, when h_1 =0 (which corresponds to standard Alumina substrate), the characteristic impedance for the line that has the width of 50μm is 110Ω. However, with the inclusion of thick-film dielectric layer (h_1 =100 μm), the characteristic impedance of the line with the same width is 156Ω (this represents an increase in the characteristic impedance of around 37%). This suggests that, by using a thin layer of thick-film dielectric, the manufacturable impedance can be increased. This is an important feature as it enables the realisation of relatively high characteristic impedance lines on high dielectric constant substrates. The high impedance capability of this structure is suitable for the implementation low-loss matching networks.

The effects of uncertainties in thickness and dielectric constant of the printed dielectric layer on the values of effective dielectric constant and characteristic impedance are summarized in Table 1.

Table 1: Sensitivity Analysis of a 50 Ω Multilayer Microstrip Line at 6GHz

Change in Microstrip Parameter (%)	Uncertainty in Thick-Film Dielectric Layer	
	$\Delta\varepsilon_{r1}$ = +10%	Δh_1 = +10%
$\Delta\varepsilon_{reff}$	+1.7	-1
$\Delta Z_0(\Omega)$	-0.73	+0.75

The characteristic impedance and relative effective dielectric constant of the multilayer microstrip line that is buried underneath the printed dielectric (as shown in Figure 1(b)) are plotted in Figure 3, along with values for the line that is on top of the 2 layers dielectric (as shown in Figure 1(a)). For comparison the values for a line on 25mil Alumina are included. It may be noted that in the situation where the printed dielectric layer is immediately under the conductor, it significantly affects Z_0 and ε_{reff}, whereas the dielectric layer above the conductor track has much less effect on

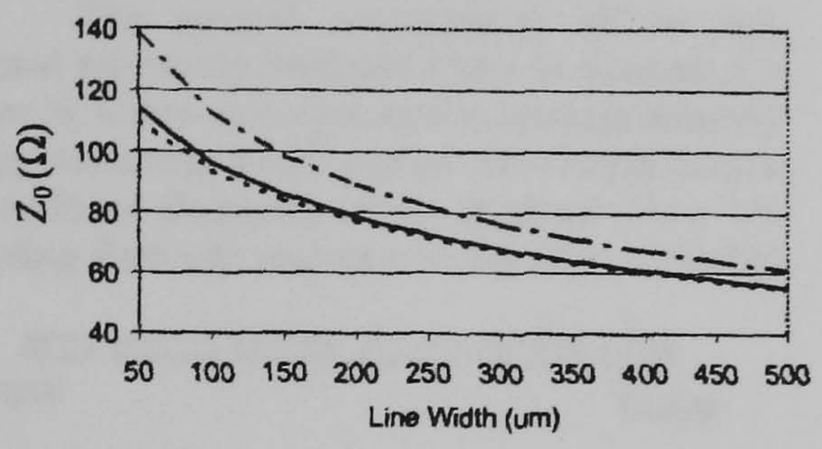

(a)

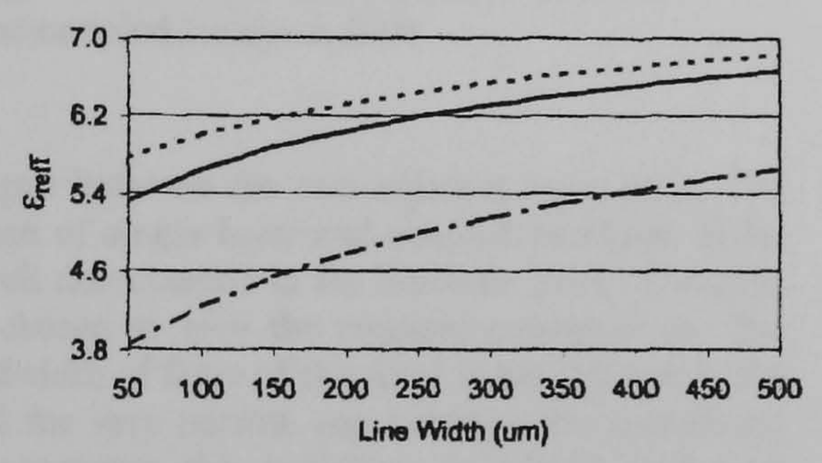

(b)

Conductor track on 2-layers dielectric
Conductor track on single layer dielectric
Conductor track buried in the 2-layers dielectric

Figure 3: Comparison of Z_0 and ε_{reff} for different lines at 6GHz (ε_r=9.9, H=635μm, ε_{r1}=3.9, h_1=30μm)

the performance of the transmission line.

Line Characterisation -Measurement

Test structures have been built to evaluate the relative effective dielectric constant (ε_{reff}) and line loss of multilayer microstrip line.

Figure 4 shows a pair of line resonators for measuring ε_{reff}. By using two resonators of different lengths we can compensate for the open-end effects at both ends of the resonator. [3]. To maintain the same resonant frequencies for the two structures, the lengths of the two resonators are chosen so that $l_2 \approx 2l_1 \approx \lambda_g$. The resonators are loosely coupled to have minimum loading effect. Knowing the length and resonant frequency, ε_{reff} can be calculated by following equation:

$$\varepsilon_{reff}(f) = \left(\frac{c(2f_1 - f_2)}{2f_1 f_2 (l_2 - l_1)} \right)^2$$

where f_1 and f_2 are the resonant frequency of resonator 1 and 2, respectively. c is the velocity of light.

Measured and simulated ε_{reff} are summarised in Table 2. It can be seen the measured data are in good agreement with the theoretical results.

Table 2: ε_{reff} of multilayer microstrip line (ε_r=9.9, H=635μm, ε_{r1}=3.9, h_1=30μm)

Line Width (μm)	Measured ε_{reff}	Calculated ε_{reff}	frequency (GHz)
760	5.97	6.13	9

The line loss of 50Ω multilayer microstrip line which is on top of 2 layers dielectric is measured and compared with the line loss of conventional 50Ω microstrip line on 25mil alumina (Figure 5). Although the inclusion of thick-film dielectric layer may cause extra dielectric loss, the width of 50Ω line is wider than that of on Alumina, and this effectively reduces the bulk conductor loss. It can be seen that the loss of multilayer line on top of 2-layer dielectric is essentially the same as that for microstrip line on Alumina.

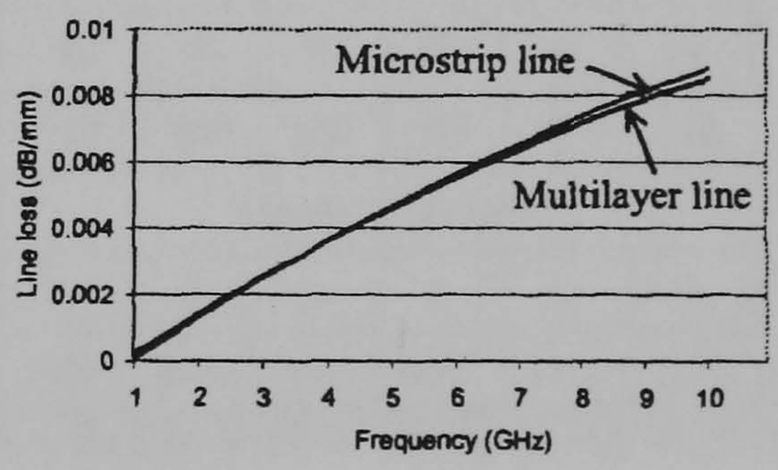

Figure 5: Measured line loss

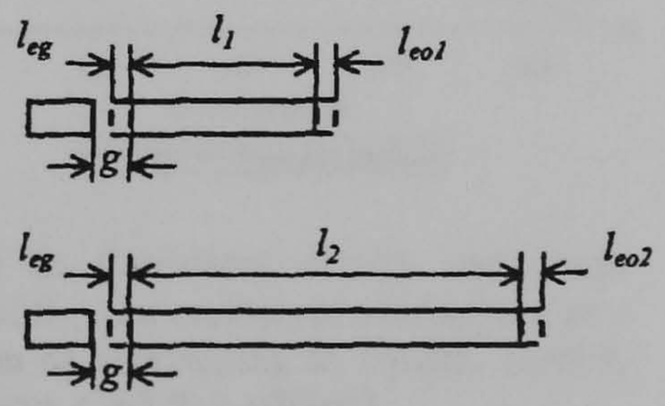

Figure 4: pairs of one-port line resonator

Multilayer End-Coupled Bandpass Filter

The general configuration of an end-coupled microstrip bandpass filters is illustrated in Figure 6, where each open-end microstrip resonator is approximately a half guided wavelength long at the midband frequency of the bandpass filter. The coupling from one resonator to the other is through

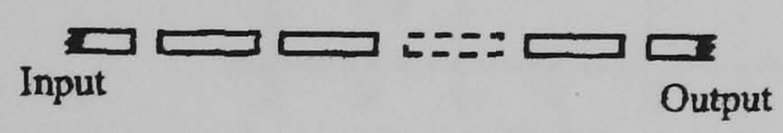

Figure 6: General microstrip layout for an end-coupled bandpass filter

the gap between the two adjacent open ends. The design of single layer end-coupled bandpass filters is well documented in the literature [4-6]. The gaps are chosen to give the required capacitances. The bandwidth of filter of this kind is limited due to the need for very narrow gap between the resonators. To overcome this problem, multilayer structures can be employed, where the end of the two

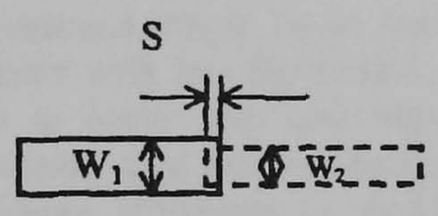

Figure 7: The layout of a multilayer overlapping.

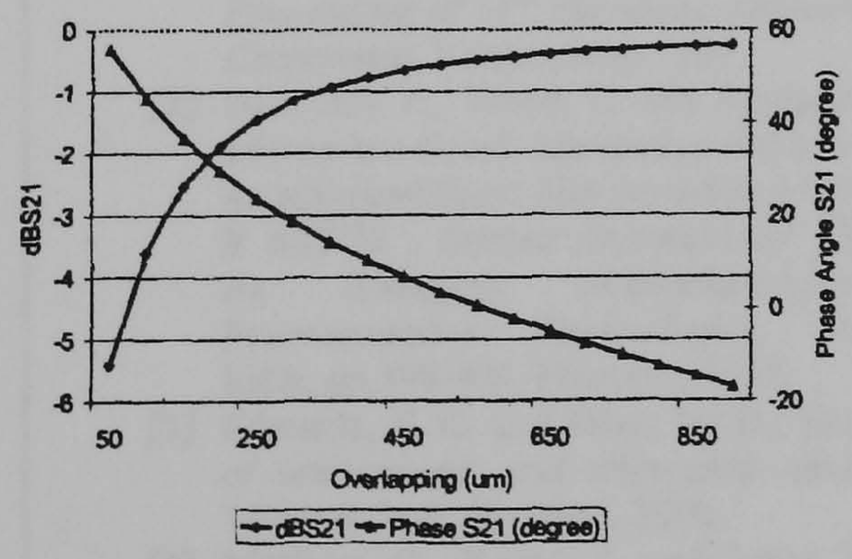

Figure 8: Calculated dBS21 and phase angle of S_{21} of a multilayer overlapping as a function of overlapping at 10GHz. (ε_r=9.9, H=635um. ε_{r1}=3.9. h_1=30um)

resonators can be positioned with an overlap as shown in Figure 7. This will give very strong capacitive coupling so as to improve the bandwidth.

The performance of multilayer overlapping filters was analysed using EM simulator and the results are plotted in Figure 8.

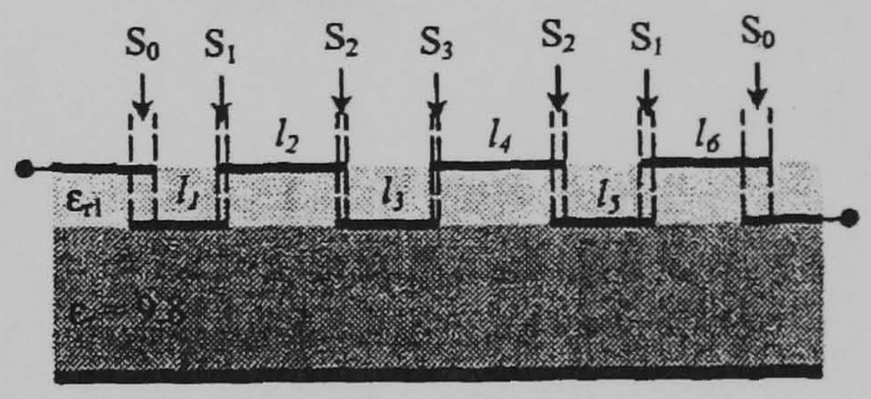

Figure 9: The layout of a multilayer end-coupled filter

The structure of a multilayer end-coupled filter is shown in Figure 9. The amount of overlapping can be chosen according to the graph obtained (Figure 8) to give the same transmission coefficient (dBS21) as the related capacitance. As the phase shift caused by the multilayer overlapping may be different from that of the ideal capacitance, correction of the resonator length is then needed to compensate for this difference. In other words, the resonator lengths depend not only upon the microstrip wavelength, but also on the phase shift performance due to the multilayer overlappings.

Table 3: Design data of a multilayer end-coupled bandpass filter at 10GHz. (unit: μm)

Line Width		Overlapping			
W_1	W_2	S_0	S_1	S_2	S_3
760	620	800	200	100	100
Resonator Length					
l_1	l_2	l_3	l_4	l_5	l_6
3688	4600	4563	4867	4312	3933

*W_1 is the line width of the line on top. W_2 is the bottom line width.

A multilayer end-coupled bandpass filter centred at 10GHz was designed and the design data are shown in Table 3. The simulated performance is

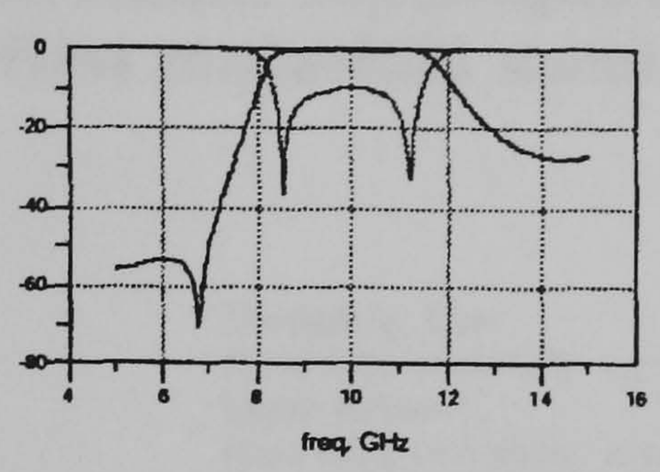

Figure 10: Simulated response of a multilayer end-coupled filter

plotted in Figure 10 where we can see a bandwidth of 30% has been achieved.

Conclusions

This study has shown that by using an extra layer of thick-film dielectric, some microwave components, such as high impedance line and broadband filter which are difficult to realise in the conventional single layer structure can be easily achieved with less fabrication stringency, and thus leads to lower cost and higher reliability. Also, siumalated data has demonstrated the potential of multilayer structures to yield higher microwave performance, primarily through very tight coupling mechanisms.

References

[1] Barnwell P. and Wood J., "Advanced thick film technology - the new generation", *Proceeding of 11th European Microelectronics Conference*, Venice, May 1997.

[2] Barnwell, P., Wood, J. and Reynolds, Q., 'A microwave circuit fabrication technology using an advanced thick-film materials system', *Proc. E MIT'98 - Second International Conference on Emerging Microelectronics and Interconnection Technologies*, Bangalore, India, pp.399-404, February, 1998.

[3] Edwards, T. C. and Steer, M. B., *Foundations of interconnect and microstrip design*, John Wiley & Sons, England, 2000.

[4] Matthaei, G., Young, L. and Jones, E. M. T., *Microwave Filters, Impedance – Matching Networks, and Coupling Structures*, Artech House, Dedham, MA, 1990.

[5] Nguyen, C. and Chang, K., 'Design and performance of millimeter-wave end-coupled bandpass filters,' *International Journal of Infrared and Millimeter Waves*, Vol. 6, No. 7, pp. 497-509, 1985.

[6] Cunningham, G. J., Blenkinsop, P. A. And Palmer, J. H., 'Microstrip end-coupled filter design at MM-wave frequencies,' *Proc. 19th European Microwave Conf.*, pp. 1210-1213, Sept. 1989.

Measurement techniques for the evaluation of thick-film materials used in wireless applications

Zhengrong Tian
Middlesex University, London, UK
Charles Free
Middlesex University, London, UK

Keywords
Measurement, Thick film, Wireless technology

Abstract
A review of the dielectric measurement techniques that are currently available for the characterization of thick film and LTCC materials at microwave and millimeter wave frequencies is presented. The intention is to show the relative advantages and limitations of the various methods, and to provide some practical guide to the particular technique that is most suitable for a given type of material, for use in a particular application. In addition, a novel slit cavity resonator method is proposed to enable substrate parameters to be more easily measured, whilst retaining high measurement accuracy. Measured data on materials from a variety of manufacturers are presented to show the validity and usefulness of this method.

This paper appeared at Microtech 2001, in London, UK.

Microelectronics International
18/2 [2001] 21–25

[ISSN 1356-5362]

Introduction

Knowledge about the dielectric constant and loss tangent of thick film and LTCC materials at microwave and millimeter wave frequencies is essential for micro-electronic packaging applications at these frequencies as well as for traditional microwave circuits designs. These material parameters are critical for obtaining the correct characteristic impedances of the interconnections as well as for determining propagation delays and predicting line loss. In general the dielectric constant and loss tangent are functions of frequency and must be measured at the frequency appropriate to the circuit application. However, the variation of dielectric constant with frequency is sufficiently small that it can be considered to be constant over a fairly wide frequency band. The loss tangent, on the other hand, will normally vary significantly with the frequency and thus it is particularly important that this parameter be characterized at the frequencies of interest.

There are numerous methods for dielectric material characterization reported in the literature. However, each method may vary significantly in respect of accuracy, applicable frequency range, requirements for sample preparation and geometry, measurement system equipment, measurement speed, and also in the level of complexity of required in processing the measured data. There is a lack of standardization in this field and it is not always obvious which of the existing techniques may be appropriate for measuring a particular type of sample over a given frequency range.

This paper summarizes the relative advantages and limitations of several of the most commonly used techniques and is intended to provide a useful design guide for the materials or packaging specialist, who requires accurate information on material properties at microwave and millimeter wave frequencies.

In particular, a recently developed technique for measuring the loss of a dielectric using a resonant cavity with a slit will be described, as this appears to offer significant advantages to the industrial user.

In addition to techniques for determining the properties of dielectric substrates the paper also addresses the issue of measuring microstrip line properties, so as to enable some estimation of conductor performance to be obtained.

Substrate permittivity

The most general description of a dielectric material is given by the complex permittivity, ε^*

$$\varepsilon^* = \varepsilon_0(\varepsilon_r' - j\varepsilon_r'') = \varepsilon_0\varepsilon_r'(1 - j\tan\delta)$$

where ε_0 is the dielectric constant of air (or vacuum), ε_r' is the real part of the relative permittivity and often referred to simply as the dielectric constant (and represented just by ε_r), and tan δ is the loss tangent. In simple terms, the dielectric constant determines the velocity with which the signal travels through the medium and tan δ determines the loss in the medium.

Thus dielectric measurement techniques are focussed on the determination of these two critical parameters, ε_r and tan δ.

In order to put the effect of the dielectric properties into a more practical context, we have used circuit simulation to show how the two parameters of interest would affect the performance of a microstrip filter. In Figure 1 we see how a change of ±2 per cent in the dielectric constant affects the match of the filter. It can be seen that the magnitude of the match is essentially unchanged but there is a shift in the centre frequency of the response of around ±1 per cent. This results is in agreement with the fundamental theory, which predicts that the dielectric constant will affect the velocity of propagation through the filter, and hence the optimum frequency. It is expected that the loss tangent will affect the loss through the filter and to examine this effect we show, in Figure 2, how a tenfold increase in the loss tangent will affect the transmission loss through the filter. The simulated data shows that the tenfold increase in loss tangent, from 0.0005 to 0.005, increase the insertion loss by around 2dB. This could be very significant in a practical design, not only because it represents a loss of signal, but also because it could substantially increase the noise figure of the component. To put the data used for the loss tangent into a practical context: 0.0005 represents the loss tangent that would be expected from microwave grade, lapped alumina, and 0.005 the value that would be expected from LTCC material.

Dielectric measurement techniques

In this section we review the standard methods that are available, and introduce a recent technique that is based on a slit resonant cavity.

Resonant cavity perturbation method

Among various dielectric measurement techniques, resonant cavity perturbation method has been proved to be the most successful and accurate technique for measuring the complex permittivity of low-loss materials (Gallone *et al.*, 1996; Horner *et al.*, 1946; Huang *et al.*, 1995; Janezic and Grosvenor, 1991; Kraszewski and Nelson, 1996; Li *et al.*, 1998; Martinelli *et al.*, 1985; Meng *et al.*, 1995; Parkash *et al.*, 1979; Pohl *et al.*, 1995; Vanzura and Kissick, 1989).

These measurements are performed by cutting and placing a small sample of the dielectric material into a microwave resonant cavity, generally at the center of the cavity where the field is a maximum, so as to achieve the greatest measurement sensitivity. Since the resonance characteristics of a cavity are dependent on the material loading the cavity, both the dielectric constant and loss

Zhengrong Tian and Charles Free
Measurement techniques for the evaluation of thick-film materials used in wireless applications

Microelectronics International
18/2 [2001] 21–25

tangent of the specimen can be obtained from measurements of the resonant frequency and quality factor (Q-factor) of the cavity with and without the specimen. Perturbation theory then enables the parameters to be found:

$$\varepsilon_r = 1 + \frac{2}{\eta}\cdot\frac{f_e - f_s}{f_s}$$

$$\tan\delta = \frac{f_s}{2f_e + (\eta - 2)f_s}\cdot\left(\frac{1}{Q_s} - \frac{1}{Q_e}\right)$$

where f_e and Q_e are the resonant frequency and Q factor of the empty cavity; f_s and Q_s are the resonant frequency and Q factor of the cavity loaded with the specimen.

The filling factor, η, is given by:

$$\eta = \frac{\int_{v_s} \vec{E}_1 \cdot \vec{E}_2 \cdot dv}{\int_{v_c} |E_1|^2 \cdot dv}$$

v_s and v_c are the specimen and cavity volume, respectively, and E_1 and E_2 are components of the electric field vector.

The calculations for the perturbation method are relatively simple and complex numerical processes are not involved.

Figure 3 is a sketch of a typical microwave resonant cavity, which is usually formed by taking a standard rectangular or circular waveguide of a certain length, with transverse metallic plates bolted to the end flanges. An iris hole in each end plate feeds energy in and out of the cavity.

The accuracy of the cavity perturbation method largely depends on the fit of the sample in the waveguide. The samples need to be precisely formed to the inside dimension of the waveguide and carefully located in the transverse plane, perpendicular to the axis of the waveguide, usually within ± 0.05°. The sample preparation is much more time-consuming in the case of a circular waveguide resonator. Also, for both the rectangular and circular cases the preparation and positioning of thin samples can be quite difficult.

As the name "perturbation" implies, the two situations, i.e. the cavity conditions with and without the sample, must be very similar. Thus the resonant cavity system must be set up very critically so the cavity resonant and Q properties can be stable and consistently repeatable after introducing or removal of a specimen. This imposes stringent requirements on the mechanical assembly of the cavity.

The measurement is normally performed over a very small frequency range, determined by the limited bandwidth of the waveguide. When investigations of microwave material over a wide frequency range are required, a set of resonant cavity structures has to be built. Also the frequency range of this method is limited by the reasonable waveguide size. As shown in Table I, as frequency extends into Q band the size of the cavity becomes so small that it is not practical to machine and position the sample into the waveguide.

Figure 1
Response of a 30GHz filter with ε_r ± 2 per cent

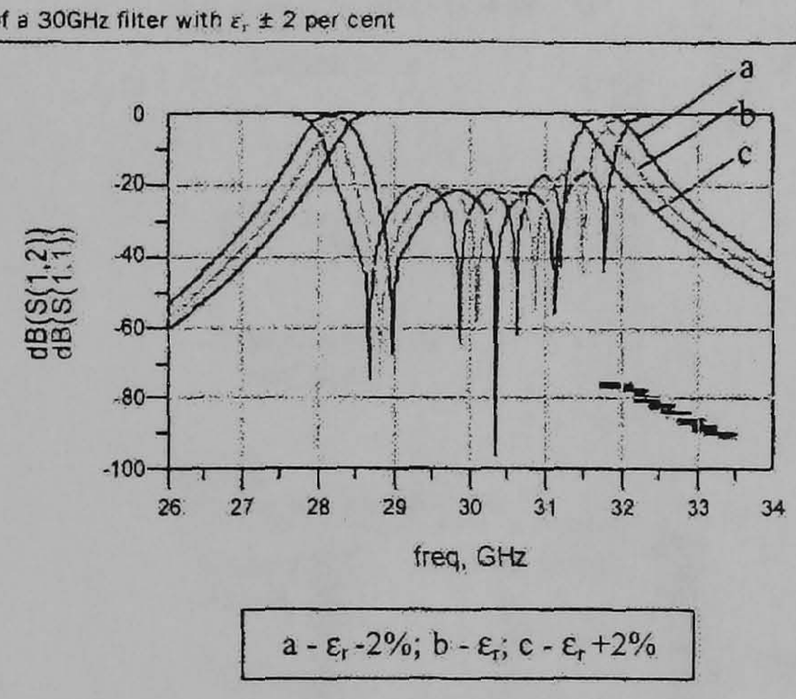

Figure 2
Insertion loss of a 30GHz filter with tan δ = 0.0005 and 0.005

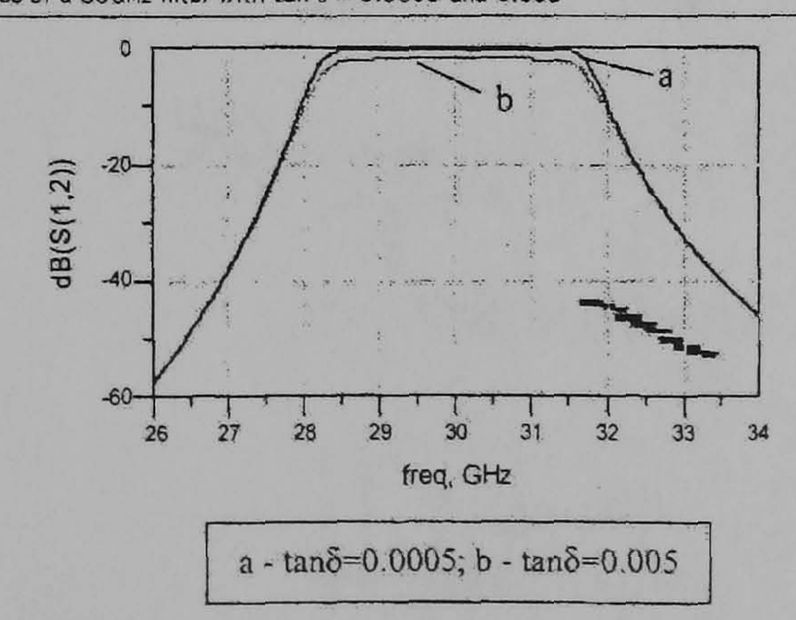

Open-ended transmission line method

The dielectric sample being tested is placed in close contact with the end of an open-ended microwave transmission line, which may be a coaxial cable (Pournaropoulos and Misra, 1997) (Figure 4) or a piece of circular waveguide (Tantot *et al.*, 1996). The input reflection coefficient is measured using an automatic vector network analyser and the dielectric properties of the sample can be inferred through numerical electromagnetic analysis.

The benefit of this method is it can be used to measure samples over a wide frequency range rather than just at a single fixed resonant frequency as in the cavity perturbation method. It is also quick to set up the measurement system and the sample preparation is rather simple. This method is also useful when it is difficult or impossible to cut the sample when on-line quality control is needed. But the problem is the data process is complicated since it involves a large amount of electromagnetic calculation.

Open resonator methods

Open resonator methods are regarded as precise measurement methods of low loss dielectric materials in the millimetre wave range 30-300 GHz (Afsar *et al.*, 1990, 1999; Cullen and Yu, 1971; Hirvonen *et al.*, 1996; Jones, 1976; Komiyama *et al.*, 1991; Yu and Cullen, 1982). Commonly used open resonators are either confocal type in which two spherical mirrors form the Fabry-Perot cavity or hemispherical type in which one spherical mirror and one flat mirror form the cavity. Figures 5 and 6 show the configurations of spherical and hemispherical type open resonators respectively. Both types of mirrors were machined from brass and gold-plated after polishing. By

Figure 3
Microwave resonant cavity

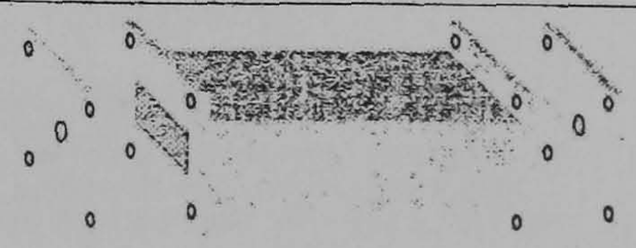

Zhengrong Tian and Charles Free
Measurement techniques for the evaluation of thick-film materials used in wireless applications
Microelectronics International
18/2 [2001] 21–25

measuring the resonant frequency and Q factor of the resonator loaded with and without sample, the complex permittivity of the materials can be determined.

It was reported that the uncertainty of the measurement is 0.02 per cent to 0.04 per cent for εr ($\varepsilon r \geq 2$) and 6 – 40 × 10-6 for tanδ (10-4 ≤ tanδ ≤ 10-3) at 100GHz.

Slit cavity resonator method

As stated earlier, the cavity perturbation measurement technique can be highly accurate provided that the properties of the cavity can maintained exactly the same after the system is dismantled and reassembled each time a new sample is tested. Otherwise, the small differences in the mechanical cavity assembly can cause significant errors in the resonant frequencies and Q factors being measured. This will obviously lead to errors in the measured dielectric data. Simulation has shown that a shift in the resonant frequency of ±2MHz caused by the inaccurate cavity set-up may cause the errors in loss tangent of ±10 per cent.

Similarly, it has been shown that a change of ±3 per cent in the Q-factor causes errors greater than ±10 per cent in the measured loss tangent. Also, the higher the dielectric constant, the worse these error become.

We identified the sample positioning as being another critical aspect of the perturbation method. This error has been quantified through simulation and the results are shown in Figure 7.

All of these problems of the conventional cavity perturbation technique suggest that a measurement technique is needed that does not require the cavity to be disassembled and reassembled between measurements on different samples. This further indicates that a measurement technique should be sought that involves loading the sample under test through an opening in the resonant cavity. If this can be achieved it will greatly improve the consistency of the measurement.

Figure 8 shows the electromagnetic field distribution of TE_{10n} mode in a rectangular cavity. If we cut a slit in the narrow wall of the cavity, as shown in Figure 9, the cavity performance will be essential unchanged since the slit is parallel to the current flow. Only if a slit is cut in such a way as to interrupt the current flow lines will there be radiation from the slit, and a consequent change in cavity performance.

With this arrangement, all that is needed is to insert the sample into the slit, and to measure the resonant frequencies and Q factor, of the arrangement before and after the insertion of the sample. Any errors associated with cavity loading or poor assembly of the cavity will be the same in both of the measurement states and therefore will effectively cancel out. A further advantage of the method is that the sample size and precise position are no longer significant.

The measurement set-up is quite simple as shown in Figure 10. The slit cavity resonator (DUT) is connected with the network analyser between Port 1 and Port 2 through waveguide and coaxial transitions. S21 is measured for the cavity with and without the sample to obtain the resonant frequency and Q factor of the cavity.

Table II shows the measured result at S band and X band by slit cavity resonator method.

Table I
Standard size of rectangular waveguide

British WG	Width a (in)	Height b (in)	Recommended operating frequency range (GHz)
7	5.100	2.550	1.45–2.20
13	1.5900	0.7950	4.9–7.05
16	0.9000	0.4000	8.20–12.4
20	0.4200	0.1700	18.0–26.5
22	0.2800	0.1400	26.5–40.0

Figure 4
Open-ended coaxial line measurement

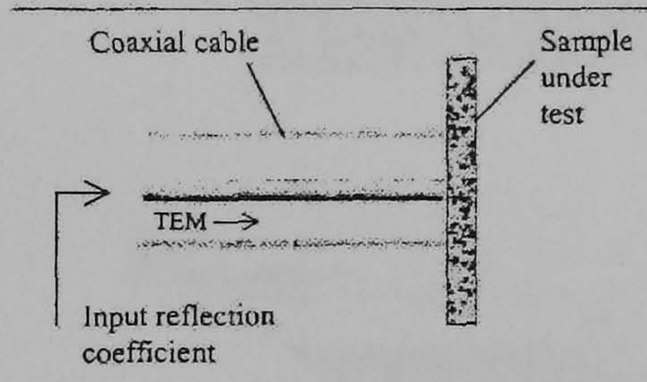

Figure 5
Spherical type open resonator

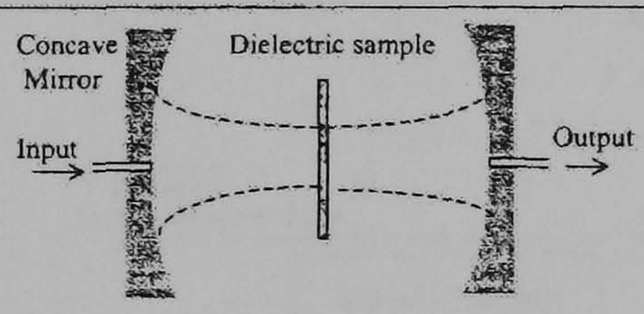

Figure 6
Hemispherical type open resonator

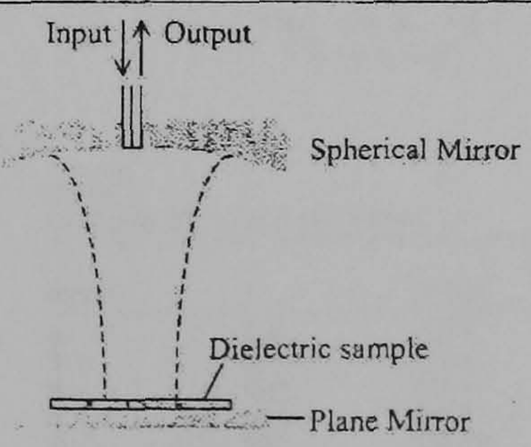

Microstrip test structures

In the previous sections we have discussed the methods that are available for measuring the properties of dielectric materials. Equally important in any practical circuit, are the properties of the conductors being used. The conventional method to establish the properties of the conductors at microwave frequencies is to build a microstrip test structure, from which the total behavior (conductor + dielectric) can be obtained, and hence the properties of the conductor, since the dielectric characteristics can be obtained through the methods previously described. Two common mictostrip test structures are used; the microstrip resonant ring and the meander line.

A microstrip resonant ring is shown in Figure 11. From measurements of the resonant frequency and Q factor of the ring, the effective dielectric constant and line loss can be deduced. For rings in which w/h < 1 and mean circumference l >> w, at resonance,

$$\varepsilon_{eff}(f) = \left(\frac{150n}{fl}\right)^2$$

Where n is the integer order of resonance. ε_{eff} is the effective microstrip permittivity.

However, this technique suffers from one basic limitation, namely that there is always a loading effect associated with the coupling of energy into and out of the ring.

Figure 7
Percentage error in ε_r caused by the positioning error of ±0.002mm

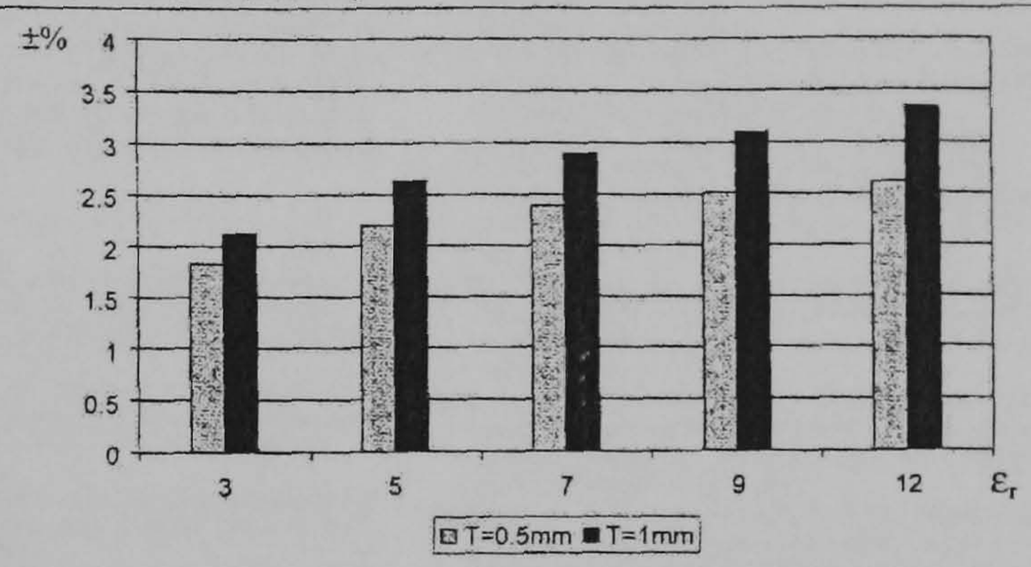

Figure 8
Electromagnetic field distribution of TE_{10n} mode in a rectangular cavity

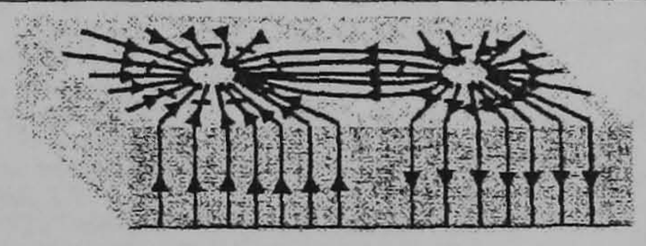

Figure 9
Slit cavity resonator

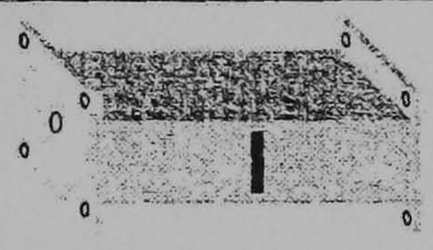

Figure 10
Measurement set-up

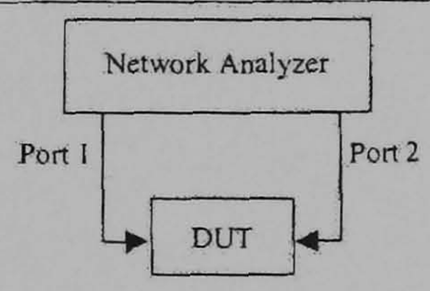

Table II
Measured results at S and X band

Sample	ε_r	tan δ S band	tan δ X band
A	7.33	0.004	0.008
B	7.2	0.001	0.003
C	6.84	0.004	0.005
D	8.89	0.002	0.007
E	9.98	0.0009	0.002

An alternative test structure that is gaining increasing acceptance, particularly for industrial users, is the meander line (Figure 12). This is used in an absolute measurement, in which the loss and phase change through the meander line are compared with the loss and phase change through a shorter, straight, line. The line loss, in dB/unit length, is then found directly by dividing the difference in the measured values of loss by the difference in the line lengths. The effective dielectric constant is found in a similar manner from the difference in the measured phase values. The advantage of this method is that there are no loading effects, and any errors associated with the coaxial-to-microstrip transitions that are used to couple energy to the lines are effectively cancelled when the difference between the measured data is computed. The only disadvantage to this technique is that there is not the voltage magnification associated with a resonant structure, and therefore the technique might be considered to be less sensitive than the resonant ring. However, this sensitivity is largely dependent on the measuring equipment being used and this is no longer a significant factor with modern network analyzers.

Figure 11
Ring resonator

Figure 12
Microstrip meander line test pattern

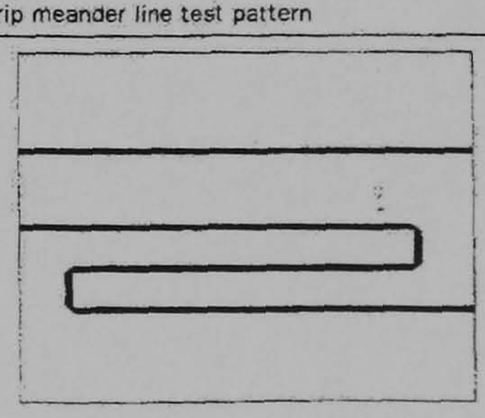

Microelectronics International
18/2 [2001] 21–25

Conclusion

The discussion has indicated that for the vast majority of commercial applications the dielectric loss can be obtained, easily and efficiently, and with sufficient accuracy using a resonator with a narrow loading slit. Where it is necessary to obtain some indication of conductor loss at microwave frequencies, the meander line technique offers a simple and accurate method.

References

Afsar, M.N., Ding, H. and Toursham, K. (1999), "A new open-resonator technique at 60 GHz for premittivity and loss-tangent measurement of low-loss materials", *1999 IEEE MTT-S Digest*, pp. 1755-8.

Afsar, M.N., Li, X. and Chi, H. (1990), "An automated 60GHz open resonator system for precision dielectric measurement", *IEEE Trans. Microwave Theory Tech.*, Vol. 38 No. 12, December, pp. 1845-53.

Cullen, A.L. and Yu, P.K. (1971), "The accurate measurement of permittivity by means of an open resonator", *Proc. R. Soc. Lond*, A325, pp. 493-509.

Gallone, G., Lucardesi, P., Martinelli, M. and Rolla, P.A. (1996), "A fast and precise method for the measurement of dielectric permittivity at microwave frequencies", *Journal of Microwave Power and Electromagnetic Energy*, Vol. 31 No. 3, pp. 158-64.

Hirvonen T.M., Vainikainen P., Lozowski, A. and Raisanen, A.V. (1996), "Measurement of dielectrics at 100 GHz with an open resonator connected to a network analyzer", *IEEE Trans. Instrum. Meas.*, Vol. 45 No. 4, August, pp. 780-86.

Horner, F., Taylor, T.A., Dunsmuir, R., Lamb, J. and Jackson, W. (1946), "Resonance methods of dielectric measurement at centimetre wavelengths", *J. IEE*, Vol. 93 Pt. III, pp. 53-68.

Huang, H., Free, C.E., Pitt, K.E.G., Berzins, A.R. and Shorthouse, G.P. (1995), "Relative permittivity measurement of thick-film dielectrics at microwave frequencies", *Electronics Letters*, Vol. 31 No. 21, October, pp. 1812-14.

Janezic, M.D. and Grosvenor, J.H. (1991), "Improved techniques for measuring permittivity of thin dielectrics with a cylindrical resonant cavity", *1991 IEEE Instrumentation and Measurement Technology Conference*, pp. 580-84.

Jones, R.G. (1976), "Precise dielectric measurements at 35 GHz using an open microwave resonator", *Proc. IEE*, Vol. 123 No. 4, April, pp. 285-90.

Komiyama, B., Kiyokawa, M. and Matsui, T. (1991), "Open resonator for precision dielectric measurements in the 100 GHz band", *IEEE Trans. Microwave Theory Tech.*, Vol. 39 No. 10, October, pp. 1792-6.

Kraszewski, A.W. and Nelson, S.O. (1996), "Resonant cavity perturbation – some new applications of an old measuring technique", *Journal of Microwave Power and Electromagnetic Energy*, Vol. 31 No. 3, pp. 178-87.

Li, D., Free, C.E., Barnwell, P.G. and Pitt, K.E.G. (1998), "Pertubation method for dielectric constant measurement of thick-film dielectric material", *Electronics Letters*, Vol. 34 No. 21, October, pp. 2042-44.

Martinelli, M., Rolla, P.A. and Tombari E. (1985), "A method for dielectric loss measurements by a microwave cavity in fixed resonance condition", *IEEE Trans. Microwave Theory Tech.*, Vol. 33 No. 9, pp. 779-83.

Meng, B., Booske, J. and Cooper, R. (1995), "Extended cavity perturbation technique to determine the complex permittivity of dielectric materials", *IEEE Trans. Microwave Theory Tech.*, Vol. 43 No. 11, pp. 2633-6.

Parkash, A., Vaid, J.K. and Mansingh, A. (1979), "Measurement of dielectric parameters at microwave frequencies by cavity perturbation technique", *IEEE Trans. microwave Theory Tech.*, Vol. 27 No. 9, pp. 791-5.

Pohl, V., Fricke, D. and Muhlbauer, A. (1995), "Correction procedures for the measurement of permittivities with cavity perturbation method", *Journal of Microwave Power and Electromagnetic Energy*, Vol. 30 No. 1, pp. 10-26.

Pournaropoulos, C.L. and Misra, D.K. (1997), "The coaxial aperture electromagnetic sensor and its application in material characterization", *Measurement Science and Technology (UK)*, Vol. 8 No. 11, November.

Tantot, O., Chatard-Moulin, M. and Guillon, P. (1996), "Dielectric measurement of multi-layered medium using an open-ended waveguide", *Microwave Processing of Materials V Materials Research Society Symposium Proceeding*, Vol. 430, pp. 245-51.

Vanzura, E.J. and Kissick, W.A. (1989), "Advances in NIST permittivty measurement sapability using a mode-filtered cylindrical cavity", *IEEE MTT-S International Microwave Symposium Digest*, Vol. III, Part EE, pp. 901-4.

Yu, P.K. and Cullen, A.L. (1982), "Measurement of premittivity by means of an open resonator: I. theoretical", *Proc. R. Soc. Lond*, A380, pp. 49-71.